Novel Intramolecular Charge Transfer Materials and their Optoelectronic Properties

MOSS, KATHRYN,CLARE

Novel Intramolecular Charge Transfer Materials and their Optoelectronic Properties

Kathryn Clare Moss
Ustinov College

Department of Chemistry
Durham University

A Thesis Submitted for the Degree of Doctor of Philosophy at Durham University

January 2012

STATEMENT OF COPYRIGHT

DECLARATION

The work described in this thesis was carried out in the Department of Chemistry at Durham University between September 2008 and December 2011. All the work was carried out by the author unless otherwise stated and has not previously been submitted for a degree at this or any other university.

Table of Contents

Abstract

Novel Intramolecular Charge Transfer Materials and their Optoelectronic Properties

Kathryn Clare Moss, Durham University, 2012

A summary of aspects of the literature surrounding organic donor-acceptor systems for a variety of optoelectronic applications (OLEDs, OFETs, OPVs) is presented with a particular focus on two key moieties; 9,9-dialkylfluorene (**F**) and dibenzothiophene-*S*,*S*-dioxide (**S**). The development of these "building blocks" into novel systems capable of intramolecular charge transfer, i.e. donor-acceptor containing materials, is then discussed.

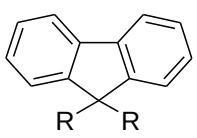

F

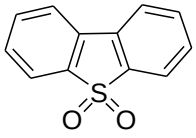

S

The syntheses and photophysics of a number of novel fluorescent ambipolar trimers based on **F** and/or **S** are presented which allow investigations to be performed into the excited state behaviour of the systems. Tuning of the emission colour is demonstrated from deep blue to green by varying the strength of the donor and/or by manipulating the extent of conjugation through the systems. Related trimers are investigated which exhibit the unusual phenomenon of (low temperature) phosphorescence from all-organic systems. Development of the **F**/**S** trimers into polymers gives systems which are capable of emitting white light and all-fluorescent white-emitting devices are presented.

Following on from this, the use of **F** as a molecular bridge between donor (ferrocene) and acceptor (C_{60}) moieties is presented, with the aim of modulating charge transfer between the two by varying the linker between ferrocene and **F** as well as the length of the fluorene bridge. The synthesis and electrochemical behaviour of the compounds is discussed and photophysical studies are currently being undertaken.

Finally, random co-polymers of **F**, **S** and related analogues are presented to investigate the morphology of such systems with regard to beta phase formation. A number of **F** and/or **S** based systems are also presented with the aim of finding novel high triplet energy host materials for OLEDs. The syntheses and photophysical studies of these materials are discussed.

Overall, the work demonstrates the great potential of **F** and **S** in donor-acceptor systems for a wide variety of optoelectronic applications.

Acknowledgements

Firstly I would like to thank Professor Martin R. Bryce for offering me a PhD position; I have really enjoyed being part of the Bryce group. I would also like to thank Durham University for awarding me a Doctoral Fellowship in order to fund my research.

I would like to thank all the chemists who have been involved in this work and related projects. The work described in Chapters 2 and 3 was part of a number of wider projects involving Dr. Haiying Li, Dr. Kiran Kamtekar and Dr. Vandana Bhalla. The work described in Chapter 4 was developed from studies started by Dr. Cornelia van der Pol. Dr. Mark Fox is acknowledged for the computational work discussed in Chapter 3 and Dr. Andrei Batsanov for the X-ray crystallography mentioned in Chapter 2. I would also like to thank the Durham University analytical staff for all the services they provide and maintain.

I would like to thank the physicists of Professor Andrew Monkman's group (Durham University) for all their helpful contributions to the work described in this thesis. Work discussed in Chapters 2 and 3 involved Dr. Helen Vaughan, Dr. Konstantinos Bourdakos and Dr. Fernando Dias; the white light-emitting devices discussed in Chapter 3.3 were fabricated by Mr. Gareth Griffiths and the beta phase photophysical studies discussed in Chapter 5 were performed by Dr. Daniel Bright. I would especially like to acknowledge Dr. Fernando Dias for his advice and ideas over the course of my PhD. The compounds discussed in Chapter 4 will be studied in the group of Professor Dirk Guldi (University of Erlangen-Nürnberg) and studies involving these materials are currently underway.

Lastly, I would like to thank all the members of the Bryce group, past and present for helping to solve many different chemistry problems over the years and for providing great company and friendship along the way.

Publications and Presentations

The following papers are based on work described in this thesis:

- H. Li, A. S. Batsanov, K. C. Moss, H. L. Vaughan, F. B. Dias, K. T. Kamtekar, M. R. Bryce, A. P. Monkman; **The interplay of conformation and photophysical properties in deep-blue fluorescent oligomers**, *Chem. Commun.*, **2010**, *46*, 4812

- K. C. Moss, K. N. Bourdakos, V. Bhalla, K. T. Kamtekar, M. R. Bryce, M. A. Fox, H. L. Vaughan, F. B. Dias, A. P. Monkman; **Tuning the intramolecular charge transfer emission from deep blue to green in ambipolar systems based on dibenzothiophene-*S*,*S*-dioxide by manipulation of conjugation and strength of the electron donor units**, *J. Org. Chem.*, **2010**, *75*, 6771

- D. W. Bright, K. C. Moss, K. T. Kamtekar, M. R. Bryce, A. P. Monkman; **The β phase formation limit in two poly(9,9-di-*n*-octylfluorene) based copolymers**, *Macromol. Rapid Commun.*, **2011**, *32*, 983

The following presentations were based on work described in this thesis:

- Durham University Chemistry Department Postgraduate Student Research Symposium, June 2011, (*winner of organic chemistry presentation prize*)

- RSC Organic Division Northeast regional symposium, Northumbria University, April 2011, (*winner of poster prize*)

- 43rd IUPAC World Polymer Congress Macro2010, Glasgow, July 2010; oral presentation

- 42nd IUPAC Congress, Glasgow, August 2009; flash oral presentation and poster presentation

- 13th International Symposium on Novel Aromatic Compounds ISNA-13, Luxembourg, July 2009, poster presentation

List of Abbreviations

A	Acceptor
ArN	Arylamine
BHJ	Bulk heterojunction
BT	2,1,3-benzothiadiazole
^{n}BuLi	^{n}Butyl Lithium (2.5 M in hexanes)
Cbz	Carbazole
CCT	Colour correlated temperature
CIE	Commission internationale d'eclairage
CRI	Colour rendering index
CT	Charge Transfer
CV	Cyclic voltammetry
D	Donor
DBT	Dibenzothiophene
DCM	Dichloromethane
DMF	Dimethylformamide
DPA	Diphenylamine
EL	Electroluminescence
EQE	External quantum efficiency
E_T	Triplet energy level
ET	Electron transport
F	Fluorene
Fc	Ferrocene
HOMO	Highest occupied molecular orbital
HT	Hole transport
ICT	Intramolecular charge transfer
ISC	Inter-system crossing
LE	Local excitonic
LUMO	Lowest unoccupied molecular orbital
MCH	Methylcyclohexane
NBS	N-bromosuccinimide
OF	Oligofluorene
OFET	Organic field effect transistor

OLED	Organic light-emitting device
OPV	Organic photovoltaic
OXD	Oxadiazole
P3HT	Poly(3-hexylthiophene)
PCBM	[6,6]-phenyl-C_{61}-butyric acid methyl ester
PF	Polyfluorene
PF6	Poly-9,9-di-*n*-hexylfluorene
PF7	Poly-9,9-di-*n*-heptylfluorene
PF9	Poly-9,9-di-*n*-nonylfluorene
PF10	Poly-9,9-di-*n*-didecylfluorene
PFO (PF8)	Poly-9,9-di-*n*-octylfluorene
PICT	Planarised intramolecular charge transfer
PL	Photoluminescence
PLED	Polymeric light-emitting diode
PLQY (ϕ_{PL})	Photoluminescence quantum yield
RGB	Red, green, blue
S	Dibenzothiophene-S,S-dioxide
S-M	Suzuki-Miyaura
TBT	4,7-bis(2-thienyl)-2,1,3-benzothiadiazole
THF	Tetrahydrofuran
TICT	Twisted intramolecular charge transfer
TPA	Triphenylamine
WOLED	White organic light-emitting device

Chapter 1: Organic Ambipolar Materials for Optoelectronic Applications

1.1 Introduction

The development of novel materials for optoelectronic applications e.g. organic light-emitting devices (OLEDs), organic field effect transistors (OFETs) and organic photovoltaics (OPVs) is essential to realise the full potential of plastic electronics. These materials represent the future in more energy efficient displays, lighting and solar cells for our future energy needs. The use of organic (i.e. carbon-based) materials in these applications is an attractive prospect as these materials offer the possibility of generating lightweight, flexible materials, which can be produced at a low cost and are easily applicable to large scale roll-out. Some of these materials are already in use in the OLED display screens of mobile phones, personal digital assistants and car displays, as well as prototype television displays.

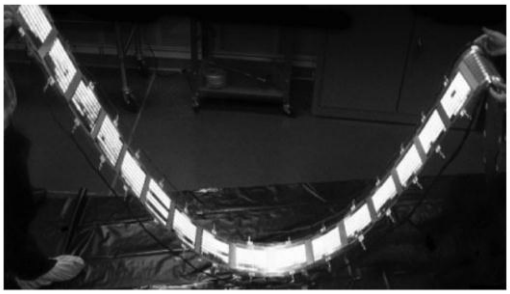

Figure 1.1 – Example of a "plastic electronics" application; a roll-to-roll printed OLED from General Electric Company (reproduced from reference[1])

The requirement of materials used in these applications is that they act as organic semiconductors i.e. are capable of transporting charge carriers (electrons and holes) through the devices. In OLEDs it is the recombination of an electron and a hole to form an exciton, within the correct region of the device, which then decays radiatively, producing light in the visible region of the spectrum. OFETs act as capacitors and generally consist of a source, a drain and a gate. The gate controls the flow of current between the source and the drain and can therefore be switched on or off with the applied voltage; a negative applied voltage allows hole transport through the device (*p*-channel), a positive applied voltage allows electron transport (*n*-channel). In OPVs the absorption of visible light allows the generation of an exciton which can migrate through the device before dissociating into its constituent electron and hole. These charge carriers are then transported through the device to their relevant electrodes, thus generating a current. Materials for these applications can be small molecules or polymers.

Ambipolar systems (also referred to as "bipolar" systems[2,3]) are those capable of balanced charge transport and must therefore contain both electron-accepting and hole-accepting moieties i.e. have donor-acceptor type architectures. Without these contrasting moieties, either migration of electrons or holes will dominate which will reduce device efficiencies. Balanced charge transport can either be achieved with blends of hole transport and electron transport materials within the devices, or by covalently linking the two moieties together. Blends have the potential to phase separate during device operation which can reduce efficiencies, but the required materials can be synthetically easier to access. Covalent ambipolar systems avoid the problems associated with phase separation but can often be synthetically more difficult to access as the energy levels of the constituent parts must be carefully tuned. In OLEDs, the emission from a donor-acceptor (D-A) system often originates from intramolecular charge transfer (ICT) excited states which are formed when the donor radical cations combine with the acceptor radical anions.

There are already numerous reviews covering various aspects of materials for optoelectronic applications including ambipolar conjugated molecules,[4] co-polymers,[5,6] single-material molecular emitters for OLEDs,[7] light-emitting conjugated polymers,[8] charge carrier transporting materials,[9] as well as a recent review covering the design of bipolar small molecules for OLED applications.[2] This chapter focuses on the introduction of covalently linked D-A (i.e. ambipolar) systems for optoelectronic applications with a particular focus on the key moiety, fluorene (**F**, **1**) followed by a brief introduction to the heterofluorene analogue, dibenzothiophene-*S*,*S*-dioxide (**S**, **2**) (Figure 1.2). Subsequent chapters then focus on the development of novel D-A systems, both oligomers and polymers, based on one or both of these moieties in order to understand key properties/address key issues related to the optoelectronics field.

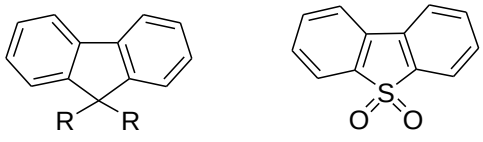

1 **2**

Figure 1.2 – Structures of fluorene (F) and dibenzothiophene-*S*,*S*-dioxide (S)

1.2 Non-fluorene containing donor-acceptor systems

There have been many donor units utilised in ambipolar systems including carbazole, arylamine, fluorene, phenoxazine and phenothiazine. Among the commonly used acceptors are arylboranes, benzimidazoles, triazoles, oxadiazoles, quinolines and C_{60} (for OPVs – a topic which is discussed further in Chapter 4).

The Jenekhe group presented a series of ambipolar molecules containing phenoxazine as the donor unit with acceptors including quinoline, quinoxaline, benzoquinoxaline and benzoylquinoxaline (selected examples, Figure 1.3) with the aim of understanding the structure-property relationships in D-A systems relevant to optoelectronic device applications.[10] The materials exhibit ICT fluorescence with photoluminescence quantum yields (PLQYs) ranging from a low 16% (**3**) to a high 81% (**4**) in value depending on the identity of the acceptor.[10] Electrochemical studies demonstrated the ambipolar nature of the materials. Subsequent work probed these systems further and a tuning of the emission colour of the molecules across the visible spectrum from blue through to red was reported with increasing electron accepting character.[11] Field-effect hole mobilities of up to 7 x 10^{-4} cm^2 V^{-1} s^{-1} were reported, demonstrating the potential utility of these systems as *p*-type semiconductors in OFETs as well as emitters in ambipolar OLEDs.[11]

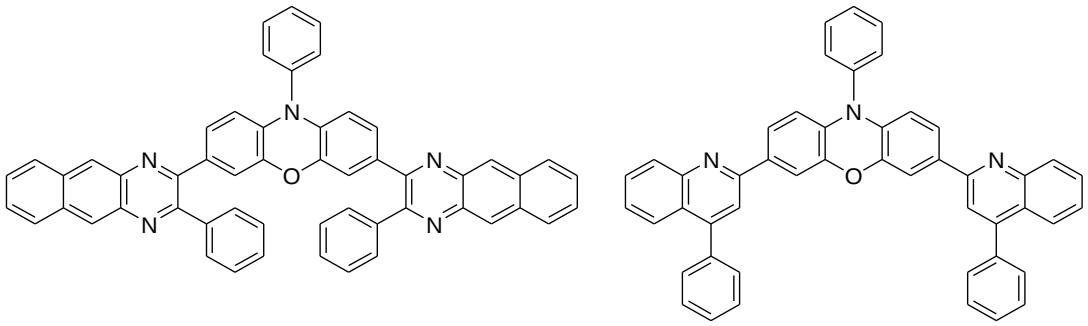

3 **4**

Figure 1.3 – Structure of ambipolar phenoxazine-based molecules

The quinoline acceptor unit was also used in alternating D-A conjugated co-polymers (and their corresponding A-D-A oligomers) with both carbazole (**5**) and phenothiazine (**6**) donors (Figure 1.4).[12] Strong ICT effects were seen in both co-polymers; however, the effects were more pronounced in the phenothiazine-containing material in line with the increased donor capability of phenothiazine compared with carbazole.[12]

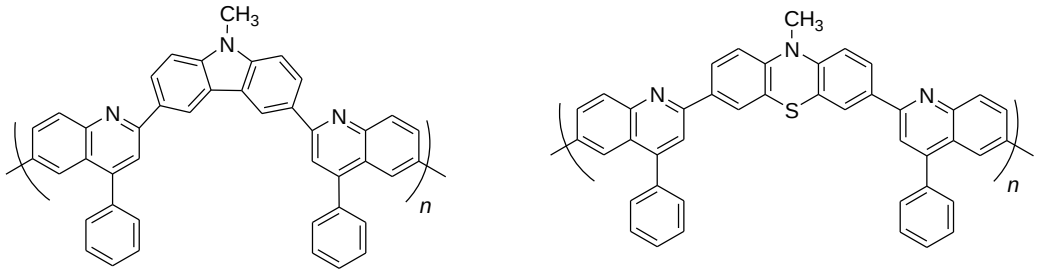

5 **6**

Figure 1.4 – Structures of alternating D-A co-polymers

A D-A dimer based on the phenothiazine-quinoline system (**7**) was used to fabricate a green-emitting OLED which exhibited a maximum device external quantum efficiency (EQE) of 2.5% with a reasonable brightness of 1735 cd m^{-2} and a luminous efficiency of 8.5 cd A^{-1} (Figure 1.5).[13]

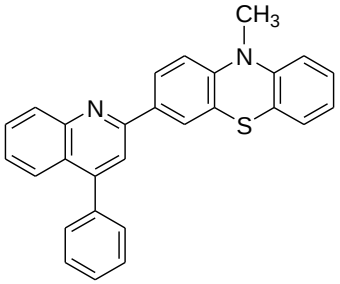

7

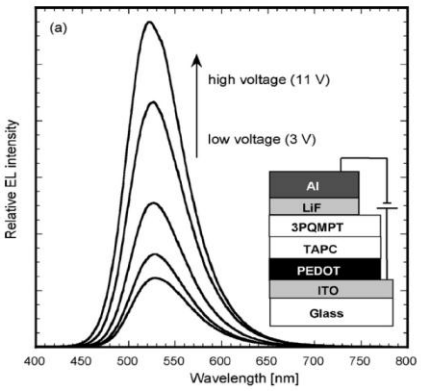

Figure 1.5 – Structure of A-D dimer; EL spectra at different voltages; inset shows device schematic[13]

The strongly donating phenothiazine unit has also been used with anthraquinone as an electron acceptor, for example in the systems reported by Zhang *et al*. (Figure 1.6).[14] The different architectures of the two ambipolar molecules allowed their ICT properties to be probed. From DFT calculations it was determined that the greater conjugation through the larger molecule (**9**) gave the material its smaller HOMO-LUMO gap and explained the greater extent of ICT behaviour seen.[14] Compound **9** was determined to have a co-planar geometry, favouring π-orbital overlap.[14] These results highlight how structural details of D-A systems can affect photophysical behaviour, and that conjugative effects must be taken into consideration in order to tune the properties of the systems to their required applications.

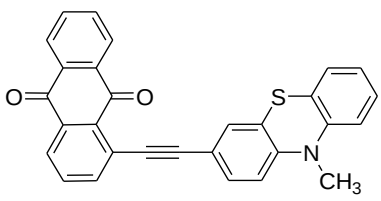

8

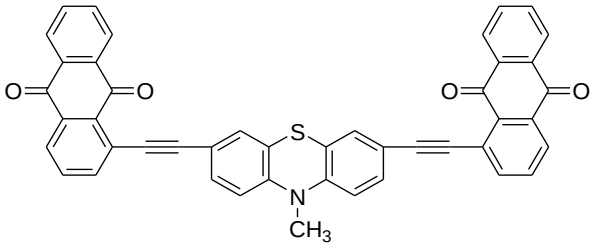

9

Figure 1.6 – Structures of phenothiazine-anthraquinone systems

Lin *et al*. reported a series of ambipolar molecules based on carbazole and an aryl borane for non-doped blue OLEDs (e.g. **10**, **11**, Figure 1.7).[15] Blue OLEDs are the most difficult colour to achieve due to the requirement for a material with a large band gap. A common way to achieve blue emission is to dope a high triplet level host polymer with an organometallic

complex; however, this can create problems with controlling the level of dopant and phase separation. The molecules reported by Lin *et al*. circumvent this problem by using a covalently linked D-A, blue-emitting molecule in the active layer of the devices.[15] Carbazole was chosen as the electron donor due to its relatively weak donor capabilities; too much ICT within a molecule generally leads to more red-shifted emission. Aryl borane was chosen as the acceptor moiety due to its electron deficient nature and luminescent properties and the dimesityl groups hinder close packing of the molecules in the solid state, which could also red-shift the emission.[15] Different linker groups between donor and acceptor were compared.

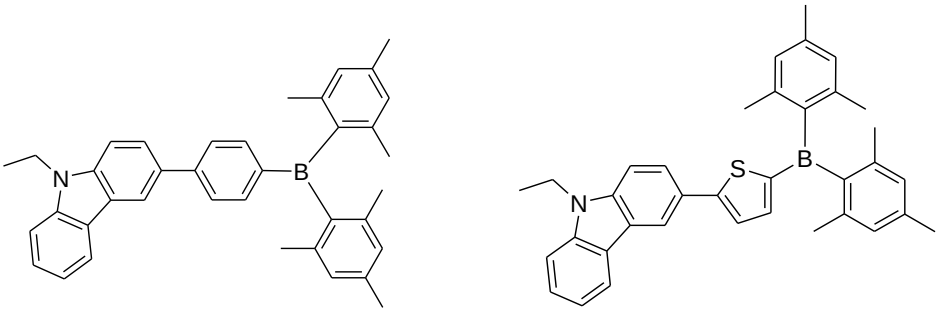

10 **11**

1.7 – Structures of carbazole-aryl borane ambipolar blue-emitting molecules

OLEDs were fabricated from **10** and **11** which emitted electroluminescence (EL) in the deep blue (449 nm) and blue (473 nm) regions of the spectrum respectively, with reasonably high maximum device efficiencies (EQEs) of 4.3% and 6.9% respectively (Figure 1.8, note *CzPhB* refers to compound **10**, *CzThB* refers to compound **11**).[15] Reasonably high solid state fluorescence efficiencies were also reported (~ 50%). The strong performance of these molecules is attributed to the efficient charge-confinement within the molecules and the correct matching of the HOMO/LUMO energy levels to the device requirements.[15] These systems therefore show good potential for use in blue-emitting OLEDs.

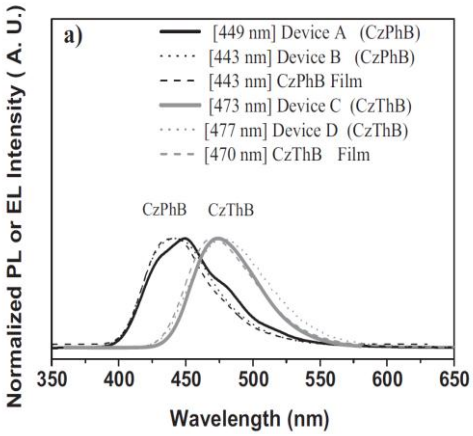

Figure 1.8 – EL spectra of devices based on compounds 10 (CzPhB) and 11 (CzThB) together with their PL spectra in thin film[15]

Another unresolved problem of materials for OLED applications is the development of a red-emitting material which fluoresces with a high efficiency. While there are many reports of red-emitting materials, there are few reports of saturated red emission from organic systems. Chen *et al*. recently addressed this problem by designing novel D-A-D' systems based on electron-withdrawing 2,1,3-naphthothiadiazole (NT) or 2,1,3-benzoselenadiazole (BS) units and electron-donating TPA units (e.g. **14** and **15**, Figure 1.9).[16] Compared with similar compounds where 2,1,3-benzothiadiazole (BT) is used as the acceptor unit (e.g. **12** and **13**), the extended conjugation of the NT units means the emission is red-shifted from orange to red. Similarly, the selenium atom of the BS unit shows stronger polarity than the sulfur atom of the BT unit, hence these compounds also show longer wavelength (ICT) emission in the red region.[16] Compound **13** emits in the red region but with a low PLQY of 0.25.[16] This was partly attributed to the addition of the thiophene rings, which red shift the emission, but may also enhance non-radiative decay pathways due to the heavy atom effect of the sulfur atoms. Compounds which do not have these extra thiophene rings emit red light with higher fluorescence efficiencies (0.33 – 0.51).[16] Compound **14** shows the strongest performance as a red emitter with a fluorescence PLQY of 0.51, indicating this material has good potential for use in red-emitting OLEDs. The authors report that preliminary device studies based on covalently attaching **14** to the side chain of a polyfluorene host, gave efficient red OLEDs.[16]

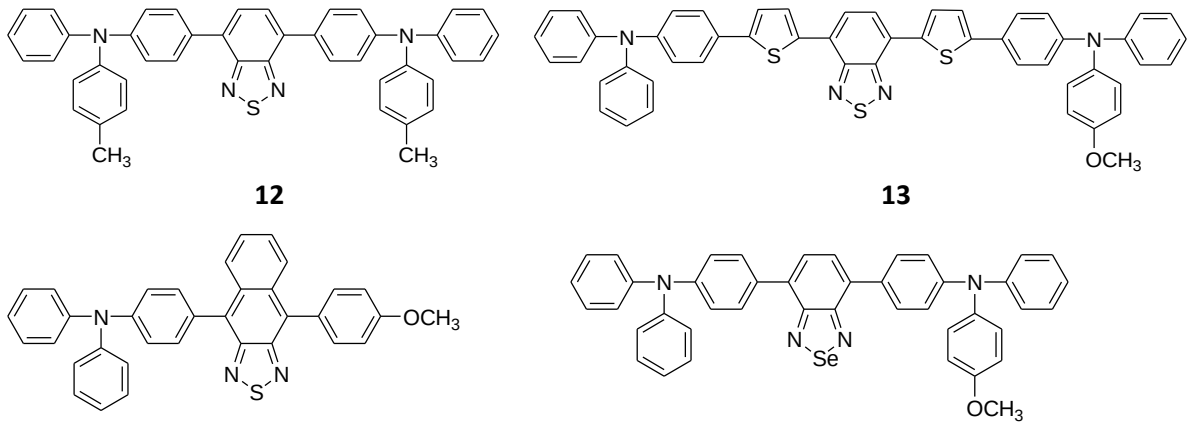

12 **13**

14 **15**

Figure 1.9 – Structures of red-emitting D-A systems

Carbazole has been used in ambipolar host materials for OLEDs, as well as being the emitting unit. Tao *et al*. presented a series of carbazole-oxadiazole-based materials (e.g. Figure 1.10) with the aim of synthesising a material capable of hosting green-emitting iridium complexes.[17] The key requirement for a host material is that it has a triplet energy level (E_T) higher than that

of the guest emitter (i.e. the iridium complex) in order to prevent back energy transfer from the guest to the host thus reducing the luminous efficiency of the guest. For an ambipolar host material the key is balancing the need for a high triplet level with enough charge transport capabilities for efficient devices (increased ICT interactions lead to a lowering of the triplet level).[17] A number of devices were reported with the best performance from the use of **16** (device E) as the host material with a green-emitting iridium complex as the guest (Figure 1.10). These devices outperformed other commonly used host materials under similar conditions.[17]

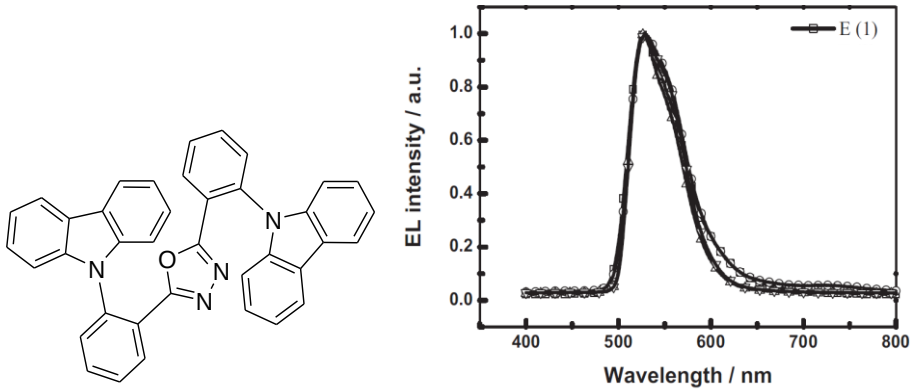

16

Figure 1.10 – Structure of a carbazole-oxadiazole ambipolar host material and EL spectra of multi-layer green-emitting devices doped with $Ir(ppy)_3$ (9 wt%)[17]

This work was developed further by the Bryce group who recently reported a series of carbazole/1,3,4-oxadiazole bipolar molecules (**17**, Figure 1.11) where the optoelectronic properties could be tuned by varying the intramolecular torsional angles through substituent modification.[18] ICT emission was observed, as expected, from the donor carbazole to the acceptor oxadiazole. The work demonstrates a strategy for achieving unusually high triplet levels from bipolar molecules (E_T = 2.64 – 2.78 eV at 14 K)[18] giving these materials strong potential for use as bipolar, small molecule host materials in OLEDs (NB this subject has recently been reviewed by Chaskar *et al*.[3]).

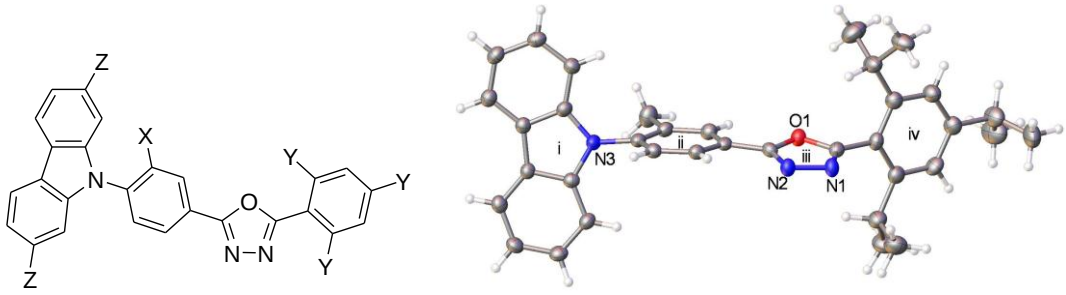

17

Figure 1.11 – Structure of high triplet level bipolar molecules where *X* = H, Me; *Y* = H, Me, ^{i}Pr, ^{t}Bu; *Z* = H, OMe and X-ray molecular structure of molecule with *X* = Me; *Y* = ^{i}Pr; *Z* = H, showing the twist between carbazole and phenyl/oxadiazole moieties

The development of high triplet level ambipolar host materials for OLEDs is discussed further in Chapter 6 where fluorene-based polymers are developed with the aim of hosting green or blue phosphorescent complexes.

As mentioned above, Tao *et al*. exploited the use of a meta linkage between donor and acceptor (**16**) to tune the properties of their system to requirement, in this case to increase triplet levels.[17] Exploiting *meta* conjugation effects in D-A systems has also been applied to solar cell research. One approach to designing materials capable of high efficiency solar energy conversion is to have an electron donor and an electron acceptor separated by a covalently bound chemical bridge. This chemical bridge is usually a conjugated organic moiety which can act as a "molecular wire" between the donor and acceptor. Unlike in OLEDs, for solar cell applications it is necessary to prevent charge recombination in order to convert the energy taken in from the sun into chemical energy i.e. electrical charge. Therefore, an ideal bridge would be able to promote charge separation in order to form the donor and acceptor radical cations and anions but prevent charge recombination. This was achieved by Thompson *et al*. by synthesising two donor-bridge-acceptor molecules using a carbazole donor and a naphthalimide acceptor separated by a phenyl acetylene bridge in which the donor and acceptor were either *meta*-linked (**18**) or *para*-linked (**19**) (Figure 1.12).[19]

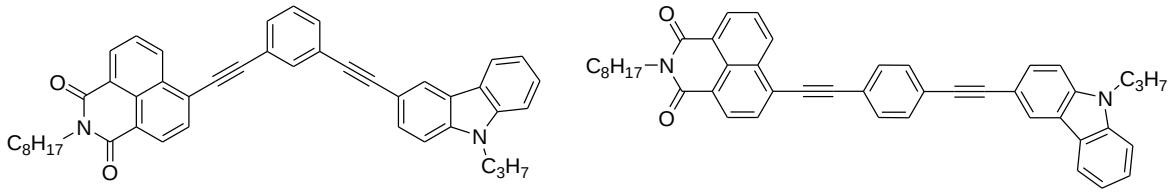

18 **19**

Figure 1.12 – Structures of *meta*- and *para*-conjugated donor-bridge-acceptor molecules

It was reported that the *meta* linkages lead to electronic decoupling in the ground state but undergo enhanced electronic coupling in the excited state.[19] This means that the *meta*-linked phenyl acetylene bridge acts like a wire in the excited state but an insulator in the ground state.[19] Both molecules are capable of efficient electron transfer from donor to acceptor upon excitation but it is only the meta-linked molecule which prevents the charge recombination, indicating its strong potential for use in solar cell applications. This topic is discussed further in Chapter 4 where fluorene oligomers are used as luminescent bridges between donor and acceptor moieties.

A similar strategy was exploited by Tang *et al*. who presented a series of star-shaped donor-π-acceptor *meta* conjugated systems based on triphenylamine (TPA) as the donor unit and 2-dicyanomethylen-3-cyano-4,5,5-trimethyl-2,5-dihydrofuran (TCF) as the acceptor unit (e.g. **20**, Figure 1.13).[20] The broad absorption profiles and intramolecular energy transfer properties of the materials gives them potential for application in solar cells. Tuning of the absorption properties of the materials was demonstrated by varying the ratio of TPA to TCF and the length of the linker unit.[20] However, no photovoltaic devices were reported.

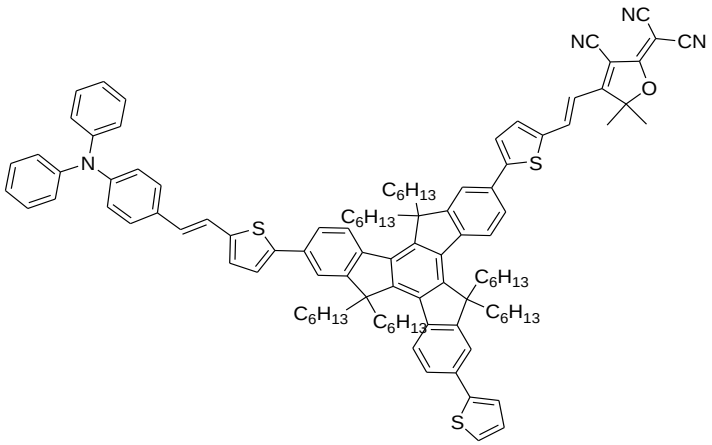

20

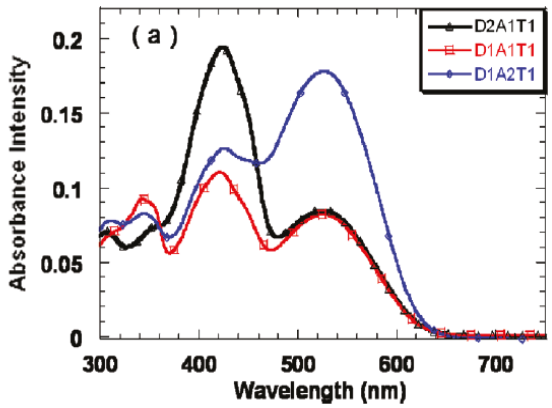

Figure 1.13 – Structure of a star-shaped donor-π-acceptor system and absorption spectra of this compound (= D1A1T1) and analogous compounds in THF solution (10^{-6} M)

For solution-processable polymer solar cells, the bulk heterojunction (BHJ) device is the most common device architecture employed as this ensures the maximum internal donor-acceptor interfacial area for efficient charge separation.[21] These devices require a *p*-type conjugated polymer blended with an *n*-type material (usually the C_{60} derivative, PCBM, **21** Figure 1.14). The main requirements for the polymer are that it has sufficient solubility in order to be solution processable, has a low band gap, broad absorption spectrum and high hole mobility.[21]

There have been numerous D-A systems used in BHJ solar cells blended with PCBM. Recent examples include the phthalimide-based D-A co-polymer synthesised by the Jenekhe group

(**22**, Figure 1.15), which was blended with PCBM and exhibited high hole mobility values of 4.0 x 10^{-4} cm^2 V^{-1} s^{-1}, with device power conversion efficiencies of a moderately high 2.0%, suggesting these materials are promising new candidates for further investigation.[22] Since those reports, the Jenekhe group have presented a series of thieno[3,4-*c*]pyrolle-4,6-dione (TPD)-based D-A co-polymers (e.g. **23**, Figure 1.15) for use in BHJ solar cells.[23] Hole mobilities of up to 8.9 x 10^{-3} cm^2 V^{-1} s^{-1} were observed for this polymer and BHJ devices fabricated, blended with PCBM, achieved power conversion efficiencies of 3.06%, higher than that of the phthalimide-based co-polymer.[23] Dithienopyrrole-quinoxaline/pyridopyrazine D-A co-polymers have also recently been reported by Jenekhe and co-workers (e.g. **24**, Figure 1.15).[24] A series of co-polymers was presented, varying the acceptor unit, but, BHJ devices blended with PCBM exhibited lower power conversion efficiencies of up to 1.4%.[24]

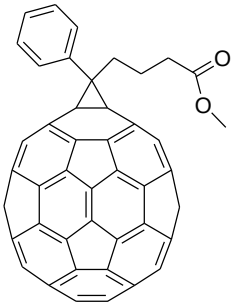

21

Figure 1.14 – Structure of PCBM

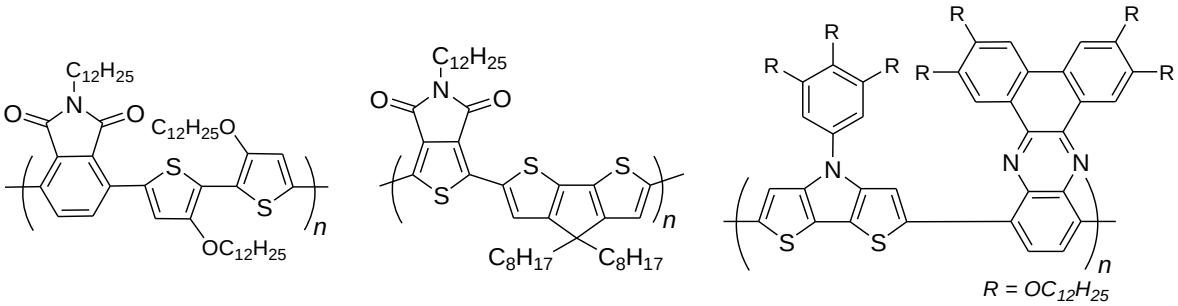

22 **23** **24**

Figure 1.15 –Structures of three D-A co-polymers

As well as for BHJ solar cells, other recent work from the Jenekhe group has included the synthesis of materials for ambipolar OFETs, such as the naphthalenebiscarboximide-bithiophene co-polymer (**25**, Figure 1.16).[25] High electron and hole mobilities (0.04 cm^2 V^{-1} s^{-1} and 0.003 cm^2 V^{-1} s^{-1}, respectively) were reported in devices fabricated from the material.[25] Previous work on the development of D-A co-polymers with high charge carrier mobilities led to the synthesis of a series of pyridopyrazine-based co-polymers (**26**, Figure 1.16).[26] Whilst these materials did show ambipolar redox behaviour and broad absorption bands, the charge

carrier mobilities were much lower (10^{-4}–10^{-3} cm^2 V^{-1} s^{-1} for holes),[26] hence co-polymer **25** is a much better candidate for use in ambipolar OFETs than **26**.

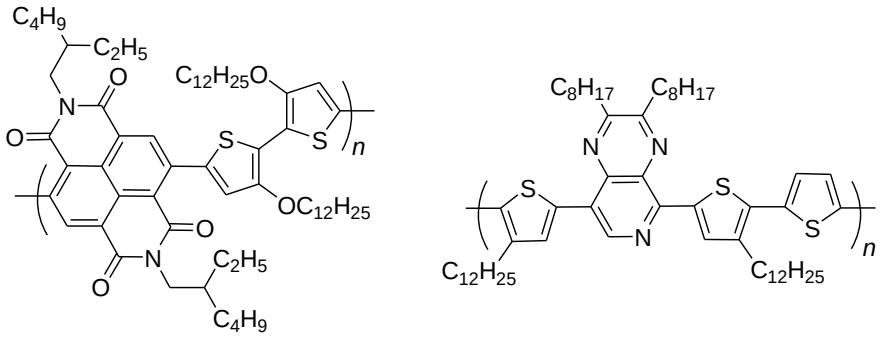

25 **26**

Figure 1.16 – Structures of two D-A co-polymers

These numerous reports highlight the utility of donor-acceptor systems for optoelectronic applications as well as the wide variety of structural variants which are accessible by changing the donor and acceptor units as well as the linkers and conjugation patterns between the two moieties. The following sections focus on the use of fluorene (**F**) and its analogues, including dibenzothiophene-*S*,*S*-dioxide (**S**) (**1**, **2**, Figure 1.2), in ambipolar systems.

1.3 Fluorene in ambipolar systems

1.3.1 Introduction to fluorene

Fluorene (**F**) is a polycyclic aromatic molecule which emits intense violet fluorescence. **F** has been used in a variety of optoelectronic applications, but its most widespread use has been in OLEDs, mainly due to its utility as a blue light-emitter. The facile functionalisation of fluorenes in the 2,7- positions (**27** shows atom numbering) allows for couplings to a wide variety of other moieties in order to modify charge transport properties and/or the emission colour of the materials. Substitution of **F** in the 3,6-positions is also possible, although much less widely investigated due to the more complex synthetic procedures required. Investigations into reactions of **F** in these positions is discussed further in Chapter 6. **F** can also be easily modified at the C_9 position due to the acidity of the bridgehead hydrogen atoms which allows solubility and aggregation properties to be modified. Common substituents in this position include alkyl chains, either branched or linear (e.g. in the commonly used poly-9,9-di-*n*-octylfluorene, PFO) and aryl groups. Schemes 1.1 (a) to (c) show the syntheses of the most common substitution patterns of **F** monomers.

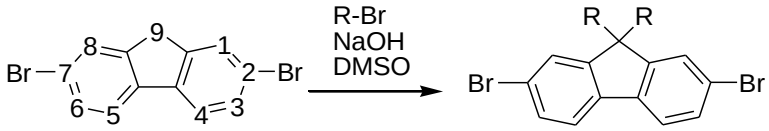

27 **28**

Scheme 1.1(a) – Example synthesis of dialkyl-substituted fluorenes

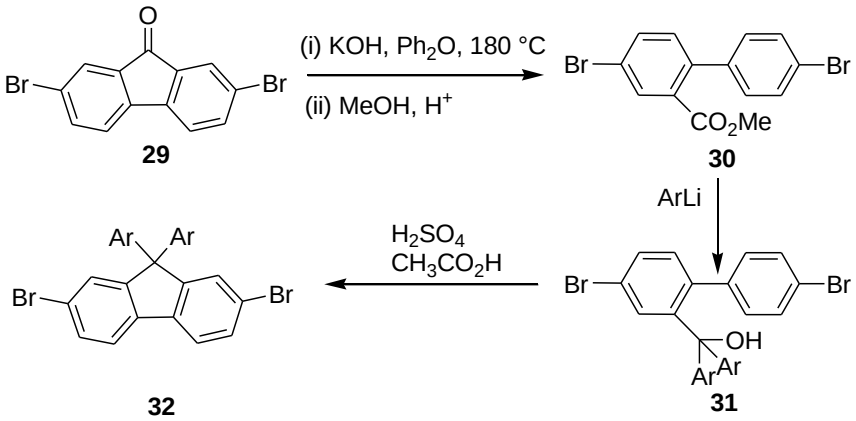

29 **30** **31** **32**

Scheme 1.1(b) – Example synthesis of diaryl-substituted fluorenes

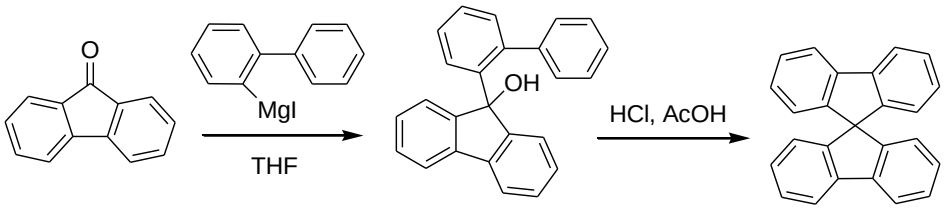

33 **34** **35**

Scheme 1.1(c) – Example synthesis of spiro fluorenes

The charge transport capability of polyfluorenes, i.e. electron-transporting vs. hole-transporting, has been widely debated. In reference to the use of semiconducting polymers for field effect transistors, the Friend group reported the hole mobility of PFO as 3 x 10^{-4} cm^2 V^{-1} s^{-1} and the electron mobility as an order of magnitude higher at 5 x 10^{-3} cm^2 V^{-1} s^{-1}.[27] While it is a widely held view that PFO has a higher electron mobility than hole mobility, once electrons move through a device (e.g. an OFET or an OLED) they can begin to congregate at the hole injection layer, where they build up, thus allowing an excess of holes to then move through the device. This imbalance of charge mobility can have detrimental effects on the devices. **F** has thus been incorporated into ambipolar systems in order to improve charge injection and migration, whilst maintaining efficient blue light emission. **F** has been used as the "donor" unit in ambipolar systems, the "acceptor" unit and as a luminescent linker between donor and acceptor; examples of these systems are discussed in subsequent chapters.

In order to incorporate **F** into ambipolar systems (oligomers or polymers), various cross-coupling pathways are utilised, namely Yamamoto coupling[28] and Suzuki-Miyaura (S-M) coupling[29] (Schemes 1.2 (a) and (b)).

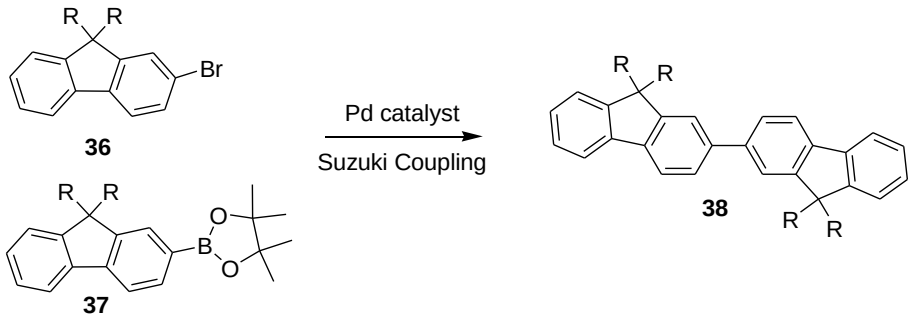

Scheme 1.2(a) – Suzuki-Miyaura coupling of fluorene units

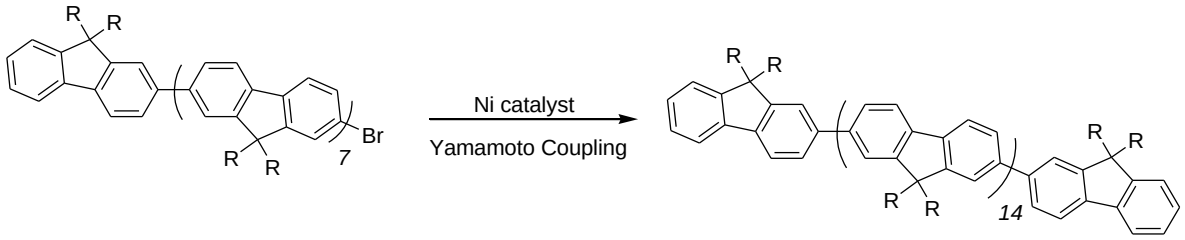

39 **40**

Scheme 1.2(b) – Yamamoto coupling of fluorene units

Yamamoto couplings involve stoichiometric amounts of expensive nickel and generally give low molecular weight polymers. However, the synthesis is often less complex than that of S-M couplings as only one starting material is required (e.g. the bromo-substituted **F**, **39**). S-M is the method favoured by many groups (including the Bryce group) due to the catalytic amounts of metal (palladium) needed and the high molecular weight polymers which can be achieved. However, the palladium catalysts can be expensive and it can sometimes be difficult to purify the boronic acids/esters which are required, as well as the halogenated starting materials.

One of the key problems associated with the use of dialkyl-substituted PFs (e.g. the commonly used PFO) in devices is that a low energy green emission band tends to appear in the spectrum during device usage which degrades the emission colour from blue to green. It was previously reported that this low-energy green emission band was due to aggregate and/or excimer formation.[30] However, it has subsequently been reported that it is in fact due to the presence of fluorenone units in the PF backbone, which is now the widely held view.[31] It is proposed that these "keto defects" act as low-energy guest emitters, effectively trapping singlet excitons which are created on the PF backbone.[31] The mechanism proposed for the formation of the

defects is shown in Scheme 1.3, starting from any mono-alkylated fluorene units present from incomplete alkylation reactions.[31]

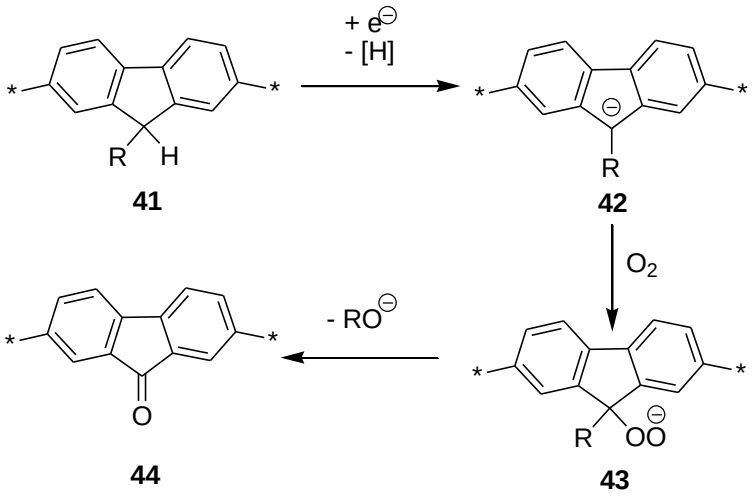

Scheme 1.3 – Proposed mechanism for the formation of fluorenone units in the PF chain

This mechanism was elucidated based on the Yamamoto polymerisation reaction, whereby the authors reported that the active nickel(0) species used as a catalyst would reduce any monoalkylated fluorene units to aromatic fluorenyl anions. These fluorenyl anions could then form hydroperoxide anions and rearrange to give the fluorenone units.[31] The reaction using Suzuki-Miyaura (S-M) conditions can be assumed to occur via a similar pathway. Indeed work from Liu *et al*. found that the commonly used S-M catalyst tetrakis(triphenylphosphine) palladium(0) could also effectively catalyse the oxidation of monoalkylated fluorene into fluorenone.[32] The oxidation of fluorenyl anions to fluorenones in air is a known reaction,[33] although full details of the oxidation mechanism are yet to be completely understood. It has also been proposed that keto defect sites can be formed directly from dialkylated fluorene units during device performance, as a result of photo- or electro-oxidative degradation.[31] It has been shown that as little as 0.06 mol% of monoalkylated fluorene within the backbone can lead to the unwanted green emission dominating the spectrum.[34]

A synthetic strategy to produce defect-free fluorene monomers was reported by Cho *et al*. using the cyclisation of a tertiary alcohol to guarantee the incorporation of both alkyl substituents in good yields (Scheme 1.4).[34] These fully dialkylated monomers did not exhibit any green emission when incorporated into OLEDs, thus providing evidence for the origin of the keto defect sites.

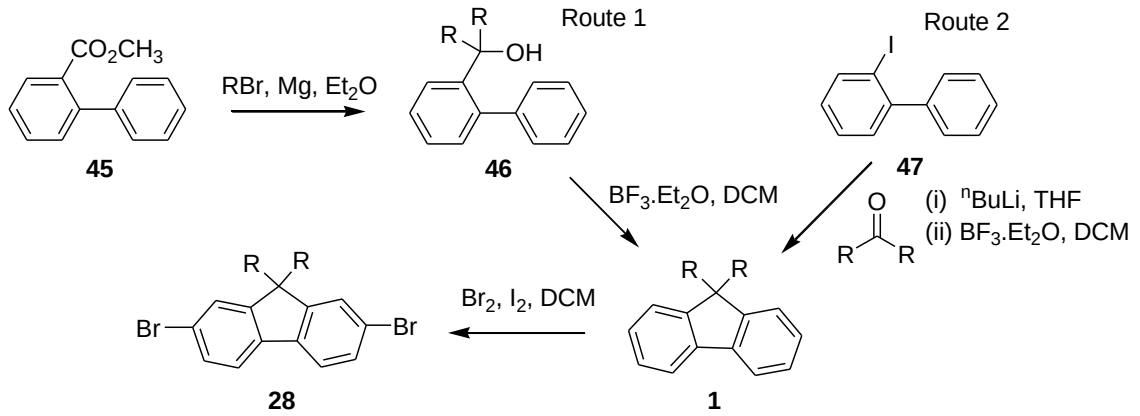

Scheme 1.4 – Synthesis of defect free F monomers

It is possible that the origin of defect sites in PFs is not exclusively from the presence of fluorenone units. Kappaun *et al*. reported that while ketonic defects were largely responsible for the unwanted green emission in fluorene-based OLEDs, these defects could not explain all the features in the EL spectra.[35] It was established that the presence of hydroxyl end groups in the material also contributed to the appearance of the green emission band. It was thought that these end groups could be formed from the protiodeboronation of the boronic acids or esters (**48**) used in S-M coupling reactions which could then be deprotonated by the calcium electrode within a device (**50**, Scheme 1.5).[35] It was therefore concluded that for defect-free PF materials to be synthesised, not only ketonic defects, but also the formation of hydroxyl end groups must be avoided.[35]

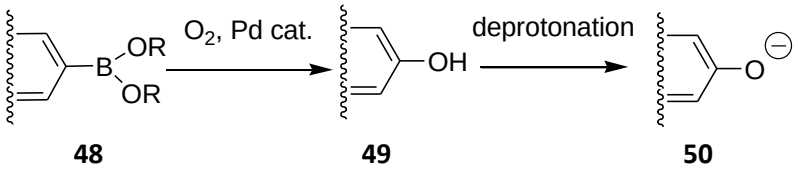

Scheme 1.5 – Synthesis of hydroxyl end group defects

The synthesis of defect-free alkyl substituted PFs remains a current research topic. An alternative approach to avoiding fluorenone formation is to synthesise aryl or spiro substituted PFs (Schemes 1.2 (b), (c)). Aryl substituted PFs avoid the possibility of fluorenone formation as no bridgehead hydrogen atoms are present during the synthesis and the bulky aryl groups can also help to prevent excimer formation; however, many have solubility problems. Spiro-substituted PFs have been widely investigated for OLEDs as they have been reported to be stable blue emitters and their structural rigidity increases thermal stability and glass transition temperatures.[36] While these classes of compounds are interesting and do have potential for OLED applications, alkyl substituted PFs are more widely investigated in academia due to the need for fewer synthetic steps from relatively cheap starting materials. Chapter 5 details

further investigations into charge migration to keto defect sites in PFO-based co-polymers in order to better understand the charge transport processes occurring in these systems.

As mentioned above, **F** has been incorporated into a number of different ambipolar systems, including the addition of electron accepting and/or electron donating moieties and efforts towards these systems are now discussed.

1.3.2 Addition of hole transport units to fluorene

As previously mentioned there is an imbalance of charge mobilities in PFs. The ionization potential for PF is 5.8 eV, thus there can be a large energy barrier to hole injection (the work function of the commonly used anode, indium tin oxide (ITO) is ~ 5.0 eV). Fluorene monomers are therefore often functionalised with hole transporting (i.e. electron donor) units such as arylamines and carbazoles. In these cases ambipolar systems are created where **F** is acting more as an electron acceptor than a donor.

The group of Ullrich Scherf reported the synthesis of a PF end-capped with TPA moieties (**51**, Figure 1.17) which when incorporated into OLEDs gave devices with performances an order of magnitude higher than those based on uncapped PF.[37]

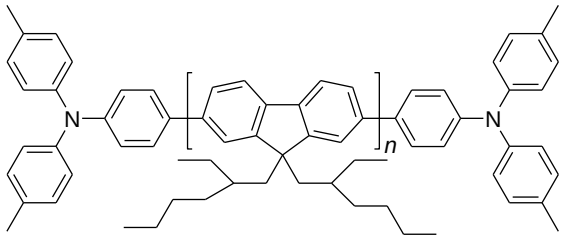

51

Figure 1.17 – Structure of PF end-capped with TPA moieties

TPA units have also been incorporated at the C_9 position of PFs (**52**, Figure 1.15) to increase the hole transporting properties of PFs.[38] The incorporation of bulky substituents in this position also helps to suppress excimer/aggregate formation in the materials.

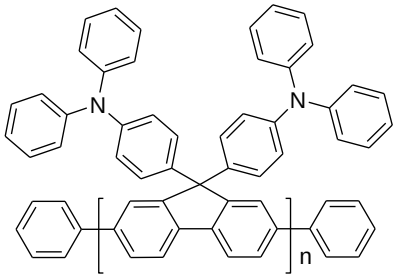

52

Figure 1.18 – Structure of PF functionalised with TPA moieties at the C_9 position

Alternating co-polymers of the C_9 functionalised **F** monomer with the "standard" dialkyl-substituted **F** monomer (**53**, Figure 1.19) show good morphological and thermal stability as well as improved hole injection properties and reduction of defect/aggregate emission.[39] The solid state quantum yield for **53** was reported as 55%, higher than that of standard PFO.[39] However, this did not translate to device characteristics as OLEDs based on the co-polymer showed low EQEs of 0.49% and a low energy emission band at 630 – 650 nm appeared during device operation (Figure 1.19), attributed to emission from TPA excimers.[39]

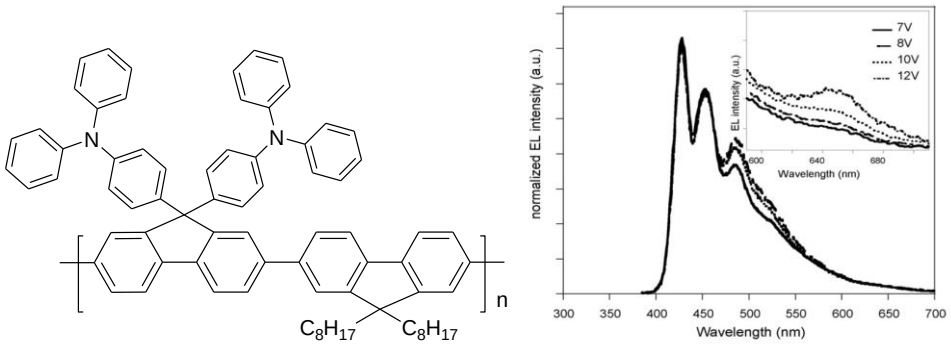

53

Figure 1.19 – Structure of TPA functionalised co-polymer and time evolution of EL spectrum of device (ITO/PEDOT:PSS/polymer/Ca/Al) at *t* = 0 min (solid line), 180 min (dotted line), 300 min (dashed line) at constant V. Inset shows V dependence of low energy emission band[39]

The use of TPA was further developed by Jiang *et al*. who designed a novel aryl-bridged TPA derivative, co-polymerising this monomer with dihexylfluorene (**54**, Figure 1.20).[40] The optical properties of this polymer were investigated and the results compared with a co-polymer of TPA and dihexylfluorene (**55**, Figure 1.20). It was reported that the rigidity of the novel bridged TPA monomer improved the thermal and morphological stability of the polymer, whilst still lowering the barrier to hole injection (compared with PFO).[40] OLEDs fabricated from **54** outperformed those based on **55** under similar conditions, indicating the potential of this new monomer to replace TPA as a hole transport unit.[40]

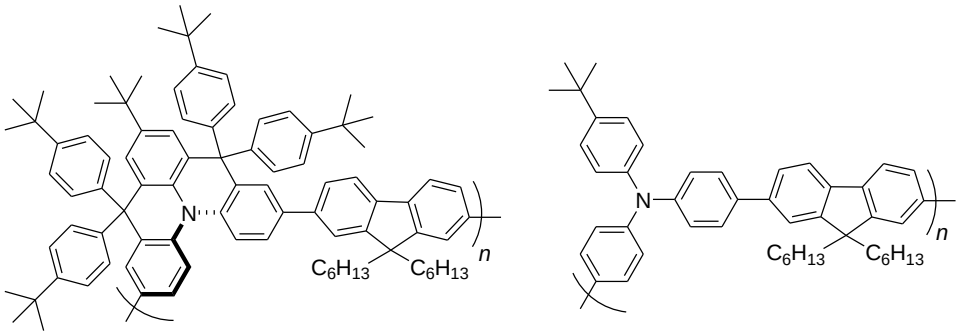

54 **55**

Figure 1.20 – Structures of TPA-based co-polymers

TPA has also been incorporated in a non-conjugated architecture with fluorene, for example in the work of Zhang *et al*. who recently reported the synthesis and optical properties of two 3D monodisperse oligofluorenes with non-conjugated TPA-based cores (e.g. **56**, Figure 1.21(a)).[41] The 3D structure effectively reduced the ability of the fluorenes to crystallise, thus increasing the morphological stability of the material. The oligomers emit deep blue fluorescence with high efficiencies even in thin films (67% and 86%).[41] It was reported that the introduction of the TPA units promoted hole injection in the materials whilst still maintaining the blue emission of fluorene (presumably due to the non-conjugation of the TPA units) and also not sacrificing the electron-injection ability of the materials.[41] OLEDs based on these materials exhibited deep blue electroluminescence at low turn-on voltages, unfortunately, the appearance of a low energy emission band at ~ 580 nm was also observed, which increased in intensity with increased applied voltage (Figure 1.21(b)).[41]

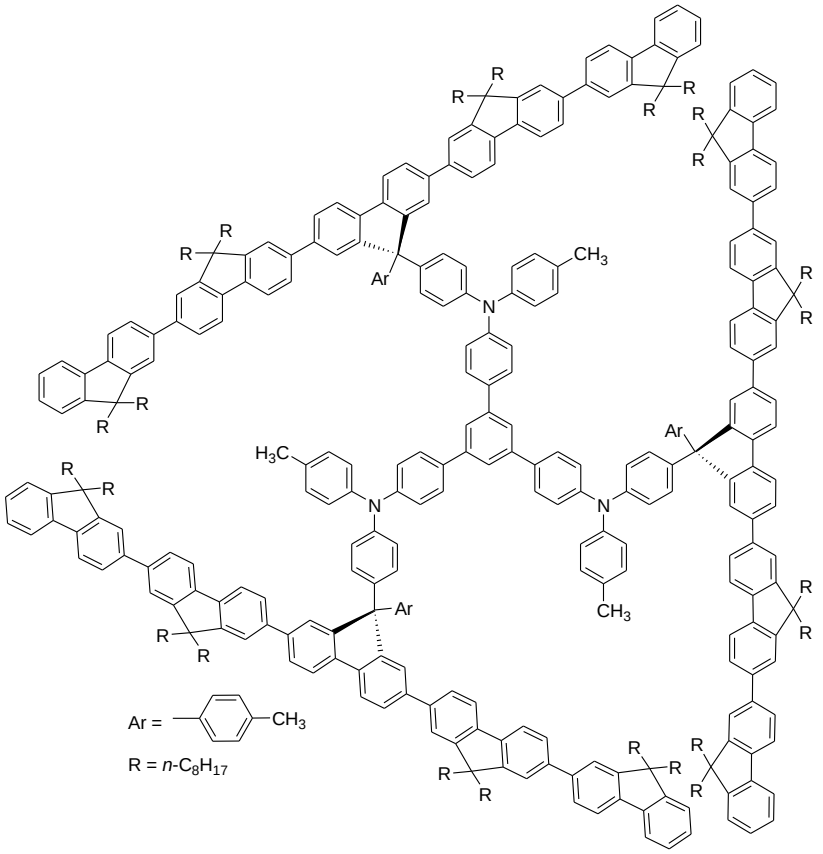

56

Figure 1.21(a) – An example structure of a 3D oligofluorene with a TPA-based core

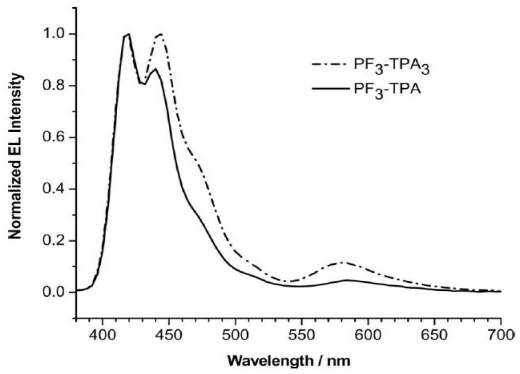

Figure 1.21(b) – EL spectra of oligomers at 5 V (compound 53 = PF_3-TPA_3); device structures ITO/PEDOT:PSS/oligomer/TPBI/LiF/Al[41]

Carbazole has also been used as a hole transporting moiety within **F**-based materials. For example, Li *et al*. reported the synthesis and optical properties of a series of **F**/carbazole co-polymers (**57**, Figure 1.22) for use in blue-emitting OLEDs.[42] The incorporation of the carbazole moiety (linked through the 3,6-positions) suppresses the tendency of PFs to crystallise which improved device performances and raised the HOMO level of the materials, thereby facilitating hole injection.[42] The co-polymers showed similar EL spectra to that of PFO, but with decreased photoluminescence quantum yields.[42] The use of arylamine and carbazole as electron donors in ambipolar systems is discussed further in chapter 3 with the synthesis of novel ambipolar systems.

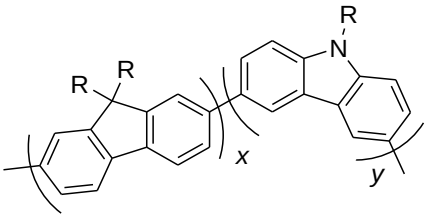

57

Figure 1.22 – Structure of F/carbazole co-polymers

1.3.3 Addition of electron transport units to fluorene

As well as being functionalised with hole transporting moieties, **F** has also been covalently bound to electron acceptor moieties in order to improve electron transport through the materials. Zhu *et al*. reported a series of co-polymers of **F** with increasing amounts of dibenzo[*a*,*c*]phenazine (**58**, Figure 1.23).[43] The phenazine unit was chosen due to its strong electron accepting abilities compared with other commonly used acceptors such as quinoxaline and quinoline.[43] Co-polymers incorporating 2, 5, 10, 15 and 20% of the acceptor unit were synthesised and OLEDs fabricated based on these polymers. With the exception of the 20% co-polymer, the devices showed superior performances compared with devices based

on PFO.[43] The 2% co-polymer exhibited the best device performance with a two-fold increase in device brightness and efficiencies compared to the homo-polymer, without compromising the blue emission colour expected from PFO (Figure 1.23).[43] These results again stress the need for balanced charge transport properties within devices.

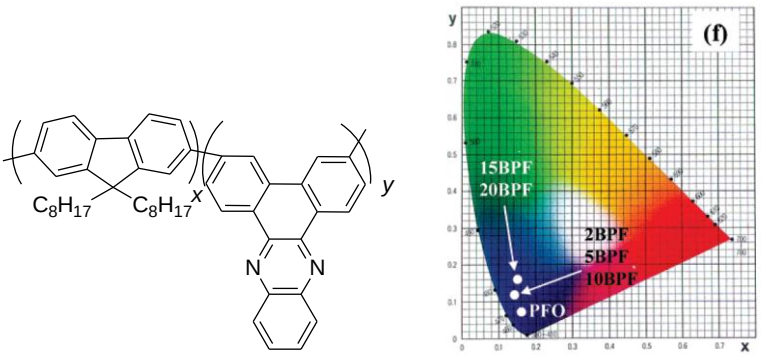

58

Figure 1.23 – Structure of F/phenazine co-polymers (*y* = 2 – 20 mol%) and CIE diagram showing deep blue colour of devices operating at maximum efficiency, compared with PFO[43]

The bisphenazine unit has also been used with **F** as a strong electron accepting unit due to the two pyrazine rings in its molecular structure. Co-polymers were synthesised by Wang *et al*. with varying amounts of bisphenazine (1 – 20%) incorporated into PFO backbones (**59**, Figure 1.24).[44] The LUMO levels of the co-polymers were reported to be - 3.06 eV, lower than that of PFO (- 2.65 eV) indicating the benefit of the bisphenazine as an electron transport unit.[44] In contrast to the blue fluorescence emission observed in the **F**/phenazine co-polymers, the emission in the **F**/bisphenazine co-polymers is more green-yellow in colour, in both the photoluminescence and electroluminescence spectra. This difference in emission colour is also evidence of the stronger electron accepting nature of bisphenazine compared with phenazine; the stronger the electron acceptor, the more ICT is observed which generally leads to a more red-shifted emission band. These results indicate the delicate balance that is required between charge carrier mobilities and device characteristics when choosing donor and acceptor units for optoelectronic systems.

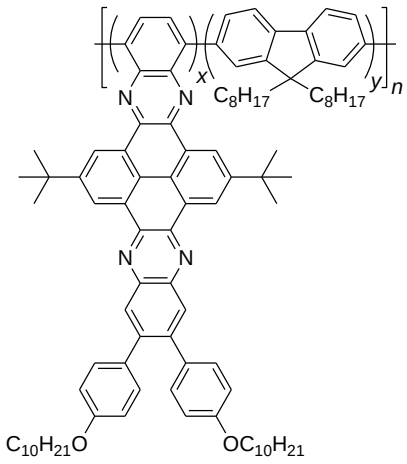

59

Figure 1.24 – Structure of F/bisphenazine co-polymers

Zou *et al*. reported the synthesis and optical properties of star-shaped donor-π-acceptor molecules with a triazine acceptor and donors including arylamine, carbazole and fluorene (e.g. **60**, **61**, Figure 1.25).[45] The compounds all show reversible or quasi-reversible redox properties and strong ICT behaviour as a result of the D-A interactions. The molecules also have large two photon absorption cross-sections. Two photon absorption is when the simultaneous absorption of two low energy photons allows a molecule to reach a high energy excited state. Systems with large two photon absorption cross-sections are suitable for many applications such as two-photon fluorescence excitation microscopy, 3D optical data storage and photodynamic therapy.[45] By increasing the donor strength (fluorene to carbazole to arylamine) the ICT and two photon absorption properties could be tuned.[45]

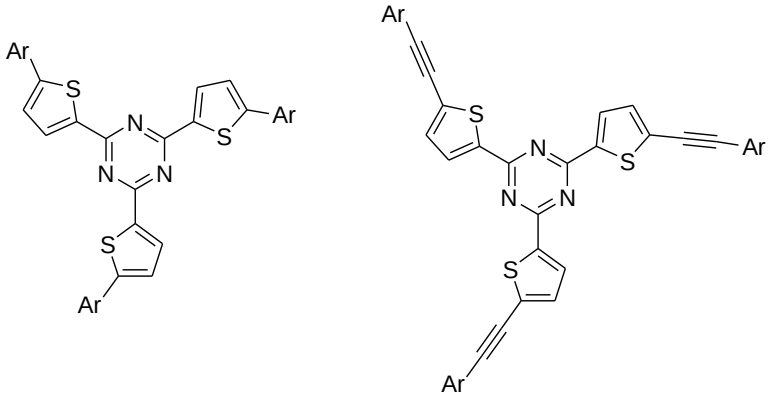

60 **61**

Figure 1.25 – Structure of star-shaped D-π-A molecules (Ar = triphenylamine, carbazole, fluorene)

For many optoelectronic applications, such as OFETs and solar cells, semiconducting, conjugated polymers are preferred over oligomers due to their solution processability.

Fluorene has been a widely used monomer unit in these types of polymers, particularly when co-polymerised with electron rich thiophene and electron deficient benzothiadiazole units. Chen *et al*. reported the synthesis of fluorene-based co-polymer poly(4-(3,4'-dihexyl-2,2'-bithiophen-5-yl)-7-(5'-(9,9-dioctyl-9*H*-fluoren-2-yl)-3,4'-dihexyl-2,2'bithiophen-5-yl)benzo[*c*][1,2,5]-thiadiazole) (**63**) compared to the analogous polymer which is commonly used in solar cell research, with two fewer thiophene units, poly((9,9-dioctylfluorene)-2,7-diyl-alt-[4,7-bis(3-hexylthien-5-yl)-2,1,3-benzothiadiazole]-2',2''-diyl) (**62**) (Figure 1.26).[46] The addition of the extra thiophene units improves charge injection and enhances ambipolar charge transport in field effect transistors. Hole mobilities of 5 x 10^{-2} cm^2 V^{-1} s^{-1} and electron mobilities of 4 x 10^{-3} cm^2 V^{-1} s^{-1} were reported for **63**.[46] The polymer was also tested in a solar cell which showed promising initial device results.

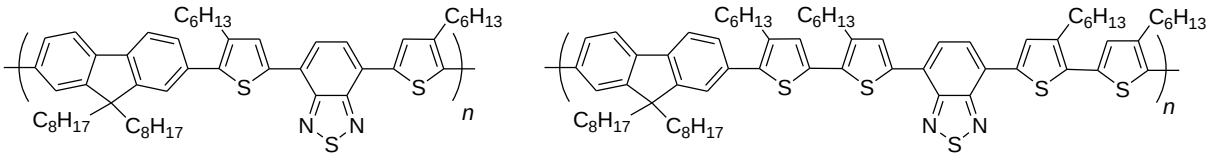

62 **63**

Figure 1.26 – Structures of conjugated co-polymers for solar cell applications

A co-polymer of fluorene with bithiophene (**64**) and a co-polymer of fluorene with 2,1,3-benzothiadiazole (**65**) were synthesised as hole- and electron-transport materials, respectively (Figure 1.27). However, once incorporated into OFETs both polymers showed ambipolar characteristics, i.e. were capable of transporting both electrons and holes with similar hole and electron field-effect mobilities (~ 10^{-3} cm^2 V^{-1} s^{-1}).[47] This was attributed to the fact that the work function of the ITO electrode is approximately intermediate between the HOMO and LUMO levels of the fluorene derivatives.[47] These results indicate the versatility of fluorene as a monomer in these applications in terms of charge carrier ability. Light-emitting OFETs based on **64** exhibited yellow-green emission and those based on **65** exhibited yellow EL emission.[47]

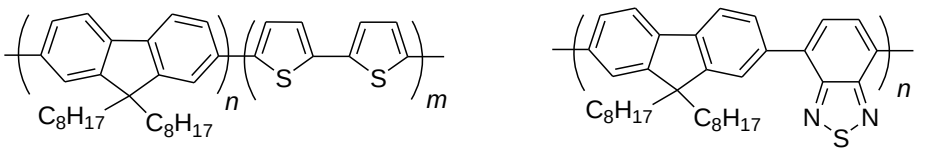

64 **65**

Figure 1.27 – Structures of hole transporting and electron transporting co-polymers

An effective solution to designing a low band gap polymer capable for use in BHJ solar cells blended with PCBM is to take advantage of ICT effects by incorporating both electron donor and electron acceptor segments, such as in the co-polymers shown in Figures 1.26 and 1.27. Increased ICT interactions along a conjugated polymer backbone will lead to a red-shift in emission and therefore a reduction in the band gap. Extensions of these co-polymers for solar cells includes work from Lee *et al*. who investigated the effect of changing the central acceptor unit from 2,1,3-benzothiadiazole, (Figure 1.28).[48] The co-polymers were blended with PCBM in BHJ solar cell devices. The power conversion efficiencies of the photovoltaic cells decreased in the order **67** > **66** > **68**, indicating that 2,1,3-benzothiadiazole is the optimum acceptor in these systems.[48]

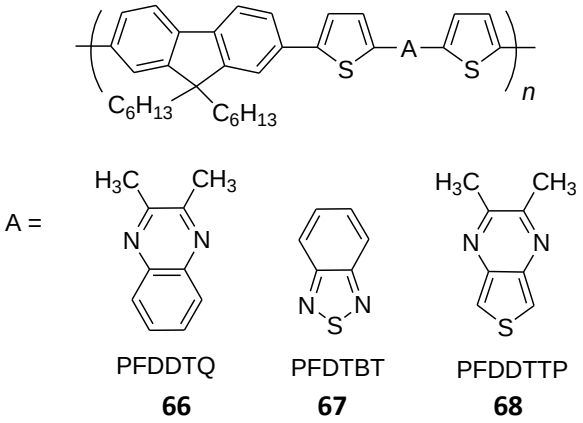

Figure 1.28 – Structures of co-polymers for solar cells

In order to facilitate electron delocalisation along the polymer chains (thus decreasing the band gap further and aiding charge transport), Wu *et al*. recently presented a polymer system in which the thiophene units are fused onto the fluorene units (**69**, Figure 1.29).[21] Alkyl and aryl groups at the C_9 positions of the fluorene units allow solubility and aggregation properties to be modified. The polymer shows strong ICT behaviour and both *p*- and *n*-type behaviour in CV studies, indicating the ambipolar nature of the material and the good charge transport properties.[21] An analogous carbazole-based polymer was also synthesised showing the same characteristics, with stronger ICT behaviour reported due to the stronger donating ability of carbazole compared with fluorene.[21] Both polymers exhibited high hole mobilities (~ 10^{-4} cm^2 V^{-1} s^{-1}) and preliminary BHJ photovoltaic devices showed strong performances with power conversion efficiencies of 2.8% (fluorene) and 3.7% (carbazole).[21]

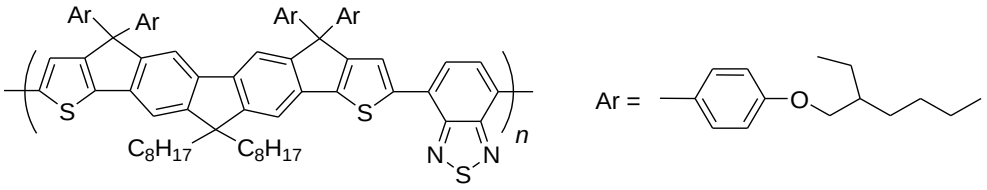

69

Figure 1.29 – Structure of fused fluorene co-polymer

1.3.4 Fluorenes functionalised with hole- and electron-transport units

As discussed above, fluorene is a relatively weak donor unit and although it is capable of transporting electrons reasonably well, it is not a strong electron acceptor. However, **F** does have a number of favourable optoelectronic characteristics such as its blue light emission, conjugated structure, solubility and ease of structural modification. Therefore, **F** has also been used in conjunction with stronger electron donating and accepting moieties in ambipolar systems for a number of different applications.

Wu and Feng and co-workers utilised the blue-emitting properties of fluorene to synthesise a series of donor-**F**-acceptor oligomers capable of two- and three-photon excited photoluminescence and lasing in the blue region of the spectrum.[49,50] As discussed previously, molecules with high two photon absorption cross-sections have many potential applications and three-photon absorption may be an even more advantageous property, e.g. for frequency up-converted lasing. To achieve a large two photon absorption cross-section it is necessary to have a highly polarisable D-A chromophore, however, it is not guaranteed that these molecules will also exhibit useful three photon absorption properties.[49] To exhibit multi-photon absorption up-converted lasing, molecules must have high fluorescence quantum yields, large multi-photon absorption cross-sections and low fluorescence re-absorption.[49] Wu *et al*. were the first to report three-photon induced up-converted pure blue lasing from an organic system, using a series of diphenylamine and 1,2,4-triazole end-capped oligofluorenes (**70**, Figure 1.30).[49,50]

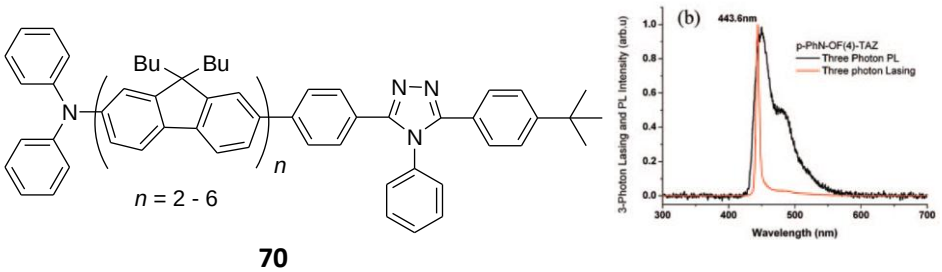

70

Figure 1.30 – Structure of donor-oligofluorene-acceptor system and the three-photon up-conversion photoluminescence and lasing spectra for (*n* =4)[49]

Highly efficient three-photon excited deep blue photoluminescence and lasing was reported from these oligofluorene-based molecules. In the initial series of compounds (*n*=2 to *n*=4) it was determined that the three-photon absorption cross-section and lasing efficiency increased with oligofluorene length, without affecting the lasing emission wavelength.[49] This series was therefore extended to include pentafluorenes (*n*=5) and sexifluorenes (*n*=6) (**70**, Figure 1.30), as well as a set of similar molecules containing oligothienylfluorenes (**71**, Figure 1.31).[50] The absorption and emission maxima of the extended oligofluorenes (*n* = 5, 6) reached a saturation limit, implying there is an effective conjugation length for optimum three photon absorption.[50] The introduction of the thienyl unit led to a significant increase in the three photon absorption cross-section attributed to enhanced electron delocalisation and ICT processes.[50] These results indicate the utility of **F** in D-A systems for photonic applications such as lasing.

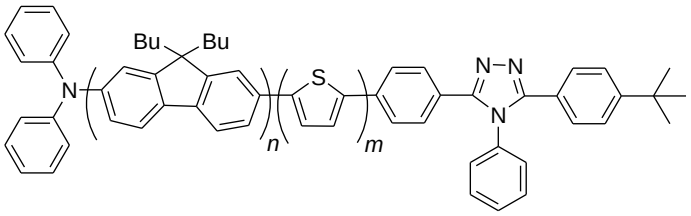

71

Figure 1.31 – Structure of donor-oligothienylfluorene-acceptor molecules

Fluorene has also been functionalised with additional donor and acceptor moieties for OPV applications, such as the cyanofluorene-TPA co-polymers reported by Lin *et al*. (**72**, Figure 1.32).[51] **F** was chosen due to its high photo- and electro-luminescence efficiencies and good solubility. The functionalisation of **F** with cyano groups increases the electron affinity of the materials and the incorporation of TPA into the main polymer backbone acts as an electron donor or hole transporter.[51] The co-polymers exhibit greater thermal stability than PFO attributed to the presence of the TPA units.[51] For D-A materials to have the potential for use in solar cell applications, the charge separation process must be rapid, i.e. transfer of electrons from donor to acceptor, but the rate of recombination of electrons and holes must be slow, as this would mean energy would be lost to non-radiative (or radiative) transitions instead of the charges being able to be used to store energy i.e. create a current in the device. Investigations into the cyanofluorene-TPA materials determined that the co-polymers exhibited fast photoinduced electron transfer (~ 10^{11} s^{-1}) from donor to acceptor, with the rate of charge recombination being much slower so that long lived radical ion pairs (CN**F**$^{\bullet-}$ – TPA$^{\bullet+}$) form.[51]

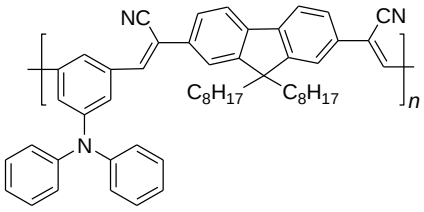

72

Figure 1.32 – Structure of cyanofluorene-TPA co-polymer

The blue emission properties of fluorene have also been exploited in donor-acceptor systems for OLEDs. Wu *et al*. presented an efficient green-emitting polymer which incorporated low-bandgap 2,1,3-benzothiadiazole, electron donating TPA groups and electron withdrawing oxadiazole groups within a polyfluorene backbone (**73**, Figure 1.33).[52] Devices were presented with a high maximum brightness of 10,232 cd m^{-2}, luminance efficiency of 8.9 cd A^{-1}, but a high drive voltage of 19 V.[52]

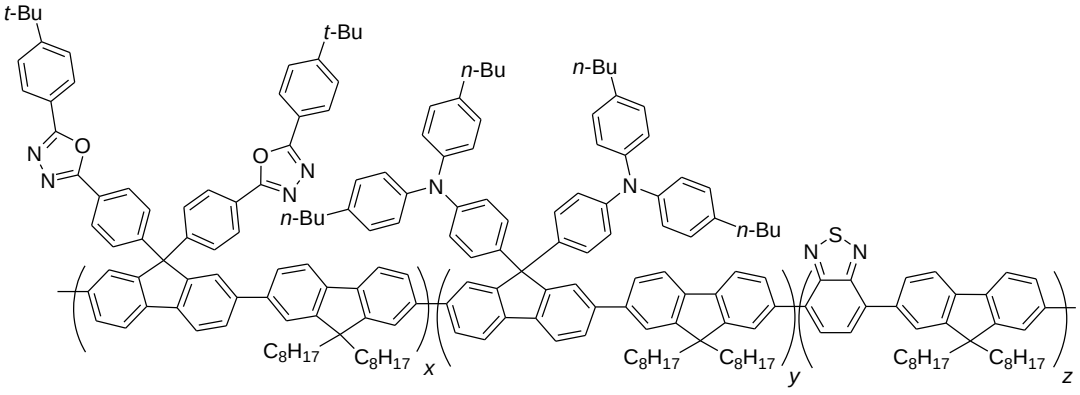

73

Figure 1.33 – Structure of green-emitting ambipolar fluorene co-polymer

Similar ambipolar co-polymers based on **F** have recently been reported by Wang *et al*. (**74**, **75**, Figure 1.34) consisting of "electron-deficient" main chains with "electron-rich" pendant side groups.[53] The incorporation of the rigid electron deficient 1,2,4-triazoles and the electron rich TPA units enhances the thermal stability of the co-polymers.[53] The co-polymer with **F** and 1,2,4-triazole in its main chain (**74**) emits blue fluorescence in chloroform solution and in thin films, but with low PLQY values (ϕ_f 0.29 and 0.08, respectively); whereas the polymer with the additional **F** and BT units in its backbone (**75**) fluoresces in the green-yellow region of the spectrum with higher PLQYs in solution and film (ϕ_f 0.9 and 0.4, respectively).[53] OLEDs were fabricated from the two co-polymers, but devices based on polymer **74** were reported to be non-emissive and it was proposed that triphenylaminyl radical cations formed during the hole

injection process were quenching the blue EL.[53] Devices based on polymer **75** exhibited green-yellow emission similar to the PL spectrum, implying no such quenching effect occurred in these co-polymers.[53] These results were compared to a previously studied analogue of polymer **75** where the TPA unit is in the main chain of the polymer and the 1,2,4-triazole is the pendant side group. This alters the HOMO-LUMO levels of the system; however, this polymer showed similar device performances, with slightly higher luminance values, but lower device efficiencies.[53]

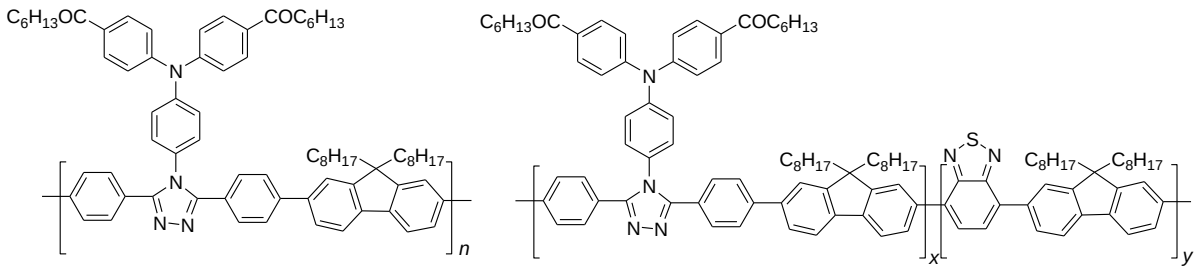

74 **75**

Figure 1.34 – Structures of ambipolar F-based co-polymers

As well as in polymers for OLEDs, **F** has also been used in ambipolar molecules with additional donor and acceptor units, such as the systems reported by the Bryce group incorporating TPA or carbazole hole transport units and oxadiazole electron transport units within both symmetrical and unsymmetrical fluorene-based molecules (e.g. **76**, **77**, Figure 1.35(a)).[54,55] OLEDs fabricated from the ambipolar carbazole analogue (**77**) exhibited higher device performances than the analogous arylamine molecule (**76**), emitting in the deep blue region of the spectrum with a high device efficiency of 4.7% (Figure 1.35(b)).[55] These devices are among the highest performing deep blue molecular OLEDs reported to date, hence the fluorene-based molecules have great potential for further development in this field.[55]

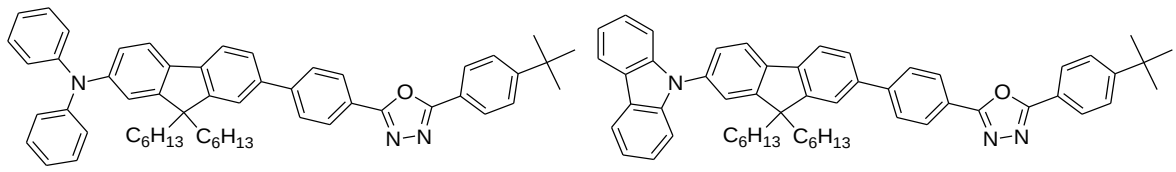

76 **77**

Figure 1.35(a) – Structures of ambipolar fluorene-based molecules

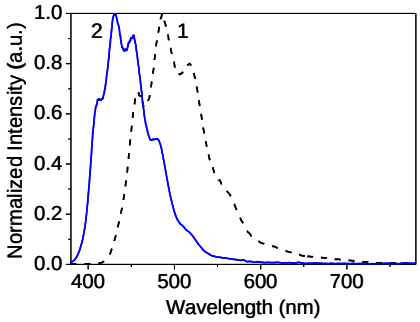

Figure 1.35(b) – EL spectra of devices based on spin-coated layers of 1 (76) and 2 (77)[55]

F has proven its utility in materials for optoelectronic applications with the sheer number of different architectures within which it has been used, the number of different applications its systems have and its versatility in performing different roles within the materials. There is, therefore, still much research interest in extending the use of **F** to other novel ambipolar systems, as well as trying to gain a fuller understanding of the photophysical and charge transport properties of **F**-containing materials; topics which are addressed in the following chapters of this thesis.

1.4 Heterofluorenes for optoelectronic applications

The previous sections have demonstrated the huge research interest generated by fluorene (**F**). It is therefore not surprising that numerous analogues to **F** have been researched in the context of organic materials for optoelectronic applications, for example, where the C_9 carbon atom is replaced by silicon, germanium, phosphorus, sulfur or nitrogen (i.e. to give the hole-transporting unit, carbazole).

The synthesis of 2,7-functionalised dibenzosilole monomers and their incorporation into polymers (**78**, Figure 1.36) via Suzuki cross-couplings was first reported by the Holmes group in 2005.[56] The optical properties of the homo-polymer were found to be directly comparable to PFO, e.g. emission in the blue region of the spectrum. However, the poly(dibenzosilole)s showed higher thermal stability than PFO and there was no evidence of any long wavelength defect emission (i.e. from keto sites).[56,57]

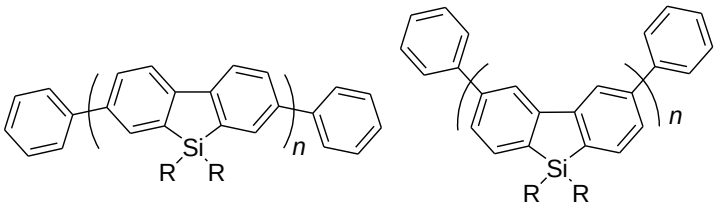

78 **79**

Figure 1.36 – Structures of 2,7- and 3,6- substituted poly(dibenzosilole)s

The Holmes group also reported the synthesis of 3,6-functionalised dibenzosilole monomers and their incorporation into polymers (**79**, Figure 1.36).[58] The short conjugation length of this polymer (due to the 3,6-linkages) means it is well suited to act as a high triplet level host material. The triplet level of the polymer was reported to be 2.55 eV and an OLED fabricated from this polymer doped with a green-emitting iridium complex (Ir(*m*-ppy)$_3$, Figure 1.37) showed only emission from the phosphorescent guest emitter i.e. no back energy transfer to the host at a low turn-on voltage of 4 V.[58]

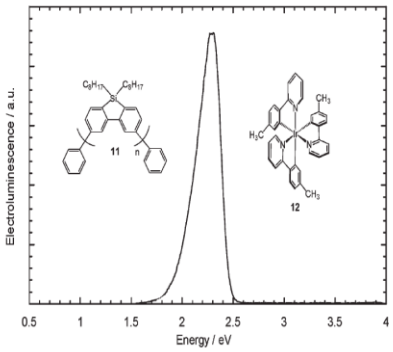

Figure 1.37 – EL spectrum of an OLED based on polymer 79 doped with Ir(*m*-ppy)$_3$ (8 wt.%)

A recent paper from the same group reported a series of conjugated polymers containing either 2,7- or 3,6-functionalised dibenzosilole monomers co-polymerised with either hole-transport units (carbazole and triarylamine) or electron-transport units (oxadiazole and triazole) (example structures, **80** and **81**, Figure 1.38).[59] The 3,6-linked co-polymers showed a blue shift in absorption and emission maxima due to the reduced conjugation through the systems (compared with their 2,7-linked analogues) and accordingly, an increase in their respective energy gaps. OLEDs fabricated from the co-polymers exhibited poor performance (low luminescence intensity) which was primarily attributed to the poor film-forming properties of the polymers due to their low molecular weights.[59] However, an OFET fabricated from co-polymer **81** was demonstrated to exhibit good hole mobility and a high current on/off ratio.[59]

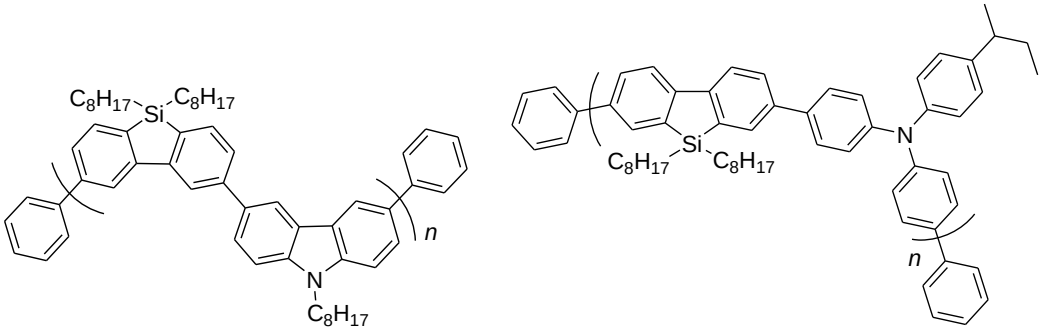

80 **81**

Figure 1.38 – Examples of the dibenzosilole-containing co-polymers recently reported

As with fluorene, dibenzosilole monomers have also been incorporated into donor-acceptor co-polymers for use in organic solar cells blended with PCBM (e.g. Figure 1.39).[60,61] Co-polymer **82** was blended with PCBM to achieve a solar cell with a high power conversion efficiency of up to 5.4%. This material was reported to have a broader absorption spectrum, higher hole mobility and thus better device performance compared to a PFO-based analogous co-polymer.[59] **83** is an example of a silafluorene-based ambipolar co-polymer, synthesised by the Cao group with a hole-transporting arylamine moiety in the backbone and a pendant electron-accepting moiety. Solar cells fabricated from this co-polymer achieved a power conversion efficiency of 3.15% and it was demonstrated that the energy levels and band gap of the materials could be tuned by changing the electron-accepting strength of the side-chain.[60]

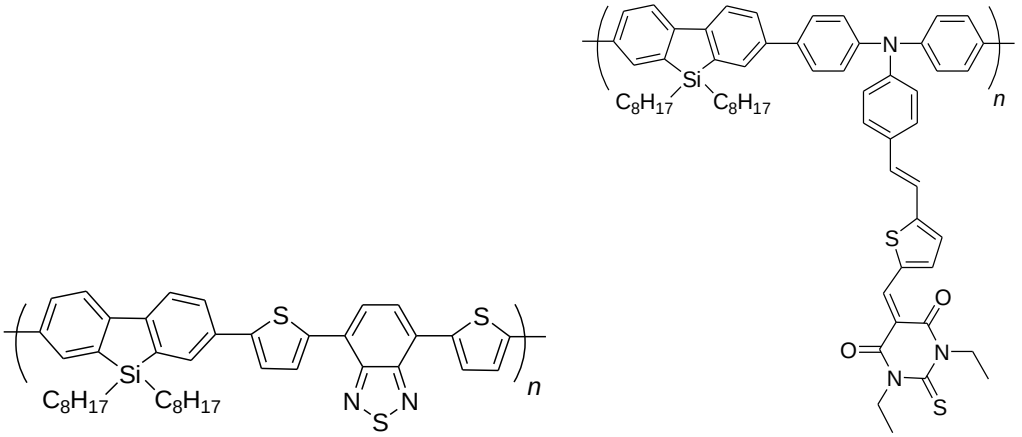

82 **83**

Figure 1.39 – Structures of dibenzosilole-based co-polymers for solar cell applications

A novel series of fluorinated heterofluorenes was reported by Geramita *et al*. who presented 2,7-substituted hexafluoroheterofluorenes as building blocks for electron transport materials (**84**, Figure 1.40).[62-64] The materials were prepared via nucleophilic aromatic substitution reactions of phenyllithium, thienyllithium and lithium phenylacetylide with various octafluoroheterofluorenes.[63] The inclusion of fluorine atom substituents aimed to improve the electron-accepting nature of the heterofluorene as well as the molecular packing arrangement of molecules in the solid state. Photophysical studies showed the compounds emitted light in the blue region of the spectrum, with wide-ranging PLQY values.[63] The low PLQY values were attributed to the heavy atom effect of the heteroatom and in the case of the thienyl derivatives, the lone pair on the sulfur atoms enhancing non-radiative decay pathways. The fluorinated compounds all exhibited lower LUMO values than their non-fluorinated analogues, indicative of the increased electron affinity imparted by these substituents.[63] The fluorinated molecules also showed co-facial packing in the solid state as opposed to the herringbone

structure often adopted for non-fluorinated fluorenes. It was suggested that this may help with electron transfer through the molecules; unfortunately this theory could not be quantified as it was not possible to solution cast the molecules into films.[63]

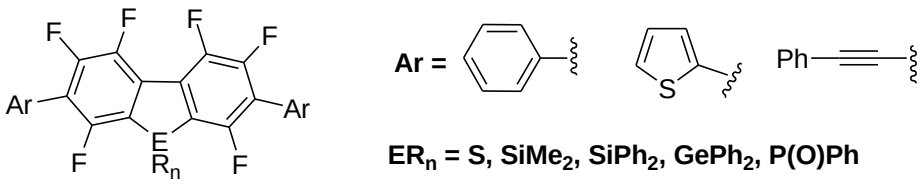

84

Figure 1.40 – Structures of 2,7-substituted hexafluoroheterofluorene derivatives

These materials were further developed into D-A architectures with a series of oligothiophene-perfluoro-9-heterofluorene based compounds (e.g. **85**, Figure 1.41).[64] A thiophene-based donor unit was chosen due to its well-documented hole transport ability and widespread use in systems for OPV applications. Preliminary OPV devices were reported using the D-A molecules blended with P3HT which exhibited improved performance compared with P3HT-only devices, indicating the importance of the D-A molecule in balanced charge transport.[64] However, the overall efficiencies of the devices (0.002 – 0.031%) are still much lower than the alternative systems based on P3HT blended with PCBM as an electron transport material.[64]

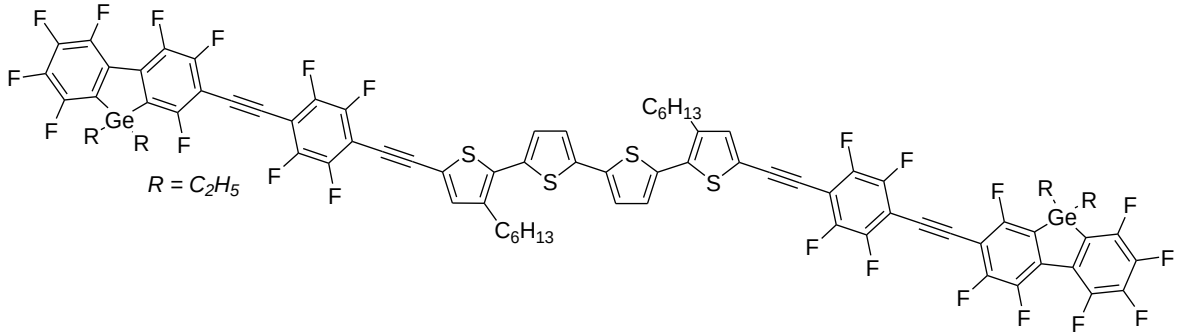

85

Figure 1.41 – Structure of germanium-based A-D-A system

While silafluorene-type systems show good promise for use in a number of different applications and they do offer advantages over polyfluorenes (e.g. increased stability), the complexity of their syntheses and the requirement for the use of toxic reagents may limit their applicability and reduces the desirability for them to fully replace polyfluorenes. Similarly, to date, no other fluorene analogues have proved as versatile in their uses as fluorene itself.

1.4.1 Dibenzothiophene-*S*,*S*-dioxide

A type of heterofluorene which may offer similarly straightforward synthetic routes to its formation, compared to fluorene, as well as applicability to a variety of different molecular architectures is dibenzothiophene-*S*,*S*-dioxide (**S**) (**2**, Figure 1.2). **S** is a molecule topologically similar to **F** where the C_9 carbon is replaced with an electron-withdrawing sulfone (SO_2) group, thus **S** is a high electron affinity moiety. **S** is easily synthesised from the oxidation of commercially (and cheaply) available dibenzothiophene (**86**). Dibromo-derivatives of **S** (**87**, **89**) are also easily accessible, leading to the possibility of a variety of coupling reactions to incorporate **S** into both small molecules and polymers (Scheme 1.6).

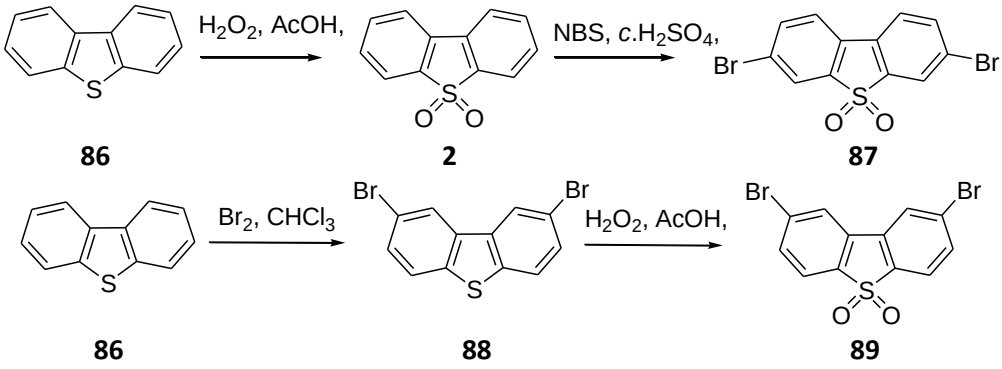

Scheme 1.6 – Syntheses of dibromo-S derivatives

The Bryce group were the first to utilise **S** as an electron acceptor in ambipolar molecules for OLED applications.[65] A series of conjugated oligomers based on **F** and **S** were synthesised (**90**-**92**, Figure 1.42), as well as an analogous **F**-only trimer (**93**) for comparison. The **F**/**S** materials are highly fluorescent and exhibit stable blue emission both in solution and the solid state.[65]

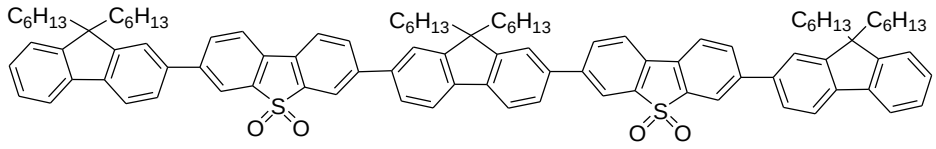

90

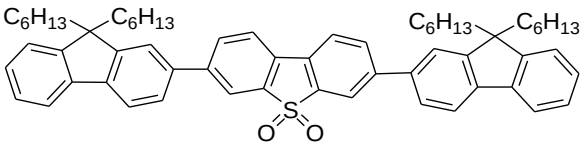

91

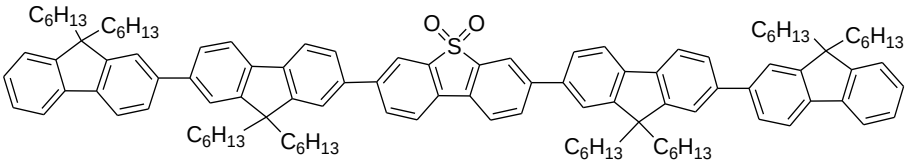

92

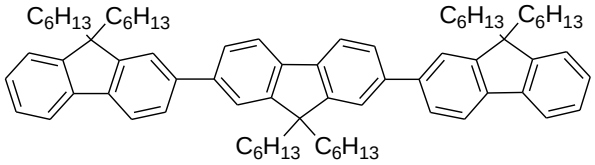

93

Figure 1.42 – Structures of F/S oligomers and FFF trimer

The **F/S** oligomers (**90** – **92**) were synthesised using palladium-catalysed Suzuki coupling conditions. Their emission maxima range from 430 – 450 nm in solution and 447 – 462 nm in the solid state with PLQY values ranging from 65 – 67% (solution) and 44 – 63% (solid state) (Figure 1.43).[65] The oligomers are thermally stable with decomposition temperatures above 300 °C and no low energy green defect emission is observed upon annealing films of the materials. From DFT calculations it was determined that the LUMO levels of the **F/S** oligomers are decreased compared to analogous **F**-only oligomers (e.g. **93**), indicative of the increased electron accepting character of the sulfone.[65]

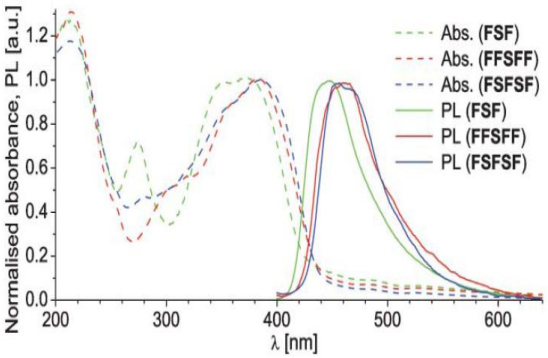

Figure 1.43 – Normalised UV-Vis absorption and PL spectra of FFF (93), FFSFF (92) and FSFSF (90) co-oligomers in thin film[65]

As previously mentioned, the presence of a fluorenone unit in a **PF** chain quenches its blue emission; however, from photophysical studies of the **F/S** oligomers, it appears this is not the case for **S**. A similar effect was previously reported by Barbarella *et al*. who inserted a thienyl-*S,S*-dioxide moiety into the aromatic backbone of a series of thiophene oligomers (e.g. **94**, Figure 1.44) and observed both an increase in electron affinity (measured through cyclic voltammetry) and an increase in the solid-state PL efficiency (compared to the thienylene-only oligomers).[66] Charas *et al*. reported the use of the thienyl-*S,S*-dioxide moiety together with **F** in

co-polymers.[67] In the case of the polymers, the electron affinity of the systems increased (as was seen for the oligomers), but PLQY values were much lower (16% in solution, <1% in film).[67]

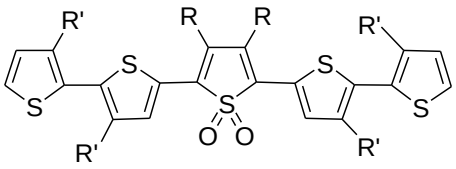

94

Figure 1.44 – Structure of thienyl-*S*,*S*-dioxide/thiophene co-oligomer

Detailed photophysical studies of the **F**/**S** systems show they exhibit efficient dual emission, where the molecular excited state can have both local excitonic (LE) and charge transfer (CT) character depending on the nature of the local environment, e.g. solvent polarity.[68,69] In non-polar solvents, such as toluene, a well-structured LE emission is observed, whereas in more polar solvents such as chloroform, broad featureless (and red-shifted) CT emission is dominant (Figure 1.45, **FSF** (**91**) and **FFF** (**93**) as example oligomers). In the non-ambipolar **FFF** trimer (**93**), this localised emission is seen in both non-polar and polar solvents as no ICT interaction can occur. On recording the emission spectrum of **F**/**S** systems in polar media at low temperature, both types of emission are seen simultaneously, implying the dual emission is related to molecular conformation, a topic which is investigated further in chapter 2.

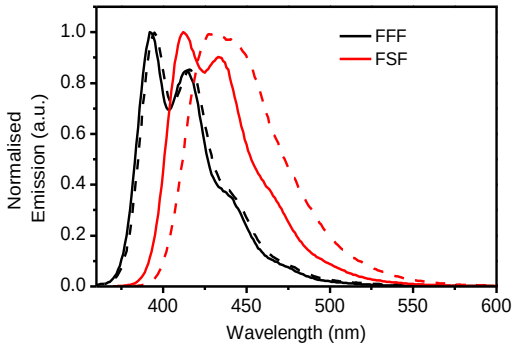

Figure 1.45 – Emission of FSF (91) and FFF (93) in toluene (solid lines) and chloroform (dashed lines)

As well as oligomers, random co-polymers of **F** and **S** have been synthesised using palladium-catalysed Suzuki conditions where the proportion of **S** is increased from 2 – 30 mol%.[70] The polymer molecular weights are ~ 20 - 33 kDa and all exhibit excellent thermal stability.[70] All **S**-containing polymers show the same dual emission characteristics as the oligomers, i.e. the presence of CT emission in polar solvents, which becomes more dominant with increasing amounts of **S**. Most importantly, unlike the polymers of the thienyl-*S*,*S*-dioxide-based materials (**94**),[67] the **F**/**S** polymers show high PLQYs of up to ~ 69% in solution.[70] OLEDs fabricated using these polymers show increased external quantum efficiencies (EQEs) with increased **S** unit

content up to a maximum of 1.3% at 100 mA cm^{-2}, for 30% **S** content. This efficiency is higher than that of pure PFO-based devices, which under similar conditions produced EQEs of 0.05 – 0.1%.[70] A decrease in device performance was reported at low **S** unit incorporations which was attributed to the **S** units acting as electron traps in the PF backbone, hence changing the balance between electron and hole transport.[70] The role of **S** as an exciton trap in **F/S** co-polymers is discussed further in chapter 5. The improvement of device characteristics with the incorporation of **S** is an effect which has also been reported by the Cao group who demonstrated an increase of spectral stability and efficiency of blue-emitting polyfluorenes by the addition of **S** as a co-monomer.[71] The dual fluorescence effect of **S** has also been exploited in polymers to achieve broad spectrum emission (i.e. towards white light) from a single-polymer device, a topic which is discussed further in Chapter 3.[70]

Interestingly, the incorporation of an *N*-arylphenothiazine-*S*,*S*-dioxide unit into **F**-based trimers and polymers (e.g. **95**) does not lead to the same ICT emission bands as the **F/S** systems, despite the presence of the electron-accepting sulfone moiety (Figure 1.46).[72] This is attributed to the breaking of the conjugation through the backbone by the *N*-Ar functionality.[72] While these materials show good potential as deep blue emitters for OLEDs, the results demonstrate the importance of conjugation effects in ambipolar systems as well as donor and acceptor identities if ICT emission is to be utilised.

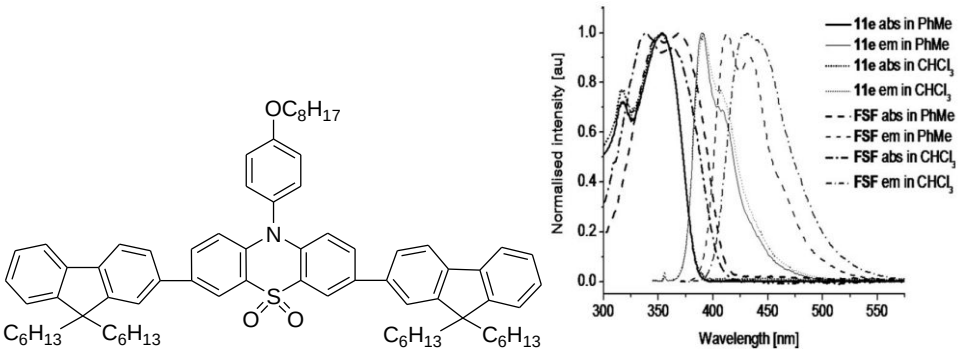

95

Figure 1.46 – Structure of F-phenothiazine trimer (11e) and its absorption/emission spectra in toluene and chloroform, compared with compound 91 (FSF)[72]

Numerous other **S**-containing systems for OLED applications have been reported, both oligomers[73-75] and polymers.[71,76,77] These include: co-polymers of **S** with dialkoxyphenyl substituted fluorenes (**96**) which exhibited an increase in PLQY values compared to non-**S** containing polymers;[76] and a series of random poly(arylenevinylene)s containing **F**, **S** and a bis(2-ethylhexyloxy)-2,5-phenylene donor unit (**97**) which were used for green-yellow emitting OLEDs (with relatively low performances).[77]

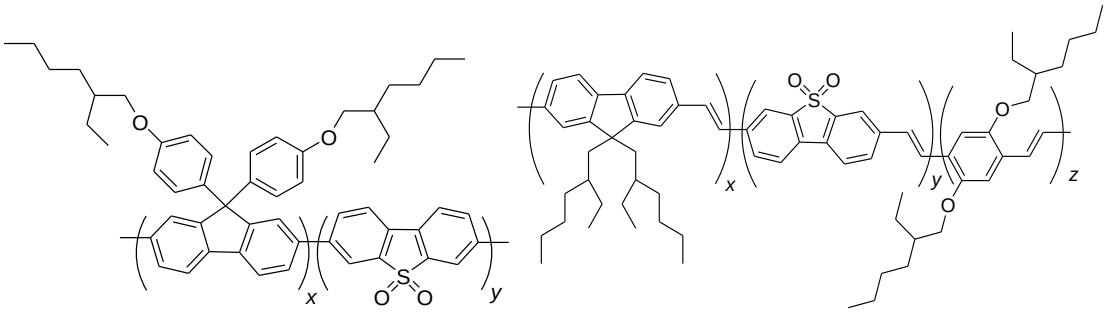

96 **97**

Figures 1.47 – Structures of F/S type co-polymers

The incorporation of **S** into conjugated organic systems has led to an interesting new class of ambipolar materials with potential for use in a number of optoelectronic applications, in particular, OLEDs. This topic is developed further in chapters 2 and 3 where the ICT characteristics of novel **S**-containing D-A systems are probed in order to gain insights into the fundamental photophysical processes occurring.

1.5 Conclusions

The widespread use of donor-acceptor systems in optoelectronic applications has been discussed and the clear advantages of using these ambipolar systems highlighted. The wide variety of structural variations possible has given rise to a huge wealth of materials, whose properties can be tuned to the required applications. The use of these materials has allowed a number of fundamental issues to be addressed which will allow novel materials to be designed with the specific properties required.

The utility of fluorene (**F**) in these systems has been demonstrated and its ability to function in different roles within various types of systems presented. **F** has emerged as a key structural unit in virtually all optoelectronic applications and there is still much research interest in extending its use to other novel ambipolar systems in order to fully understand its photophysical and charge transport properties. The emergence of dibenzothiophene-*S*,*S*-dioxide (**S**), a molecule topologically similar to **F**, as an electron transport moiety in ambipolar systems has been discussed and its clear favourable properties for these uses highlighted.

The following chapters focus on the development of novel ambipolar systems, both oligomers and polymers, which are based on either **F**, **S**, or both, in order to understand key properties and address key issues relating to their potential uses in a variety of different optoelectronic applications.

Chapter 2: Novel Trimers of 9,9-Dihexylfluorene and Dibenzothiophene-*S*,*S*-dioxide

2.1 Introduction

In Chapter 1 an introduction to the literature surrounding donor-acceptor (D-A) systems for optoelectronic applications was presented with particular focus on 9,9-dialkylfluorene (**F**, **1**) and a brief introduction to dibenzothiophene-*S*,*S*-dioxide (**S**, **2**). This chapter (and subsequent chapters) demonstrates the use of these moieties in addressing key issues and understanding important fundamental features of the D-A systems in which they are employed. This chapter focuses on probing the origins of the dual emission in **F**/**S** systems by designing, synthesising and studying the photophysical properties of a novel series of **F**/**S** co-oligomers.

As previously discussed (section 1.4.1), **F**/**S** co-oligomers and co-polymers are D-A systems which show improved electron affinity characteristics compared with fluorene-only analogues and exhibit high photoluminescence quantum yields (PLQYs).[65,68-70] Dual fluorescence from both local excited (LE) and intramolecular charge transfer (ICT) states is observed in solution and thin film. The phenomenon of dual fluorescence and its origins have been widely investigated and debated in the literature (e.g. reviewed in detail by Grabowski *et al*.[78]). The majority of the early studies were on 4-(*N*,*N*-dimethylamino)benzonitrile (**98**, Figure 2.1) as it was observed that this compound emits two fluorescence bands, the relative intensities of which depend strongly on solvent polarity and temperature.[78] In non-polar solvents only one band appears (LE emission), whereas in more polar solvents, a red-shifted fluorescence band emerges. It later became apparent that this phenomenon was not limited to this particular molecule; it is in fact common to many D-A containing molecules, e.g. our **F**/**S** systems.

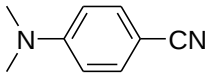

98

Figure 2.1 – Structure of 4-(*N*,*N*-dimethylamino)benzonitrile

There have been numerous mechanisms proposed to explain the origin of the dual fluorescence band in compound **98**, and these are discussed in detail by Grabowski *et al*.[78] However, the dominant explanations in the literature are the formation of either a twisted ICT state where the donor and acceptor rotate to be perpendicular to each other in the excited state (termed TICT) or a planarised ICT state where the donor and acceptor adopt a near planar conformation in the excited state (termed PICT).[78] There is much debate about which of

these mechanisms can best explain the dual fluorescence in D-A systems and evidence has been presented to support both theories.

Zachariasse and co-workers have presented numerous studies into D-A molecules with evidence for the excited states adhering to a PICT model.[79-83] Studies were performed comparing the planarised molecule fluorazene (**99**) with its flexible counterpart *N*-phenylpyrrole (**100**) (Figure 2.2) which showed that ICT transfer to a planar state occurred efficiently and that the formation of a twisted ICT state was not required.[80,82] Detailed photophysical studies showed that the onset of ICT emission was observed in solvents of lower polarity for **99** than for **100** and that ICT formation was quicker in the planarised **99**.[82] A similar trend was reported when comparing 4-fluorofluorazene (**101**) with its flexible counterpart 4-fluoro-*N*-phenylpyrrole (**102**).[81] X-ray data showed that the pyrrole group of **102** was twisted by an angle of 25˚ relative to the fluorophenyl moiety (in the ground state), whereas the same angle in **101** was 2˚ and it was the more planar **101** which exhibited the strongest ICT behaviour.[81]

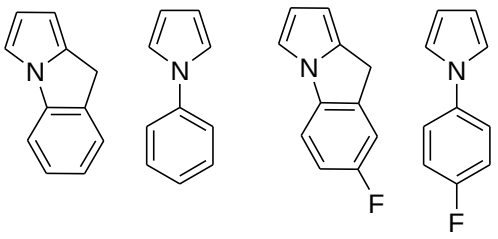

99 **100** **101** **102**

Figure 2.2 – Structures of planarised and non-planarised donor-acceptor molecules

There is also evidence for D-A molecules following a TICT model.[84-87] For example, Ooyama *et al*. presented a series of heteropolycyclic D-π-A structural isomers of benzofuro[2,3-*c*]oxazolo[4,5-*a*]carbazole-type fluorescent dyes with various acceptor groups (**103**, Figure 2.3) where it was reported that in highly polar solvents the predominant excited state species was the TICT state.[86]

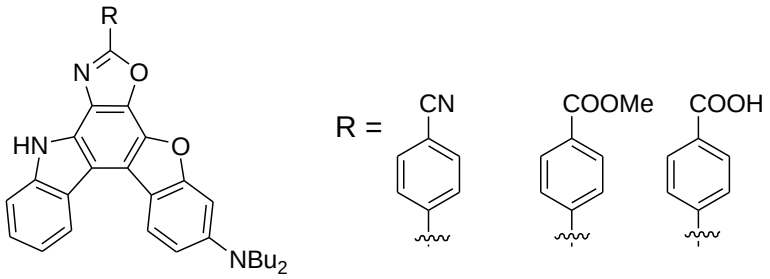

103

Figure 2.3 – Structure of fluorescent dye with varying acceptor groups

Similarly, Kotaka *et al*. reported the synthesis and photophysical properties of a number of π-extended fluorene derivatives including a dinitro compound (**104**, Figure 2.4(a)).[87] This compound exhibited fluorescence emission which was highly dependent on solvent polarity; in non-polar solvents such as cyclohexane and toluene no emission was seen, whereas in more polar solvents such as chloroform, dimethylsulfoxide and dimethylformamide strong fluorescence emission was observed.[87] Interestingly, no emission in ethanol (a polar solvent) was observed; however, no comment was made on this by the authors. The "on-off" behaviour of compound **104** in the various solvents was attributed to the reorganisation of the molecule into a TICT state where the *para*-nitrophenyl groups were nearly perpendicular to the central fluorene unit (Figure 2.4(b)).[87] The theory was proposed, but no further photophysical studies were presented to substantiate it.

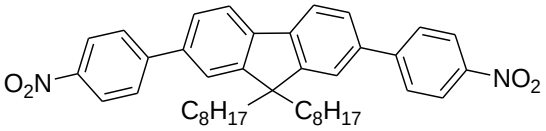

104

Figure 2.4(a) – Structure of dinitro substituted π-extended fluorene derivative

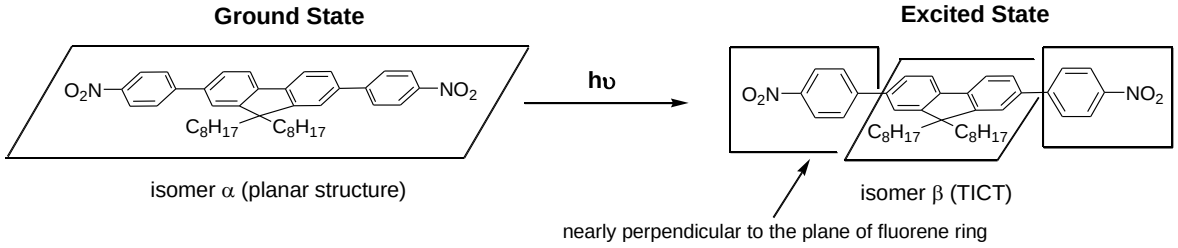

Figure 2.4(b) – Schematic representation of TICT structure adopted in the excited state
(redrawn from reference [87])

Previous work from the Bryce group on **F/S** oligomers (e.g. **90** – **92**) provisionally indicated that the excited state in these systems could also be described by a TICT model, but it was reported that further clarification on this point required the syntheses of new derivatives which possessed either enforced planar or twisted architectures.[68]

In pursuit of this clarification a series of novel **F/S** based systems was designed and synthesised, details of which will be discussed in this chapter. **S** has been used in a number of different molecular architectures; however, there has been very little work on the incorporation of functionalised **S** units. The Bryce group recently presented the synthesis of

hexyl substituted **S** units (**105**, **106**) for incorporation into random co-polymers with 9,9-dioctylfluorene monomers (**109** -**111**).[88] The aim of the work was to provide a system in which the backbone would be twisted compared to the parent **F/S** (unfunctionalised) co-polymers to study the effects of reduced π–conjugation on the emission properties. It was proposed that the hexyl chains would increase the dihedral angle between **F** and **S** units in the backbone which would blue shift the emission and impart additional solubility for ease of processing (when using unsubstituted **S**, co-polymers with > 30% **S** incorporation could not be synthesised due to monomer insolubility).[88] Scheme 2.1 shows the syntheses of the monomer units and the final polymers.

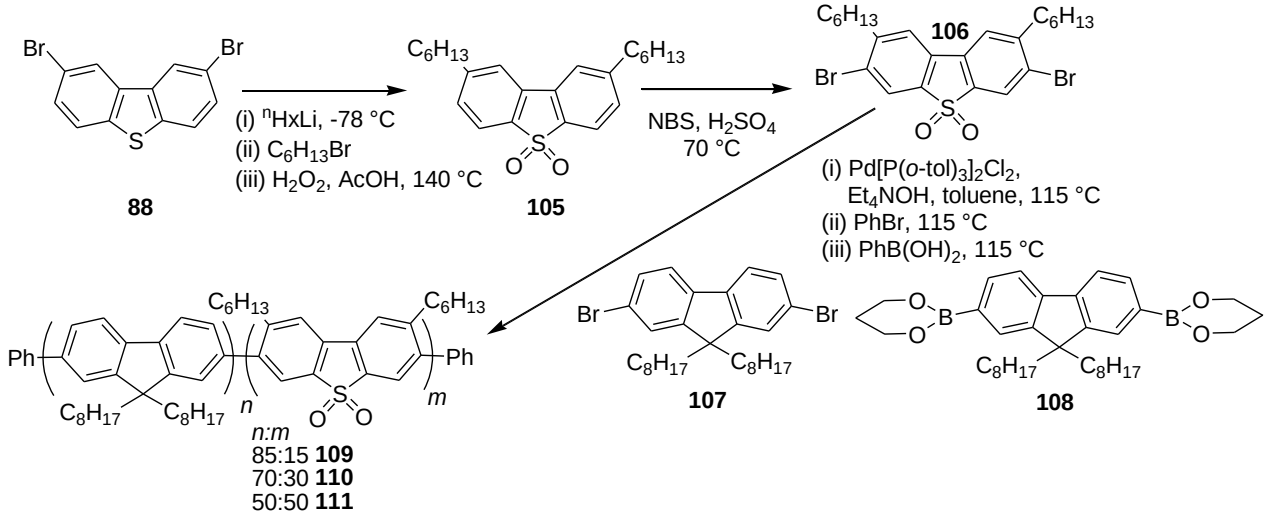

Scheme 2.1 – Syntheses of hexyl substituted S monomers and their incorporation into polymers

The synthesis of the required dihexyl substituted **S** unit (**105**) proceeded in relatively low yield, but the final polymers were obtained in high yields with high molecular weights.[88] Photophysical studies of the three co-polymers **109 – 111** revealed that the hexyl substituents have a strong effect on the ICT emission. Compared with the parent (unfunctionalised) **F/S** co-polymers, the emission of co-polymers **109 – 111** is blue shifted, indicative of reduced conjugation through the backbones.[88] Interestingly, in co-polymers **109** and **110** the formation of the ICT band is restricted even in the more polar solvent (Figure 2.5(a)).[88] These data suggest that the ICT state in these systems is de-stabilised by a more twisted architecture so a TICT model would not be appropriate in this case. In the alternating co-polymer, **111**, this effect is overcome; the emission is further blue shifted compared with **109** and **110** (by ~ 12 nm) but strong ICT emission is observed.[88] This can be attributed to the increased interaction between **F** and **S** as they are now adjacent to each other. The triplet energy (E_T) of the alternating co-polymer was determined to be 2.46 eV (E_T increases with **S** content due to reduced conjugation) making it a strong candidate as a host material for green light-emitting

complexes. Indeed a device fabricated using a blend of co-polymer **111** with a green-emitting iridium complex showed emission only from the guest complex (Figure 2.5(b)).[88]

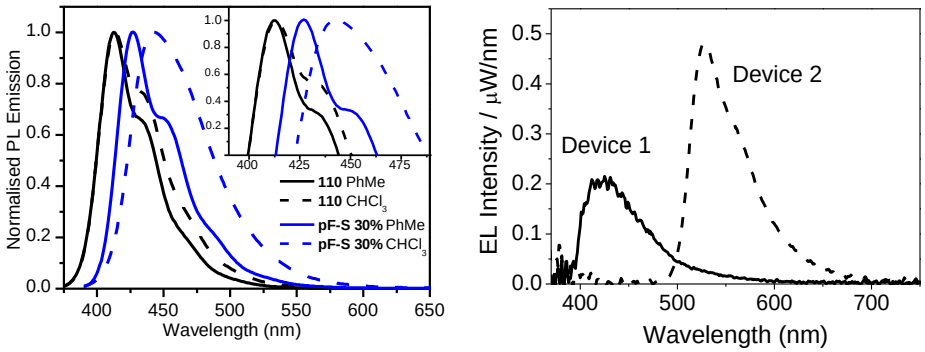

Figures 2.5(a) – PL emission of co-polymer 110 compared with parent pF-S (30% S) in toluene and chloroform and (b) – EL emission from device 1 (co-polymer 111), device 2 (co-polymer 111 blended with Ir complex)[88]

This novel **F/S** system sheds some light on the origin of the ICT band in these systems, i.e. disfavouring a TICT model, as well as demonstrating a new class of potential host materials for OLEDs. To take this work further a new series of substituted **S** units was designed and synthesised for incorporation into oligofluorene D-A-D type oligomers. The following sections present the syntheses and photophysical properties of these systems.

2.2 Results and Discussion

In order to gain a fuller understanding of the ICT processes involved, a set of **S** units with a variety of substituents was required, e.g. electron-donating, electron-withdrawing, bulky, non-bulky etc. A novel set of alkoxy-substituted **S** units was synthesised within the Bryce group (discussed later) with bulky electron-donating substituents. To complement these compounds, the syntheses of derivatives with other substituents on the **S** unit were required.

2.2.1 The difluoro-substituted S unit

A key target was the difluoro substituted **S** unit, (**117**/**120**)**.** A fluorine atom is approximately intermediate in size between a hydrogen atom and a hydroxyl group.[89] Therefore, fluorine substituents should have little steric effect, i.e. induce little twist in the backbone compared with bulky alkoxy substituents, but will of course have a different electronic effect due to their strong electron-withdrawing capabilities. First it was necessary to synthesise 2,8-difluorodibenzothiophene (**117**), which could then be oxidised and brominated to give the required monomer (**120**) for Suzuki coupling to two fluorene moieties to obtain the required D-A-D trimer.

A number of different routes were attempted in order to functionalise **S** with fluorine atoms:

1. Sandmeyer reaction of the diamino derivative
2. Use of an electrophilic fluorine source
3. Cyclisation of bis(4-fluorophenyl)sulfone

Route 1

The synthesis plan was to nitrate dibenzothiophene (**86**) to give compound **112** which could then be reduced to the amino derivative (**113**), followed by a Sandmeyer reaction to form 2-fluorodibenzothiophene (**114**). This compound could then be oxidised to the corresponding sulfone and brominated to give a functionalised monomer. Similarly it was envisaged that the di-substituted analogues (**115 – 117**) could be synthesised in the same way (Scheme 2.2).

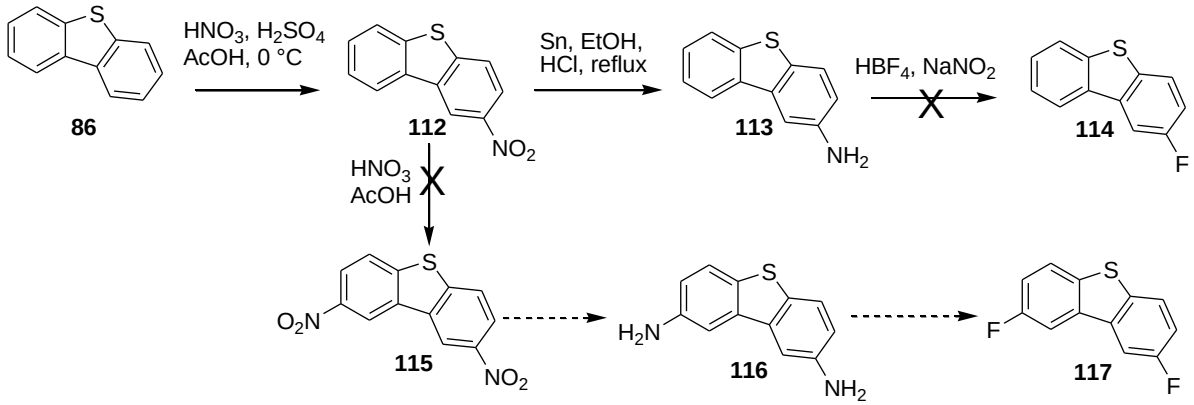

Scheme 2.2 – Attempted syntheses of fluoro-substituted S units

Compound **112** was synthesised, but in a low yield (34%) and was reduced to **113**, again in a low yield (32%). However, the attempted Sandmeyer reaction of compound **113** to compound **114** was unsuccessful, giving a mixture of unidentified decomposition products. An attempted synthesis of compound **115** from compound **112** gave no product, just unreacted starting material. Due to the difficulty and number of steps involved in this scheme, the route was abandoned in favour of options with fewer steps.

Route 2

A commonly used method for functionalising organic compounds with fluorine atoms is to use an electrophilic fluorinating agent, i.e. an F^+ source. 2,8-Dibromodibenzothiophene (**88**) was lithiated (^{n}BuLi, -78 °C) and an excess of *N*-fluorodi(benzenesulfonyl)amine ("F^+") added (Scheme 2.3). Upon work up and purification the product fraction was obtained as a white solid. However, this fraction was determined by NMR and GC-MS to be a mixture of dibenzothiophene (**86**), 2-fluorodibenzothiophene (**114**) and the desired product, 2,8-

difluorodibenzothiophene (**117**). Although **117** was the major product (~ 38% yield), it was not possible to separate the three compounds either by column chromatography or through recrystallisation. The mixture was reacted on to see if separation would be possible at a later stage, but after each reaction (oxidation, followed by bromination), the mixture of products remained inseparable.

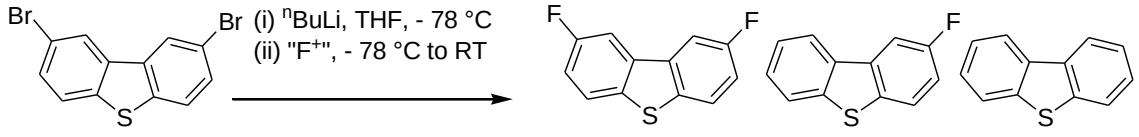

88 **117** **114** **86**

Scheme 2.3 – Reaction with electrophilic fluorine source and mixture of products obtained

Although it was not possible to isolate the product **117** using this method, it was established that the bromination reaction on our electron-deficient system was possible. We opted, therefore, to pursue a route which avoided the formation of the monofluoro by-product.

Route 3

An in-depth literature search revealed a report of the lithiation and subsequent cyclisation reaction of diphenylsulfone (**118**) to dibenzothiophene (**86**) in a high yield (Scheme 2.4).[90]

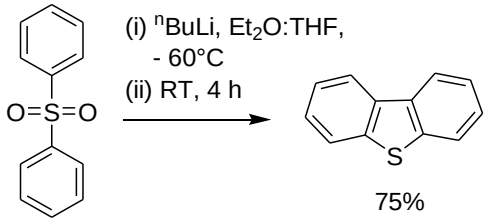

118 **86**

Scheme 2.4 – Reported cyclisation of diphenylsulfone to dibenzothiophene

Unfortunately, only the abstract of this work[90] was available (despite attempts to obtain the full article), so no further experimental information could be obtained. However, the difluoro analogue (**117**) was referenced to this paper by SciFinder. This encouraged us to attempt the analogous reaction using commercially available bis(4-fluorophenyl)sulfone (**119**, Scheme 2.5).

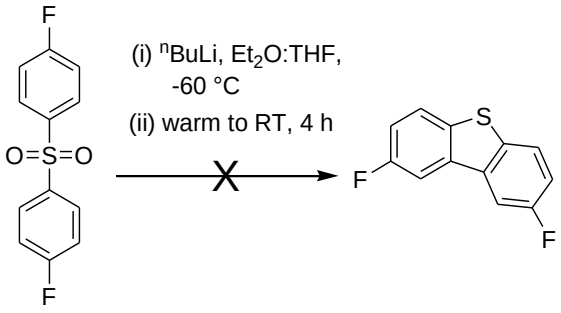

119 **117**

Scheme 2.5 – Attempted cyclisation of bis(4-fluorophenyl)sulfone to 2,8-difluorodibenzothiophene

The suggested mechanism for this reaction (Scheme 2.6) is based on a process reported by Soki *et al*. who observed a "surprising" cyclisation of diphenylsulfone upon treatment with ^{n}BuLi in their synthesis of a new chiral diol.[91] The abstract from Brinon *et al.* implies that the lithium hydride (LiH) by-product then reduces the sulfone (SO_2) to the sulfide to give the reported product.[90]

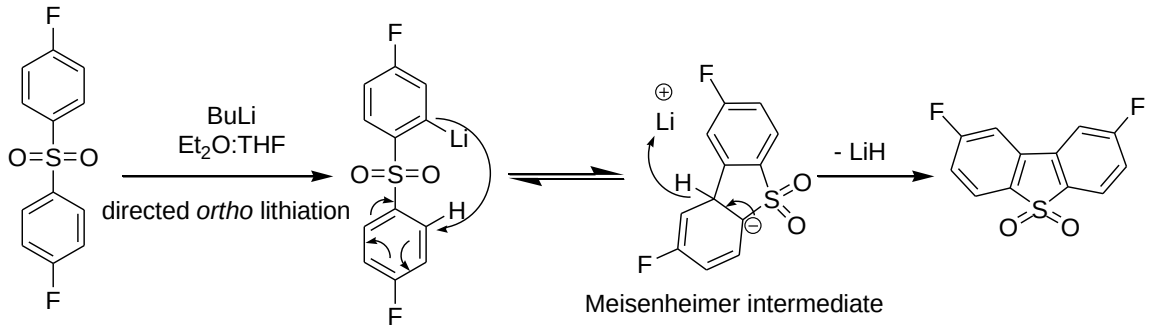

119 **120**

Scheme 2.6 – Proposed mechanism for the cyclisation reaction

The reaction shown in Scheme 2.5 was attempted using a range of conditions; varying the temperature, the solvent and the number of equivalents of lithiating agent. However, in all cases the major product obtained was unreacted starting material, with only trace amounts of the product (**117**) seen by GC-MS. A lithiation reaction followed by a D_2O quench of the starting material (bis(4-fluorophenyl)sulfone, **119**) was performed. The proton NMR spectrum showed the same shifts as that for the starting material, but the integrations and splitting patterns were consistent with full conversion to the doubly *ortho*-deuterated product (**121,** Figure 2.6). This implied that the problem with the reaction was the cyclisation, not the lithiation step.

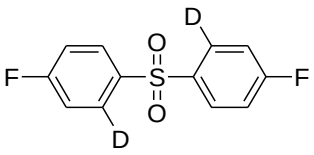

121

Figure 2.6 – The molecular structure of the lithiation product quenched with D_2O

In an attempt to improve the cyclisation reaction, research revealed conditions reported by Yamazaki *et al*. who synthesised radical cations of dibenzothiophene with bicyclo[2.2.2]octene units, using four equivalents of copper(II) chloride (Scheme 2.7).[92]

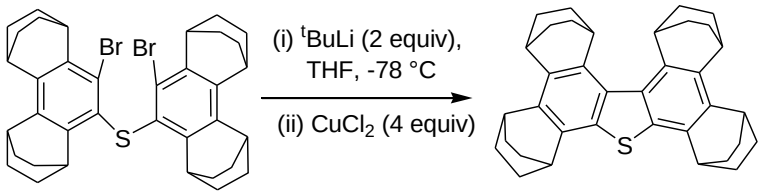

122 **123**

Scheme 2.7– Reaction conditions reported by Yamazaki et al.[92]

The cyclisation reaction of bis(4-fluorophenyl) sulfone (**119**, Scheme 2.5) was repeated with the addition of copper(II) chloride which was dried by heating under vacuum (120 °C, ~ 1 mb) for 2 h prior to use. Using these conditions, 2,8-difluorodibenzothiophene-*S*,*S*-dioxide (**120**) was successfully obtained. The sulfone (**120**) was the only isolated final product, with none of the reduced species as referred to by Brinon *et al*.[90] (i.e. compound **117**). The product was obtained in repeatable (low) yields of 20 - 25%, mainly due to the messy work up involving the large amounts of copper salts which formed and made purification difficult. Scheme 2.8 shows the synthesis of this product as well as the subsequent bromination reaction to give monomer **124** and the Suzuki cross-coupling reaction performed to obtain trimer **126**, herein also referred to as **FS$_F$F**. Figure 2.7 shows the single crystal molecular structure (determined by X-ray analysis) of one of the four independent molecules in the asymmetric unit.

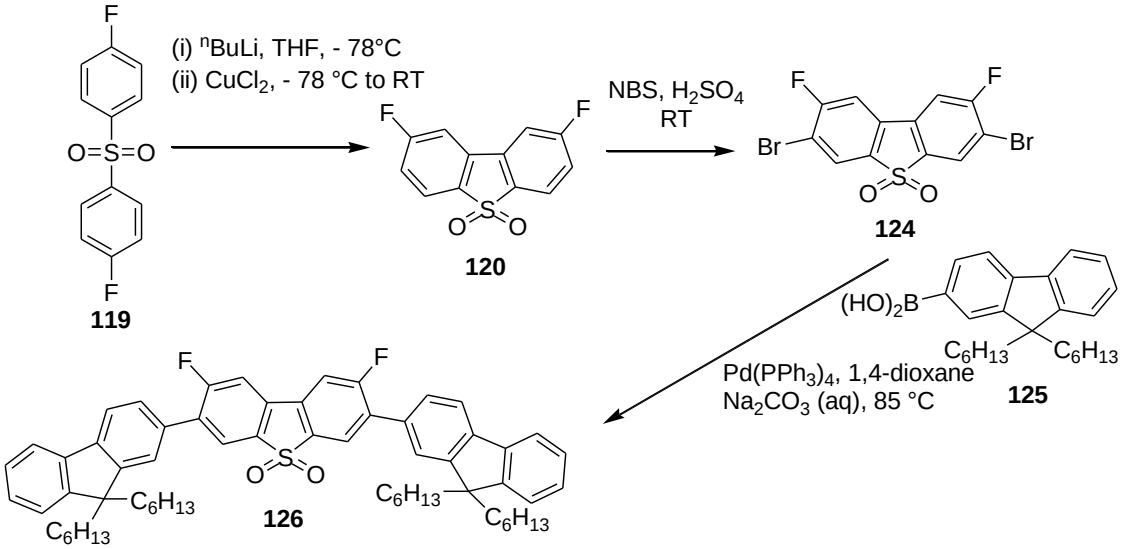

Scheme 2.8– The successful syntheses of difluoro-substituted S and its fluorene-based co-oligomer

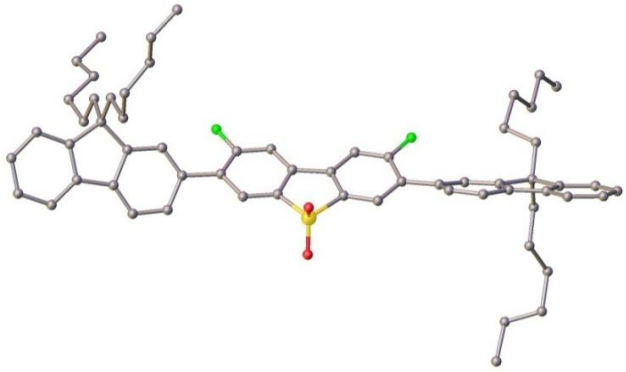

Figure 2.7 – The single crystal molecular structure of the FS_FF trimer (126)
(H atoms omitted; F, S and O atoms are shown in green, yellow and red, respectively)
(Structure determined by Dr. A. S. Batsanov)

The 3,7-dibromo-2,8-difluorodibenzothiophene-*S*,*S*-dioxide monomer (**124**) was also used to synthesise two random co-polymers (**pF-S_F-x%**, **127**, **128**) together with 9,9-dioctylfluorene monomers (**107**, **108**) (Scheme 2.9). The polymers were synthesised using Suzuki-Miyaura coupling conditions, end-capping with bromobenzene/phenyl boronic acid (see Chapter 7 for full details of experimental procedures). Both polymers were obtained as fluffy pale yellow solids.

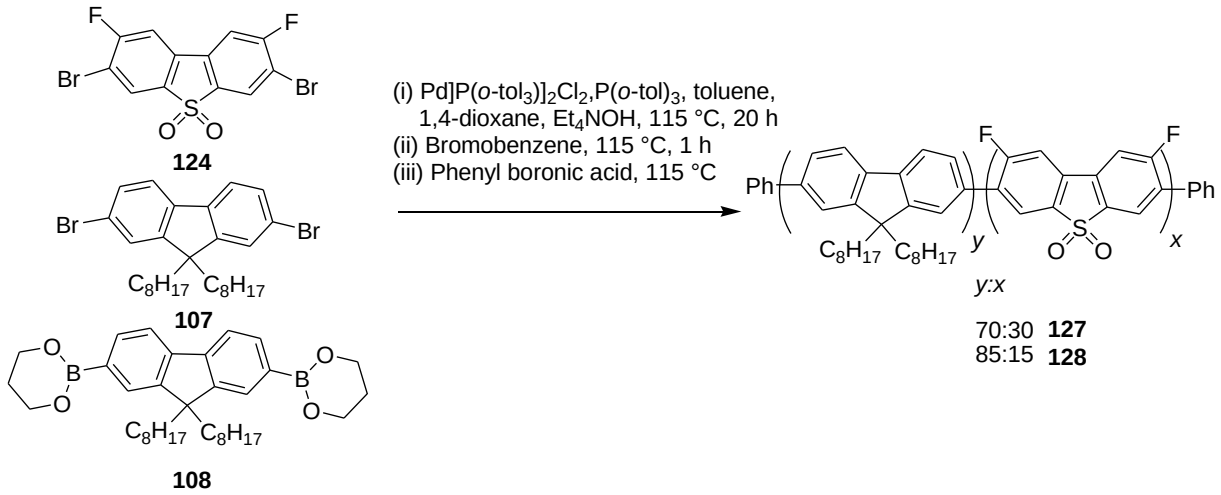

Scheme 2.9 – Syntheses of pF-S_F-x% random co-polymers
(Compounds **107**, **108** synthesised by Dr.K.T.Kamtekar)

2.2.2 Other attempted syntheses of substituted S units

Following the successful syntheses of the difluoro-substituted **S** unit (**124**) and its **FS_FF** trimer (**126**), the syntheses of a number of other analogues were attempted to compare with this compound and others being synthesised within the Bryce group.

2.2.2.1 The bis(trifluoromethyl)-substituted S unit

In order to extend the effect of the fluorine atoms, trifluoromethyl-substituted analogues were attempted. Trifluoromethyl groups are more electronegative and larger than fluorine atoms. However, these groups can be difficult to add to molecules often requiring the use of high pressure experiments. It was, therefore, decided to use trifluoromethyl-functionalised starting materials. In order to follow a similar reaction scheme to that used in the synthesis of monomer **124**, the analogous starting sulfone (**132**) was required. This was obtained by synthesising a Grignard reagent (**130**) from 4-bromobenzotrifluoride (**129**) and reacting it *in situ* with 4-trifluoromethylbenzene sulfonyl chloride (**131**) (Scheme 2.10). Compound **132** was then subjected to the same cyclisation conditions as for the difluoro analogue to give the trifluormethyl-functionalised S unit, (**133**).

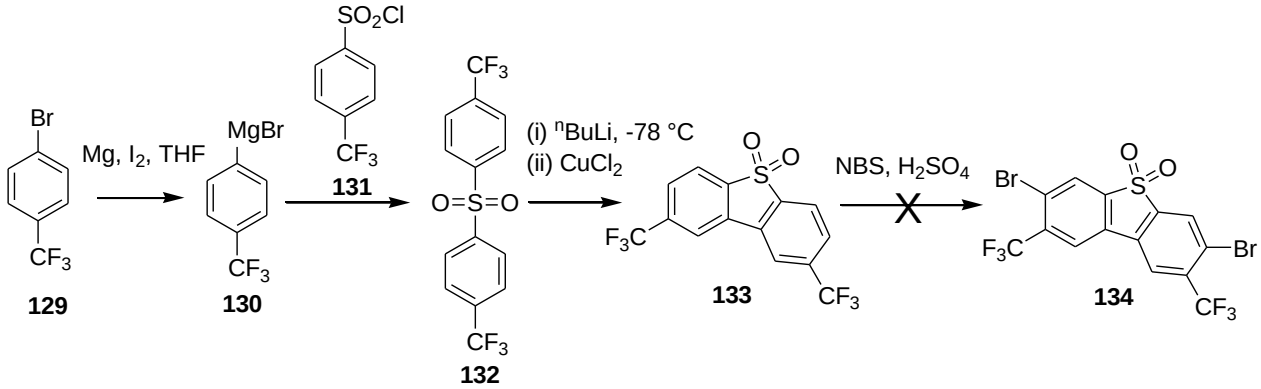

Scheme 2.10 – Synthesis of trifluoromethyl-substituted S unit

Bromination of **133** was attempted in order to produce the monomer required for coupling to fluorene (**134**); unfortunately, this reaction was unsuccessful even using harsh conditions (*c*.H_2SO_4, NBS), giving a mixture of unreacted and decomposed starting material. We attributed this to the strongly electron-withdrawing trifluoromethyl groups (as well as the electron withdrawing sulfone moiety) which deactivates the system to bromination, hence the subsequent fluorene-based trimer could not be synthesised.

2.2.2.2 The dimorpholine-substituted S unit

After the bromination problems encountered with the electron deficient compound (**133**), it was decided to investigate an electron-rich analogue. A nitrogen donor ligand (morpholine) was chosen to complement the series of alkoxy substituted **S** units which were being synthesised within the group (discussed in section 2.2.3), by inducing twist into the backbone. A carbon-nitrogen (C-N) cross-coupling reaction was performed on 2,8-dibromodibenzothiophene-*S*,*S*-dioxide (**89**) (Scheme 2.11). The resulting dimorpholine-

substituted compound (**135**) was brominated (in a high yield of 75%) to give compound **136** and then coupled to two fluorene moieties to give the resultant trimer (**137**) as a yellow solid.

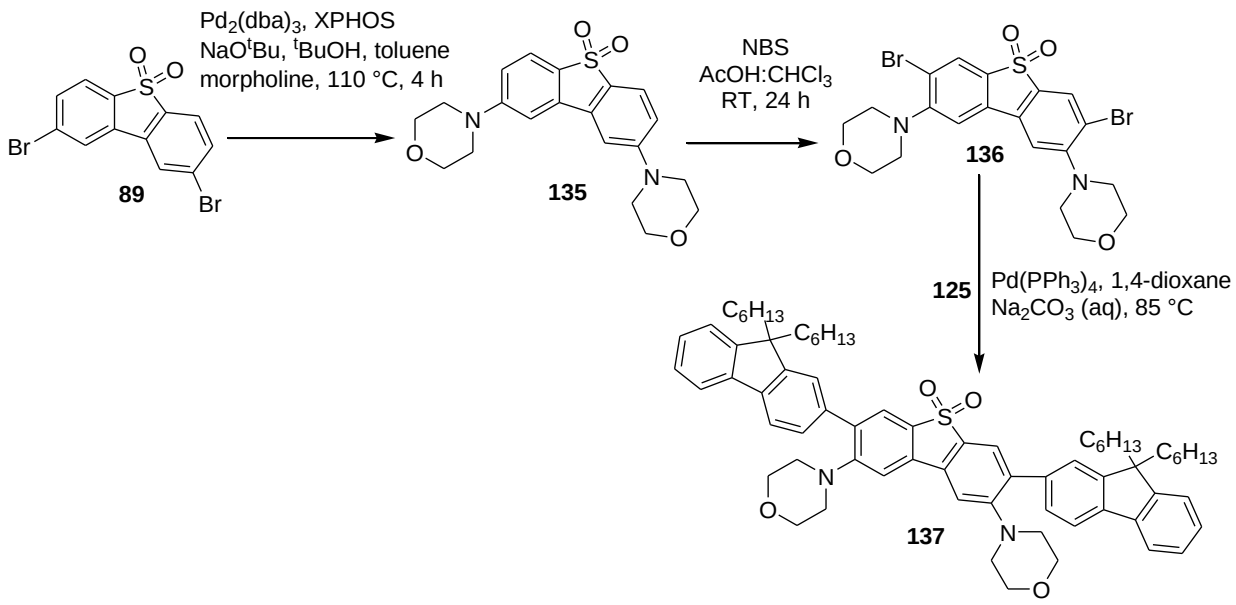

Scheme 2.11 – Syntheses of the morpholine-substituted S unit and its fluorene-based trimer

2.2.3 Photophysical results

The photophysical properties of the difluoro-substituted **FS$_F$F** trimer (**126**) were studied together with a variety of other functionalised **S** unit trimers and compared with the "parent" trimers, previously reported, **FFF** (**93**) and **FSF** (**91**). The structures of these compounds are shown in Figure 2.8. The alkoxy substituents of trimers (**138**-**140**) impart both solubility (allowing **S**-**F**-**S** and **S**-**S**-**S** type trimers to be synthesised for the first time), as well as twisting the backbone. Compound **141** is a planarised model compound where the backbone cannot twist at all and compound **142** is its diaryl analogue.

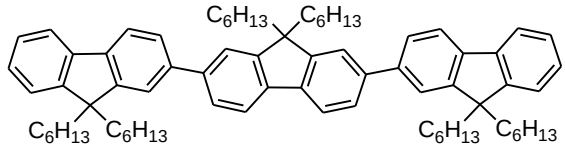

93 (**FFF**)

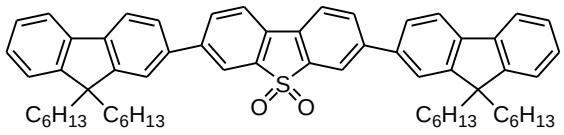

91 (**FSF**)

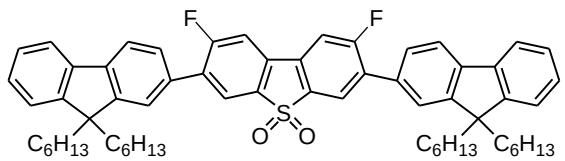

126

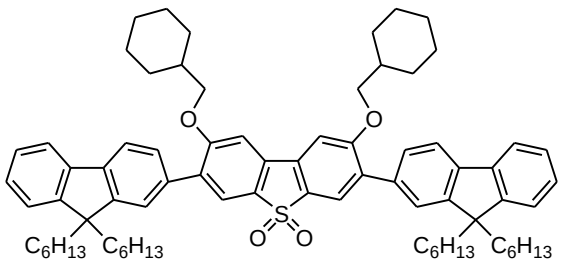

138

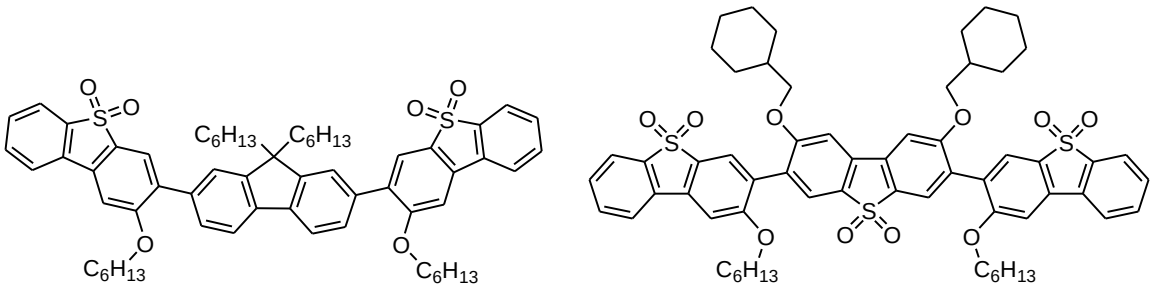

139 **140**

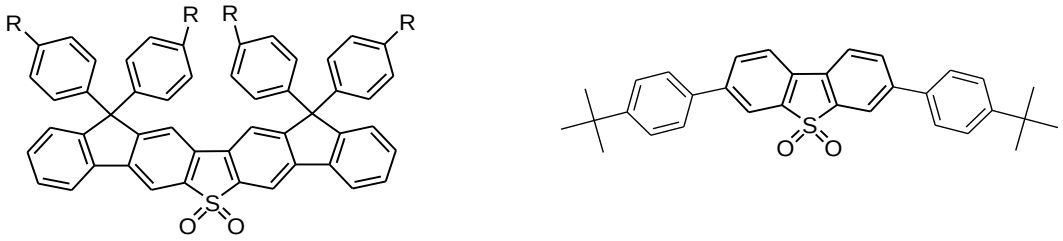

141 **142**

Figure 2.8 – Structures of the F/S oligomers with substituted S units
Compounds (**138**-**140**) synthesised by Dr. H. Li; compounds (**141**,**142**) synthesised by Dr. K. T. Kamtekar (see reference[93] for synthesis details)

All the compounds exhibit bright deep blue fluorescence. The key feature of the series is that compounds containing both **F** and **S** show broad, red-shifted ICT bands in polar solvents (e.g. chloroform), whereas **FFF** (**93**) and **SSS** (**140**) type compounds do not (spectra are shown in Figures 2.9 and 2.10) thus demonstrating that both donor and acceptor units are required for ICT. Also, importantly, the ICT interaction between donor and acceptor is not prevented by twisting the backbone of the oligomers (as was seen in the hexyl substituted **F/S** co-polymers discussed in section 2.1[88]). Table 2.1 shows selected photophysical data for all the trimers. The photoluminescence quantum yields (PLQY/ϕ_{PL}) are generally very high in both solution and the solid state. Indeed, the fluorinated trimer (**126**), exhibits a PLQY of 1.0 i.e. a 100% (within error) conversion of energy into light, making it a very attractive material in terms of OLED applications. This increase in PLQY with the addition of fluorine atom substituents may be attributed to the fact that it has been reported that C-H bonds can promote radiationless decay from the excited state back down to the ground state of a molecule, but the replacement of a C-H bond with a C-F bond of lower vibrational frequency can reduce this radiationless decay and hence increase the PLQY.[94]

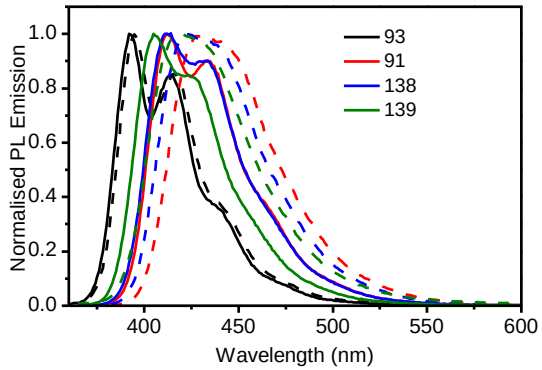

Figure 2.9 – Normalised emission of trimers in toluene (solid lines) and chloroform (dashed lines)

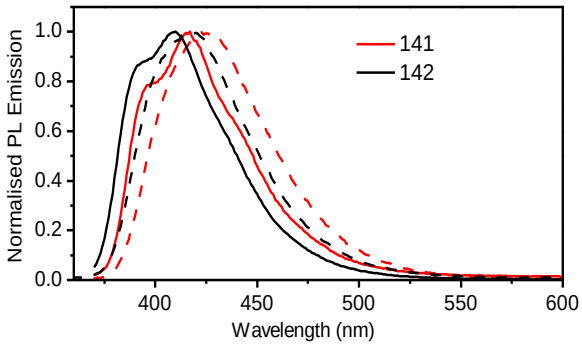

Figure 2.10 – Normalised emission of trimers in toluene (solid lines) and chloroform (dashed lines)

Lifetime studies of the compounds show that those with ICT bands have much longer lifetimes in polar solvents compared with non-polar solvents, consistent with polar solvents stabilising the donor-acceptor interaction. The planarised compound (**141**) shows the longest lifetimes in both polar and non-polar solvents (~ 1.7 and 3.8 ns, respectively), compared to oligomers **93, 91, 126, 138 – 140** (~ 0.7 - 1.0 and 0.8 - 1.5 ns, respectively), and the model compound (**142**) (~ 1.5 and 2.8 ns, respectively). These data suggest that planarisation is stabilising the ICT state in these systems, implying a PICT model for the excited state. This is consistent with the previously reported findings for the hexyl substituted **F/S** co-polymers.

Compound	Solvent/Film	λ_{abs} (nm)	λ_{PL} (nm)	ϕ_{PL} (%)
93	Toluene	358	395, 416	0.8 ± 0.1
FFF	Chloroform	358	395, 416	
	Film	357	416, 440	0.7 ± 0.05
91	Toluene	352, 370	415, 434	0.9 ± 0.1
FSF	Chloroform	352,370	430	
	Film	360	441	0.5 ± 0.1
126	Toluene	361	409, 429	1.0 ± 0.1
FSF_FF	Chloroform	361	422	
	Film	360	435	0.7 ± 0.1
138	Toluene	371	414, 433	0.8 ± 0.1
F-$S(OR)_2$-F	Chloroform	372	423, 440	
	Film	375	443	0.5 ± 0.1
139	Toluene	364	406, 427	0.9 ± 0.1
S(OR')-F-S(OR')	Chloroform	364	420	
	Film	374	435	0.14 ± 0.05
140	Toluene	368	408, 429	0.7 ± 0.1
S(OR')-$S(OR)_2$-S(OR')	Chloroform	355	408	
	Film	408	428	0.72 ± 0.05
141	Toluene	350	396, 414	0.7 ± 0.1
Planar Ar-S-Ar	Chloroform	355	425	
	Film	353	423	0.1 ± 0.05
142	Toluene	325, 360	390, 410	0.38 ± 0.05
Ar-S-Ar	Chloroform	325, 360	418	
	Film	360	429	0.4 ± 0.1

Table 2.1 – Selected photophysical properties of F/S trimers

2.3 Conclusions

A successful route to 2,8-difluorodibenzothiophene-*S*,*S*-dioxide has been developed based on the lithiation of bis(4-fluorophenylsulfone) followed by an *in situ* copper(II)chloride mediated cyclisation reaction. This product can be successfully brominated to afford 3,7-dibromo-2,8-difluorodibenzothiophene-*S*,*S*-dioxide which has been incorporated into oligo-/poly-fluorene backbones to produce materials which show bright, deep blue fluorescence with high efficiencies. The very high PLQY value of the resultant trimer indicates the potential of this

building block in materials for OLED applications with particular regard to blue light emission. This trimer was studied as part of a series of substituted **S**-based oligomers in which the backbones of the oligomers were either twisted or planarised in comparison to the "parent" **FFF** and **FSF** systems. The formation of the ICT band from the interaction between donor **F** and acceptor **S** was not prevented by the twisted architectures, but it was found to be stabilised by a planarised conformation. This provides evidence for the theory that in these **F**/**S** systems the ICT interaction can be described by a planarised intramolecular charge transfer (PICT) model. Thus the donor-acceptor interactions in these very promising OLED-related systems have been further explored and understood.

Chapter 3: Exploiting ICT Emission From Ambipolar Systems Based on Dibenzothiophene-*S*,*S*-dioxide

3.1 Introduction

In chapter 2 the origin of the dual emission band seen in **F/S** systems was investigated by the design and synthesis of novel functionalised **S** units for incorporation into fluorene-based co-oligomers and co-polymers with twisted/planarised backbones. In this chapter ICT interactions in D-A systems based on **S** will be further probed by varying the donor units and the extent of conjugation through the systems. Tuning of the emission colour from deep blue to green in D-A oligomers will be presented (section 3.2) as well as work demonstrating how these systems can be applied to white light-emitting OLEDs (section 3.3) and how they are being used to investigate the unusual phenomenon of all-organic phosphorescence (section 3.4).

3.2 Tuning the ICT emission from deep blue to green by manipulation of conjugation and strength of the electron donor units

3.2.1 Introduction

In this section the synthesis, photophysical and computational properties of a series of novel ambipolar trimers incorporating **S** is described. The objective was to tune the emission properties by combining the strategies of conjugation control (varying the substitution pattern between donor and acceptor) and varying the redox potential of the donor unit, i.e. donor strength, comparing fluorene, carbazole and arylamine.

As discussed in Chapter 1, polyfluorene-based systems have been extensively investigated due to their utility as blue emitters, with fluorene-based co-polymers and co-oligomers emitting deep blue light with high efficiencies both in solution and the solid state.[95] The use of **S** in polyfluorene-type systems increases the electron transport properties of the materials and a number of ambipolar oligomers and polymers have been synthesised which show potential for use in OLED applications.[65,68-71,73,88,93,96]

In the previous chapter the ICT state in **F/S** systems was probed by synthesising new functionalised **S** units for incorporation into trimers and polymers. An alternative strategy for probing the ICT state is to increase the strength of the donor unit. Carbazole (**cbz**) has been widely investigated for OLED applications (see reviews from Morin *et al*.[97] and Boudreault *et al*.[98]) and is a stronger electron donor than fluorene. Similarly, the use of arylamine units in

OLED-related materials is well documented mainly due to their high hole transporting ability.[99] This ability makes arylamine units attractive candidates for incorporation into polymers and/or oligomers with bipolar charge transport characteristics. Small molecule systems have been demonstrated which include **S** as an acceptor and triphenylamine (**TPA**)/diphenylamine (**DPA**) donor moieties for OLED applications (**143**, **144**).[73,74] Huang *et al*. reported strong ICT from donor amine units to acceptor **S** in the two trimers shown in Figure 3.1.[74] An OLED device fabricated using trimer **144** as the emissive material showed good performance for a small molecule device (EQE 3.1%, 3.9 lm W^{-1} and 7.5 cd A^{-1} at 100 mA cm^{-2}).[74]

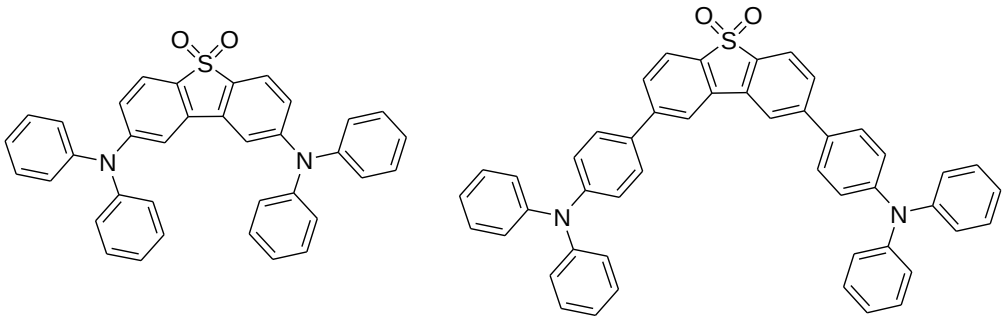

143 **144**

Figure 3.1 – Structures of arylamine-S-arylamine trimers

Kulkarni *et al*. demonstrated that careful choice of donor and acceptor units could control HOMO/LUMO levels and hence vary the emission colour of ambipolar molecules.[100] ICT effects were found to be more pronounced when using a stronger phenothiazine-based donor (**145**, Figure 3.2) compared to a weaker carbazole-based donor (**146**, Figure 3.2), with phenylquinoline acceptor units was reported in A-D-A trimers.[100] The thin film emission from **145** was significantly red-shifted compared to **146** (~ 98 nm), attributed to the increased amount of ICT emission.[100] Greater positive solvatochromism was also noted in the more strongly donating system.

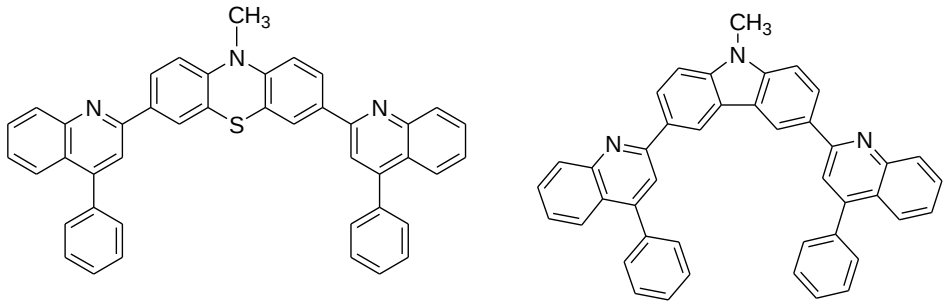

145 **146**

Figure 3.2 – Structure of A-D-A trimers with varying donor units

Another method for controlling the amount of ICT emission in D-A systems is to vary the extent of conjugation through the system. Manipulation of conjugation was a strategy

employed by Brunner *et al*., whose aim was to tune the triplet levels of carbazole-based oligomers in order to achieve OLED host materials.[101] Their work was also expanded to polymeric systems where the triplet energy of a carbazole-fluorene type co-polymer was increased from 2.3 eV to 2.6 eV purely by changing the substitution pattern of the monomer units.[102] Chen *et al*. also reported that it was necessary to control the conjugation lengths of fluorene/carbazole co-polymers in order to maintain high triplet levels and demonstrated tuning of the HOMO/LUMO levels through substitution at the 9-position of carbazole.[103] The extent of conjugation should have an effect on the extent of the ICT emission seen in D-A systems as this depends on the communication between donor and acceptor. As demonstrated from work discussed in section 2.1, substituting **S** units with hexyl chains and incorporating them into fluorene co-polymers affects both the triplet levels (through reduced conjugation) and the amount of ICT emission observed, compared with unfunctionalised **S** unit co-polymers.[88]

While our work was in progress Estrada and Neckers reported ambipolar 2,7- and 3,6-disubstituted fluoren-9-ylidene malonitrile derivatives (**147**, **148**, Figure 3.3) with the aim of investigating the extent of electronic communication between these substitution positions and the C_9 position of fluorene.[104] Their work suggests effective electronic communication between the 3,6- positions and C_9. However, unlike the **F/S** systems, the ICT state in these systems was reported to be one of the *non-radiative* deactivation pathways (i.e. *non-emissive*), with the carbazole-based 3,6-disubstituted oligomer (**148**) showing total emission quenching in polar solvents such as ethyl acetate and dichloromethane.[104] This compound displayed efficient charge separation (from photophysical and computational studies) in moderate to high polarity solvents which the authors claim will aid in the search for novel materials as candidates for electron transfer systems which require efficient charge separation.[104]

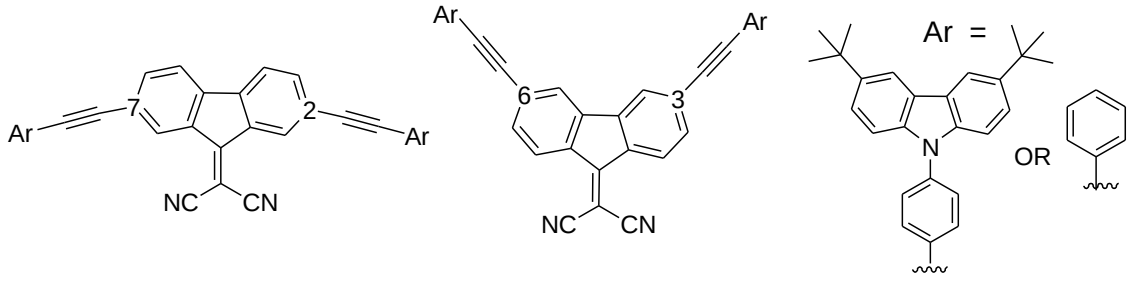

147 **148**

Figure 3.3 – Structure of D-A-D trimers linked through different positions on the acceptor

The work presented in this section aims to combine these strategies in order to investigate the effect on the ICT emission of systematically varying the donor unit from fluorene (**F**) to carbazole (**cbz**) to arylamine (**ArN**) in **S**-based trimers, as well as changing the substitution pattern between donor and acceptor moieties.

3.2.2 Results and Discussion

A series of **cbz**-**S**-**cbz** trimers and their analogous **F**-**S**-**F** trimers were synthesised by palladium-catalysed Suzuki-Miyaura coupling conditions (Schemes 3.1 – 3.3). The 3,7-dibromo- (linear) and 2,8-dibromo-substituted (bent) **S** units (**87**) and (**89**) were synthesised according to previously reported procedures (see chapter 7 for full synthesis details). The carbazole boronic acid derivatives (**151** and **157**) were synthesised in good yields from their brominated precursors (**150** and **156** respectively), by a sequence of lithiation, borylation and hydrolysis. The 2-ethylhexyl substituent at the 9-position of the carbazole was chosen to enhance solubility. The cross-couplings were performed using either dichlorobis(triphenylphosphine) palladium(II) or tetrakis(triphenylphosphine)palladium(0) as the catalyst to afford the trimers **152**, **153**, **154**, **158**, **126** and **159** in moderate to good yields as white or yellow solids (see chapter 7 for full synthesis details; the synthesis of trimer **126** was discussed in Chapter 2).

The *N*-substituted trimers (**161**) and (**162**) were synthesised by palladium-catalysed C-N cross-coupling reactions of carbazole (**160**) with either “linear” or “bent” dibromo-**S** (Scheme 3.4). The low solubility of these products makes reaction and work up difficult and the trimers were obtained in low yields as amorphous solids with high melting points (> 350 ˚C). The diphenylamine (**DPA**) analogue (**164**) was also synthesised in this way (Scheme 3.5). The triphenylamine (**TPA**) analogue was synthesised by a different route whereby the diboronic ester **S** derivative (**165**) underwent Suzuki cross-coupling with **166** to give the TPA-based trimer (**167**). Both arylamine-based trimers are bright yellow solids with good solubility due to the *n*-butyl substituents.

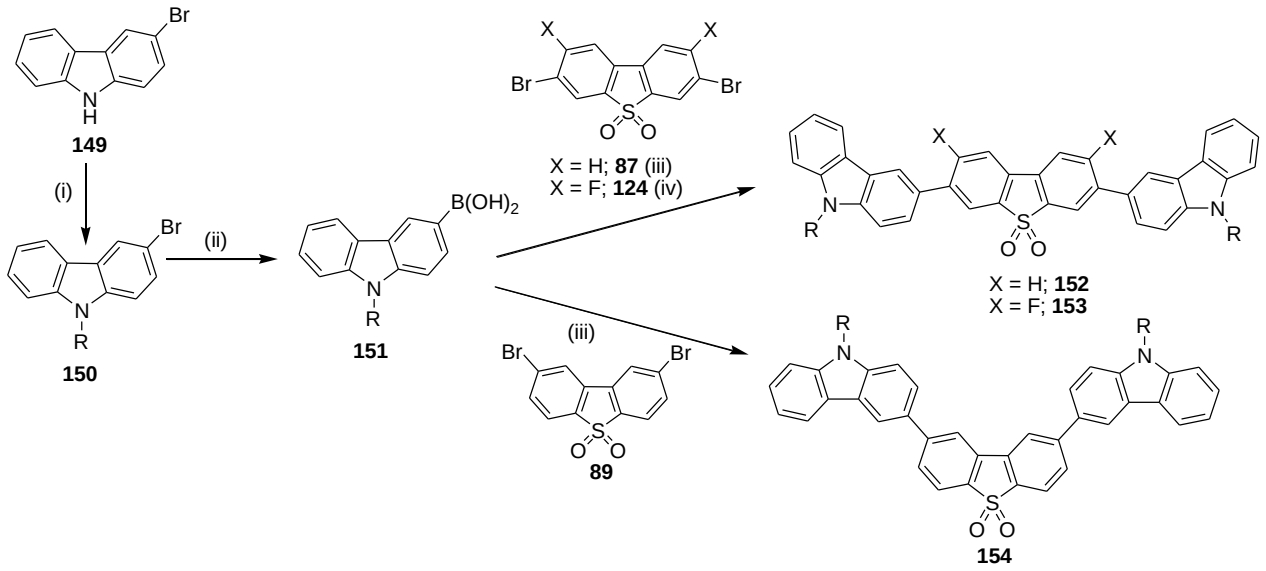

Reagents and conditions: (i) 2-ethylhexyl bromide, KO^tBu, DMF, 130 ˚C, 63%; (ii) ^nBuLi, $(^iPrO)_3B$, NH_4Cl (aq), THF, - 78 ˚C to 20 ˚C, 61%; (iii) $Pd(PPh_3)_4$, Na_2CO_3 (aq), 1,4-dioxane, 85 ˚C, 82% for **152**, 74% for **154**; (iv) $Pd(PPh_3)_2Cl_2$, K_2CO_3 (aq), 1,4-dioxane, 110 ˚C, 50%. *NB. R = 2-ethylhexyl*

Scheme 3.1 – Synthesis of cbz-S-cbz trimers
(Compound **153** synthesised by Dr. V. Bhalla)

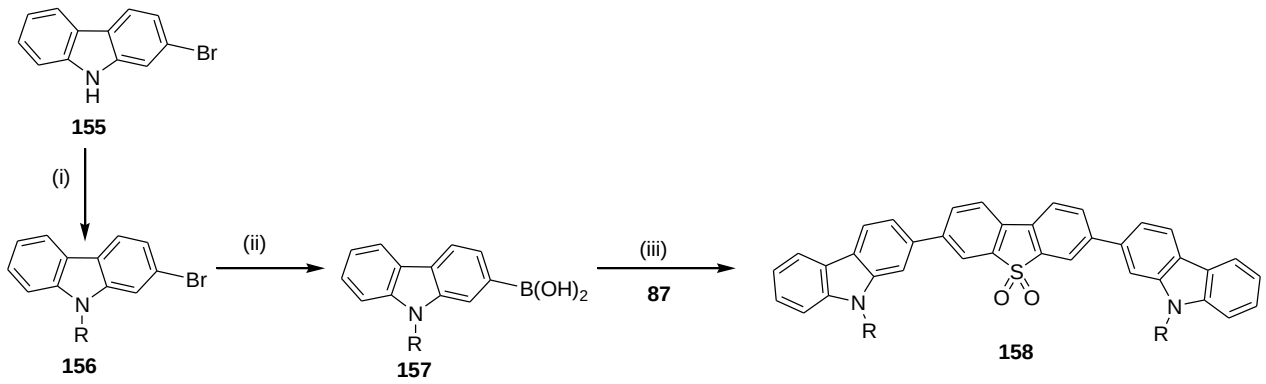

Reagents and conditions: (i) 2-ethylhexyl bromide, KO^tBu, DMF, 130 ˚C, 80%; (ii) ^nBuLi, $(^iPrO)_3B$, conc. HCl, THF, - 78 ˚C to 20 ˚C, 67%; (iii) **87**, $Pd(PPh_3)_2Cl_2$, K_2CO_3 (aq), 1,4-dioxane, 110 ˚C, 78%. *NB. R = 2-ethylhexyl*

Scheme 3.2 – Synthesis of meta substituted cbz-S-cbz trimer
(Compounds **155**-**158** synthesised by Dr. V. Bhalla)

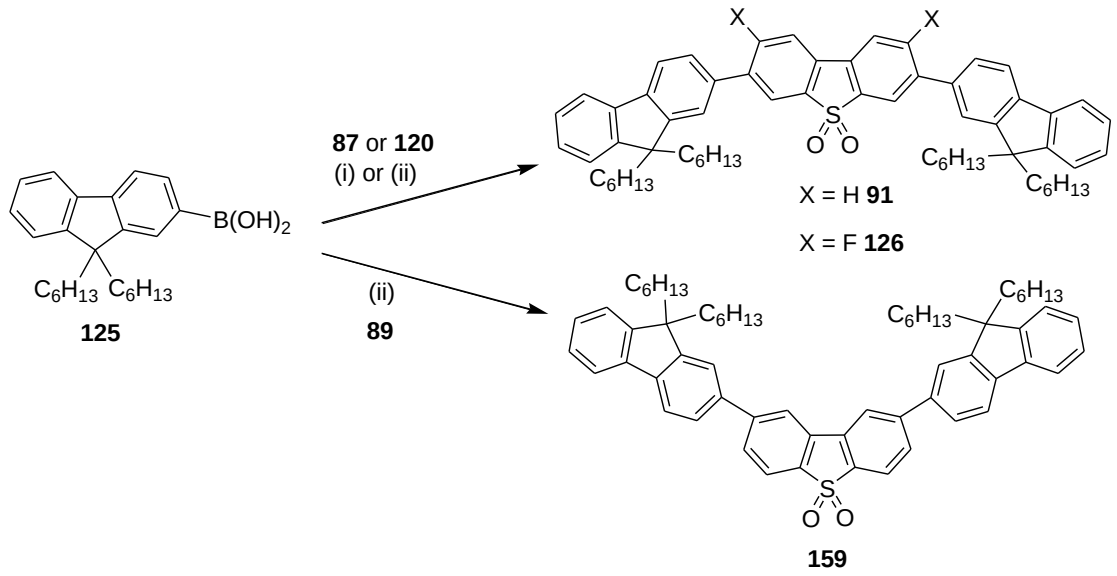

Reagents and conditions: (i) **87**, $Pd(PPh_3)_2Cl_2$, K_2CO_3 (aq), 1,4-dioxane, 110 ˚C, 86% for **91**; (ii) **120** or **89**, $Pd(PPh_3)_4$, Na_2CO_3 (aq), 1,4-dioxane, 85 ˚C, 50% for **126**, 21% for **159**.

Scheme 3.3 – Synthesis of F-S-F trimers
(Synthesis of compound **91** reported previously[65])

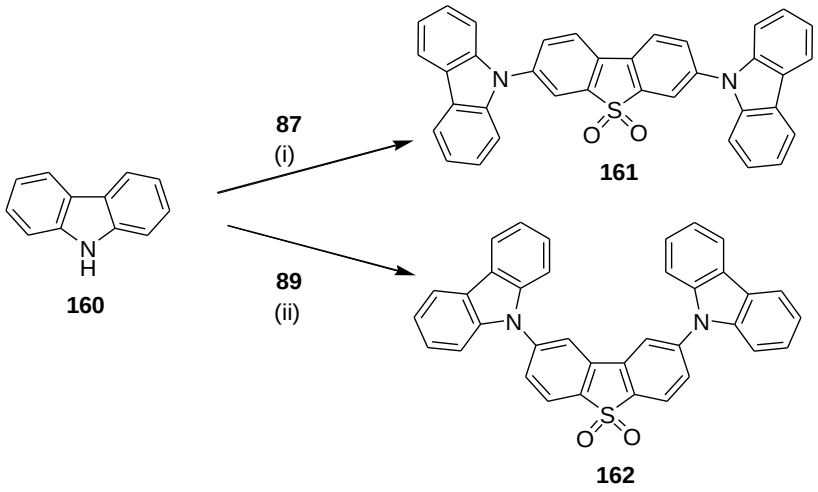

Reagents and conditions: (i) **87**, $Pd_2(dba)_3$, xphos, NaO^tBu, ^tBuOH, toluene, 110 ˚C, 24%; (ii) **89**, $Pd_2(dba)_3$, $^tBu_3PHBF_4$, NaO^tBu, ^tBuOH, toluene, 110 ˚C, 20%.

Scheme 3.4 – Synthesis of N-substituted cbz-S-cbz trimers

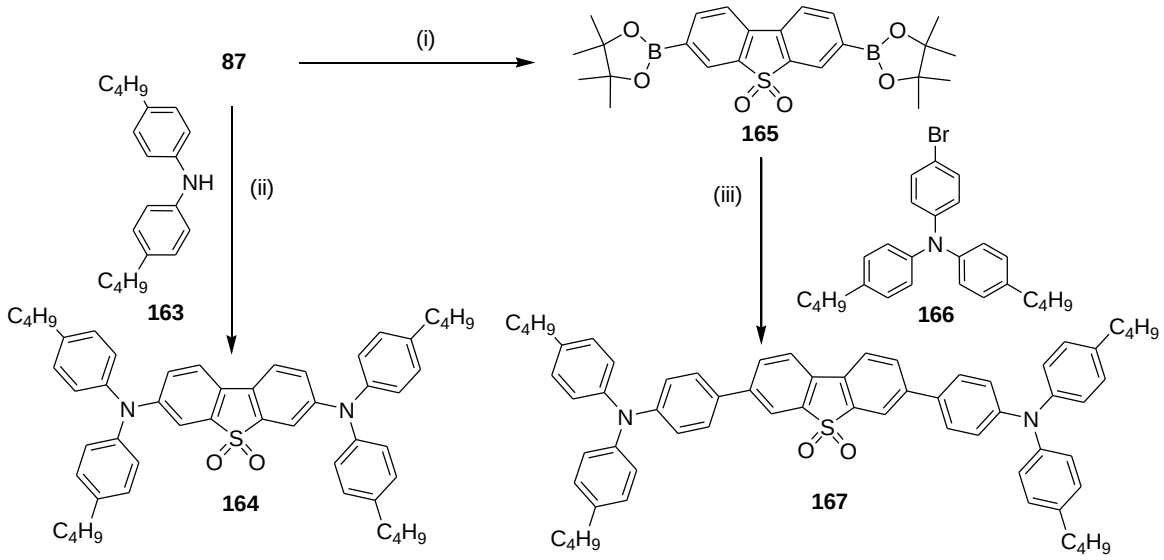

Reagents and conditions: (i) B_2pin_2, $Pd(dppf)_2Cl_2$, KOAc, DMF, 90 ˚C, 26%; (ii) $Pd_2(dba)_3$, $^tBu_3PHBF_4$, NaO^tBu, toluene, 107 ˚C, 44%; (iii) $Pd(PPh_3)_2Cl_2$, K_2CO_3 (aq), toluene, 110 ˚C, 33%.

Scheme 3.5 – Synthesis of ArN-S-ArN trimers
(Compounds **163**-**167** synthesised by Dr. K.T.Kamtekar)

Cyclic voltammetry measurements were carried out on all the trimers; selected scans are shown in Figures 3.4(a) – (d) (for other scans, see Appendix I) and the full results are summarised in Table 3.1. The carbazole-based trimers show irreversible oxidation waves at ~ 0.8 – 1.0 V, similar to those typically seen for carbazoles.[101] These potentials are lower than those of the reversible oxidation waves observed at ~ 1.2 – 1.4 V for the fluorene-based trimers. Even lower oxidation potentials at ~ 0.4 V are seen for the arylamine-based trimers. These data are consistent with the expected decrease in oxidation potential as the electron donor strength increases from fluorene to carbazole to arylamine. The **TPA**-substituted trimer (**167**) shows a reversible two-electron oxidation wave (Figure 3.4(c)), indicating that oxidizing one amine group has little influence on the oxidation of the other amine group. In contrast, **DPA**-substituted trimer (**164**) shows two well separated one-electron reversible oxidation waves (Figure 3.4(d)), indicating that in this case oxidation of one amine group does have an influence on the oxidation of the other amine group, suggesting significant conjugation across the linear **S** unit. The reduction potentials observed for the reversible waves of these trimers are within the range ~ - 1.9 to - 2.4 V, arising from the one-electron reduction of the **S** unit. The two fluorinated trimers (**153** and **126**) are more easily reduced than their non-fluorinated analogues (by ~ 0.1 – 0.3 V) in accordance with their more strongly electron-accepting **S** units. These data demonstrate the ambipolar nature of all the trimers and show how the donor strength increases from fluorene to carbazole to arylamine.

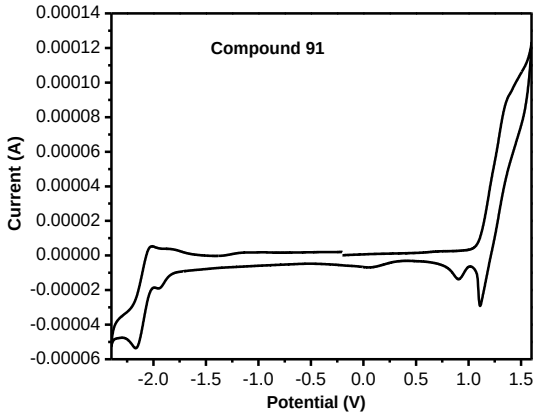

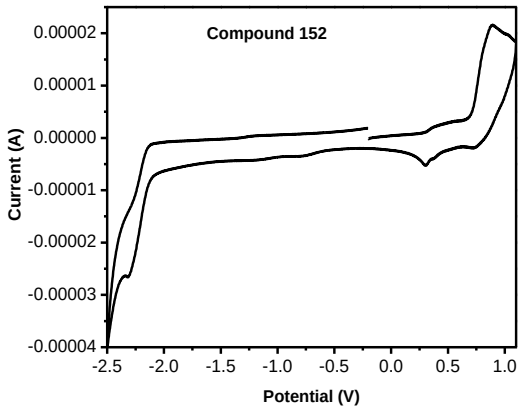

Figures 3.4(a) and (b) – CV scans of compounds 91 (a) and 152 (b)
(referenced to the ferrocene/ferrocenium couple)

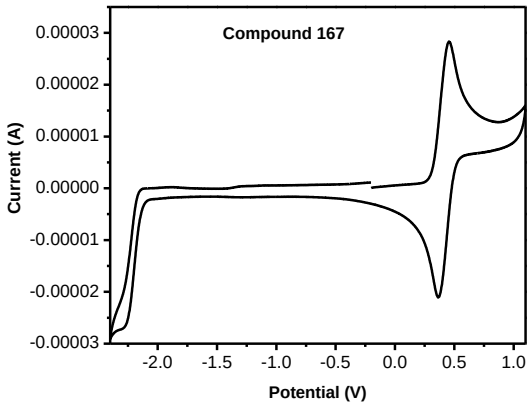

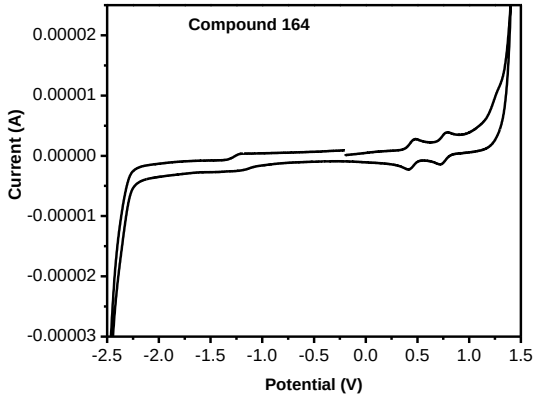

Figures 3.4(c) and (d) – CV scans of compounds 167 (c) 164 (d)
(referenced to the ferrocene/ferrocenium couple)

Compound	Donor	Acceptor	E_{ox} (V) [a,b]	E_{red} (V) [a]
91	F	Linear **S**	1.20	- 2.17
152	3-Cz	Linear **S**	0.83 [c]	- 2.23
153	3-Cz	Linear **S** (F_2)	1.04 [c]	- 2.14
154	3-Cz	Bent	0.75 [c]	- 2.22
158	2-Cz	Linear **S**	0.81 [c,d]	- 2.13
126	F	Linear **S** (F_2)	1.39	- 1.91
159	F	Bent **S**	1.24	- 2.26
161	N-Cz	Linear **S**	0.96 [c,d]	- 2.18
162	N-Cz	Bent **S**	0.94 [c,d]	- 2.19
164	DPA	Linear **S**	0.40 [e]	- 2.39
167	TPA	Linear **S**	0.45	- 2.20

[a] $E_{1/2}$ values with reference to the ferrocene/ferrocenium couple at 0.00 V using 0.2 M NBu_4PF_6 in DCM. [b] Poorly defined oxidation wave arising from two simultaneous one-electron oxidation processes in most cases. [c] Irreversible; $E_{1/2}$ values estimated from deconvolution data. [d] Irreversible reduction wave at ~ -2.0 V observed after oxidation. [e] Well-defined one-electron reversible wave with second reversible wave at 0.70 V.

Table 3.1 – Electrochemical data for the trimers

Compound	λ_{abs} (nm) PhMe	ε ($M^{-1}cm^{-1}$) PhMe	λ_{abs} (nm) $CHCl_3$	λ_{PL} (nm) PhMe	λ_{PL} (nm) $CHCl_3$	Φ_{PL} PhMe	λ_{ex} (nm) for Φ_{PL}
91	344	55800	352	412[a]	427[a]	0.90 ± 0.10	380
	366	57100	367	433	440		
152	355	35900	355	433[a]	458	0.45 ± 0.05	380
	379	34900	382	450			
153	352[b]	30700	357	432[a]	454	0.58 ± 0.05	380
	377	36300	387	450			
154	299	62800	300	408	438	0.25 ± 0.10	360
	340	27000	355				
158	339	38800	339	420[a]	438	0.55 ± 0.05	380
	370	53000	371	440			
126	360	49100	362	411[a]	425[a]	1.00 ± 0.10	380
				429	440		
159	300	47000	300	377	409	0.59 ± 0.05	320
	320	43700	326	387[a]			
161	338	18850	350	431	454	0.57 ± 0.10	380
	379	14760	384	442[a]			
162	323	13000	322	424	456	0.26 ± 0.10	360
	336	16500	334				
	351[b]	9100	354[b]				
164	298	20600	296	482	516	0.60 ± 0.05	375
	380	33600	380				
	428[b]	13440	436[b]				
167	300	35100	302	471	520	0.75 ± 0.05	375
	411	40500	418				

[a] highest maxima, [b] shoulder

Table 3.2 – Photophysical properties of the trimers

Photophysical studies were carried out on all the trimers and the results are summarised in Table 3.2, showing the absorption and emission data for the compounds in toluene and chloroform, as well as PLQY values. As for the **F/S** systems, all the trimers show red-shifted ICT emission in more polar solvents; chloroform compared to toluene. A progressive red-shift in

absorption and emission is also seen with increasing donor strength from fluorene to carbazole to arylamine, e.g. λ_{PL} ($CHCl_3$) for **FSF** (**91**) 427 nm; λ_{PL} ($CHCl_3$) for **cbz-S-cbz** (**152**) 458 nm; λ_{PL} ($CHCl_3$) for **TPA-S-TPA** (**167**) 520 nm. The fluorene-based trimers emit deep blue fluorescence, which becomes sky blue for carbazole-based trimers and green for arylamine-based trimers (Figure 3.5)

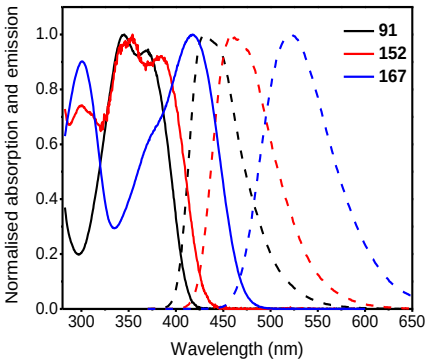

Figure 3.5 – Absorption and emission of selected trimers in chloroform

All of the trimers show positive solvatochromism in their PL spectra due to ICT emission, thus the emission colour can be tuned by varying solvent polarity. As previously discussed, **FSF**-type trimers show structured LE emission in toluene (two band values quoted in Table 3.2), which becomes a broad red-shifted single (ICT) emission band in chloroform. The linear cbz-based trimers behave in a similar way with a structured LE emission seen in toluene and a broad ICT emission seen in chloroform. However, for the bent trimers this structured LE emission in toluene is no longer seen, instead a single emission band is observed (Figure 3.6).

When comparing the bent vs. linear trimers some clear differences arise: bent trimers lack the fine structure in toluene seen in the linear trimers; the peak emission values are blue-shifted for the bent trimers compared to their linear analogues and there is a larger positive solvatochromic shift in the emission bands going from toluene to chloroform for the bent compounds. These differences relate to the extent of ICT character in the systems; compounds with strong ICT character are the bent trimers **154**, **159** and **162**; compounds with weaker ICT character are the linear trimers **91**, **152**, **153**, **158**, **126** and **161**. The linear arylamine-based trimers (**164**) and (**167**) are intermediate in their ICT character due to the strong donating ability of **DPA** and **TPA**.

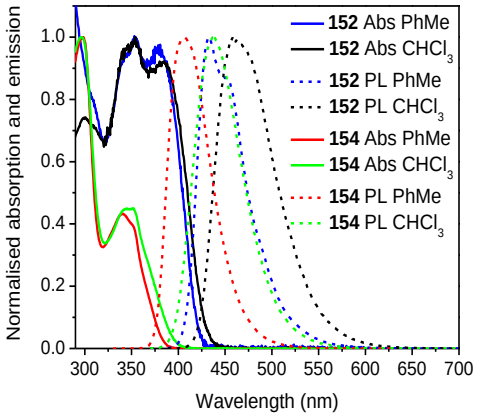

Figure 3.6 – Absorption and emission of linear cbz-S-cbz (152) compared to its bent analogue (154)

In order to compare the relative ICT strengths between a bent and linear system, the emission and absorption peak maxima in different solvents were recorded for **154** as this bent cbz-based trimer is representative of a trimer with strong ICT character. Figure 3.7 shows the solvatochromic study of this compound. These data were then compared to data previously obtained for the linear **FSF** trimer (**91**) which is representative of a trimer with weak ICT character. Figure 3.7 shows that the emission spectra are strongly red-shifted and broadened as the solvent polarity is increased from MCH to methanol, a typical feature of ICT excited states. The vibronic structure of the emission spectrum can be seen in MCH, but not in any of the more polar solvents.

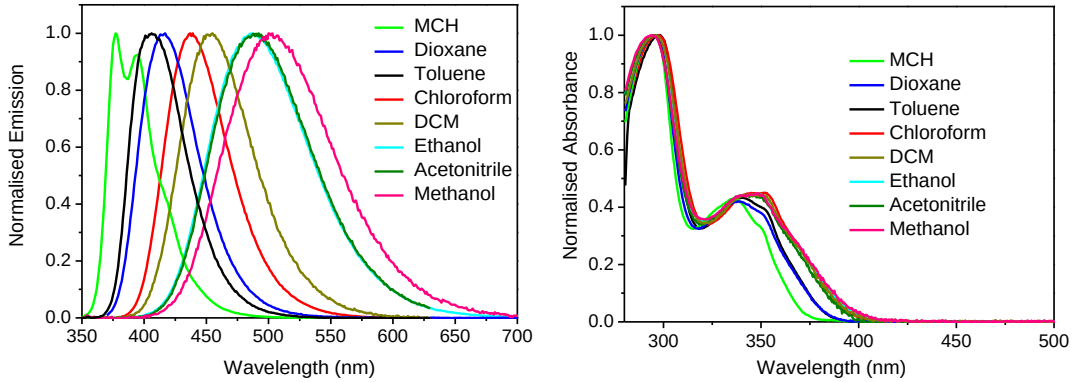

Figure 3.7 – Emission and absorption spectra of bent cbz-S-cbz trimer (154) in various solvents

By plotting the wavelengths of the emission maxima in the various solvents as a function of the solvent orientation polarizability, given by the Lippert-Mataga equation (equation 3.1), the corresponding Lippert plot can be obtained (Figure 3.8).

$$\Delta f = (\varepsilon - 1) / (2\varepsilon + 1) - \tfrac{1}{2}((n^2 - 1)/(2n^2 + 1)) \qquad \text{(eqn 3.1)}$$

Figure 3.8 shows the Lippert plots for the bent **cbz-S-cbz** (**154**) and the linear **FSF** (**91**) trimers. From these plots it can be seen that spectral shifts of emission with solvent polarity follow an approximately linear trend in both cases. The fact that aprotic solvents, such as dichloromethane and acetonitrile, are included demonstrates that the shifts observed are due to solvent polarity rather than hydrogen bonding. The negative slopes of the plots indicate that the excited state dipole moments are larger than the ground state dipole moments. The steeper slope for the bent trimer indicates a larger difference between the dipole moments of the ground and excited states, suggestive of greater charge separation in the excited state for the bent trimer compared with the linear trimer. A qualitatively similar result was also found by Estrada *et al*. when comparing carbazole-containing fluoren-9-ylidene malonitrile derivatives (**147**, **148**, Figure 3.3).[105] When the carbazole substituents were in the 3,6-position (i.e. "bent"), the difference between S_1 and S_0 state dipole moments was much larger than when the substituents were in the 2,7-position (i.e. "linear"). It was reported that there was a more favourable path for electron transfer through the trimers in the 2,7-disubstituted derivatives.[105]

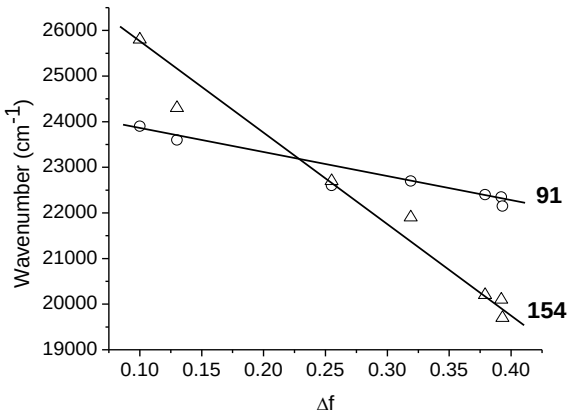

Figure 3.8 – Lippert plots for bent Cbz-S-Cbz (154) and linear FSF (91)

The blue shift in emission of our bent trimers compared with their linear analogues can be explained in terms of π–conjugation through the systems. For example, in the linear **cbz-S-cbz** trimer (**152**), four rings are in conjugation, whereas in the bent trimer (**154**), only two rings are in conjugation. Figure 3.1 shows the structure of two previously reported trimers **143**, **144** which can be considered to be bent analogues (without the butyl chains) of **DPA** and **TPA**-based linear trimers **164** and **167**.[74] The reported emission of these trimers in toluene is blue-shifted from the linear compounds, following the same trend as the **F**-based and **cbz**-based trimers. A similar trend was observed by Grisorio *et al*. who, during the course of our work, reported the N-methyl analogues of cbz-based trimers **152** and **154**.[75] Due to the lack of solubility imparted by the methyl groups (in contrast to our 2-ethylhexyl) no solvatochromic

studies were reported; however, it was noted that the bent trimer gave more blue-shifted emission in chloroform than the linear trimer, attributed to a reduced conjugation effect.[75]

In order to further investigate the conjugation effects in the trimers, ground state (S_0) geometry optimizations were carried out on the trimers at the B3LYP/6-311G** level of theory. Methyl chains were used instead of 2-ethylhexyl or *n*-butyl for ease of computation. Figure 3.9 shows the frontier molecular orbitals for the linear and bent **cbz**-**S**-**cbz** trimers (i.e. N-methyl analogues of **152** and **154**).

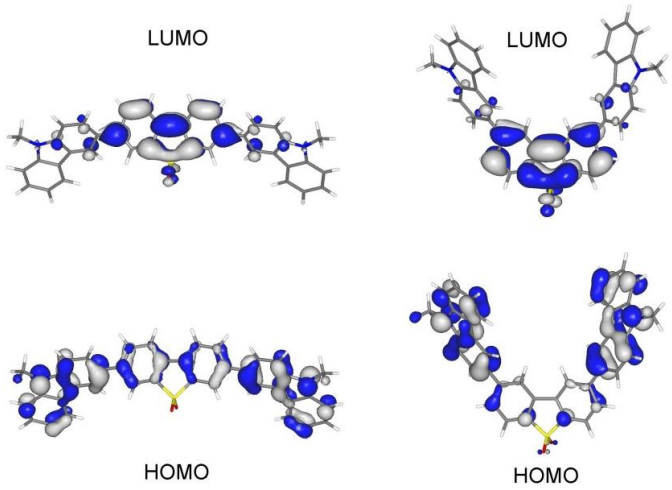

Figure 3.9 – Frontier molecular orbital plots for linear and bent cbz-S-cbz trimers
(Computations performed by Dr. M. Fox)

These plots show that in both trimers the LUMO remains localised on the **S** unit acceptor. However, in the linear trimer the HOMO is delocalised throughout the molecule, whereas in the bent trimer the HOMO is localised on the donor units. These plots are representative of the other linear vs. bent trimers, i.e. for linear trimers there is a delocalised HOMO, whereas for bent trimers the HOMO remains localised on the donor units. These data support the photophysical results that bent trimers have more blue shifted emission (due to reduced conjugation) and increased charge separation in the excited state. The same effect was reported by Estrada and Neckers for the ambipolar 2,7- and 3,6-disubstituted fluoren-9-ylidene malonitrile derivatives discussed in section 3.2.1 (**147**, **148**, Figure 3.3).[104] In the linear systems, the HOMO was delocalised over the molecule, whereas in the bent systems, the HOMO was localised on the donor units and efficient charge separation was reported.[104]

3.2.3 Conclusions

Donor-acceptor-donor **S**-based oligomers have been synthesized where the donor strength has been increased in the series fluorene → carbazole → arylamine. Photophysical properties have been investigated, with particular emphasis on probing the charge transfer character of the singlet excited state. The substitution of fluorene by carbazole red-shifts the emission from deep blue to sky blue, becoming green for arylamine-based trimers. The effect of conjugation between donor and acceptor units has also been investigated and it is demonstrated that "bent" trimers i.e. where the donor is *para*-conjugated to the sulfone have increased CT character compared to their linear analogues. Bent trimers also exhibit blue-shifted emission (due to reduced conjugation) compared to linear trimers, and hence show increased charge separation in the excited state.

Overall we have demonstrated that ICT emission in D-A systems can be systematically tuned by varying the redox potentials of the donor and/or acceptor units, as well as by changing the conjugation pattern between donor and acceptor. The results demonstrate promising strategies for exploiting ICT states in ambipolar oligomers for various optoelectronic applications.

3.3 Enhancing ICT emission for white light-emitting polymeric OLEDs

3.3.1 Introduction

In the previous section it was demonstrated how the ICT emission in trimers based on **S** can be tuned from deep blue to green in the visible spectrum. The ambipolar nature of the trimers was also demonstrated, a key requirement for device applications. In this section the expansion to polymers of these systems is discussed and how the incorporation of additional fluorescent dopants adapts the systems to white light emission.

One of the key objectives for OLED research is white light emission (WOLEDs) either for use as solid state lighting or for displays. Current light sources including the incandescent bulb as well as fluorescent tube lighting have many drawbacks. Incandescent bulbs lose ~ 95% of their energy as heat rather than light with very low power efficiencies.[1] Fluorescent tube lighting is more efficient but can have problems such as reduced lifetimes as they are constantly switched on and off. Fluorescent lighting has a low colour rendering index (CRI) which is a measure of how true the colour of an object appears under that light source. Additionally, the small levels of mercury which fluorescent tube lights contain make them an environmental hazard for disposal.[1] As a result of this and the fact that worldwide demand for lighting is ever

increasing (currently ~ 19% of total global energy consumption), new, more energy efficient light sources must be developed.

There are a number of different characteristics used to assess the quality of a white light source: (i) the Commission Internationale d'Eclairage (CIE) coordinates which locate the emission colour on the chromaticity diagram shown in Figure 3.10; the colour rendering index (CRI); the colour correlated temperature (CCT) which is the temperature of a black body radiator emitting the same colour of the light source (shown as the black curve on the CIE diagram).[106] The white point of the CIE diagram is given by coordinates (0.33, 0.33). However, there is an area around this point which is still considered white light as different markets require different types of white, e.g. cooler white (further into the blue) or warmer white (further into the red). For lighting, the CRI should be around 90 – 100, with CCT values in the range 2500 – 6500 K.[106]

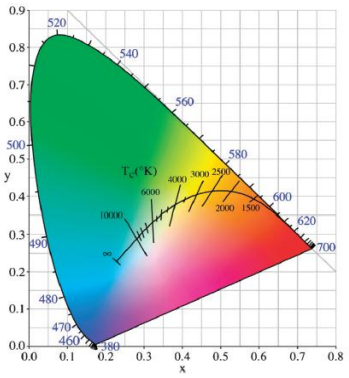

Figure 3.10 – The CIE diagram showing emission colours

When describing the efficiency of devices, a number of different quantities can be quoted including: (i) the external quantum efficiency (EQE) which is essentially the ratio of photons out compared to electrons injected in; (ii) power efficiency (or efficacy), measured in lm W^{-1}, which represents the efficiency of the device taking into account the response of the human eye to the different wavelengths within the visible region; (iii) luminous efficiency, measured in cd A^{-1}, which is the ratio of the luminous intensity and the current through the device; (iv) lifetime which describes the average number of hours of constant device operation before the light intensity given out has fallen to half its original value.[1,106]

The progress and development of materials for WOLEDs has been reviewed extensively over the last few years, indicative of the intense research interest in this area.[1,106-108] As a brief summary, there are a number of different ways of achieving white light emission including: (i) multilayer devices where two or more emissive materials (small molecules) are blended

together to emit different colours which overall give white light; (ii) devices based on blends of polymers often with phosphorescent complexes as dopants; (iii) devices based on excimer emission; (iv) single polymer devices where white light is achieved from a single material in the emissive layer. The main advantage of single polymer devices is that they avoid the problems of phase segregation which frequently occurs with more than one material in the emissive layer. The solution processability of polymers over small molecules also makes them applicable to large-scale solid state lighting sources. However, they are often the most synthetically challenging as it is necessary to balance the energy levels of the different components very carefully in order to obtain white light.

To obtain white light from a single emissive polymer requires monomers capable of emitting the different primary colours which can then combine to give white light. This can either be achieved by utilising blue- and orange-emitting units within one polymer[109-111] or by combining red-, green- and blue-emitting segments.[112-114] The different colour dopants can be incorporated as side chains, e.g. Liu *et al*. covalently attached blue (B), green (G) and red (R) dopants to a PF-based host material (**168**, Figure 3.11) so that white electroluminescence (EL) could be produced.[112] Devices were presented with CIE coordinates (0.33, 0.36) with a CRI of 88, a maximum luminous efficiency of 8.6 cd A^{-1} and power efficiency of 5.3 lm W^{-1}.[112]

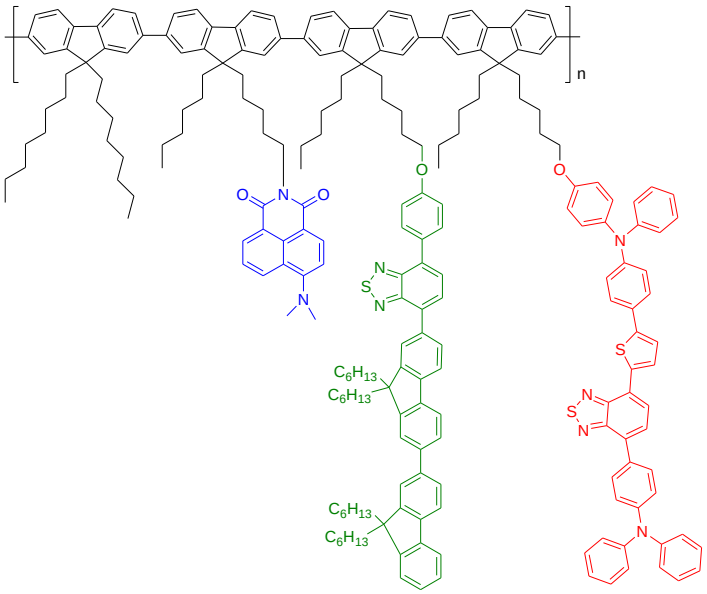

168

Figure 3.11 – Structure of white polymer with RGB side-chain dopants

Alternatively, the RGB dopants can be incorporated into the main backbone of the polymer such as the system reported from the Cao group, where PFO was used as the blue emitter, 2,1,3-benzothiadiazole (**BT**) as the green emitter and 4,7-bis(2-thienyl)-2,1,3-benzothiadiazole (**TBT**) as the red emitter (**169**, Figure 3.12).[113] By incorporating the low energy (red and green)

dopants in small amounts (e.g. < 0.3%) and in carefully controlled ratios, the dopants can become saturated leading to emission from all three components. The best device results gave a reasonable EQE of 3.84% with a luminance efficiency of 6.20 cd A^{-1} and CIE coordinates of (0.35, 0.34).[113]

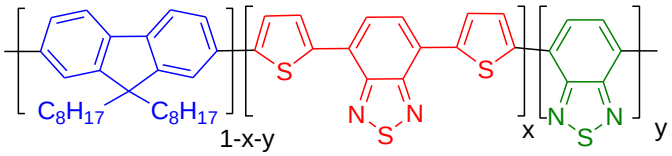

169

Figure 3.12 – Structure of white polymer with RGB dopants in the main chain

A recent paper from the Cao group introduced a set of white light-emitting polymers derived from 2,7-fluorene and 4,7-dithienylbenzotriazole (DTBTA) (**170**, Figure 3.13).[115] An alternating co-polymer of the two segments showed orange EL, however, incorporating the DTBTA in much smaller amounts (0.03 – 0.1%) allowed partial energy transfer to the low energy dopant to occur, leading to white light emission. The best device performances were achieved using a PVK inter-layer with the 0.1% co-polymer exhibiting a high luminous efficiency of 7.08 cd A^{-1} with a good EQE value of 3.29% and CIE coordinates in the white region of the spectrum at (0.30, 0.46).[115]

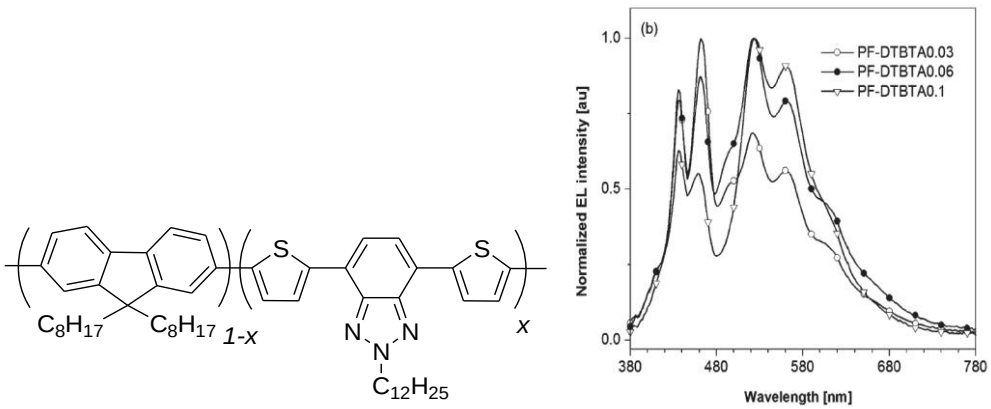

170

Figure 3.13 – Structure of white light-emitting polymer and EL spectra of devices (*x* = 0.03, 0.06, 0.1) Device architecture: ITO/PEDOT:PSS/PVK/polymer/CsF/Al

A slightly different strategy has been presented by the Bryce group for white light emission from a single polymer by exploiting the dual fluorescence characteristics of the **F/S** systems.[70] By increasing the amount of **S** in fluorene co-polymers from 2 – 30%, the EL emission colour can be tuned from blue to greenish-white (0.24, 0.41) as the red-shifted ICT band becomes stronger (Figure 3.14).[70] Incorporation of small amounts (0.1%) of the red-emitting **TBT** unit then shifts the CIE coordinates further towards the white point (0.36, 0.28).[70]

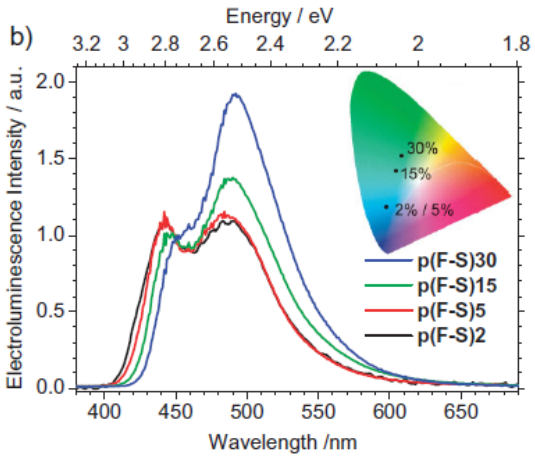

Figure 3.14 –EL spectra of F/S-based devices with increasing S content; inset shows CIE diagram[70]

3.3.2 Results and Discussion

In this section we discuss how the types of strategies described above have been applied to the ambipolar trimers discussed in section 3.2 in order to achieve white light emission. Random co-polymers of **F** and **S** have already been developed which show blue light emission (or greenish-white depending on **S** unit content).[69-71,88] However, these polymers are lacking a hole transport unit which should improve the balance of charge migration through the system (**S** is a good electron transport unit). As discussed in section 3.2, carbazoles and arylamines are very good hole transport units and the ambipolar nature of **cbz**-**S**-**cbz** and **ArN**-**S**-**ArN** trimers has been proven, therefore, expansion of these materials to polymers should give systems with well-balanced charge transport properties. For a single polymer white-emitting system, the whole of the visible light spectrum should be covered, i.e. red, green and blue. If this could be achieved as well as efficient hole transport (HT) and electron transport (ET), in theory only a very simple device structure would be required. Figure 3.15 shows a schematic of such a system, which should have advantages over those previously reported, e.g. from the Cao group, which do not have any HT units incorporated.[113]

Figure 3.15 – Schematic of single white-emitting polymer with balanced charge transport

Initially two "parent" random co-polymers were synthesised; one based on a **cbz**/**S** system (**171**) and one based on an **ArN**/**S** system (**172**). Figure 3.16 shows their structures.

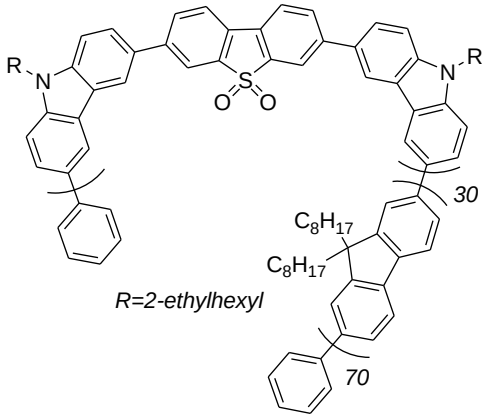

171

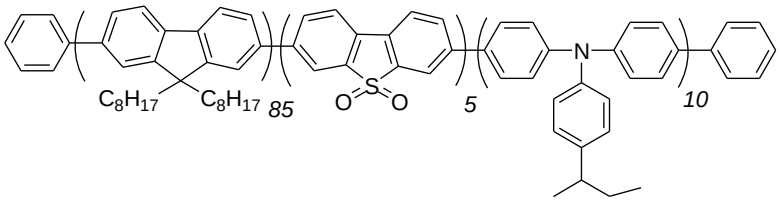

172

Figure 3.16 – Structures of "parent" cbz- and ArN-based co-polymers
(**171** synthesised by Dr. V. Bhalla; **172** synthesised by Dr. K.T.Kamtekar)

Thin films of the polymers showed emission maxima at 476 nm for **171** and 466 nm for **172** (Figures 3.18 and 3.19) which are both in the sky blue region of the spectrum (NB decreasing the amount of arylamine content to 5% (**173**) blue shifts the PL emission; maximum at 460 nm). In order to obtain white light emission, the lower energy regions of the spectrum need to be "filled in". Based on previous reports,[70,113] it was decided to incorporate the red-emitting dopant 4,7-bis(2-thienyl)-2,1,3-benzothiadiazole (**TBT**, **177**). Figure 3.17 shows the structures of all the monomer units used to synthesise these sets of polymers.

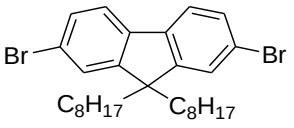

107

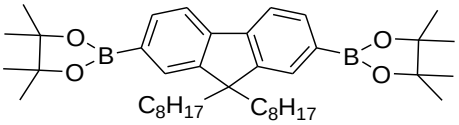

174

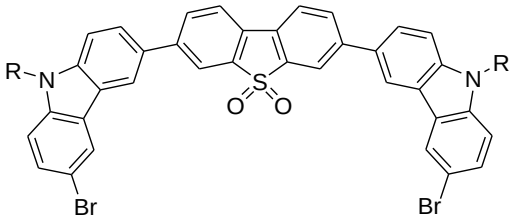

175

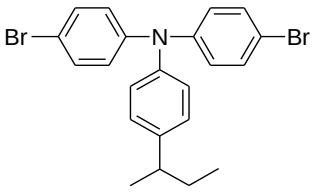

176

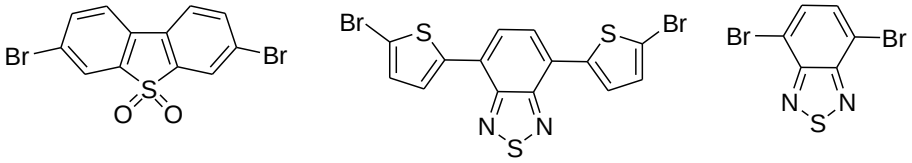

87 **177** **178**

Figure 3.17 – Structure of all monomer units used to synthesise white polymers
(**107**, **174**, **176** synthesised by Dr. K.T.Kamtekar)

The polymers were synthesised using palladium-catalysed Suzuki cross-coupling conditions: $PdCl_2[P(o\text{-}tol_3)]_2$ catalyst, degassed tetraethylammonium hydroxide solution, in toluene refluxed at 115 ˚C for 20 h and end-capped with bromobenzene and phenylboronic acid (see chapter 7 for full details). The key to achieving good quality, high molecular weight polymers is thorough purification of the monomer units, hence each of the compounds shown in Figure 3.17 was recrystallised numerous times, ideally until > 99% pure by HPLC. It is also very important to weigh out the monomer units highly accurately as any errors can have a significant impact on polymer formation and hence molecular weight.

Starting with the carbazole-based polymers, to fill in the red region of the spectrum the analogous polymer to **171** was synthesised (**179**) but with 0.050% **TBT** (only extremely low incorporations of **TBT** are needed based on previously reported systems). The thin film PL emission spectrum of this polymer (Figure 3.18) now shows the same sky blue peak at ~ 476 nm as **171** but with an additional peak at 605 nm, which is in the red region of the spectrum, as expected. The intensity of this red peak is relatively low compared with the sky blue peak, therefore, another polymer was synthesised (**180**) with 0.075% **TBT**. This polymer again shows an emission peak in the sky blue region, but now shows a higher intensity peak in the red region (maximum ~ 613 nm), which overall shows good spectral coverage of the visible region.

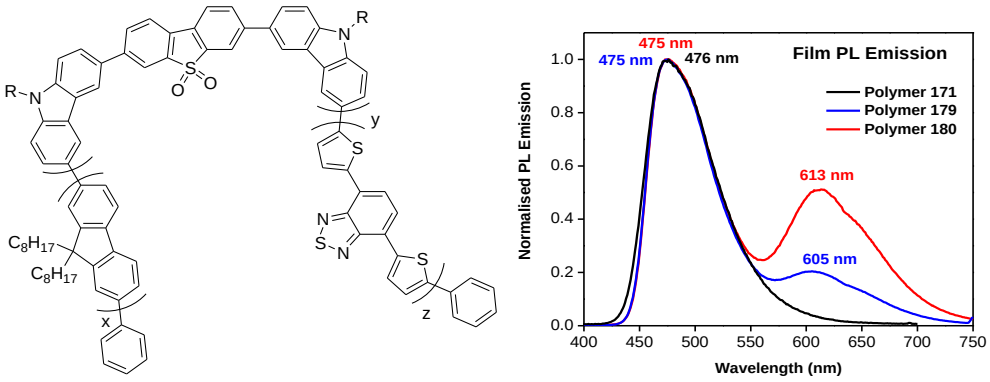

Figure 3.18 – The structure and thin film PL emission of the carbazole-based co-polymers

Table 3.3 shows the composition of the three carbazole-based co-polymers as well as the molecular weight analyses. The molecular weights of the polymers are relatively low which is attributed to the lack of crystallinity of the **cbz-S-cbz** monomer (**175**). This monomer is a fluffy yellow solid which is not at all crystalline making recrystallisation to the required level of purity extremely difficult. Thermal gravimetric analysis (TGA) indicated good thermal stability with decomposition temperatures corresponding to 5% weight loss in the range $T_{d5\%}$ 462 – 510 °C.

Polymer	x (%)	y (%)	z (%)	M_n (Da)	M_w (Da)	$T_{d5\%}$*
171	70	30	0	6,000	15,000	465
179	69.950	30	0.050	10,000	25,000	510
180	69.925	30	0.075	14,000	43,000	462

Table 3.3 – Composition and molecular weight analyses of carbazole-based co-polymers
* samples heated from 30 – 900 °C at a rate of 10 °C min^{-1}, under nitrogen

The arylamine based monomer units are crystalline and hence more easily purified to the required standard than the carbazole monomers, so it was expected that the arylamine-based polymers would have higher molecular weights. Following on from the "parent" polymer (**172**), an analogue was synthesised incorporating 0.075% **TBT** (amount chosen based on the peak intensities seen in the **cbz**-analogues), **181**. Figure 3.19 shows the thin film PL emission of the arylamine-based co-polymers. The parent polymer shows a maximum emission at ~ 466 nm, in the sky blue region of the spectrum. Adding the TBT allows a peak in the red region of the spectrum to appear, with a maximum of ~ 611 nm. Whilst **181** does show good spectral coverage there is still a gap in the green part of the spectrum (to which the human eye is particularly sensitive). The green-emitting 2,1,3-benzothiadiazole (**BT**) (a precursor in the synthesis of **TBT**) was, therefore, incorporated in a comparable amount (0.1%), **182**. As can be seen from Figure 3.19, this polymer now has a sky blue peak at ~ 465 nm, a green peak at ~ 507 nm and a red peak at ~ 607 nm and is providing broad spectral coverage of the entire visible region from ~ 425 nm to 750 nm.

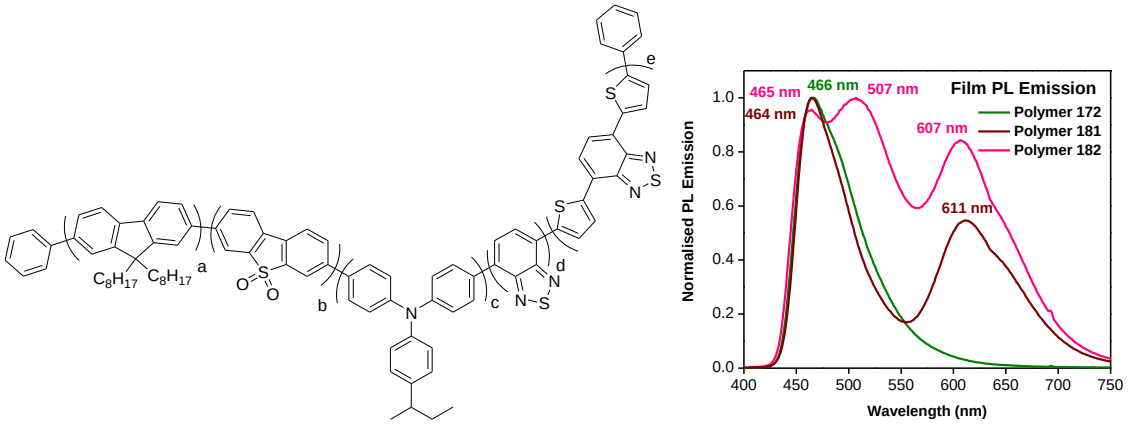

Figure 3.19 – Structure and thin film PL emission of the arylamine-based co-polymers

Table 3.4 shows the composition and molecular weight analyses for these polymers, with the predicted increase in molecular weight compared to the carbazole analogues. TGA analysis demonstrates the thermal stabilities of these polymers with decomposition temperatures corresponding to 5% weight loss in the range $T_{d5\%}$ 457 – 561 °C.

Polymer	a (%)	b (%)	c (%)	d (%)	e (%)	M_n (Da)	M_w (Da)	$T_{d5\%}$
172	85	5	10	0	0	45,000	125,000	561
181	84.925	5	10	0	0.075	48,000	138,000	457
182	84.825	5	10	0.1	0.075	47,000	139,000	472

Table 3.4 – Composition and molecular weight analyses of arylamine-based co-polymers
* samples heated from 30 – 900 °C at a rate of 10 °C min^{-1}, under nitrogen

By comparing the film PL emission of the six polymers on a CIE diagram (Figure 3.20) it can be seen how the emission is tuned from the blue across towards the central white area.

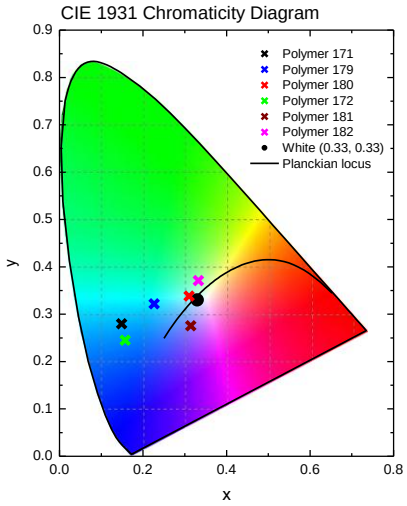

Figure 3.20 – CIE coordinates of the PL emission of the co-polymers

While these polymers show good potential as white emitters based on their PL spectra, it is important to look at their performance once incorporated into WOLEDs. Devices were fabricated by Mr. Gareth Griffiths, Department of Physics, Durham University. Polymer **182** was chosen due to its high molecular weight and broad PL spectral coverage. Initial devices based on a single layer structure were fabricated which emitted light across the visible spectrum from ~ 400 nm to ~ 750 nm. Figure 3.21 shows a photograph of a single layer device based on this polymer under an applied voltage of 11 V emitting white light at (0.38, 0.39).

Figure 3.21 – Photograph of white light emitting single layer device based on co-polymer 182. Device architecture: ITO // PEDOT:PSS (50 nm) // 182 (69 nm) // LiF (0.8 nm) // Al (92 nm) operating at 11V

Unfortunately these single layer devices exhibited relatively poor performance with EQEs of <0.20% and luminous efficiencies of <0.12 lm W^{-1}. However, this was improved by the use of an interlayer of PVK doped with the well-known hole-transport material, 1,1-bis((di-4-tolylamino)phenyl)cyclohexane (TAPC).[116] Figure 3.22 shows the EL spectra of devices with an inter-layer of increasing amounts of TAPC (0 – 60%). This device architecture increases EQEs to ~ 0.6% with device efficiencies of ~ 1.0 cd A^{-1} and luminous efficiencies of ~ 0.4 lm W^{-1}. Whilst these device performances are still relatively low, work is currently on-going to improve this by varying the device architectures and experimenting with different inter-layer formulations. The good spectral coverage shown by these polymers gives them great potential for OLED applications. However, it remains necessary to find the right device structure in order to realise this potential for white-emitting polymeric OLEDs.

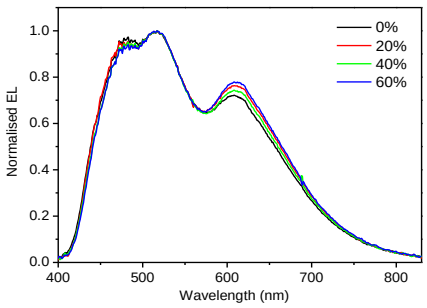

Figure 3.22 – Device EL with increasing amounts of TAPC doped into a PVK interlayer. Device architecture: ITO // PEDOT:PSS (50 nm) // PVK + x% TAPC // 182 (44 nm) // Ba (4 nm) // Al (100 nm)

In conjunction with these device studies, an analogous polymer was synthesised without the **S** unit (**183**, Figure 3.23) in order to determine its role in the devices. GPC analysis established the polymer was of high molecular weight (M_n = 49,000, M_w = 151,000 Da) and TGA analysis showed it possessed high thermal stability with $T_{d5\%}$ = 446 °C. Figure 3.24 (a) shows device EL for two devices based on **S**-containing polymer **182** and two devices based on non-**S** containing polymer **183**. As can be seen in Figure 3.24(a), the polymer without **S** exhibits less intense emission in the blue region of the spectrum, although the peak emission in this area is blue shifted compared with polymer **182**. This can be attributed to the presence of a CT band caused by the interaction between **F** and **S**, which red-shifts and broadens the blue emission band (as discussed for the trimers in Chapters 2 and 3.2), giving much broader spectral coverage in this region. From Figure 3.24(b) it can be seen that without the broadening of the blue emission due to the presence of **S**, the emission of the polymers falls into the yellow/orange region, rather than white. From these results it seems that the **S** unit is necessary in order for white light emission to be achieved and is, therefore, a vital component in these systems. Initial results indicate that devices without **S** are slightly more efficient than those with **S**: EQE ~ 1.5%, device efficiency ~ 3.5 cd A^{-1}; however, their emission colour means they are not suited for use in white-emitting OLEDs.

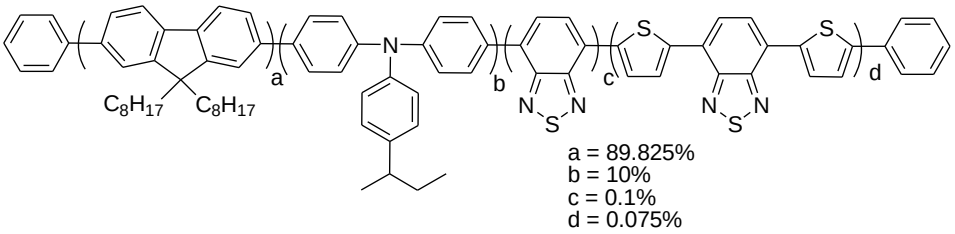

183

Figure 3.23 – Structure of analogous co-polymer without S

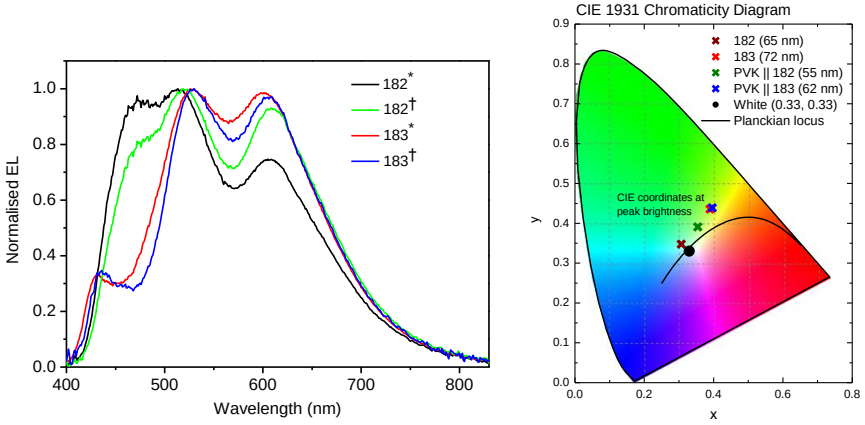

Figure 3.24 (a) – EL of devices with S (182) and without S (183); (b) Corresponding CIE diagram
Device architectures: *ITO // PEDOT:PSS (50 nm) // 182 or 183 // Ba (4 nm) // Al (100 nm); †ITO // PEDOT:PSS (50 nm) // PVK (30 nm) // 182 or 183 // Ba (4 nm) // Al (100 nm)

3.3.3 Conclusions

Ambipolar trimers based on carbazole/**S** and arylamine/**S** have been successfully developed into high molecular weight polymers emitting in the blue/sky blue region of the spectrum. Incorporation of additional fluorescent red and green dopants shifts the PL emission into the white region, very close to the white point. Initial device results show that this broad emission is also seen in the EL spectra and devices have been produced which emit white light. By comparison to a non-**S** containing analogous co-polymer, it has been determined that the incorporation of **S** into these systems is essential in order to achieve white light. Overall a novel polymer has been demonstrated which contains electron donor units, electron acceptor units, as well as the ability to emit in the red, green and blue regions of the spectrum. These polymers, therefore, represent a very promising class of material in the next generation of white light-emitting devices. Work is currently underway to improve the device characteristics.

3.4 Enhancement of phosphorescence by molecular structure modification

3.4.1 Introduction

In the previous section it was demonstrated how the ambipolar trimers discussed in section 3.2 have been developed for application in white light-emitting polymeric OLEDs. In this section an unusual photophysical property observed in the trimers is investigated and its origins probed.

Luminescent materials can emit light in one of two ways, namely fluorescence or phosphorescence depending on whether the excited state is a singlet or triplet state. Radiative decay from an excited singlet state down to the ground (singlet) state is fluorescence; radiative decay from an excited triplet state to the ground (singlet) state is phosphorescence.[117] The transition between the ground (singlet) and excited (triplet) states is formally forbidden, so for phosphorescence to occur there needs to be intersystem crossing (ISC) from the singlet to the triplet manifold.[117] ISC is promoted by heavy metal atoms (most commonly organometallic complexes) due to their significant spin-orbit coupling properties. The majority of purely organic compounds do not show strong spin-orbit coupling (some exceptions are discussed later). Based purely on charge recombination statistics, triplets would account for 75% of the excited states within a material, with singlets accounting for 25%,[118] therefore, OLED devices based on phosphorescent emitters are likely to be more efficient. However, devices based on all-organic systems often have advantages over phosphorescent emitters in terms of colour-tuning through synthetic modifications, applicability to more simple device structures, as well as cost; organometallic complexes tend to be expensive to use which may be a problem

industrially. If the triplet manifold of all-organic systems could be utilised, a new class of metal-free materials could be developed for highly efficient light emission. However, there have been very few reports of any such systems in the literature.

There have been a number of investigations into the phosphorescence of conjugated polymers, in particular polythiophenes.[118-120] In polythiophenes, ISC to the triplet manifold has been demonstrated to be one of the main non-radiative decay routes for singlet excitons, attributed to the "heavy atom" effect of sulfur.[118] This effect was also reported by Fonseca *et al*. who studied the triplet states of a series of fluorene-based alternating co-polymers including those shown in Figure 3.25.[119] When thiophene was used as a co-monomer (**186**) a decrease in fluorescence quantum yield was observed which was attributed to the heavy atom effect of the sulfur, enhancing spin-orbit coupling, leading to increased ISC to the triplet manifold.[119] Interestingly, on de-aromatising the sulfur lone pair electrons, i.e. by incorporating thiophene-*S*,*S*-dioxide (**185**), little ISC was observed and higher singlet yields were achieved.[119]

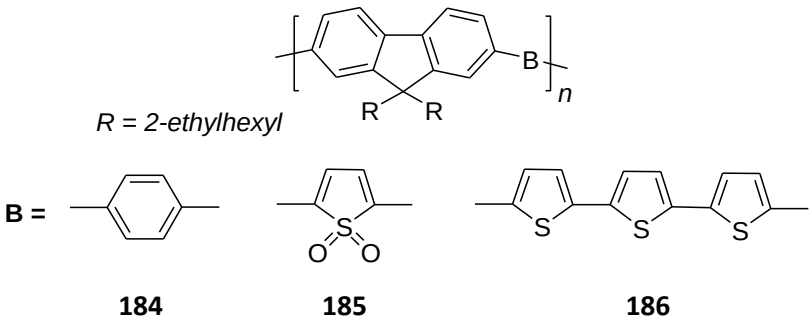

184 **185** **186**

Figure 3.25 – Structure of alternating fluorene-based co-polymers

For oligo- and poly-thiophenes the probability of spin-orbit coupling (as required for ISC) is reduced for highly symmetrical, planar, conjugated structures.[118] Beljonne *et al*. proposed that for polythiophene systems to emit efficiently (i.e. reduce any non-radiative decay from the triplet manifold), a highly delocalised, conjugated structure should be designed with a planar backbone to reduce spin-orbit coupling and therefore, also reduce ISC.[118] Conversely it could be conceived that to enhance phosphorescence (e.g. if emission from the triplet were a radiative transition), the opposite principles could be applied.

One of the few reported organic molecules to exhibit phosphorescence is benzophenone (**187**, Figure 3.26).[121,122] The phosphorescence is attributed to the spin-orbit coupling induced by the carbonyl oxygen.[121,123] Devices were fabricated based on **187** which was dispersed into an inert polymer matrix of poly(methylmethacrylate) (PMMA).[122] The EL of the device was attributed to

the phosphorescence of benzophenone with peaks at 420, 450 and 480 nm (Figure 3.26). This phosphorescence was only observed at 100 K, it was not observable at room temperature, as non-radiative decay processes become dominant with increasing temperature.[122]

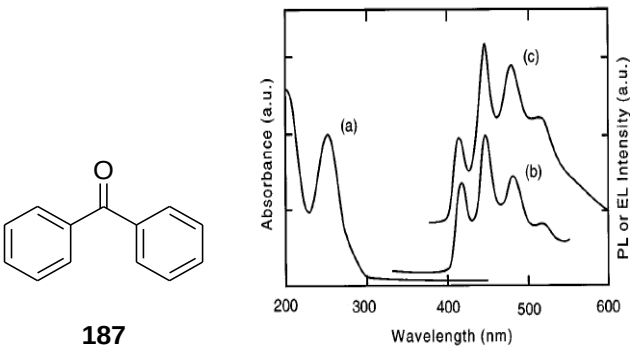

Figure 3.26 – Structure of benzophenone with the absorption (a) and PL (b) of the 187:PMMA layer, together with the EL (c) of the device at 100 K (EL spectrum displaced vertically for clarity)[122]

In an unusual case, room temperature phosphorescence has been reported from a carbazole derivative (*N*-ethylhexylcarbazole) and its dimer (*N*,*N*'-diethylhexyl-3,3'-bicarbazolyl) dispersed into a PMMA matrix and irradiated with laser pulsed UV light.[124] The PL spectra of the compounds show blue fluorescence emission together with green phosphorescence emission with maxima at 444 nm (monomer) and 486 nm (dimer) (Figure 3.27).[124]

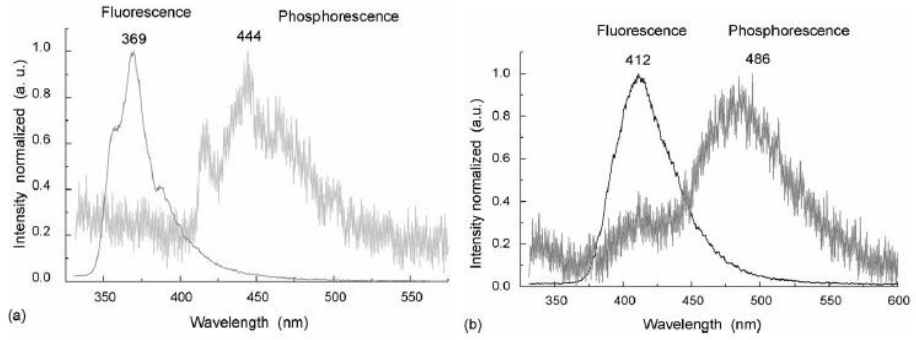

Figure 3.27 – Fluorescence and phosphorescence spectra of monomer (a) and dimer (b)[124]

A recent report focussed on a strategy for achieving phosphorescence from non-metal containing systems by combining a number of effects known to enhance ISC.[123] Systems were designed containing triplet-producing aromatic aldehydes, triplet-promoting bromine atoms and the ability of the molecules to halogen bond in their crystalline form.[123] As seen in benzophenone, the oxygen atom of carbonyls can promote spin-orbit coupling; bromine is a heavy atom capable of enhancing ISC and halogen bonding between the bromine and the carbonyl enhances both of these effects. Once the molecules are doped into a suitable host material (to prevent excimer formation), efficient, room temperature phosphorescence is observed in the solid state (Figure 3.28).[123] In solution, halogen bonding does not occur and

only fluorescence emission is observed. Room temperature phosphorescence in these systems is reported to be as high as 55% which is the first report of such a material.[123]

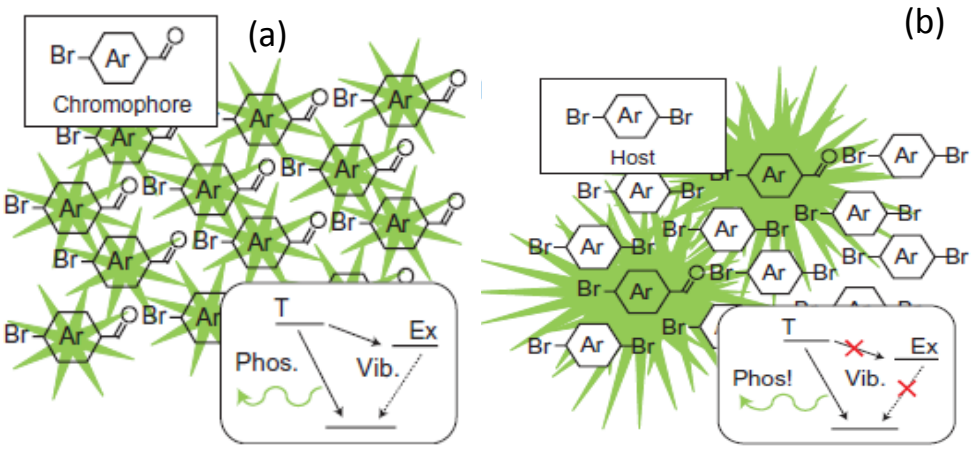

Figure 3.28 – Schematic of phosphorescence emission from all-organic system:
(a) halogen bonding between carbonyl O and adjacent Br enhances phosphorescence, but excimer (Ex) formation is significant leading to self-quenching; (b) doping into a dibromo host material prevents Ex formation, increasing the phosphorescence yield. [123]

The following section focuses on the identification and investigation of phosphorescence emission seen from some of the ambipolar trimers discussed in section 3.2.

3.4.2 Results and Discussion

When the photoluminescence quantum yields (PLQYs) were recorded (in toluene) for the ambipolar trimers discussed in section 3.2, an interesting trend was seen between linear and bent analogues. The linear trimers all exhibited higher PLQYs than their bent counterparts (Table 3.5; data repeated from Table 3.2). The reduction in PLQY (which measures fluorescence quantum yields) for the bent trimers implies that the radiative rate constant for fluorescence is reduced in the bent systems compared to the linear, possibly due to poorer overlap between the ground and excited states.

Compound	Donor	Type of system	Φ_{PL} (PhMe)
91	F	Linear	0.90 ± 0.10
159	F	Bent	0.59 ± 0.05
152	3-Cbz	Linear	0.45 ± 0.05
154	3-Cbz	Bent	0.25 ± 0.10
161	N-Cbz	Linear	0.57 ± 0.10
162	N-Cbz	Bent	0.26 ± 0.10

Table 3.5 – Comparison of PLQYs for bent vs. linear trimers

In order to investigate this effect, further photophysical studies were undertaken. As discussed in the introduction to this section, if phosphorescence is occurring (or even if the triplet state is being populated without radiative decay), the singlet yields of the compounds would be reduced. The room temperature emission spectra of the trimers show no evidence of phosphorescence; however, this emission is often only observable at low temperatures. The PL spectra were therefore recorded at different temperatures ranging from room temperature down to 80 K (in ethanol). Figures 3.29 (a) to (d) show these spectra for the bent vs. linear **F**-based and **cbz**-based trimers.

For linear **FSF** (**91**) (a), as the temperature is decreased, the broad CT emission gains increasing vibronic structure, until a LE type emission starts to be observed at 150 K and below. For the bent **FSF** (**159**) (b) a similar structured emission is observed as the temperature is decreased, but in this case, at 80 K, a new set of peaks appears with maxima at ~ 520 and 550 nm. For the linear **3-cbz** trimer (**152**), the emission spectra follow a similar pattern with decreasing temperature as for linear **FSF**. For the bent analogue (**154**), the main emission peak becomes significantly blue-shifted with decreasing temperature and lower energy peaks start to be observed at 100 K, reaching intensities approximately equal to the "main" peak at 80 K. These lower energy peaks are assigned to phosphorescence based on their increased lifetimes; ms for phosphorescence, compared with ns for fluorescence (see Table 3.6).

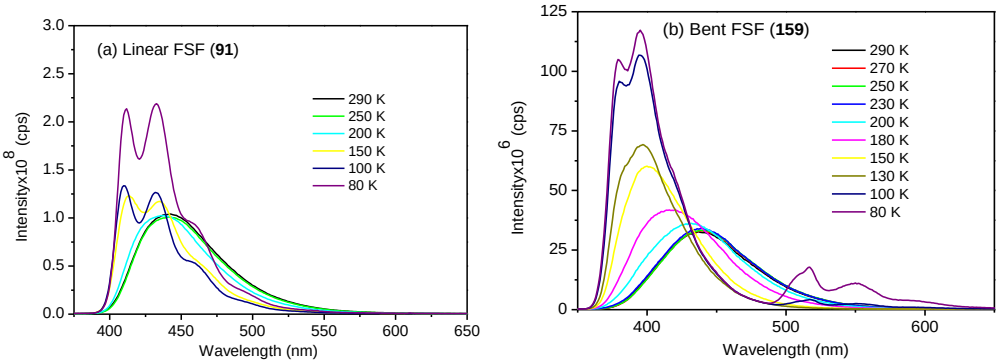

Figures 3.29 – Showing temperature dependent PL spectra in EtOH for (a) linear, (b) bent FSF trimers

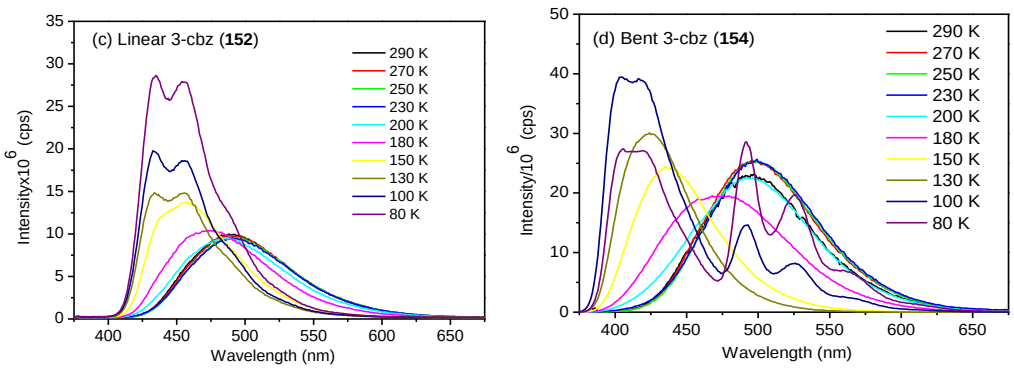

Figures 3.29 – Showing temperature dependent PL spectra in EtOH for (c) linear, (d) bent 3-Cbz trimers

The low solubility of the N-bonded carbazole trimers (**161** and **162**) made similar low temperature studies not possible, therefore, more soluble analogues were synthesised where the carbazole units were functionalised with *tert*-butyl groups, compounds **189** and **190**, Scheme 3.6. In order to compare the arylamine trimers, a bent **DPA**-**S**-**DPA** analogue (**191**) was synthesised in the same way as for the linear trimer (**164**, Scheme 3.5) but using 2,8-dibromodibenzothiophene-*S*,*S*-dioxide (**89**) (NB. (**191**) was synthesised by Dr. K.T.Kamtekar). The photophysics of these more soluble N-**cbz** bonded trimers, as well as the linear and bent **DPA**-based trimers were then studied. Figures 3.30 (a) to (d) compare the PL spectra of the different sets of linear vs. bent trimers in ethanol at low temperatures.

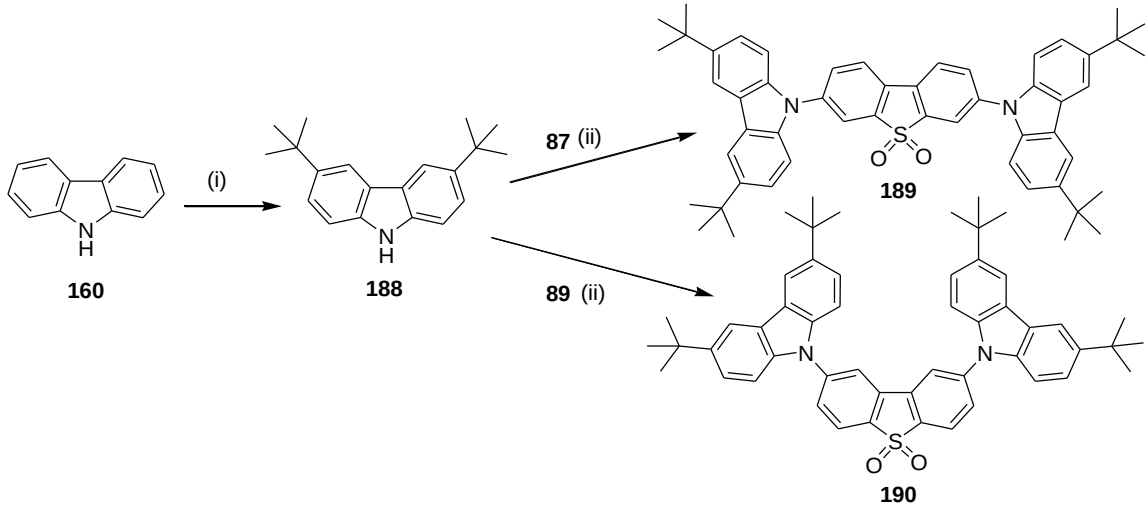

Reagents and conditions: (i) $ZnCl_2$, ^tBuCl, nitromethane, RT, 37%; (ii) **87**/**89**, $Pd_2(dba)_3$, xphos, NaO^tBu, ^tBuOH, toluene, 110 ˚C, 64% for **189**; 59% for **190**

Scheme 3.6 – Synthesis of more soluble N-Cbz bonded trimers

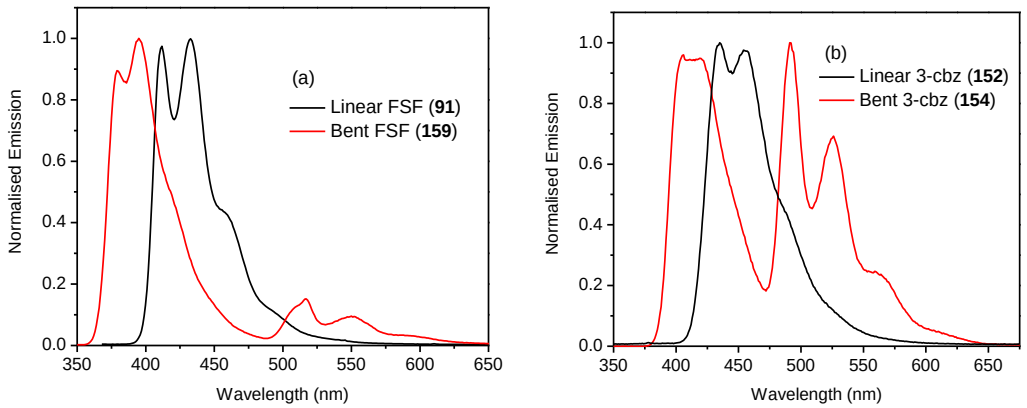

Figures 3.30 – PL spectra at 80 K in ethanol of linear and bent FSF (a), linear and bent 3-cbz trimer (b)

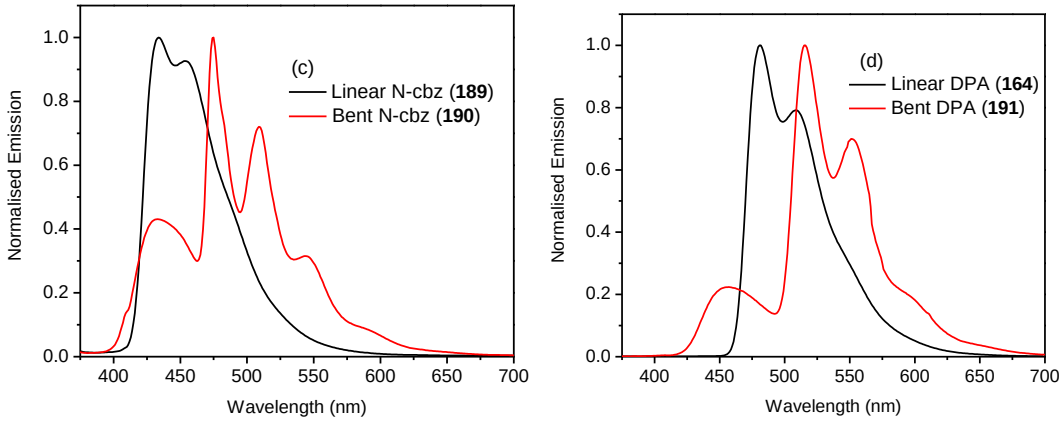

Figures 3.30 – PL spectra in EtOH of linear and bent N-cbz; 80 K (c) and linear and bent DPA; 100 K (d)

Compound	Donor	Type of System	τ_f (ns) [a]	τ_{ph} (ms) [b]
91	F	Linear	1.05	55
159	F	Bent	1.02	944
152	3-Cbz	Linear	1.21	84
154	3-Cbz	Bent	1.46	289
189	N-Cbz (^{t}Bu)	Linear	3.08	38
190	N-Cbz (^{t}Bu)	Bent	1.60	92
164	DPA	Linear	3.65	137
191	DPA	Bent	1.11	86

[a]fluorescence lifetimes recorded in hexane, λ_{ex} 363 nm; [b]phosphorescence lifetimes recorded in ethanol

Table 3.6 – Lifetimes of selected linear vs. bent compounds

The PL spectra of the bent trimers all show phosphorescence emission at low temperatures. In bent **FSF** (**159**) this emission is weak compared with the fluorescence signal; in the bent **3-cbz** bonded (**154**) it is approximately equal in intensity; and in the bent N-**cbz** (**190**) and bent **DPA** (**191**) trimers the phosphorescence emission appears stronger than the fluorescence. The appearance of strong phosphorescence explains why the fluorescence quantum yields for the bent trimers are lower than their linear analogues. In the bent trimers there is increased ISC from the singlet to the triplet manifold, i.e. the rate of ISC is much faster than the rate of radiative decay from the excited singlet state, hence fewer singlets are fluorescing thus the PLQYs are reduced. In the linear systems, this ISC is not occurring in so great an extent i.e. the rate of radiative decay from the excited singlet state is now faster than the rate of ISC, so more singlets are decaying radiatively, hence the PLQYs are higher. The data in Table 3.6 show similar fluorescence lifetimes (τ_f) for the linear and bent **FSF** and 3-**cbz** trimers. However, for the N-**cbz** and **DPA** trimers, there is a marked decrease in fluorescence lifetimes when

comparing linear and bent trimers. This is in agreement with the strong phosphorescence seen in these compounds, i.e. an increased rate of ISC compared to fluorescence.

As discussed above, strong phosphorescence is an unusual phenomenon to observe in all-organic systems. In our systems it appears that by changing the molecular architecture of the **S**-based donor-acceptor trimers, the balance between the rates of fluorescence and ISC in the systems can be changed which is observed experimentally as the "switching on and off" of (low temperature) phosphorescence. This is an interesting result as a study of this nature has not previously been reported in the literature; however, the origins of this effect were not immediately obvious. As discussed earlier, it has been reported that the sulfur atom of thiophene in conjugated polymers can aid ISC to the triplet manifold.[118,119] However, these reports centre on conjugated polymers and it has been reported that de-aromatising the thiophene ring by using the sulfone actually prevents this ISC from occurring.[119] It has also been discussed that oxygen atoms can aid ISC; however, these reports centre on carbonyl oxygen atoms, e.g. in benzophenone.[121,123] In all of our systems the common features are the **S** unit and a **D**-**A**-**D** type architecture. If it is the sulfur atom and/or the carbonyl atoms promoting ISC, there must be something about the structure of the compounds which prevents or allows this. A possible explanation lies with El-Sayed's rule which states that the rate of ISC from the singlet to the triplet manifold is increased if the radiationless transition involved is accompanied by a change of molecular orbital type e.g. a (π,π*) singlet transitioning to a (n,π*) triplet state.[117]

In order to further develop these compounds a number of novel trimers were designed and synthesised. Compound **192** was chosen as a sulfide analogue of the bent trimer **190** in order to evaluate the effect of the electron-accepting **S**. Compound **193** is another analogue of **190** but with a fluorene unit in the centre, i.e. no sulfur atom present at all. Compounds **197** and **201** were designed in order to look at the conjugation effects between donor and acceptor by adding a *meta*-phenyl spacer (**197**) and an alkynyl spacer (**201**). Schemes 3.7 – 3.9 show the syntheses of these trimers (see Chapter 7 for full details).

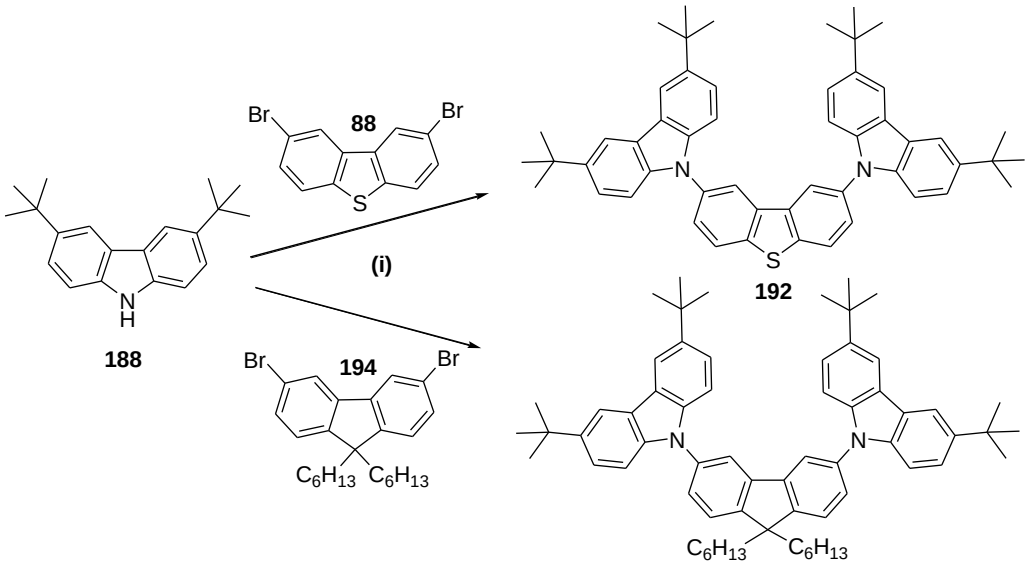

Reagents and conditions: (i) $Pd_2(dba)_3$, xphos, NaO^tBu, ^tBuOH, toluene, 110 ˚C, 86% for **192**; 86% for **193**

Scheme 3.7 – Synthesis of sulfide and fluorene-based trimers

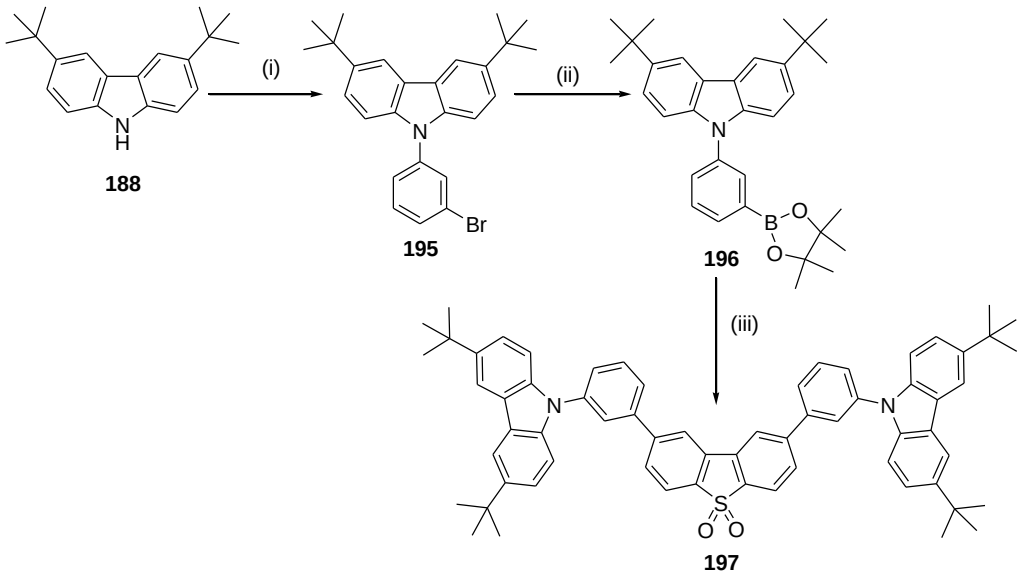

Reagents and conditions: (i) 1-bromo-3-iodobenzene, CuI, 1,10-phenanthroline, K_2CO_3, DMF, 120 °C, 51%; (ii) B_2pin_2, $Pd_2(dba)_3$, dppf, KOAc, DMF, 80 °C, 44%; (iii) **89**, $Pd(PPh_3)_4$, K_2CO_3, 1,4-dioxane:H_2O, 85 °C, 51%

Scheme 3.8 – Synthesis of meta-phenyl spaced trimer

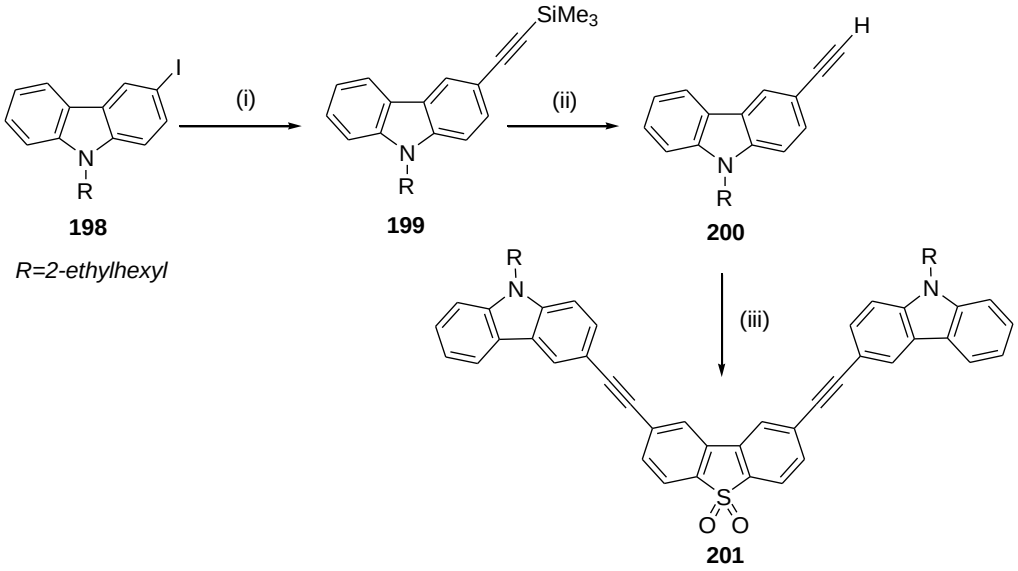

Reagents and conditions: (i) $Pd(PPh_3)_4$, CuI, TMSA, THF:Et_3N, 20 °C, 66%; (ii) K_2CO_3, THF:MeOH, 20 °C, 82%; (iii) **89**, $Pd(PPh_3)_4$, CuI, THF:Et_3N, 60 °C, 61%

Scheme 3.9 – Synthesis of alkynyl linked trimer

The absorption and PL spectra of compound **192** in non-polar hexane and polar ethanol are shown in Figure 3.31 (a). Structured emission is seen in hexane and a red-shifted, slightly broader emission is seen in ethanol. However, there is not the significantly red-shifted ICT band observed when **S** is the central unit, indicative of the fact that dibenzothiophene is not an electron-acceptor, so ICT emission is not significant in this case. Figure 3.31 (b) shows the PL spectra in ethanol of **192** at room temperature and at 100 K. At the lower temperature strong phosphorescence emission is observed in the range ~ 425 – 475 nm. This indicates that the sulfone (**S**) unit is not essential for observing phosphorescence; it is observed in bent trimers where carbazole is the donor whether the central unit is dibenzothiophene-*S*,*S*-dioxide (**S**) or dibenzothiophene. Figures 3.32 (a) and (b) show the analogous PL spectra for compound **193**.

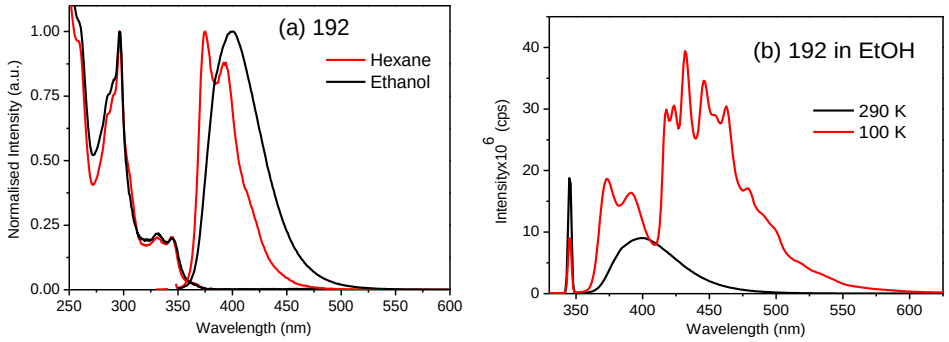

Figure 3.31 – (a) Absorption/PL in hexane/ethanol; (b) PL in ethanol at different temperatures (192)

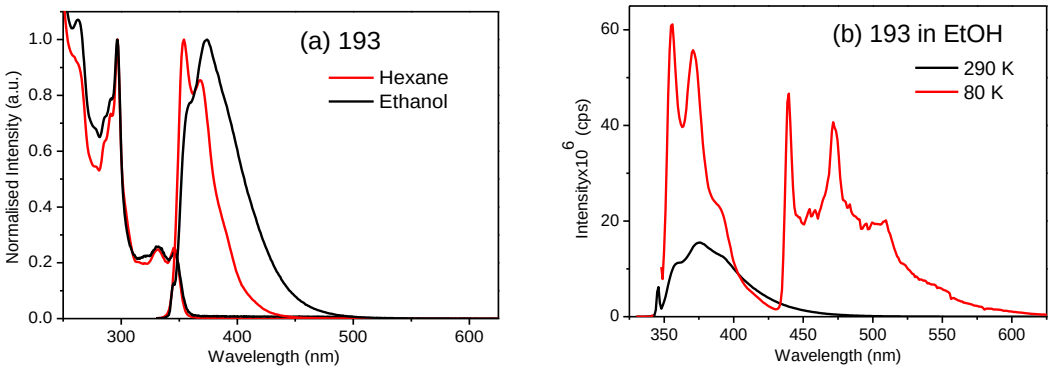

Figure 3.32 – (a) Absorption/PL in hexane/ethanol; (b) PL in ethanol at different temperatures (193)

For compound **193** a strong ICT emission band is not seen in polar ethanol because the electron-accepting **S** unit has now been replaced by fluorene. However, it has been previously demonstrated that carbazole is a stronger donor than fluorene, so some CT character may be present in this compound. At 80 K phosphorescence is observed, although it does appear to be less significant (in comparison to the fluorescence signal) compared with both compounds **190** and **192**. Overall, the bent trimers containing carbazole all exhibit phosphorescence to varying degrees, with the **S**- and dibenzothiophene-containing trimers exhibiting the strongest phosphorescence. For a study which is discussed in Chapter 6, a "bent" **FFF** trimer (**202**) was synthesised and so for comparison with this series, its PL spectra in ethanol at different temperatures were recorded (Figure 3.33).

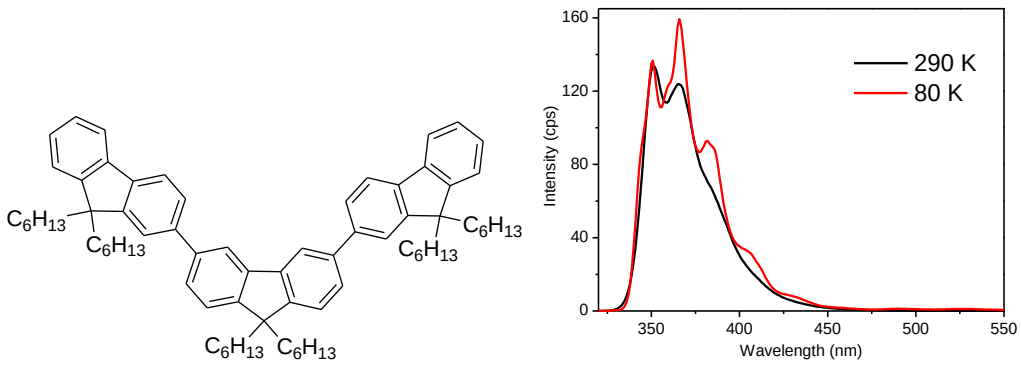

202

Figure 3.33 – Structure of bent FFF trimer and its PL spectra in ethanol at different temperatures

The low temperature PL spectrum of the bent **FFF** trimer (**202**) shows no phosphorescence emission; the only bent trimer of the series which does not show this. Two possible conclusions can be drawn from this: (i) the lone pair of the N atom of the carbazole is required; (ii) a donor-acceptor type system is required. The fact that strong phosphorescence is observed in the bent trimers based on **cbz** and **DPA** supports statement (i); however, the fact that phosphorescence (albeit weak) is observed in bent **FSF** is in disagreement with this. The fact that stronger phosphorescence is observed in the significantly bipolar systems, e.g. **190**

compared with the slightly ambipolar **193** and the non-ambipolar **202** supports statement (ii); however, the strong phosphorescence observed in compound **192** (without an electron acceptor) contradicts this statement.

One possible explanation could be that nitrogen, sulfur and oxygen are all capable of allowing spin-orbit coupling, thereby enhancing the rate of ISC and allowing phosphorescence emission to occur. In the bent **FSF** (**159**), sulfur and oxygen atoms are present and weak phosphorescence is observed. In the bent N-**cbz** compound (**190**) and the bent **DPA** trimer (**191**), sulfur, oxygen and nitrogen atoms are all present and strong phosphorescence is observed. In the bent **FFF** trimer (**202**), no such atoms are present and no phosphorescence is observed. In the sulfide-containing trimer (**192**), sulfur and nitrogen atoms are present and phosphorescence is observed. When the **S** unit is present, there is no lone pair available on the sulfur atom (usually the explanation for why sulfur can increase spin-orbit coupling), so it is possible that in **S** it is only the oxygen atoms which are causing the increased ISC, but when the sulfide is present the sulfur atom alone can achieve this.

Whilst an explanation for the trend in phosphorescence emission within the bent trimers can be proposed, it still remains to explain why no phosphorescence is observed in the linear trimers. As discussed earlier, for polythiophenes, Beljonne *et al*. reported that to reduce ISC, highly delocalised and conjugated structures should be designed with planar backbones.[118] From computational studies (Section 3.2) it has been determined that the bent trimers are much less conjugated than their linear analogues. The HOMO of the bent trimers is very much localised onto the donor unit, whereas in the linear trimers the HOMO is more delocalised throughout the molecule. This decrease in orbital overlap between HOMO and LUMO could be predicted to lead to a decrease in the rate of radiative emission from the excited singlet state. If the rate of ISC becomes faster compared to the rate of fluorescence, emission from the triplet manifold is then increased. More in-depth computational and photophysical studies (including looking at the PL emission of compounds **197** and **201**) are currently underway in order to attempt to determine the nature of the transitions occurring within these systems and thus explain their photophysical behaviour in more depth.

3.4.3 Conclusions

The reduction in PLQY values for the bent trimers discussed in section 3.2, compared with their linear analogues has been ascribed to ISC to the triplet manifold which is observed as phosphorescence in low temperature PL spectra of the bent trimers. By synthesising new

derivatives it has been demonstrated that at least one lone-pair containing atom needs to be present (nitrogen, sulfur or oxygen) within a bent trimer architecture to cause the spin-orbit coupling required for phosphorescence. It is suggested that the reduced conjugation of the bent trimers is reducing the rate of radiative decay from excited singlet states, thus allowing ISC to compete with fluorescence. The details of this are currently being investigated by our collaborators through more in-depth computational and photophysical studies.

Overall, it has been established that efficient phosphorescence can be achieved (at low temperature) from non-metal containing compounds and that this phosphorescence can be switched on or off depending on the molecular architecture. These compounds, therefore, introduce design rules which should be followed to either prevent phosphorescence (thereby increasing singlet yields) or to take advantage of phosphorescence, e.g. for a new generation of phosphorescent all-organic OLED systems.

Chapter 4: Oligofluorenes as Molecular Wires to Probe Electron Transfer in Donor-Acceptor Systems

4.1 Introduction

In Chapters 2 and 3, the role of fluorene as the electron donor in ambipolar systems, where dibenzothiophene-*S*,*S*-dioxide (**S**) is the electron acceptor, was discussed and the charge transfer processes within the systems were investigated. The emission of the charge transfer band was probed in order to understand excited state geometries. It was also demonstrated how the charge transfer emission could be exploited for OLED applications including for white light. In this chapter, the use of fluorene is again discussed in donor-acceptor (D-A) systems, where fluorene is not the donor – it is instead the bridge between a donor and an acceptor moiety. In this way fluorene is acting as a molecular wire and by monitoring the fluorescence emission of the fluorene, charge/electron transfer processes can be probed at a molecular level.

Donor-bridge-acceptor type systems are well suited for probing electron/energy transfer processes at a molecular level, where the bridging units mediate electron transfer (i.e. charge separation and recombination) processes through the systems.[125] Upon excitation with visible light, intramolecular charge transfer can be induced from the donor to the acceptor via the bridge. The kinetics of this process are governed by a number of factors including the distance between donor and acceptor, the extent of the coupling between the two moieties and the attenuation factor, β.[125] β is essentially a measure of the charge transfer capability of the bridge; a small β value implies that charge can be transferred over large D-A distances. When the acceptor is the high electron affinity moiety, C_{60} (**203**, Figure 4.1), a long-lived charge separated state may be formed upon photo-excitation. This gives these systems the potential to simulate the processes occurring during photosynthesis where light is transformed into chemical energy and stored. There is much current interest in developing this area of chemistry for our future energy needs.[126]

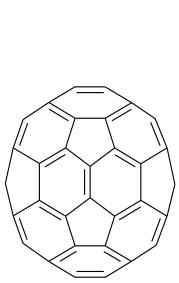

203

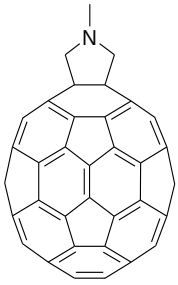

204

Figure 4.1 – Structures of C_{60} and *N*-methylfulleropyrrolidine

Since the first experimental observations of C_{60} over twenty five years ago, its chemistry has been extensively studied and developed.[126] A key reaction of C_{60} is the Prato reaction; a 1,3-dipolar cycloaddition of an azomethine ylide which is generated *in situ* from the reaction of an aldehyde with an amino acid to generate a fulleropyrrolidine (e.g. *N*-methylfulleropyrrolidine, **204**).[127] The synthesis of these fulleropyrrolidines opened up the possibility of incorporating C_{60} into a wide variety of molecular architectures, a topic which has been recently reviewed by Kharisov *et al*.[128]

To increase the solubility of C_{60} in organic solvents, [6,6]-phenyl-C_{61}-butyric acid methyl ester (PCBM, **21**) was developed by Wudl and Hummelen in 1995[129] and has since been used extensively in bulk heterojunction (BHJ) solar cells. In these devices, the PCBM is usually blended with an organic semiconducting conjugated polymer, e.g. the polythiophene derivative, P3HT (usually regioregular) (**205**, Figure 4.2), although other polymer classes have also been widely reported.[130-132]

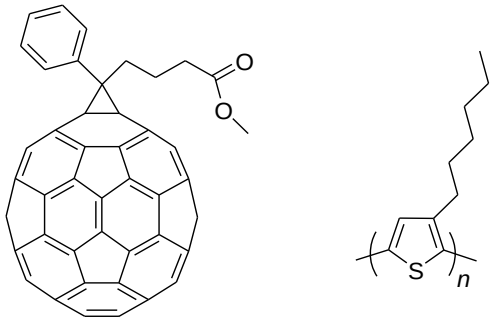

PCBM **21** P3HT **205**

Figure 4.2 – Structures of PCBM and P3HT; used in BHJ solar cells

While the results of these types of systems are promising in terms of their energy transformation efficiencies, C_{60} has a tendency to phase separate from the polymers and crystallise out during device operation which currently limits practical applications.[133] The use of π-conjugated oligomers combines the required electronic and optical properties of the polymer systems but with increased solubility and hence improved structure-function relationships.[133] There have been a wide variety of π-conjugated oligomers incorporated into D-A systems as bridging units where a fulleropyrrolidine is the accepting moiety including: oligophenylenevinylenes,[134] oligophenyleneethynylenes,[135] oligoacetylenes,[136] oligothiophenes[137] and oligovinylthiophenes.[138] Oligofluorenes (OFs) have been much less widely investigated (the majority of fluorene-based research is for OLED applications), despite their unique fluorescence properties which allows for in-depth spectroscopic monitoring of the systems to be used.

Work from Goldsmith *et al*. demonstrated that the length of OF bridges in D-A systems (phenothiazine donor and bis(dicarboximide) acceptor) could be varied without significantly changing the energies of the relevant bridge sites due to charge localisation on the two terminal fluorene units of the oligomeric bridge, indicating good electronic coupling between the donor and the bridge, as well as between the bridge and the acceptor.[139] The Bryce group were the first to report the use of fluorene oligomers as electron donor units directly attached to C_{60} moieties in investigations into photogenerated charge separated states (**206**, **207**, Figure 4.3).[133] Electrochemical studies of the compounds showed amphoteric redox behaviour with three one-electron reduction waves of each C_{60} unit, as well as irreversible oxidation waves from the OF units.[133] Steady-state fluorescence spectra and transient absorption measurements established that there was efficient transduction of the singlet excited state energy transfer from the photo-excited OF to the C_{60}. [133]

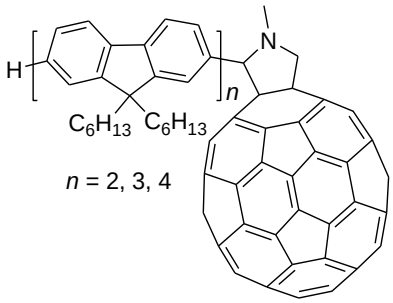

206

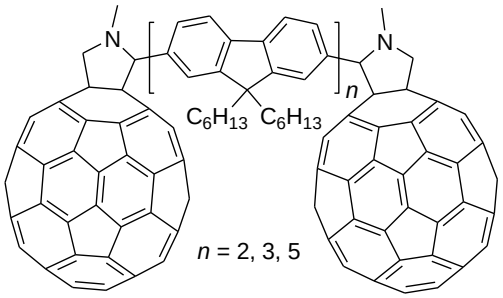

207

Figure 4.3 – Structures of the OF-C_{60} dyads and triads

The C_{60}-OF-C_{60} triad (**207**, *n* = 2) has recently been utilised in one-molecule conductance measurements.[140] One of the key features of this system which makes it suitable for this purpose are the C_{60} terminal groups which act as "molecular beacons" allowing molecules on a gold surface to be visualised and hence individually targeted using scanning tunnelling microscopy. Once the molecule has been targeted, the C_{60} can then act as an "alligator clip" to effectively wire the molecule between the tip and the surface to allow single molecule conductance measurements to be taken.[140] The excellent wire properties of the bi-fluorene spacer and the added bonus that the fluorene units can be easily functionalised at the central C_9 position, if required, mean these systems have the potential to provide a wide range of information regarding structure-property relationships in single molecule conductance situations.

As well as presenting OFs as donor units, the Bryce group have reported the use of OFs as bridging units in D-bridge-A systems where the acceptor is C_{60} and the donor is either

extended tetrathiafulvalene (exTTF)[141] (**208**) or a zinc porphyrin (ZnP)[142] (**209**, **210**). Both systems demonstrate the efficiency of OFs as molecular wires and low β values are reported; 0.09 $Å^{-1}$ for the exTTF system and 0.097 $Å^{-1}$ for the ZnP system. Wielopolski *et al*. presented a similar system where the donor is exTTF and the acceptor is C_{60}, linked by an oligo-vinylfluorene bridge.[143] This bridge was reported to facilitate charge separation and recombination processes, with π-conjugation improved by the structural rigidity imparted by the vinyl linkers, leading to systems with even lower β values (0.075 $Å^{-1}$).[143]

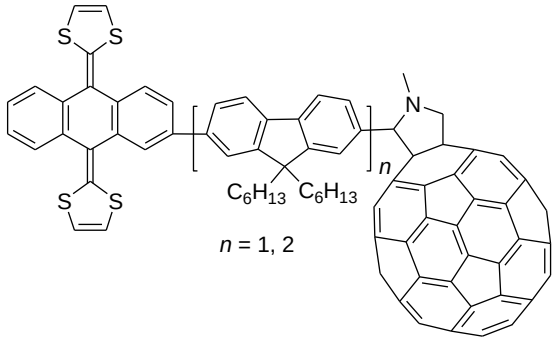

208

Figure 4.4 – exTTF-OF-C_{60} systems

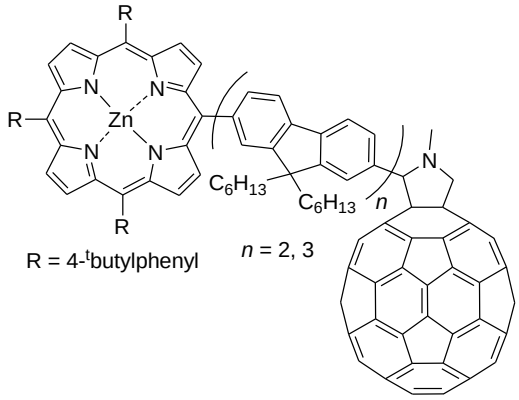

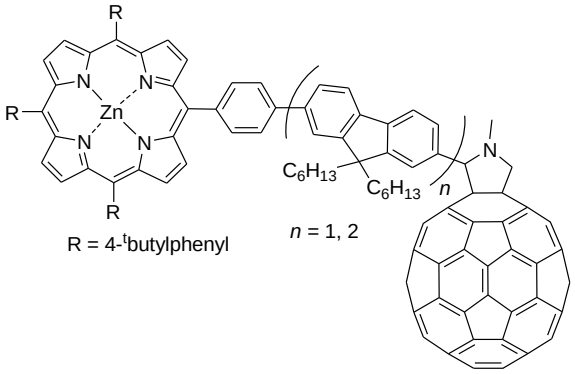

209 **210**

Figure 4.5 – ZnP-OF-C_{60} systems

For the ZnP systems photophysical studies focused on modulating the kinetics of the electron transfer processes, i.e. the β value, both by temperature control and by varying the connectivity pattern between the donor and the bridge (by the incorporation of a phenyl ring spacer).[142] It was determined that the conformation of the systems represents a compromise between minimising steric hindrance whilst maximising the π-conjugation pathway. Photophysical/computational studies determined that there are two types of charge transfer mechanism operating depending on the extent of conjugation, i.e. whether the bridge was directly bonded to the donor or was bonded via the phenyl spacer.[142]

By changing the identity of the donor unit (e.g. exTTF to ZnP) and the conjugation through the system (e.g. addition of phenyl linker) charge transfer processes through OF bridges have been probed. The following sections expand these strategies further in order to investigate the charge transfer processes in more detail with the aim of achieving OF-based systems with long-lived charge-separated states for optoelectronic applications.

4.2 Results and Discussion

4.2.1 Synthesis

In order to extend the D-OF-A systems it was decided to use ferrocene (Fc) as a donor unit and also to look at the effect of adding a spacer between the Fc and the OF bridge. There are numerous reports of Fc being used as the donor unit in D-bridge-A systems mainly due to its high electron donating ability as a result of its low oxidation potential.[134,137,138,144-147] A number of different bridging units have been reported including: oligothiophenes;[137,144] oligophenylenevinylenes;[134] and oligothienylenevinylenes.[138]

Due to the availability of a quantity of ethynylferrocene within the group two compounds had previously been synthesised (by Dr. C. van der Pol) where ethynylferrocene was coupled to an oligofluorene (mono- and bi-fluorene) which was functionalised with C_{60} (**211-212** Figure 4.6).

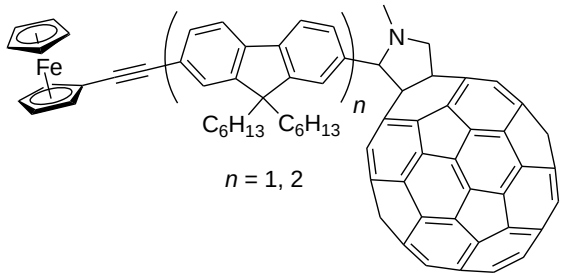

211 (*n = 1*)
212 (*n = 2*)

Figure 4.6 – Structure of ethynyl linked Fc-bridge-C_{60} compounds

This section discusses the extension of these compounds into a series of Fc-spacer-bridge-C_{60} systems. The bridge is either a mono-fluorene or a bi-fluorene and there is either no spacer (i.e. Fc directly linked to the bridge), a phenyl spacer or a vinyl spacer.

Scheme 4.1 shows the syntheses of the fluorene-based intermediates required for the directly linked (*n* = 1 and *n* = 2) compounds. Many of these compounds were synthesised according to reaction conditions previously developed in the group,[133] and the novel intermediates were

synthesised based on related procedures (see experimental procedures chapter for full details). First 2,7-dibromofluorene (**27**) was di-alkylated at the C_9 position for solubility to give **213**, followed by a mono-lithiation reaction which was quenched with DMF to obtain the mono-formyl derivative **214**. Miyaura borylation gave the key intermediate (shown in bold) for the (*n* = 1) oligomer (**215**). Suzuki coupling of this boronic ester to 2,7-dibromo-9,9-dihexylfluorene (**213**) gave compound **216**. The low yield of formation of this product is due to the large number of side products which can be formed when doing an unsymmetrical coupling reaction of this nature. Miyaura borylation of **216** then afforded the key intermediate (shown in bold) for the (*n* = 2) oligomer, **217**.

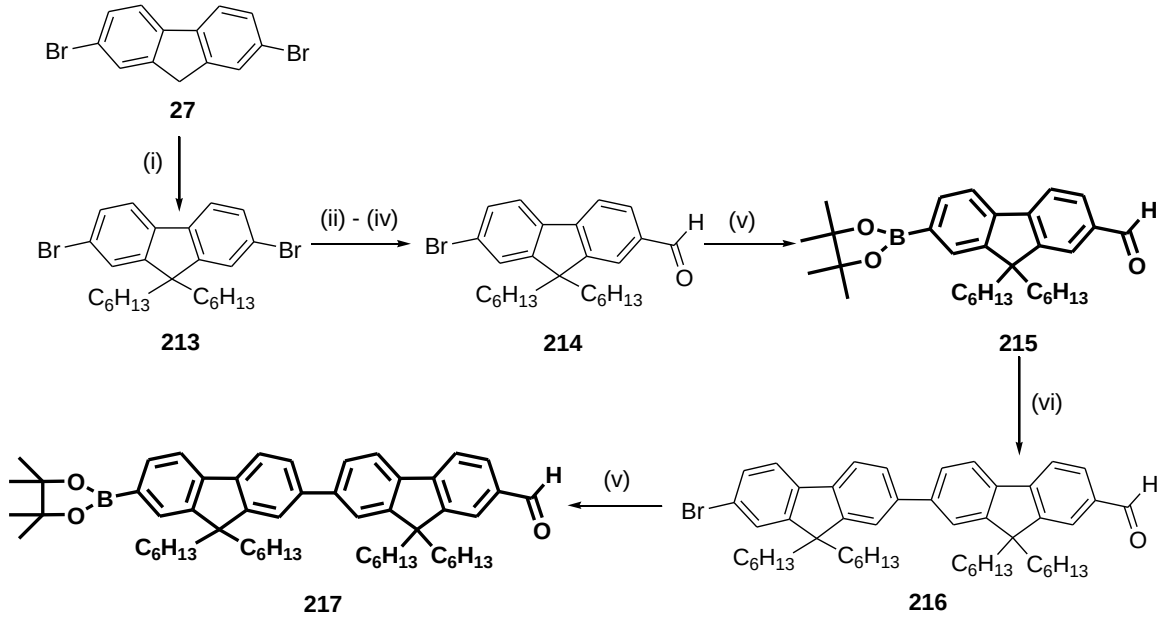

Reagents and conditions: (i) hexylbromide, $(^nBu)_4NBr$, NaOH (aq), DMSO, 20 ˚C, 72%; (ii) ^nBuLi, Et_2O, -78 ˚C to 20 ˚C; (iii) DMF, -78 ˚C to 20 ˚C; (iv) HCl (aq), 73% for **214**; (v) B_2pin_2, KOAc, $Pd(OAc)_2$, DMF, 90 ˚C, 68% for **215**; 63% for **217**; (vi) **213**, $Pd(PPh_3)_2Cl_2$, K_2CO_3 (aq), 1,4-dioxane, 85 ˚C, 45%

Scheme 4.1 – Syntheses of key intermediates (in bold) for directly linked (*n* = 1 and *n* = 2) oligomers

Schemes 4.2(a) and (b) show the syntheses of the fluorene-based intermediates required for the phenyl linked (*n* = 1 and 2) oligomers. Compound **214** was Suzuki coupled to the TMS-protected phenyl boronic ester, **218** (synthesised in two steps from 1,4-dibromobenzene) to obtain compound **219**, which was deprotected in quantitative yield using iodine monochloride. Miyaura borylation of this product (**220**) gave the key intermediate (shown in bold) for the phenyl linked (*n* = 1) oligomer, **221**. The key intermediate for the phenyl linked (*n* = 2) compound (shown in bold), **225**, was obtained in a similar way starting from bi-fluorene intermediates.

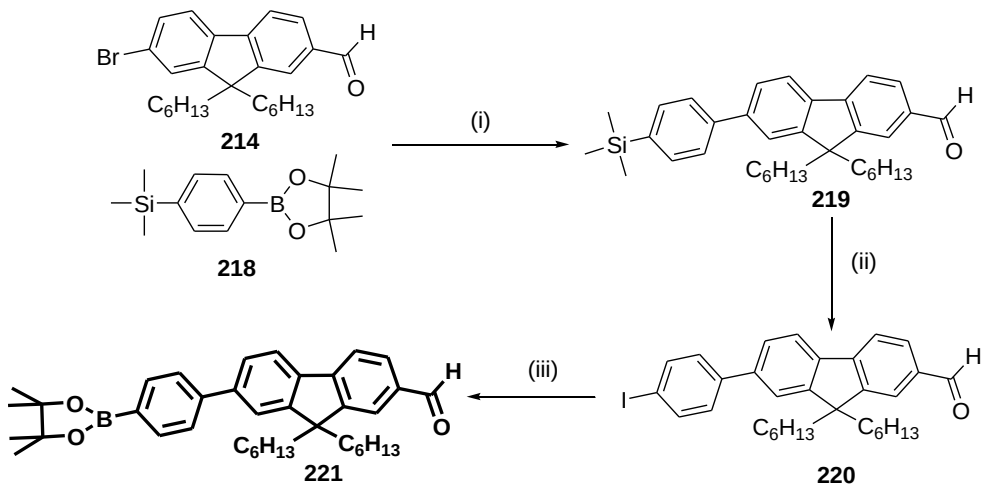

Reagents and conditions: (i) $Pd(PPh_3)_4$, K_2O_3 (aq), 1,4-dioxane, 85 ˚C, 84%; (ii) ICl, DCM, 0 ˚C to 20 ˚C, 100%; (iii) B_2pin_2, KOAc, $Pd(OAc)_2$, DMF, 90 ˚C, 60%.

Scheme 4.2 (a) – Synthesis of key intermediate (in bold) for phenyl linked (*n* = 1) oligomer

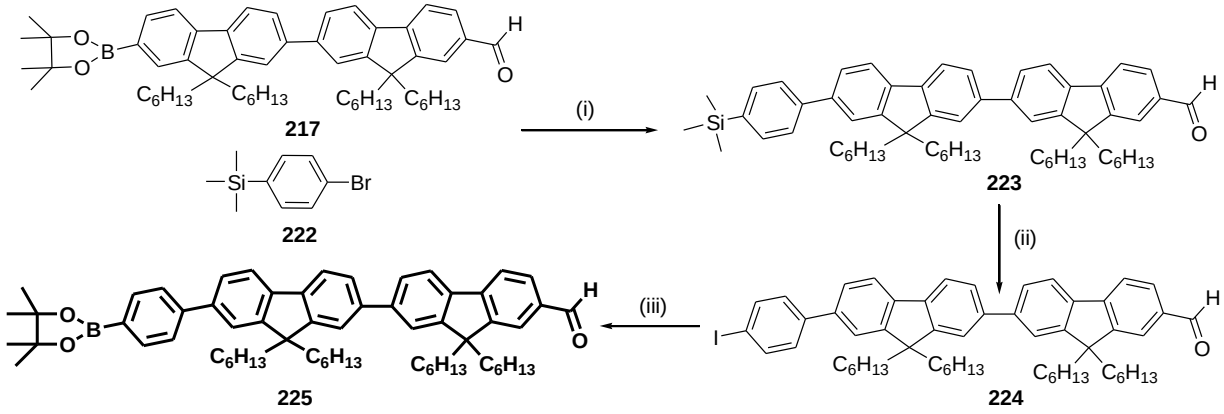

Reagents and conditions: (i) $Pd(PPh_3)_4$, K_2O_3 (aq), toluene, 110 ˚C, 87%; (ii) ICl, DCM, 0 ˚C to 20 ˚C, 100%; (iii) B_2pin_2, KOAc, $Pd(OAc)_2$, DMF, 90 ˚C, 66%.

Scheme 4.2 (b) – Synthesis of key intermediate (in bold) for phenyl linked (*n* = 2) oligomer

In order to functionalise the OF intermediates with Fc, Suzuki coupling reactions were attempted between the boronic ester fluorene derivatives and commercially available bromoferrocene. Suzuki couplings of bromoferrocene are not widely reported in the literature and initial attempts of the reaction of compound **215** with bromoferrocene were unsuccessful using "standard" Suzuki conditions i.e. $Pd(PPh_3)_4$ catalyst with 1,4-dioxane as a solvent, tribasic potassium phosphate or potassium carbonate as bases and reaction temperatures of 85 °C. These conditions returned only unreacted starting materials.

A small number of Suzuki reactions have been reported for iodoferrocene, for example, the works of Imrie *et al.*[148] and Sailer *et al.*[149] both of whom used palladium(II)acetate as a catalyst

and an aqueous ethanol solution as the solvent. Imrie *et al*. reported a systematic study of reaction conditions of iodoferrocene with a variety of aryl boronic acids and concluded that the optimal conditions were deoxygenated 90% ethanol as a solvent, palladium(II)acetate as a catalyst and either potassium carbonate or barium hydroxide as the base, at room temperature.[148] It was also noted that "scrupulous deoxygenation of the solvent was found to be most critical".[148] Whilst iodoferrocene would be expected to react more readily in these reactions than bromoferrocene, the reaction of **215** with bromoferrocene was performed successfully using these conditions, affording the Fc-based product, **226** in a moderate yield of 49% (Scheme 4.3).

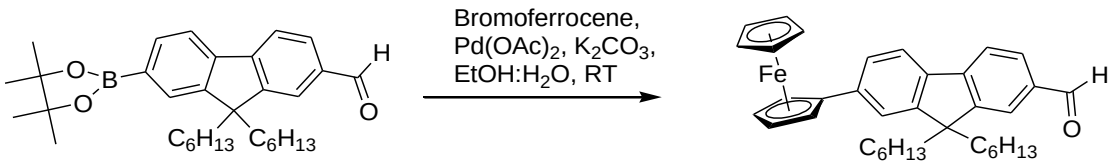

215 **226**

Scheme 4.3 – Suzuki coupling of compound 215 with bromoferrocene

After the reaction, there remained unreacted bromoferrocene (equating to a converted product yield of 65%), but stirring for a longer time and/or heating the reaction did not increase the product yield, hence the reaction conditions were not altered and the modest yield was attributed to the intrinsically lower reactivity of bromoferrocene compared with iodoferrocene. In agreement with Imrie *et al*. it was also noted in our reactions that without thorough degassing of the reaction solvent (e.g. bubbling through argon for at least 2 h prior to reaction), the product yield is indeed significantly reduced. These reaction conditions were used for the synthesis of compounds **227** (29%), **228** (37%), **229** (28%) from the other three fluorene-based boronic ester intermediates (Schemes 4.4 (a) and (b) show structures).

Once the intermediate Fc-based compounds were obtained, they were functionalised with C_{60} (to give compounds **230**-**233**) by the standard 1,3-dipolar addition reaction using sarcosine in chlorobenzene (Prato reaction) (Scheme 4.4(a) and (b)). Initial sonication of the C_{60}-containing solution helps to break up any aggregates which would reduce the reactivity. The progress of these reactions can be easily monitored by TLC as the product appears as a dark brown spot above the Fc-based starting material (which appears as a dark red spot). Once the starting material spot had disappeared (after ~ 4-7 h), the reaction was stopped. Purification by column chromatography initially eluting with carbon disulfide was necessary to remove the unreacted C_{60}; attempting to remove the C_{60} with other solvent systems, e.g. petroleum ether/hexane/toluene combinations was unsuccessful as the C_{60} streaks on the column and

contaminates the product. Once the C_{60} had been removed the products were eluted with different solvent systems, e.g. hexane:toluene 1:1 *v*/*v* to reduce the amount of toxic carbon disulfide used.

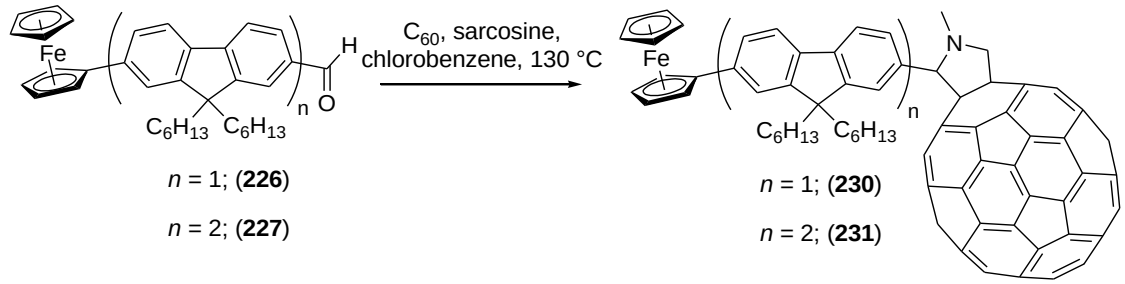

n = 1; (**226**)

n = 2; (**227**)

n = 1; (**230**)

n = 2; (**231**)

Scheme 4.4 (a) – Synthesis of directly linked (*n* = 1 and 2) oligomers

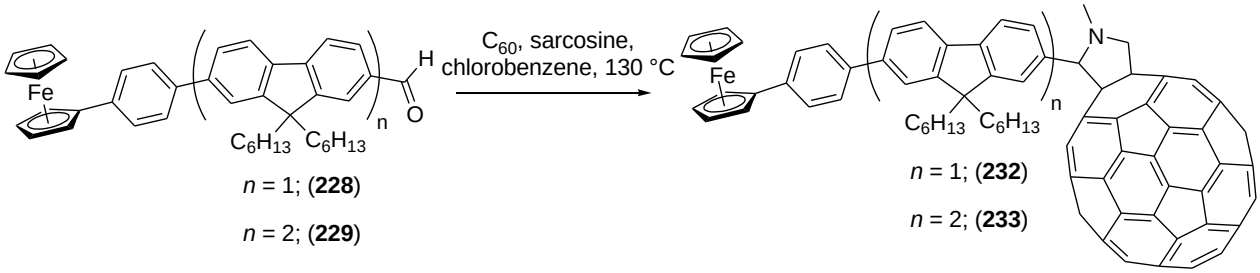

n = 1; (**228**)

n = 2; (**229**)

n = 1; (**232**)

n = 2; (**233**)

Scheme 4.4 (b) – Synthesis of phenyl linked (*n* = 1 and 2) oligomers

For the vinyl linked compounds, a different synthetic strategy was required (Scheme 4.5). Vinyl ferrocene (**235**) was synthesised from ferrocenecarboxaldehyde (**234**) which was then subjected to a Heck reaction with the mono-bromo functionalised fluorene oligomers (**214** or **216**) to give the intermediate aldehyde functionalised compounds **236** and **237** in good yields. These compounds were then functionalised with C_{60} in the same way as for the directly linked and phenyl linked compounds to give products **238** and **239**.

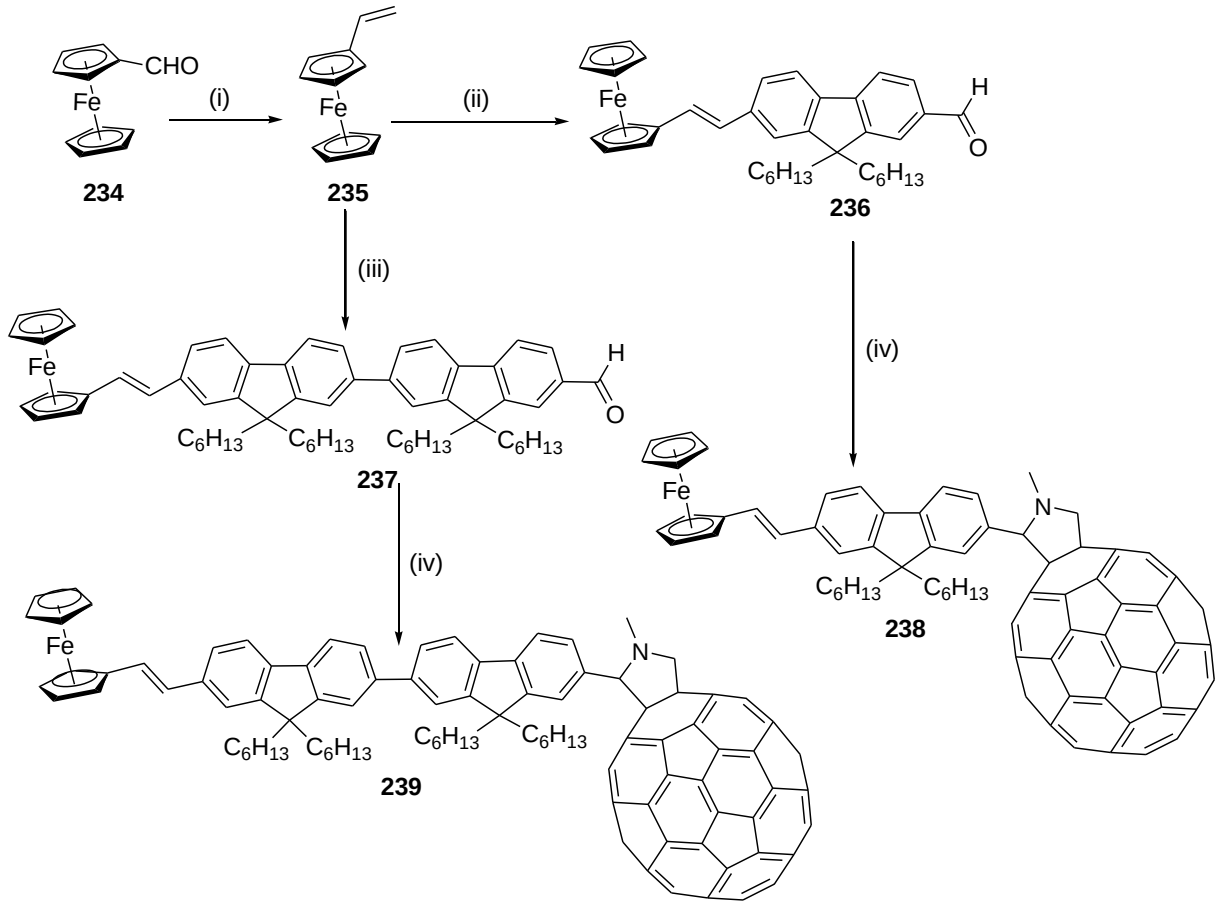

Reagents and conditions: (i) Ph_3PCH_3Br, ^nBuLi, THF, 0 ˚C, 72%; (ii) **214**, K_2CO_3, Bu_4NBr, $Pd(OAc)_2$, DMF, 95 ˚C, 62%; (iii) **216**, K_2CO_3, Bu_4NBr, $Pd(OAc)_2$, DMF, 95 ˚C, 67%; (iv) C_{60}, sarcosine, chlorobenzene, 130 ˚C, 55% for **238**; 48% for **239**.

Scheme 4.5 – Synthesis of vinyl-linked compounds

The six final compounds were obtained in good yields as amorphous black powders. The products were characterised by ^1H and ^{13}C NMR and MALDI mass spectrometry (using other mass spectrometry techniques leads to substantial fragmentation of the compounds). MALDI spectra generally show the [M+1] peaks as well as the [M-C_{60}] peaks. CHN analysis and melting points could not be obtained, which is the case for all similar compounds in the literature. Figure 4.7 shows the ^1H NMR spectrum of compound **230** as an example. The six aromatic fluorene protons are in the region ~ 8-7 ppm. Two of these protons (7.98 ppm and 7.69 ppm) appear as broad singlets which are attributed to the bulky fulleropyrrolidine preventing efficient relaxation of part of the molecule and are, therefore, assumed to be the two fluorene protons in closest proximity to this ring. The characteristic Fc protons appear in the region of ~ 4.8-4.0 ppm as three singlets (2H, 2H and 5H). The 2H signal at ~ 4.3 ppm appears as a multiplet due to the superimposition of one of the pyrrolidine protons (the other two

pyrrolidine protons appear as a triplet at ~ 5.03 ppm). The fluorene alkyl chain protons appear in the expected region as broad signals, again attributed to the reduced relaxation ability of part of the molecule, and the *N*-bonded methyl is seen as a singlet at ~ 2.9 ppm.

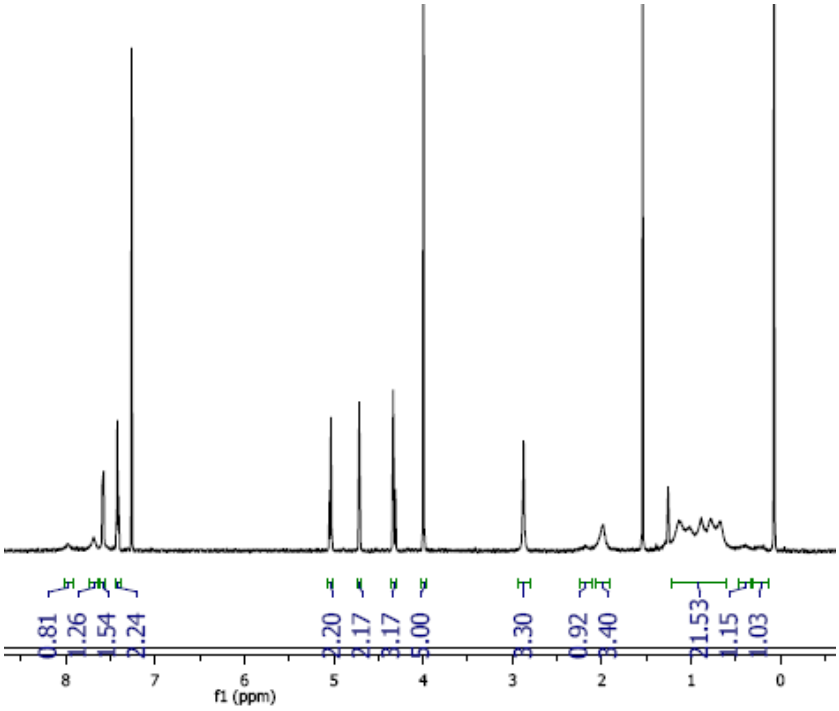

Figure 4.7 – ^{1}H NMR spectrum of compound 230 (in $CDCl_3$)

4.2.2 Electrochemical Studies

The electrochemical properties of the six final compounds **230**-**233**, **238**, **239** as well as their aldehyde precursors **226**-**229**, **236**, **237** were investigated. Cyclic voltammetry measurements were performed at room temperature in a solvent mixture of *ortho*-dichlorobenzene:acetonitrile (4:1 *v*/*v*) using a glassy carbon working electrode, a freshly prepared $Ag/AgNO_3$ reference electrode, a platinum wire counter electrode and Bu_4NClO_4 as the supporting electrolyte (0.1 M), with a scan rate of 100 mVs^{-1}. Table 4.1 summarises the relevant electrochemical data, including data from the previously synthesised alkynyl linked compounds (**211** and **212**). Figures 4.8 and 4.9 show selected scans of the products; additional scans are given in Appendix II.

Compound	$E^1_{1/2,\,red}$	$E^2_{1/2,\,red}$	$E^3_{1/2,\,red}$	$E^4_{1/2,\,red}$	$E^1_{1/2,\,ox}$	$E^2_{1/2,\,ox}$
C_{60}	803	1207	1673	2138	-	-
230 (Fc-F-C_{60})	915	1335	1886	-	209	1550*
231 (Fc-F_2-C_{60})	918	1335	1887	-	203	1556*
232 (Fc-Ph-F-$_{C60}$)	915	1333	1888	-	233	1641*
233 (Fc-Ph-F_2-C_{60})	918	1332	1887	-	218	1585*
238 (Fc-C=C-F-C_{60})	913	1330	1879	-	178	1466*
239 (Fc-C=C-F_2-C_{60})	910	1330	1878	-	173	1462*
211 (Fc-yne-F-$_{C60}$)	909	1325	1881	-	314	1456*
212 (Fc-yne-F_2-C_{60})	885	1297	1844	-	308	1462*
Fc	-	-	-	-	197	-
226 (Fc-F-CHO)	2101	-	-	-	227	-
227 (Fc-F_2-CHO)	2078	-	-	-	219	-
228 (Fc-Ph-F-CHO)	2072	-	-	-	230	-
229 (Fc-Ph-F_2-CHO)	2071	-	-	-	216	-
236 (Fc-C=C-F-CHO)	2010	-	-	-	189	-
237 (Fc-C=C-F_2-CHO)	2011	-	-	-	181	-

Potentials in mV; scan rate 100 mVs^{-1}; glassy carbon working electrode; $Ag/AgNO_3$ reference electrode; Pt wire counter electrode; 0.1 M Bu_4NClO_4 in *o*DCB/CH_3CN (4:1 *v*/*v*); * broad, irreversible oxidation wave

Table 4.1 –Electrochemical data for all compounds studied

Figure 4.8 shows scans for the four (*n* = 1) final compounds **211**, **230**, **232**, **238**. Figures 4.9(a) and (b) show the oxidation and reduction scans of the same compounds compared with unfunctionalised ferrocene (Fc) and C_{60} respectively. All compounds show amphoteric redox behaviour (NB. (*n*=2) compounds show similar trends and scans can be seen in Appendix II).

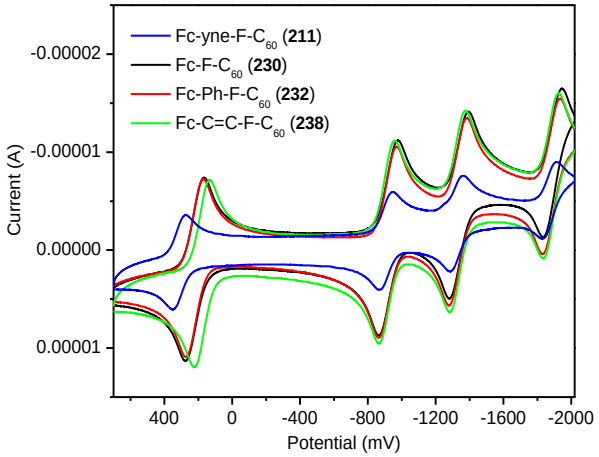

Figure 4.8 – Scans of final (*n* = 1) compounds (between + 700 and - 2000 mV)

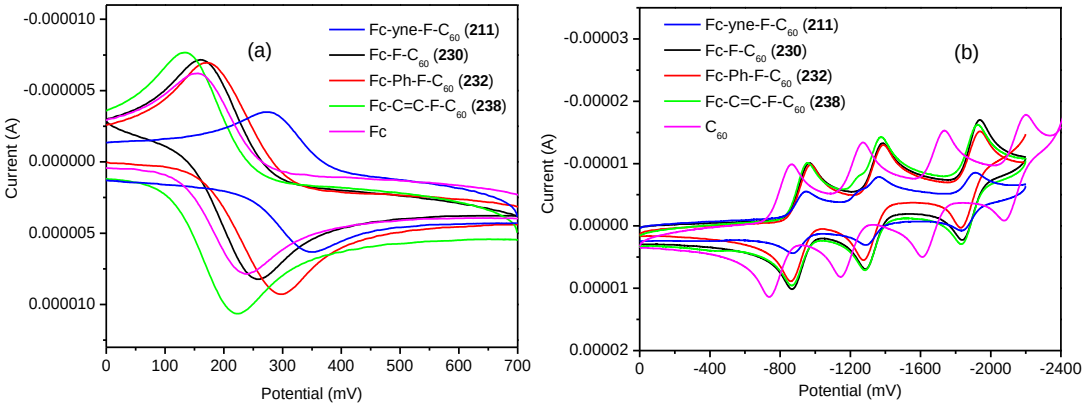

Figure 4.9 – Oxidation (a) and reduction (b) scans of (*n* = 1) compounds

Oxidative scans of the oligomers (Figure 4.9(a)) show quasi-reversible first oxidation potentials which can be assigned to the one electron oxidation of the Fc core. Full oxidation scans of the products, up to 2000 mV, show an irreversible process occurring as the fluorene units are oxidised at ~ 1500 – 2000 mV. For the directly linked (**230**) and phenyl linked (**232**) compounds, the first oxidation potential is roughly comparable to that of Fc under the same conditions. The slight increase in oxidation potentials seen can be assigned to the polarised ground state of the molecule which reduces the donor capability of the systems.

The vinyl linked compound (**238**) shows a decrease in oxidation potential compared with Fc, implying increased donor capabilities. This could potentially imply that electron donation is coming from the bridge of the molecule as well as the Fc moiety or simply that there is better communication between the donor and acceptor in these systems. This result seems to agree with the work of Wielopolski *et al*. who introduced a similar system where the donor is exTTF and the acceptor is C_{60}, linked by an oligo-vinylfluorene bridge (**240**, Figure 4.10).[143] It was reported that the incorporation of a vinyl spacer between the exTTF donor and the fluorene bridge decreased the electronic repulsion between the two electron rich systems, allowing the bridge to adopt a more planar structure thus providing a continuous π electron pathway from the donor across the bridge to the acceptor. The vinylene linked systems therefore showed better charge transfer features and lower β values than their pristine oligofluorene analogues.[143] It is therefore suggested that a similar effect is occurring in our vinyl linked system.

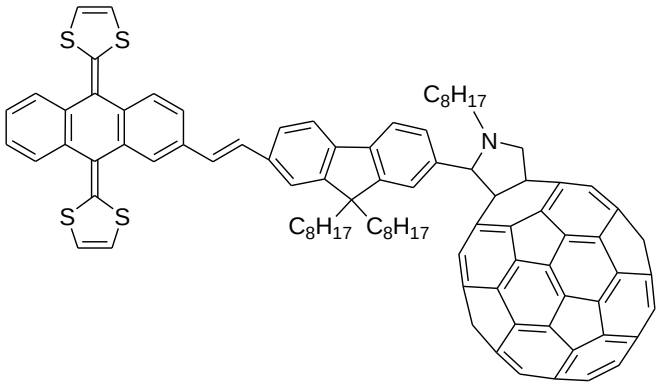

240

Figure 4.10 – Structure of exTTF-OF-C_{60} system with vinyl linker

Conversely, the alkynyl linked compound (**211**) shows an increase in oxidation potential compared with both Fc and the other compounds, implying significantly reduced donor capabilities of this system. This could mean the alkynyl linker is not a good bridging unit between Fc and fluorene i.e. is twisted between the two such that electron transfer capabilities are reduced. Photophysical studies will aim to investigate these effects further and determine the wire-like properties of each of the systems.

The reduction scans show three consecutive one-electron reduction waves which are chemically reversible. By comparison to unfunctionalised C_{60}, these waves can be assigned as the reduction steps of the electron-accepting C_{60} core of the molecules, showing the lack of substantial electronic interactions in the ground state of the molecules. These reduction peaks are cathodically shifted to more negative potentials compared to C_{60} implying reduced electron accepting ability presumably due to the polarised ground state of our donor-bridge-acceptor systems, as well as the reduced accepting ability arising from the breaking of the C_{60} symmetry due to the pyrrolidine unit.

Comparisons of the intermediate, Fc-only functionalised compounds (**226**-**229**, **236**, **237**; Table 4.1 and Appendix II) compared with their C_{60} functionalised analogues show no significant change in the oxidation potentials. However, quasi-reversible reduction peaks at ~ 2100 mV are observed which correspond to reduction of the fluorene units which are not seen once the compounds have been functionalised with C_{60}.

Photophysical studies are currently underway in the group of Professor D. M. Guldi (University of Erlangen-Nürnberg) to study these compounds in order to fully understand the charge

transfer dynamics of the systems and assess their potential for use in optoelectronic applications, e.g. molecular wires and OPVs.

4.3 Conclusions

The use of fluorene as a bridging unit in D-A systems for probing charge transfer processes on a molecular level has been extended to a set of novel donor-bridge-acceptor systems where the donor is Fc, the acceptor is C_{60} and the bridge is either a mono- or bi-fluorene which is either directly linked to the Fc or linked via a spacer (phenyl, vinyl or alkynyl). Electrochemical studies show that the compounds exhibit amphoteric redox behaviour, with three one-electron reduction waves from the C_{60} core and one oxidation wave from the Fc core. Photophysical studies are currently underway to investigate the electron/energy transfer processes occurring in the systems and hence their potential for charge separated energy storage in solar cell applications.

Chapter 5: Probing the Beta Phase in 9,9-Dioctylfluorene-Based Donor-Acceptor Co-Polymers

5.1 Introduction

In the previous chapters the role of fluorene as an electron donor with dibenzothiophene-*S*,*S*-dioxide (**S**) as an electron acceptor has been discussed in both oligomers and polymers, as well as the role of oligofluorenes as bridging units between donor (Fc) and acceptor (C_{60}) moieties. In this chapter the phase behaviour of random co-polymers of dialkylfluorenes is investigated with various co-monomers, including **S**, in order to gain a fuller understanding of the factors which control the photophysical properties of these systems.

Polyfluorenes (PFs), specifically dialkyl substituted PFs, are a class of electroluminescent conjugated polymer which have been extensively used in many molecular electronics-type applications including OLEDs, OPVs, OFETs and molecular wires.[150] It has been established by various workers that the phase behaviour of PFs (especially the commonly studied poly(9,9-dioctylfluorene), **PFO**/**PF8**, (**241**), (Figure 5.1), can have a significant effect on the emission properties.[151] Understanding the nature of these phases is therefore necessary in order to gain a fuller knowledge of the properties of PFs. Grell and Bradley *et al*. commented on a shoulder in the absorption spectrum of PFO which could become a defined peak at ~ 437 nm in certain types of films.[152,153] It was suggested that this lower energy state was associated with areas of extended chain conformation thought to be a result of the polymer's response to a physical stress, e.g. from solvent quality or temperature.[153]

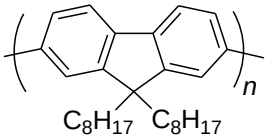

241

Figure 5.1 – Structure of PFO

This absorption peak has been attributed to the presence of beta phase within the bulk material which can be induced by spinning films of the material from poor solvents, solvent exposure and thermal cycling.[153] The beta phase is characterised by regions where adjacent fluorene units are co-planarised (rather than twisted) resulting in red shifted absorption/emission peaks[154] as shown schematically in Figure 5.2. Even a small fraction of beta phase within a polymer can strongly affect its emission by acting as a low energy trap for excitons generated within the bulk "alpha" phase of the polymer.[155]

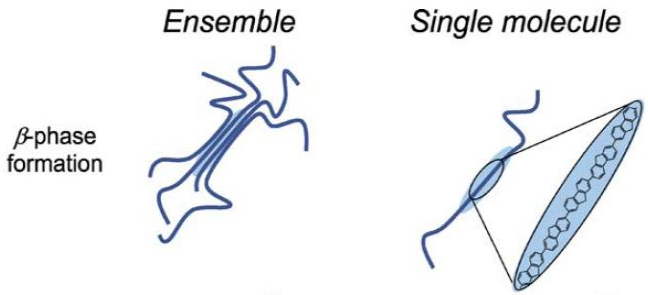

Figure 5.2 – Schematic illustration of the planarised conformation of the β phase in PFO [156]

These effects on emission can have a significant effect on device properties, hence understanding the origins of the beta phase and the factors that govern its formation are of contemporary interest.

For example, Lu *et al*. reported an increase in device performance and improved blue colour purity from a PFO-based device "self-doped" with beta phase compared to its alpha phase analogue.[157] The beta phase device performance was quoted as 3.85 cd A^{-1}, with an EQE of 3.33% and CIE (x + y) value of 0.283 ((x + y) < 0.3 is required for pure blue); compared with 1.26 cd A^{-1}, 1.08% and (x + y) = 0.323 for an analogous device where the beta phase was not induced. The increase in device performance was attributed to more balanced charge transport through the material as the areas of extended conformation of the beta phase promote hole transport, whilst also acting as electron traps. The increased blue colour purity was attributed to a decrease in the low energy wavelength emission generally seen as a "tail" at > 490 nm in the alpha phase of PFO, giving a narrower emission band and therefore a lower (x + y) value. This improved charge carrier mobility due to the planar alignment of the beta phase was also reported by Prins *et al*. investigating the beta phase of PFO for optoelectronic device applications.[158] Similarly O'Carroll *et al*. reported the synthesis of nanowires based on PFO which showed significant beta phase content, dominating the optical behaviour of the materials which were classed as a potentially important development in nanoscale optoelectronic devices.[159] The beta phase also has applications in lasing as the emission is concentrated in a very narrow spectral region which can lead to a large gain in this wavelength, i.e. amplified spontaneous emission (ASE).[160,161]

As well as in fluorene-based polymers, beta phase formation has also been investigated in oligomers, e.g. by Tsoi *et al*. who showed that beta phase could be generated in two fluorene oligomers; a pentamer and an oligomer composed of chains with a maximum length of 19

units.[162] From their studies it was determined that the enhanced structural rigidity of the beta phase gave rise to a highly extended and delocalized electronic system.

There have been numerous studies focused on determining the factors which govern the formation of the beta phase in PF homo-polymers. In 2006 Knaapila *et al*. looked at the influence of solvent quality on the phase behaviour of **PFO** (linear octyl side chains) with that of poly[9,9-bis(2-ethylhexyl)fluorene-2,7-diyl] (**PF2/6**, **242**) (branched 2-ethylhexyl side chains), Figure 5.3.[163]

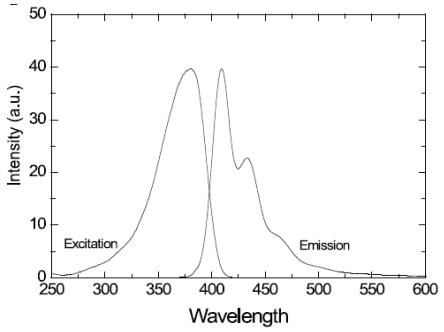

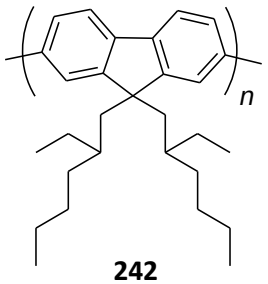

242

Figure 5.3 – Excitation and emission spectra of PF2/6 in dilute MCH solution and its structure [160]

The data showed that **PF2/6** formed long, thin aggregates in both toluene (a "good" solvent) and MCH (a "poor") solvent, whereas **PFO** showed rod-like structures in toluene, but sheet-like structures in MCH.[163] The sheet-like structures were attributed to the beta phase by comparison of solid state absorption spectra, implying that beta phase could be induced in **PFO** but not in **PF2/6**. The influence of side chain length was investigated further by studying the self-assembly of a series of PFs (in MCH) with increasing side-chain length: poly(9,9-dihexyl)fluorene (**PF6**), poly(9,9-diheptyl)fluorene (**PF7**), **PFO** (or **PF8**), poly(9,9-dinonyl)fluorene (**PF9**) and poly(9,9-didecyl)fluorene (**PF10**).[164] It was concluded that beta phase formation in the solid state was present for **PF7**, **PF8** and **PF9**, characterised by a distinct absorption peak at ~ 2.9 eV.[164] It was postulated that the side chain interactions of the various polymers are critical for beta phase formation; however no further details were provided.

Bright *et al*. investigated this set of polymers further using optical spectroscopy to show a trend between formation of the beta phase and alkyl side chain length.[155] Figure 5.4 shows the temperature dependent absorption spectra of polymers **PF6**, **PF7**, **PF8**, and **PF9** in dilute solutions of MCH. From these spectra it can be seen that: (i) in **PF6** there is no characteristic beta phase peak (expected at ~ 440 nm); (ii) in **PF7** a small beta phase peak emerges at low temperature (190 K); (iii) in **PF8** there is a strong beta phase peak appearing at 270 K (increasing in intensity with decreasing temperature) and (iv) in **PF9** there is beta phase, but it

is less intense than in **PF8**. Further investigation into the behaviour of **PF6** determined that aggregates were forming in solution at room temperature, a feature which is not seen in branched-chain **PF2/6**; however, these aggregates in **PF6** were not giving rise to beta phase formation.[155]

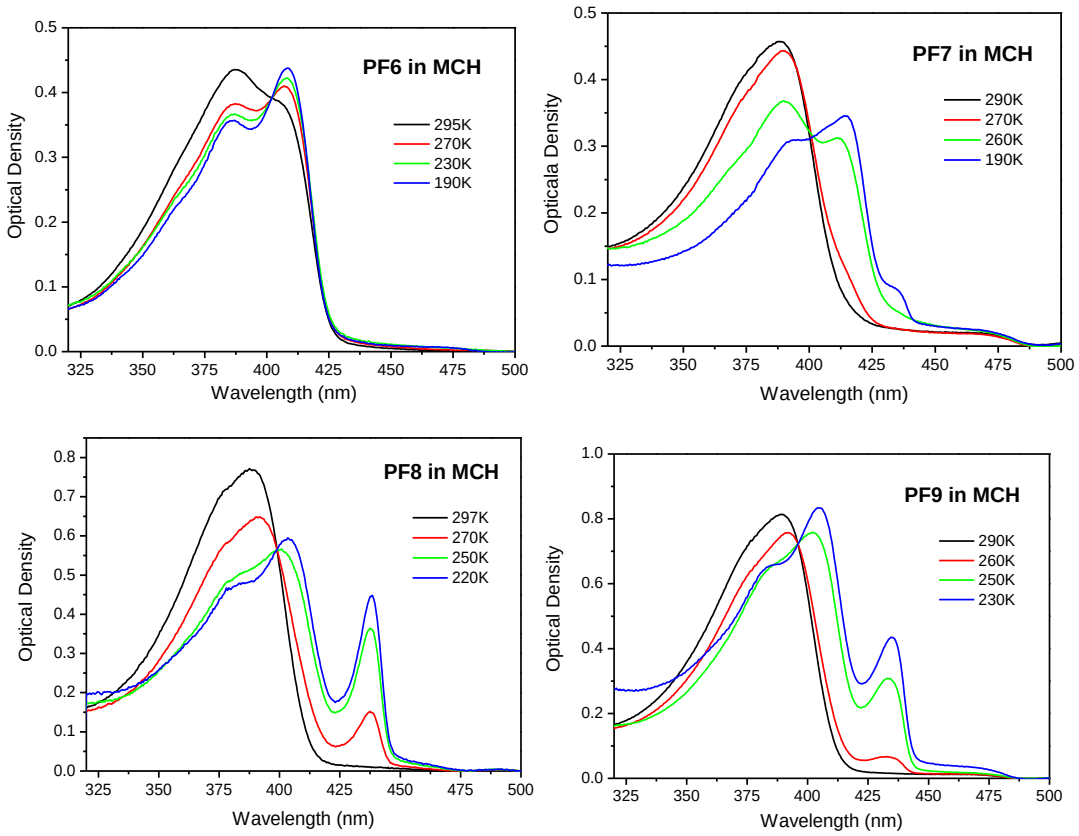

Figure 5.4 – Temperature dependent absorption spectra of PF6, PF7, PF8, PF9 in dilute MCH solutions

Bright *et al*. proposed that in poor solvents (i.e. MCH) **PF8** forms sheet-like aggregates (as observed by Knaapila *et al*.[164]) which are held together by inter-digitated alkyl side chains.[155] If the binding energy from the van der Waals forces holding the alkyl chains together is sufficiently high, the steric hindrance of the backbone interactions can be overcome and the backbone will be planarised, leading to the red-shifted beta phase absorption/emission bands. It is suggested that in **PF6**, while the aggregated structure can still form, the shorter side chains do not have sufficient energy to planarise the backbone, hence beta phase formation does not occur. Similarly in **PF7** it is reasonable to suggest that the chains now have barely enough energy to planarise the backbone, so only a small fraction of beta phase can be seen.[155] The longer side chains in **PF9** are likely to be more disordered giving rise to weaker bonding and hence lower amounts of beta phase are seen compared to **PF8**. It has been recently demonstrated that some beta phase can also be formed in thin films of **PF10**, but only trace amounts can be seen in MCH solutions due to the high solubility of the long alkyl chains

reducing aggregation.[165] In thin films of **PF10** this effect is removed, so some beta phase can be observed.[165] Overall, it is suggested that **PF8** has the optimal side chain length for formation of the beta phase.[155]

5.2 Results and Discussion

As discussed above, the formation/prevention of beta phase in PFs is of great interest and there have been numerous studies regarding this. However, in many optoelectronic applications, PFs are not used as homo-polymers; fluorene units are co-polymerised with other moieties (as discussed in Chapters 2 and 3) for example to improve charge transport or to tune the colour emission. Consequently there is interest in studying the formation of beta phase in fluorene co-polymers. For example Lee *et al*. reported an increase in EL device efficiencies attributed to the beta phase in a PFO-based co-polymer with an ambipolar co-monomer unit consisting of phenothiazine and 4-(dicyanomethylene)-2-methyl-6-[*p*-(dimethylamino)styryl]-4*H*-pyran in 0.05, 0.08 and 0.10 mol% incorporations (**243**, Figure 5.5(a)).[166] Similarly, Niu *et al*. reported a two-fold increase in device performance and increased white colour purity from the single PFO-based emissive polymer, poly(9,9-di-*n*-octylfluorene)-*co*-4,7-bis(4-N-phenyl-N-(4-methylphenyl)aminophenyl-2,1,3-benzothiadiazole) (**244**, Figure 5.5(b)) when incorporated into devices which were subject to solvent processing to induce the beta phase.[167] The following sections will discuss the syntheses and photophysical properties of three sets of PF-based co-polymers in relation to beta phase formation.

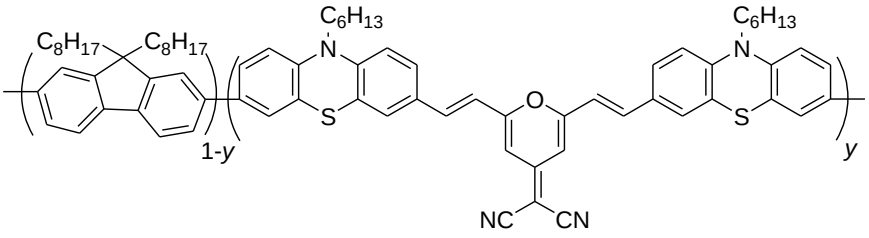

243

Figure 5.5 (a) – Structure of ambipolar PF co-polymer[166]

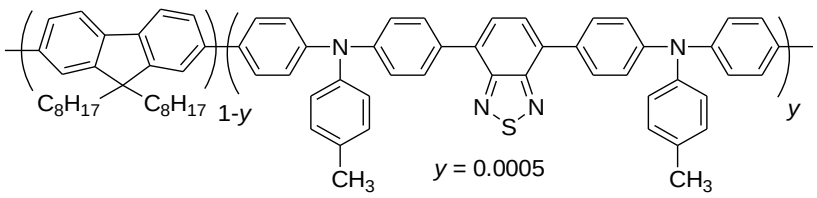

244

Figure 5.5 (b) – Structure of PF-based white-emitting co-polymer[167]

5.2.1 PF8-dibenzothiophene-*S*,*S*-dioxide and PF8-dibenzothiophene co-polymers

One of the few investigations into beta phase formation in PF co-polymers is from Knaapila *et al*. who studied PFO co-polymers with varying amounts of 9,9-bis(2-ethylhexyl)fluorene (**PF2/6**) as a co-monomer.[168] In their study it is suggested that in the case of solutions of the polymers in poor solvents the formation of beta phase is inhibited once the co-monomer (**PF2/6**) content reaches 10%.[168] Although this is mainly a theoretical study based on polymers in solution (no emission spectra are shown), it was observed that the polymers with 5% and 10% **PF2/6** content formed viscous gels in the same way as pure **PFO** upon aggregation, whilst a 50% co-polymer remained as a transparent liquid.[168] This potentially implies beta phase formation is occurring in the 5% and 10% co-polymers, but not in the 50% co-polymer – a result not highlighted in this study.

As discussed in previous chapters, the Bryce group has been instrumental in the development of **PF8** co-polymers and co-oligomers incorporating **S** units to give systems which show high luminescence efficiency and improved charge transport characteristics with respect to PF-only systems.[65,68,69,88,93,169] Thus we were keen to investigate beta phase formation in a series of random co-polymers of poly(9,9-dioctylfluorene) (**PFO**/**PF8**) with 2%, 5%, 8%, 12% and 15% of **S**; **PF8-S** (**245**-**249**), in comparison with pure **PFO** (i.e. **S** = 0, **241**) (Scheme 5.1(a)). As described in Chapters 2 and 3, the incorporation of the electron-accepting **S** unit into co-oligomers and co-polymers leads to the generation of an intramolecular charge transfer (ICT) state which appears as a broad red-shifted emission band in polar solvents and in thin films of the materials.[65,68,69,88,93,169] Therefore, a second set of PF co-polymers was synthesised for comparison where the co-monomer is dibenzothiophene (**DBT**, **86**) to allow the effects of monomer incorporation on beta phase formation to be elucidated without the potential interference of an ICT emissive state. Co-polymers **PF8-DBT** (**251**-**254**, Scheme 5.1(b)) were synthesised with 8%, 12%, 15% and 20% **DBT** content. Table 5.1 shows the M_n and M_w values for each polymer.

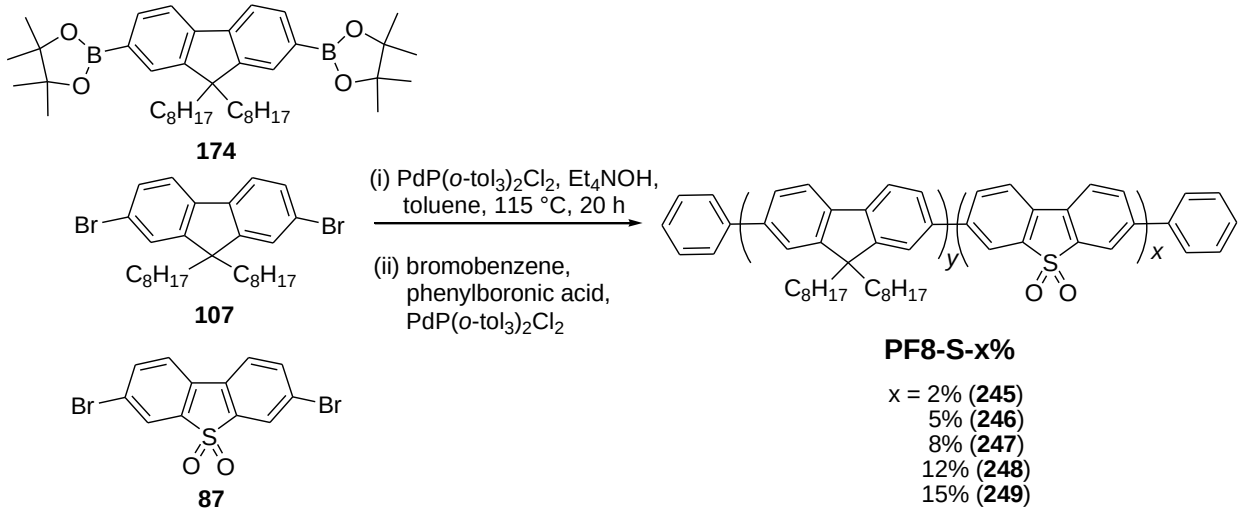

Scheme 5.1(a) – Synthesis of PF8-S co-polymers

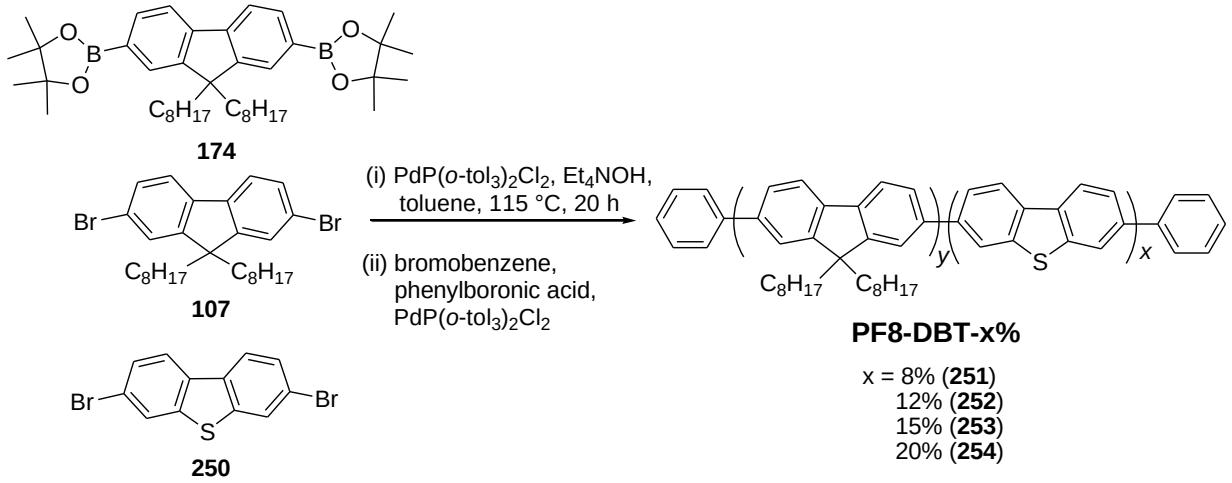

Scheme 5.1 (b) – Synthesis of PF8-DBT co-polymers

Polymer	S-Unit (%)	DBT-Unit (%)	M_n (Da)	M_w (Da)
PFO/PF8* (**241**)	0	0	73,000	258,000
PF8-S-2% (**245**)	2	0	57,000	220,000
PF8-S-5%* (**246**)	5	0	50,000	177,000
PF8-S-8% (**247**)	8	0	54,000	210,000
PF8-S-12% (**248**)	12	0	35,000	131,000
PF8-S-15%* (**249**)	15	0	39,000	124,000
PF8-DBT-8% (**251**)	0	8	47,000	157,000
PF8-DBT-12% (**252**)	0	12	40,000	140,000
PF8-DBT-15% (**253**)	0	15	55,000	181,000
PF8-DBT-20% (**254**)	0	20	53,000	158,000

**synthesised by Dr. K. T. Kamtekar*

Table 5.1 – Analysis of composition and molecular weights of the polymers

The polymers were synthesised using palladium-catalysed Suzuki cross-coupling conditions (as discussed previously, Chapters 2 and 3). All the polymers were obtained as fluffy yellow solids in high yields and were determined to have high molecular weights by GPC (see experimental procedures chapter for full details). In order to induce beta phase formation the polymers were spun into thin films and exposed to warm toluene vapour for 20 minutes. The area normalised absorption spectra for the **PF8-DBT** co-polymers after toluene exposure is shown in Figure 5.6(a). The characteristic beta phase absorption peak can be seen at ~ 435 nm in the 0% film, steadily decreasing in intensity until it has fully disappeared in **PF8-DBT-20%** (**254**). This is supported by the emission spectra shown in Figure 5.6(b) which shows the characteristic beta phase emission peak at ~ 440 nm appearing for all the films up to 15% **DBT** content (**253**), with only a very small peak visible in this region for the 20% **DBT** content polymer. The inset of Figure 5.6(b) shows beta phase formation decreasing linearly with increasing **DBT** content.

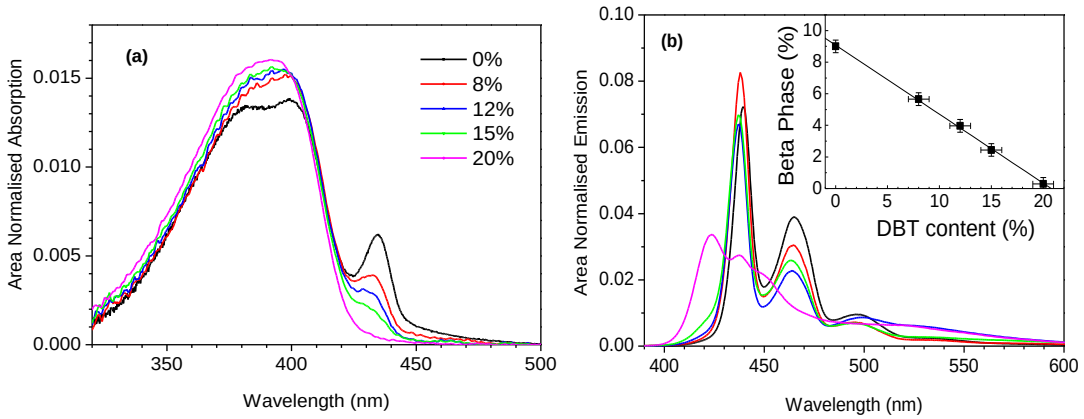

Figures 5.6(a) and (b) –Absorption and emission of PF8-DBT co-polymers after toluene vapour exposure

The normalised absorption and emission spectra for the **PF8-S** co-polymers are shown in Figures 5.7(a) and (b) before (dashed lines) and after (solid lines) exposure to toluene.

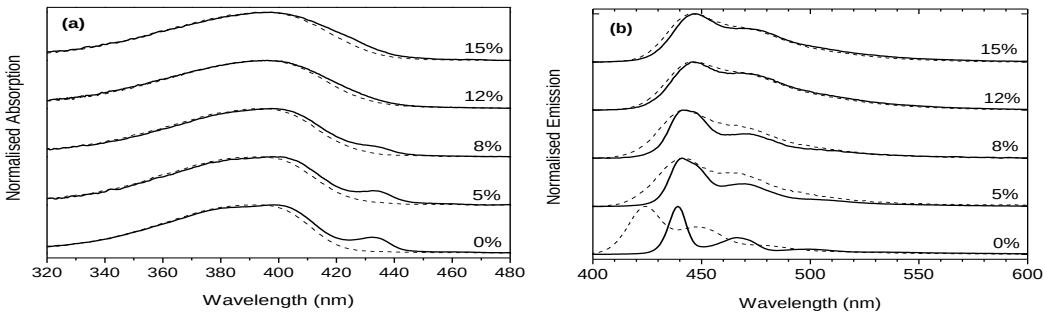

Figure 5.7(a) and (b) – Absorption and emission of PF8-S polymers for as-spun (dashed line) and toluene vapour exposed films (solid line).
NB 2% film is excluded for clarity but follows the trend shown

From these spectra we can see two clear trends for the **PF8-S** co-polymers: the absorption of the as-spun films becomes broader and red-shifted with increasing **S** unit content; the characteristic beta phase absorption at ~ 435 nm is seen in the 0%, 5% and 8% co-polymers, but not in the 12% or 15% co-polymers. The changes that are seen in the absorption spectra at these higher **S** unit concentrations can be attributed to the formation of aggregates rather than beta phase, perhaps the rod-like aggregates discussed by Knaapila *et al*.[164] The emission of the amorphous (dashed line) films shows the strong influence of the **S** unit, as the broad red-shifted ICT band is seen in all the **S**-containing polymers. It can be seen from the emission of the toluene-exposed films (solid line) that beta phase emission (at ~ 440 nm) is actually inhibiting the formation of the CT band even at **S** unit contents of 8%. The emission of each toluene-exposed film compared to its amorphous analogue shows significant sharpening of the vibronic replicas i.e. more well-resolved peaks, indicative of an increase in ordering of the polymer chains. The loss of this ordering with increasing **S** content is attributed to the lower amount of beta phase being induced in these films and hence more CT emission. Both the ICT state and the beta phase of these co-polymers can act as low energy traps for the excitons.

From the results of these two sets of co-polymers we can see that beta phase appears to be induced up to **DBT** concentrations of ~ 15% in the **PF8-DBT** co-polymers and up to ~ 12% **S** unit concentration in the **PF8-S** co-polymers. In the work from Knaapila *et al*. it is suggested that beta phase would be inhibited once the co-monomer content reached ~ 10%; a similar limit to that in these systems.[168] While this result may be unexpected as the description from Knaapila *et al*. is limited to polymers in solution and our results are for thin films, it is possible that similar energetic considerations can be used due to the way the beta phase was induced, i.e. polymers were exposed to a high concentration of solvent molecules during the swelling process to induce the beta phase.

The mechanism for beta phase formation in PFs presented by Bright *et al*., i.e. that the interdigitation of the alkyl side chains in **PF8** provided enough energy in van der Waals forces to overcome the *peri*-interactions between **F** units in the backbone, allowing planarisation (i.e. beta phase) fits in well with the results of our **PF8** co-polymer systems.[155] Based on this description it can be assumed that without sufficient side chain interactions there would be no planarisation of the backbone and no beta phase would be observed. The incorporation of co-monomer units which are topologically similar to fluorene, but do not have alkyl side chains, would therefore be expected to disrupt this interdigitation. We have seen that beta phase can still be induced in polymers where the co-monomer content is ~ 12 – 15% (decreasing linearly

from this amount) implying that at co-monomer contents higher than this (i.e. **F8** concentrations of less than ~ 85 – 88%) there are insufficient side chain interactions per chromophore to overcome the steric hindrance of the backbone and cause planarisation. These results may point to the generality of this limit and they provide further insights into the factors which govern morphology in **PF8** co-polymers, as well as offering guidelines for the design of new **PF8** co-polymers with regards to the formation/prevention of the beta phase.

5.2.2 PF8-keto co-polymers

As discussed in section 1.3.1, the presence of fluorenone (keto defects) within a PF backbone can degrade the desired blue emission into a lower energy green emission band, reducing device performance. The keto defects act as low energy traps for the excitons formed on the backbone of the polymer. As the beta phase in PFs also acts as a low energy trap it may be expected that there will be competition between these two traps for excitons which are created within the bulk alpha phase of the material. Hence investigation into keto-defect containing PFs with respect to beta phase formation is of interest in understanding the fundamental photophysical processes occurring in these systems.

A series of random co-polymers of poly(9,9-dioctylfluorene) (**PFO**/**PF8**) with varying amounts of the keto unit (0 – 2%) (**PF8-keto**, **255**-**261**) co-polymers were synthesised by S-M polymerisation conditions (Scheme 5.3). Only small amounts of keto defect are needed as at higher concentrations, the green emission band completely dominates the spectra. The polymers were synthesised in high yields, with high molecular weights. Table 5.2 shows the compositions and molecular weight analysis for the co-polymers.

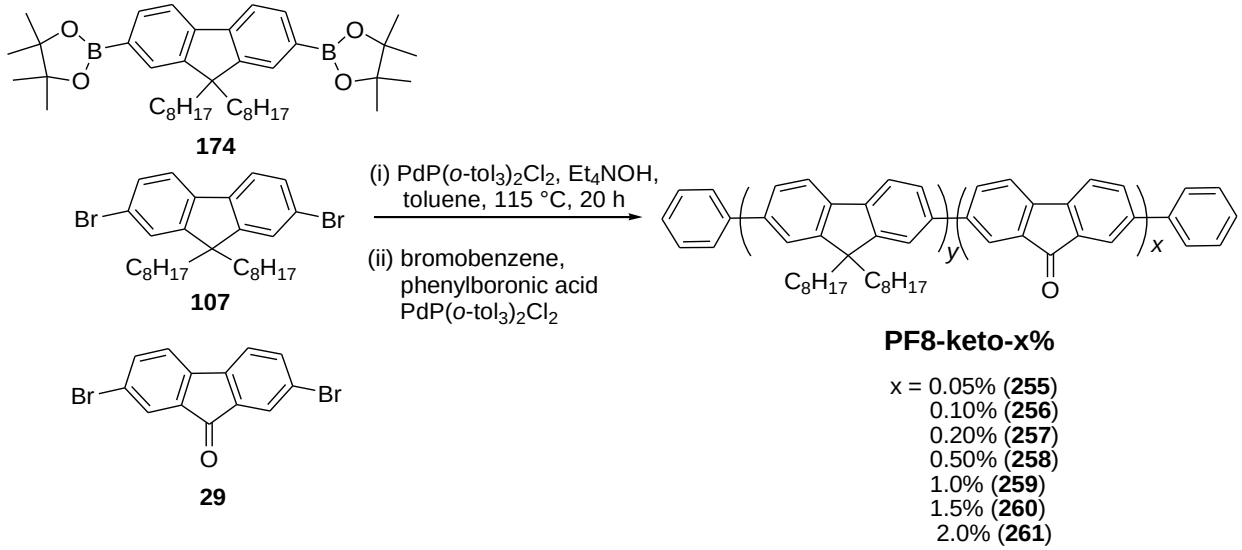

Scheme 5.3 – Synthesis of the PF8-keto co-polymers
(Compound **29** synthesised by Dr. K. T. Kametekar)

Polymer	Keto Unit (%)	M_n (Da)	M_w (Da)
PF8-keto-0.05% (**255**)	0.05	42,000	163,000
PF8-keto-0.1%* (**256**)	0.10	45,000	148,000
PF8-keto-0.20% (**257**)	0.20	28,000	152,000
PF8-keto-0.50% (**258**)	0.50	38,000	166,000
PF8-keto-1.0% (**259**)	1.0	48,000	165,000
PF8-keto-1.5% (**260**)	1.5	42,000	143,000
PF8-keto-2.0% (**261**)	2.0	52,000	221,000

* *Synthesised by Dr. K. T. Kamtekar*

Table 5.2 – Compositions and molecular weight analysis of PF8-keto co-polymers

Beta phase formation was successfully induced by the toluene vapour method (as discussed in section 5.2.1) for all the co-polymers shown in Table 5.2. The amount of beta phase induced is similar to that seen in toluene vapour-exposed **PF8** films, reaching a saturation level of ~ 5 – 6%. Figure 5.8 compares the emission spectra of the **PF8-keto-0.1%** (**256**) co-polymer film before and after exposure to toluene vapour.

Compared to the emission spectra seen for the **PF8**, **PF8-S** and **PF8-DBT** co-polymers, the emission of the **PF8-keto** co-polymers is dominated by a broad band at ~ 530 nm due to the fluorenone units which changes the emission colour of the samples from blue to green-white. The energy transfer to the fluorenone sites must be efficient due to the strong keto emission band seen with only 0.1% fluorenone content (i.e. only 1 keto unit per 1000 monomers). However, we can also see that the emission intensity from the PF is more intense in the beta phase containing sample, indicating some level of competition between these two low energy traps. The emission of both the PF and the keto bands is more structured in the beta phase containing samples, implying a more ordered system, corroborating the side-chain interaction driven mechanism for beta phase formation described earlier. The fact that beta phase emission can still be induced in these polymers shows that even with low energy traps, migration to the beta phase is efficient. However, the decrease in PF emission seen with increased keto content implies that with these low energy traps, care must be taken to balance the energy levels with those of the beta phase traps in order to prevent/utilise beta phase formation. More in-depth photophysical studies are currently underway on these polymers in order to elucidate further information about the exciton migration processes occurring in these materials.

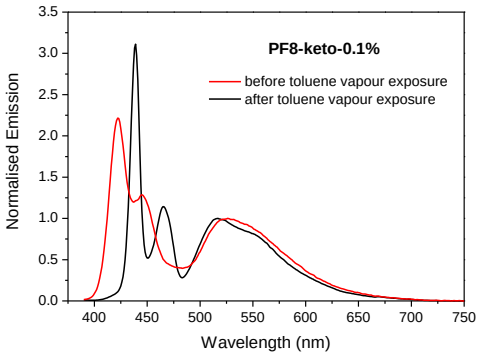

Figure 5.8 – Emission before and after toluene vapour exposure of PF8-keto-0.1% (256)

5.3 Conclusions

Overall, three sets of **PF8**-based co-polymers have been synthesised with co-monomers: dibenzothiophene-*S*,*S*-dioxide (**S**), dibenzothiophene (**DBT**) and fluorenone (**keto**). All polymers were synthesised in high yields from Suzuki-Miyaura polymerisation conditions and have high molecular weights. The beta phase has been successfully induced in all co-polymers by exposure to warm toluene vapour and the photophysical properties of these systems studied in detail. From the **PF8-S** and **PF8-DBT** co-polymers we have demonstrated that beta phase can be induced up to a co-monomer content of ~ 12 – 15%, beyond which it is no longer possible to induce the beta phase. From the **PF8-keto** co-polymers we have demonstrated that there is a competition occurring between the low energy traps of the beta phase and the keto unit. Both investigations provide support to the theory of a side-chain interaction driven mechanism for the formation of the beta phase in **PF8**-based polymers and may aid in the understanding and development of novel PF-based co-polymer systems with improved device performances by the efficient utilisation of the beta phase.

Chapter 6: Reduced Conjugation Polyfluorene-Based Oligomers and Polymers for Novel Host Materials

6.1 Introduction

In the previous chapters the use of fluorene in donor-acceptor architectures has been discussed in detail and results have been presented where fluorene is the donor unit in various co-oligomers and co-polymers, as well as the bridging unit between donor and acceptor moieties. In chapters 2 and 3 the link between reduced conjugation (either through the addition of bulky substituents to twist the backbone or through changing the molecular architecture) and blue shifting of emission was discussed. The fluorene-based systems discussed so far have focused on 2,7-disubstituted fluorene units (Figure 6.1); indeed the majority of research into oligo- and poly-fluorenes has centred on this type of system. Fluorenes have been functionalised at the central C_9 position e.g. with alkyl or aryl groups, but there is little published work involving fluorenes functionalised at, or linked through, the 3,6-positions.

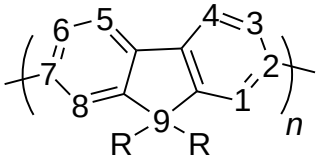

Figure 6.1 – Structure and numbering pattern of dialkyl-substituted PFs

The development of a quick and efficient strategy for the functionalisation of PFs through the 3,6-positions could give access to a novel set of materials with potential optoelectronic applications. By functionalising the fluorene units with different substituents, e.g. electron donating vs. electron withdrawing, the electronic properties of PFs could be tuned. By increasing/decreasing the steric bulk of substituents, the structural properties could be modulated which, in turn, could affect charge transport and migration through the materials. As discussed in section 2.1, the functionalisation of dibenzothiophene-*S*,*S*-dioxide (**S**) with hexyl chains blue shifts the emission of co-polymers with 9,9-dioctylfluorene compared with co-polymers of unfunctionalised **S** units, giving high triplet energy (E_T) polymers capable of hosting green-emitting iridium complexes.[88]

While a host for green-emitting complexes is useful, a key aim in OLED research is to find a material capable of hosting blue-emitting complexes as this is a rare property for conjugated organic polymers. The key requirement of a host material is that it has an E_T level higher than that of the phosphorescent emitter, e.g. the iridium complex, in order to prevent back energy

transfer to the host which would quench the emission of the complex.[170] For green or blue light-emitting devices this requires a material with a high E_T, such as the non-conjugated polymer, poly(vinylcarbazole) (PVK) which has an E_T ~ 2.5 eV.[170] However, PVK-based devices often have high operating voltages due to the high resistivity of the polymer.[170] A high E_T conjugated polymer should be able to improve device performances. In order for a fluorene-based polymer to have a high enough E_T to host blue-emitting complexes, it is necessary to design a system whereby the conjugation through the polymer is reduced compared with PFO either by twisting the backbone or by changing the linkage patterns between adjacent monomers.

In section 3.2, it was demonstrated how positioning a donor unit (e.g. fluorene) in a *para*-position to the sulfone of the **S** unit in ambipolar trimers, reduces the conjugation through the system and blue shifts the emission. A similar strategy has been applied to conjugated polymers including poly(carbazole)s and poly(silafluorene)s. Poly(3,6-carbazole)s are less conjugated than poly(2,7-carbazole)s which blue shifts their emission.[98] Similarly, poly(3,6-silafluorene)s are reported to exhibit deep blue emission with high triplet levels,[58,171] whereas poly(2,7-silafluorene)s are reported to have photophysical properties very similar to those of poly(2,7-fluorene)s.[56]

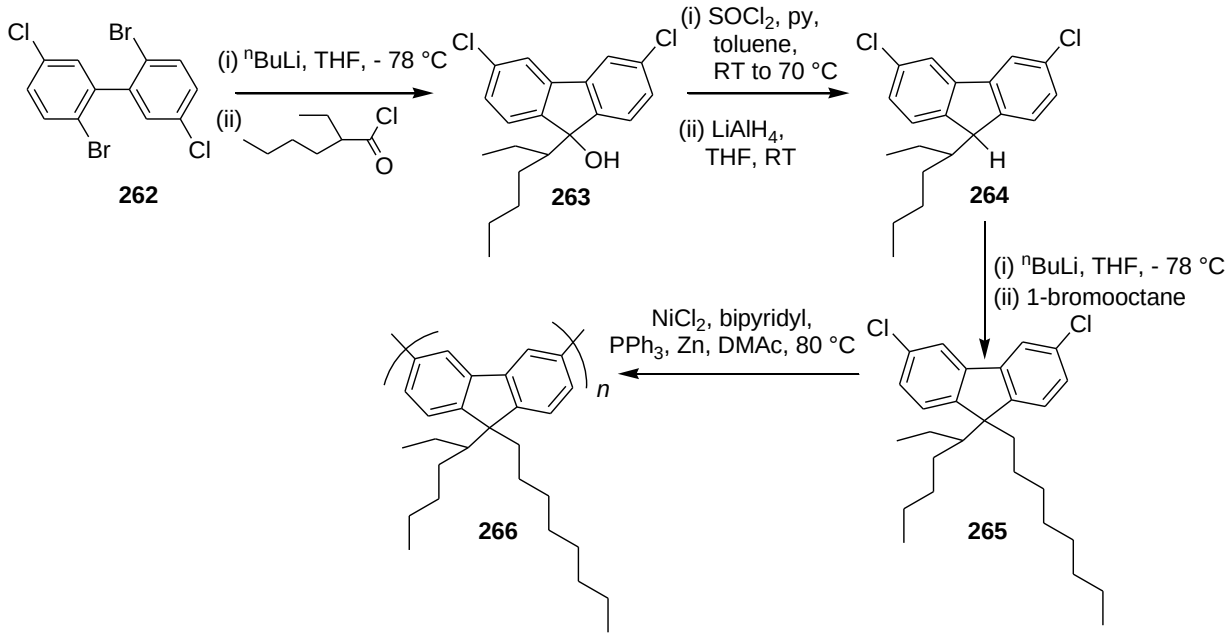

Scheme 6.1 – Synthesis of 3,6-dichloro substituted fluorene monomer [172]

Mo *et al*. reported the synthesis of a 3,6-dichloro-9,9-dialkylfluorene monomer (**265**) which was polymerised to give a 3,6-linked fluorene homo-polymer (**266**, Scheme 6.1). The optical bandgap of this polymer was reported to be 3.6 eV, but devices based on this polymer showed

very low efficiencies and not the expected deep blue emission as was reported for solutions of the polymer.[172]

The Cao group reported the synthesis of poly(9,9-bis(2-ethylhexyl)-3,6-fluorene) (**272**) as a high E_T host material.[170] A 3,6-dibromo-9,9-di(2-ethylhexyl)fluorene monomer (**271**) was synthesised in four steps from 9,10-phenanthrenequinone (**267**) (Scheme 6.2). The E_T of the homo-polymer was reported to be 2.6 eV, higher than that of poly(2,7-fluorene)s, giving it good potential to act as a host material for green- and possibly even blue-emitting complexes.[170]

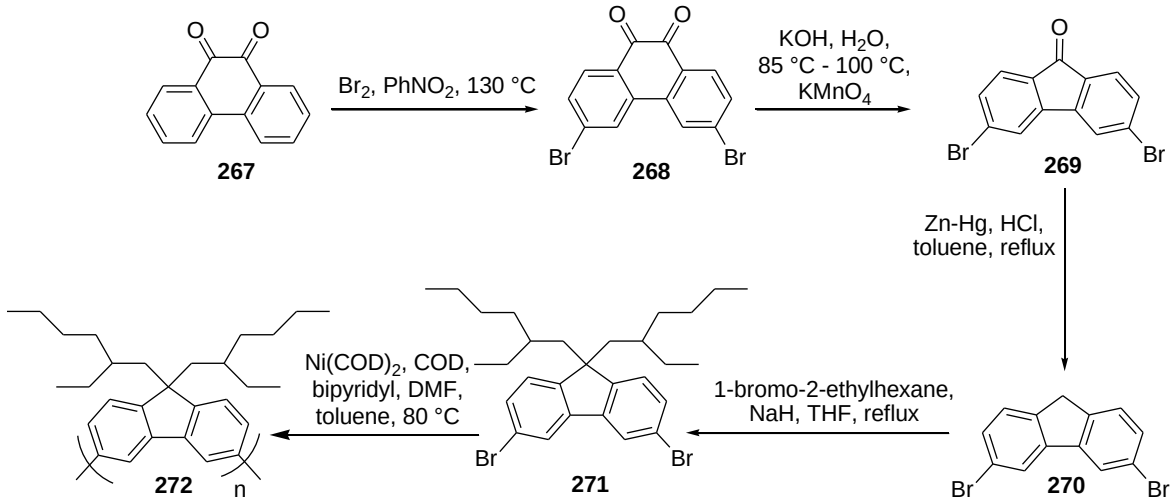

Scheme 6.2 – Synthesis of poly(9,9-bis(2-ethylhexyl)-3,6-fluorene) [170]

Fomina *et al*. reported the synthesis of 3,6-dibromo-9,9-dihexylfluorene (**194**) in a similar way to that in scheme 6.2 (but with a two-step reduction to the 3,6-dibromofluorene).[173] The synthesis and spectroscopic properties of poly(9,9-dihexylfluorene-2,7-diyl-*co*-9,9-dihexylfluorene-3,6-diyl)s (**27***co***36** co-polymers, **273**, Figure 6.2), as well as model oligomers were subsequently reported.[174] The absorption and emission spectra of the materials blue-shifted with increasing 3,6-fluorene content, in line with a reduction in conjugation.[174] E_T levels for the polymers were not reported.

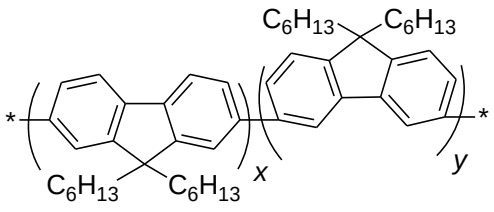

273

Figure 6.2 – Structure of 27*co*36 co-polymers [174]

In 2003 Leclerc *et al*. presented a new series of co-polymers incorporating 3,6-dimethoxy-9,9-dihexylfluorene monomers (**274**-**277**, Figure 6.3). The electron donating methoxy substituents increase the ionisation potential of the co-polymers by ~ 0.2 eV compared to their non-substituted analogues, with the aim of allowing better hole injection and therefore, better device performance in polymeric OLEDs.[175] A blue shift in emission was reported for polymer **274** compared with **275**, i.e. the polymer which would be expected to have the more twisted backbone exhibited more blue shifted emission. The monomer unit was also used in the synthesis of novel triphenylamine-based electrochromic co-polymers for military camouflage materials.[176] The dimethoxy-substituted monomer was synthesised in a multi-step process from 3,6-dimethoxy-9-fluorenone.[175] While this is a good synthetic strategy to achieve dimethoxy-substituted fluorenes, it is not applicable as a general strategy for functionalisation of fluorenes in the 3,6-positions due to the requirement for the substituents to be in place in the starting material.

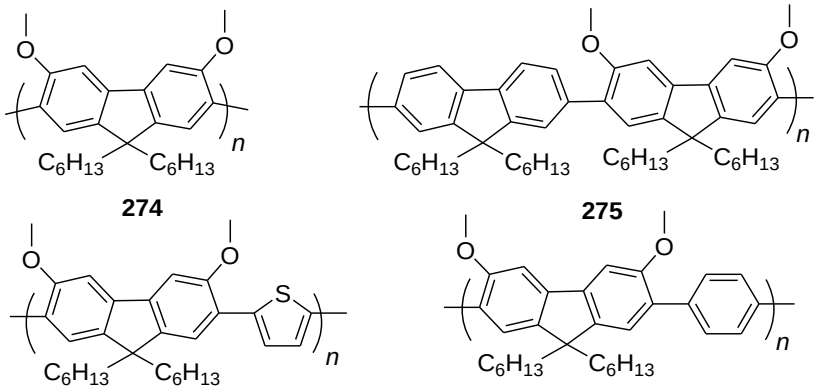

Figure 6.3 – Selection of the co-polymers synthesised by Leclerc *et al.*

From the small amount of work already reported in this area and the established need for high E_T conjugated polymer hosts for OLEDs, there is clearly interest in the development of novel reduced conjugation host materials, including investigations into the functionalisation of fluorenes in the 3,6-positions. This chapter describes efforts towards this aim.

6.2 Results and Discussion

6.2.1 Synthesis

It was decided to start the investigation into the 3,6-functionalisation of fluorenes from 3,6-dibromo-9,9-dihexylfluorene (**194**). Scheme 6.3 shows the synthesis of this monomer, using similar conditions to those reported previously.[170,173]

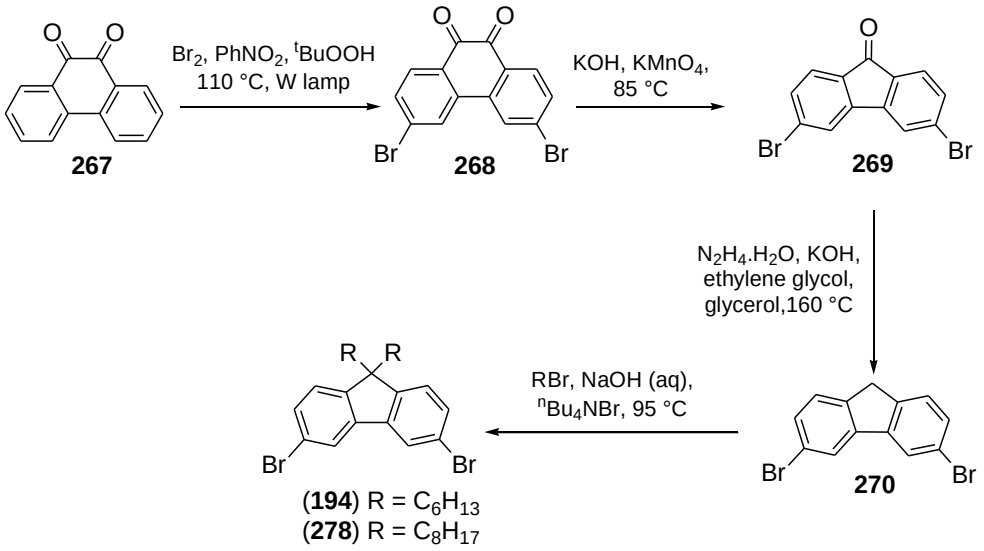

Scheme 6.3 – Synthesis of 3,6-dibromo-9,9-dialkylfluorene monomers

The first step in the synthesis shown in scheme 6.3 is the radical bromination (under irradiation from a tungsten bulb lamp) of 9,10-phenanthrenequinone (**267**) which proceeds in an excellent yield (80%) in a short reaction time. The second step is nucleophilic attack at one of the carbonyl groups to open the ring which is then closed again with the loss of carbon dioxide to give the product ketone (80%) **269**. The third step is a one-step reduction using hydrazine monohydrate followed by potassium hydroxide to give compound **270** in a 65% yield. The central C_9 position is then dialkylated with an alkylbromide to give the monomer solubility (58% for **194**; 63% for **278**).

From monomer **194** it was envisaged that a series of PF-based oligomers and polymers with functionalised fluorene units could be synthesised in order to investigate their photophysical properties. Adding substituents should twist the backbones such that the emission would be blue-shifted and the E_T increased. It was planned to convert the bromo substituents into alkyl/alkoxy/alkynyl groups (**279**), then brominate the resulting fluorene monomer in the 2,7-position (**280**) for incorporation into unsubstituted PF backbones via Suzuki-Miyaura couplings (**282**) as shown in the general scheme below (Scheme 6.4). Numerous reactions on monomer **194** were attempted but were unsuccessful; these results are summarised in Table 6.1.

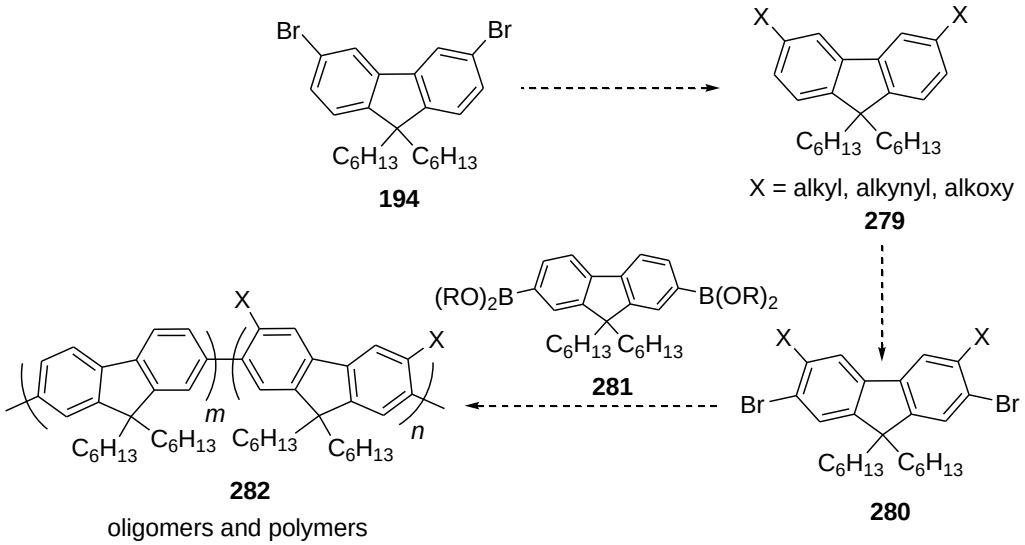

Scheme 6.4 – General scheme proposed for the synthesis of twisted PFs

Reaction	X substituent	Conditions	Result
Kumada Coupling	X = octyl (C_8H_{17})	Ni(dppp)Cl_2, octylmagnesium bromide, THF, 65 ˚C, 18 h, then HCl (2M)	Starting material recovered
Kumada Coupling	X = octyl (C_8H_{17})	Pd(dppf)Cl_2, octylmagnesium bromide, THF, 50 ˚C, 18 h	Major product is starting material (GC-MS shows no required product)
Direct Lithiation	X = hexyl (C_6H_{13})	^{n}Hexyllithium, THF then 1-bromohexane, -78 ˚C to 20 ˚C	Unreacted starting material recovered
Suzuki Coupling	X = butyl (C_4H_9)	^{n}butylboronic acid, Cs_2CO_3, Pd(dppf)Cl_2, THF:H_2O 10:1, 65 ˚C, 24 h	Trace amounts of product seen in GC-MS, only starting material isolated
Sonogashira Coupling	X = 1-dodecynyl ($C_{10}H_{22}$)	1-dodecyne, $PdCl_2(PPh_3)_2$, CuI, Et_3N, 90 ˚C, 18 h	Major product is starting material, small amount of mono-coupled product seen in GC-MS

Table 6.1 – Selection of the unsuccessful reactions performed on compound 194

From these results it appears that the reactivity of bromo substituents in the 3,6-positions of fluorene is significantly reduced compared to bromo substituents in the 2,7-positions. This

effect was also noted by Fomina *et al*. when this monomer unit was used in polymerisation reactions, the polymerisation yields and degree of incorporation of the 3,6-disubstituted unit decreased as the monomer feed was increased, implying reduced reactivity.[174]

This reduction in reactivity was also apparent in the synthesis of the 3,6-diboronic ester fluorene derivative (**283**) (Scheme 6.5). "Usual" reaction conditions (i.e. those used on 2,7-dibromo-9,9-dihexylfluorene) involve lithiation (~ 2.2 equivalents of ^{n}BuLi), followed by borylation. In the synthesis of compound **283** it was necessary to use a much larger quantity of reagent ($\geq$ 4.5 equivalents of ^{n}BuLi) otherwise mainly unreacted starting material is recovered, i.e. lithiation does not occur. One explanation for this reduction in reactivity for the 3,6-dibromofluorene monomers could be that the electron-donating C_9 position (functionalised by alkyl chains) increases the electron density on the *para*-positioned C_3 and C_6 carbons such that their reactivity towards nucleophiles is reduced.

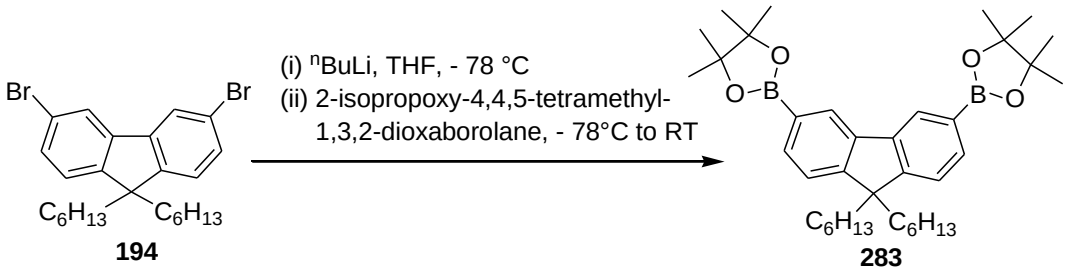

Scheme 6.5 – Synthesis of 3,6-substituted fluorene diboronic ester

Following on from the unsuccessful attempts at functionalising fluorene in the 3,6-positions, it was decided to follow on from the work of the Cao group and Fomina *et al*. by investigating reduced conjugation PFs with the aim of developing novel PF-based host materials for OLEDs. Similar to the work reported by Fomina *et al*.[174] the 3,6-dibromo-9,9-dihexylfluorene monomer (**194**) was polymerised to give a highly twisted homo-polymer (termed "fully bent"), **284**. The monomer was also co-polymerised with 2,7-fluorene units to give a 1:1 co-polymer (termed "partly bent"), **285**. Suzuki coupling to 9,9-dihexyl-9*H*-fluoren-2-ylboronic acid was also performed to give a "bent" **FFF** trimer, **202**. The polymers were synthesised by Suzuki coupling conditions, similar to those described in chapter 2. Schemes 6.6 (a) to (c) show the syntheses of these materials.

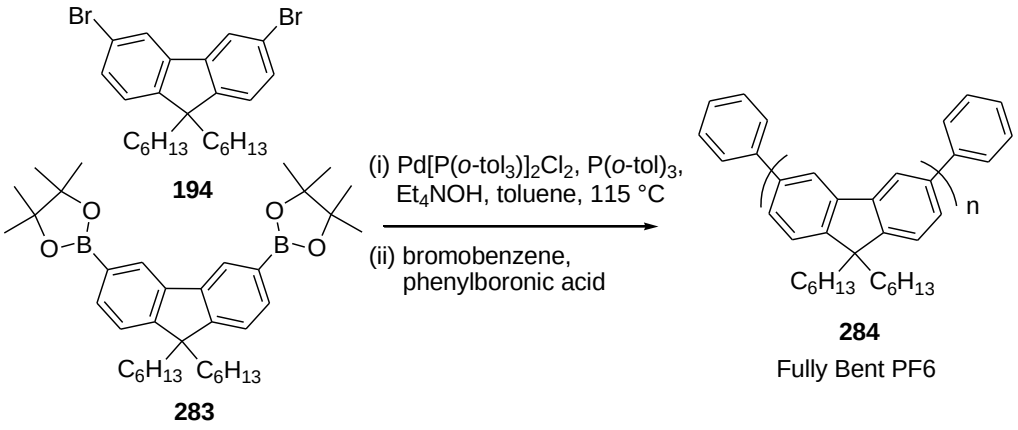

Scheme 6.6 (a) – Synthesis of Fully Bent PF6

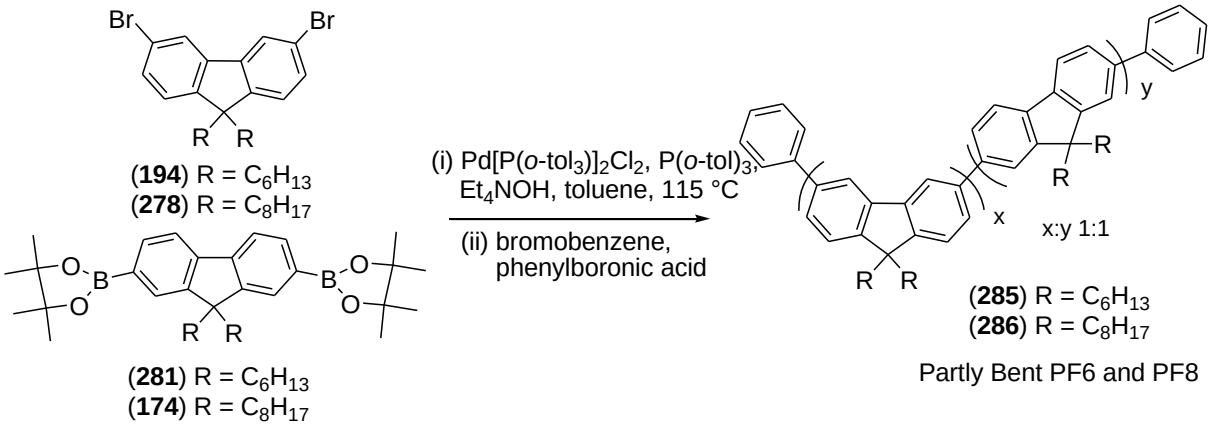

Scheme 6.6 (b) – Syntheses of Partly Bent PF6 and PF8

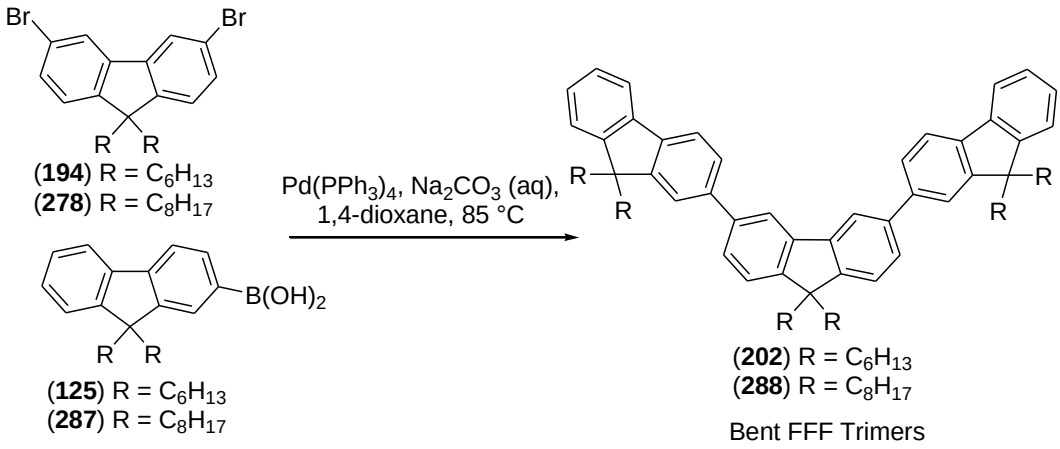

Scheme 6.6 (c) – Syntheses of Bent Trimers

For comparison, the analogous polymers and trimer were synthesised where the C_9 position of the fluorene is functionalised with octyl chains (i.e. R = octyl). The synthesis of the partly bent polymer **286** and the bent trimer **288** were carried out by the same procedures described for the hexyl-substituted materials (Schemes 6.6 (b) and (c)). However, it was not possible to

synthesise the octyl-substituted diboronic ester analogue of compound **283** either by lithiation (> 6 equivalents of ^{n}BuLi) or Miyaura borylation; both returning unreacted starting material. This supports the theory that electronic effects from the electron donation of the C_9 position are strongly affecting the reactivity of substituents in the 3,6-positions; increasing the alkyl chain length from six (hexyl) to eight (octyl) carbons decreases the reactivity of the compounds even further. Thus, for the synthesis of the fully bent polymer, **289**, nickel-catalysed Yamamoto coupling of monomer **278** was used (Scheme 6.7).

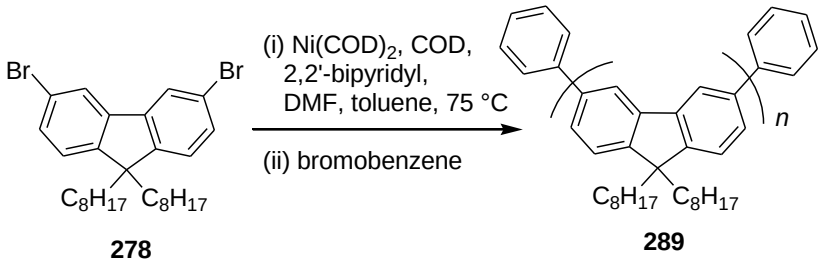

278 **289**

Fully Bent PF8

Scheme 6.7 – Synthesis of fully bent PF8

Yamamoto polymerisations only require the synthesis of one monomer, the dibromo compound, as opposed to Suzuki polymerisations which require the synthesis of both dibromo and diboronic acid/ester monomers. However, Yamamoto polymerisations require an expensive nickel catalyst which must be handled in a glove box, the use of Schlenk apparatus and extremely dry/degassed solvents. Also, any residual nickel catalyst can be difficult to remove from the final polymers, reducing their photoluminescence efficiency. Whilst the coupling reaction was successful, the fully bent **PF8** polymer, **289**, was only obtained in a low yield (26%) as a dark coloured solid (probably due to catalyst residues), again attributed to the reduced reactivity of the 3,6-positions.

6.2.2 Photophysical Results

The emission spectra (in MCH solution) of the hexyl substituted trimer (**202**) and polymers **284**, **285** are shown in Figure 6.4 (a), together with partly bent **PF8** (**286**). Figure 6.4 (b) shows the emission (in MCH solution) for standard (i.e. linear) **PF6** and **PF8**. The emission of fully bent **PF6** (**284**) is blue-shifted compared to partly bent **PF6** (**285**), which in turn is blue shifted from linear **PF6**. This corresponds to the reduction of conjugation through the polymer with increasing 3,6-content. The fully bent **PF6** (**284**) shows emission deep into the blue region of the spectrum, as does the bent trimer (**202**). The emission spectrum of the partly bent **PF8** (**286**) is similar to its hexyl analogue, although seems to have less vibronic structure.

The blue shift in emission with reduced conjugation and the fact that the fully bent **PF6** (**284**) emits in the deep blue means these materials should have high E_T levels. Further photophysical studies on these materials are currently underway in order to determine the E_T levels and to test the host capabilities of the materials.

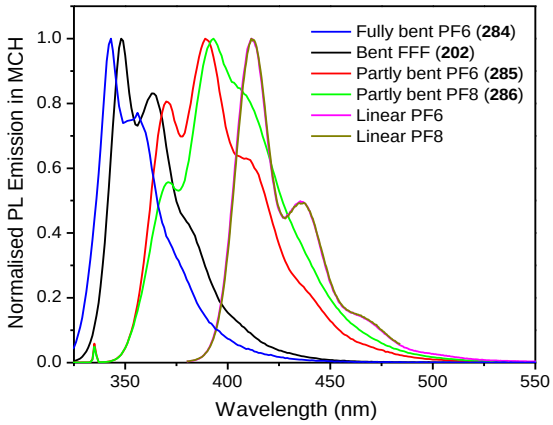

Figure 6.4 – Emission spectra (in dilute MCH) of selected bent and linear materials

6.2.3 Extension to donor-acceptor systems

As discussed in previous chapters, the introduction of **S** as a co-monomer in a PF backbone gives oligomers and polymers which exhibit stable blue emission with improved charge transport properties compared to PF-only systems. Twisting the backbone of these polymers (by substitution of hexyl chains on **S**) blue shifts this emission even further, giving systems capable of hosting green-emitting complexes.[88] To compare this strategy with the reduction of conjugation through manipulation of molecular architecture, a "bent" **F**/**S** co-polymer (**290**) was synthesised using "linear" fluorene monomers and a "bent" **S** monomer, Scheme 6.8. Figure 6.5 shows the structure of the bent co-polymer with its previously published linear analogue (**291**).

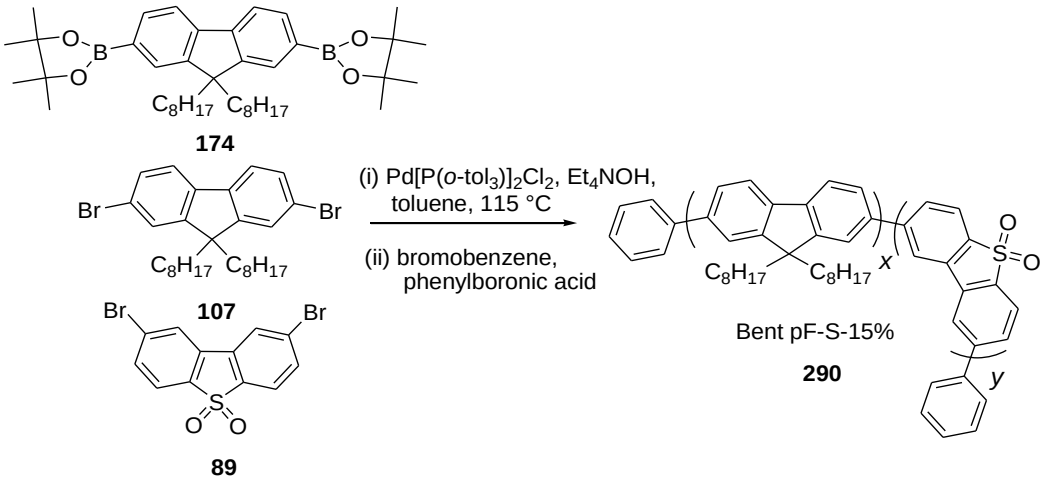

Scheme 6.8 – Synthesis of bent pF-S-15% polymer (x:y 85:15)

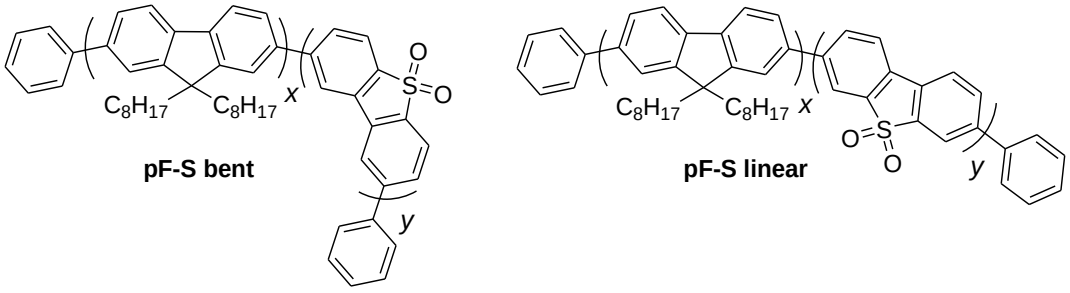

290 **291**

Figure 6.5 – Structures of linear and bent pF-S-15% co-polymers (x:y 85:15)

Figure 6.6 shows the thin film absorption and PL emission of the bent co-polymer **290**. A narrow emission band in the blue region of the spectrum is seen with a maximum at 449 nm. The thin film emission spectrum of the linear co-polymer (**291**) shows a broad emission band (due to the ICT interaction) spanning ~ 430 – 490 nm.[69] The incorporation of the bent **S** unit has therefore blue shifted the emission and significantly reduced the extent of formation of the ICT band, indicative of a loss of conjugation through the system. The analogous twisted system, i.e. the co-polymer with 15% dihexyl-substituted **S** (**109**) has PL emission at λ_{max} 429 nm in thin film, with a shoulder peak at 445 nm.[88] This indicates that the emission of the bent co-polymers needs to be blue-shifted further, e.g. by increasing the bent **S** content, in order to compete with the twisted system as a host material.

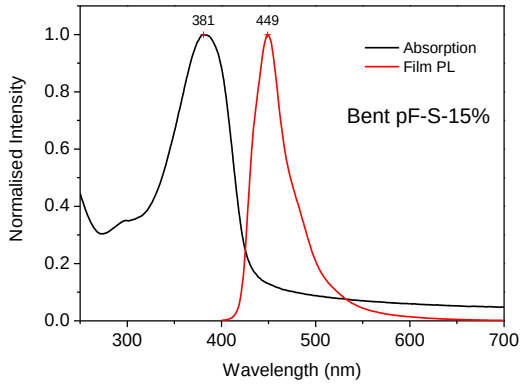

Figure 6.6 – Thin film absorption and emission of bent pF-S co-polymer (290)

Similar results from related systems have been reported by the Cao group who incorporated up to 5 mol% of a bent **S** unit into a PF backbone[177] as well as work from Huang *et al*. who observed shifting of the emission to shorter wavelengths with increasing bent **S** content.[178]

In a recent study from the Bryce group, a series of carbazole-diaryloxadiazole oligomers were synthesised (**292-295**, Figure 6.7) for use as ambipolar high E_T host materials.[179] The molecular weights of the oligomers were determined by gel permeation chromatography to be ~ 3,000 – 4,000 Da and thus can also be considered as low molecular weight polymers.[179]

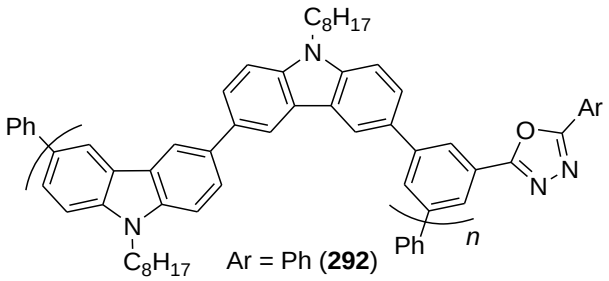

Ar = Ph (**292**)
4-pyridyl (**293**)
4-^{t}BuC$_6$H$_4$ (**294**)
4-(OC$_8$H$_{17}$)C$_6$H$_4$ (**295**)

Figure 6.7 – Structure of carbazole-diaryloxadiazole oligomers

Photophysical studies showed the existence of an ICT state which was enhanced by the addition of an electron withdrawing (pyridyl) substituent on the oxadiazole unit. Triplet levels were determined to be ~ 2.57 eV and a simple device was fabricated using oligomer **294** with a green-emitting iridium complex (**296**) which showed emission only from the phosphorescent guest complex with a good luminous efficiency of 3.93 cd A^{-1} (Figure 6.8).[179]

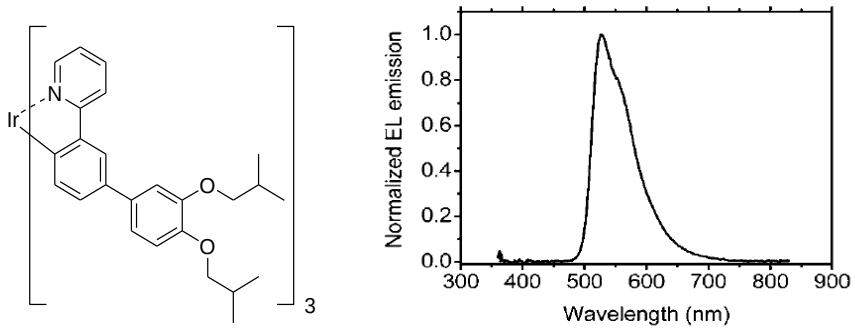

296

Figure 6.8 – Structure of iridium guest complex and EL spectrum of device based on oligomer 294 doped with iridium complex 296 [179]

To further develop this study and for comparison with the "bent" **F/S** co-polymers, two novel ambipolar polymers were synthesised (**301**, **302**) incorporating a 9,9'-dioctyl-[3,3']bicarbazolyl unit (**300**) together with either linear **S** (**301**) or bent **S** (**302**). Scheme 6.9 shows the synthesis of monomer **300** and Figure 6.9 shows the structure of the two co-polymers. The low molecular weights of these polymers (M_w ~ 5 – 8 kDa) make them comparable to the oxadiazole-based oligomers shown in Figure 6.7. The polymers were synthesised by the standard Suzuki-Miyaura polymerisation conditions and were obtained as yellow solids (see Chapter 7 for full experimental details).

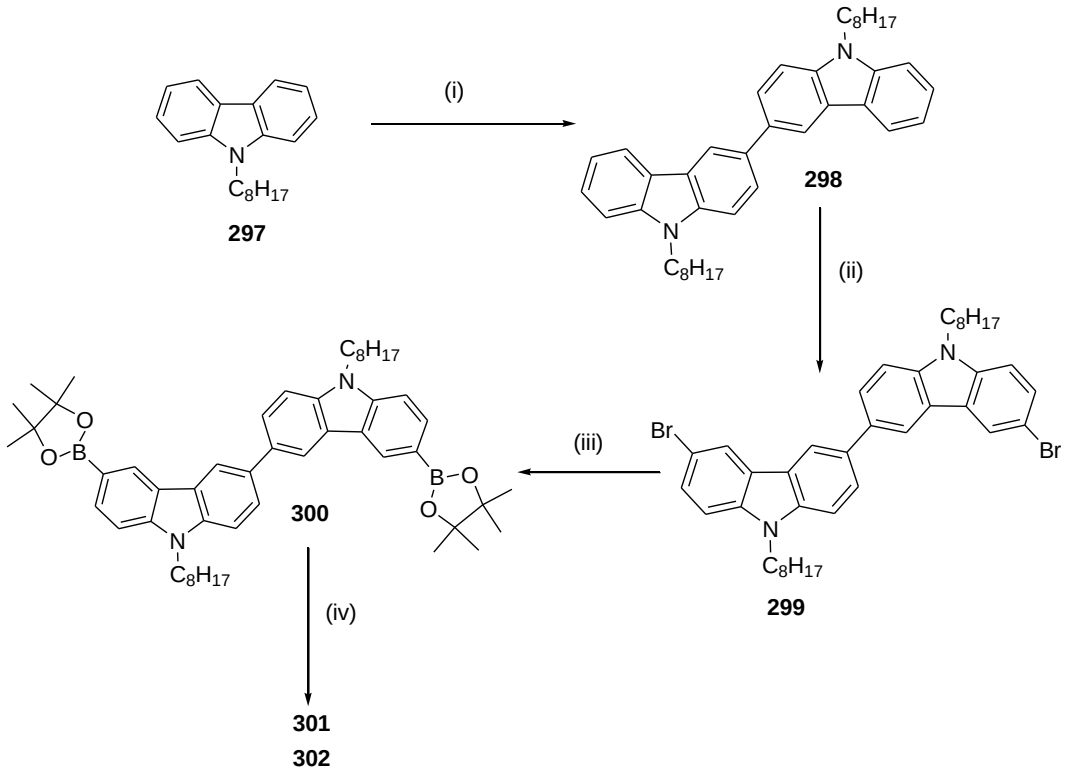

(i) $FeCl_3$, $CHCl_3$, 20 °C, 58%; (ii) NBS, THF, 0 ˚C, 89%; (iii) B_2pin_2, KOAc, $Pd(OAc)_2$, DMF, 90 °C, 26% (iv) **87** or **89**, $PdCl_2[P(o\text{-}tol_3)]_2$, Et_4NOH, toluene, bromobenzene, phenyl boronic acid, 115 °C, 67% for **301**, 57% for **302**

Scheme 6.9 – Synthesis of 9,9'-dioctyl-[3,3']bicarbazolyl unit (300) and the resultant co-polymers

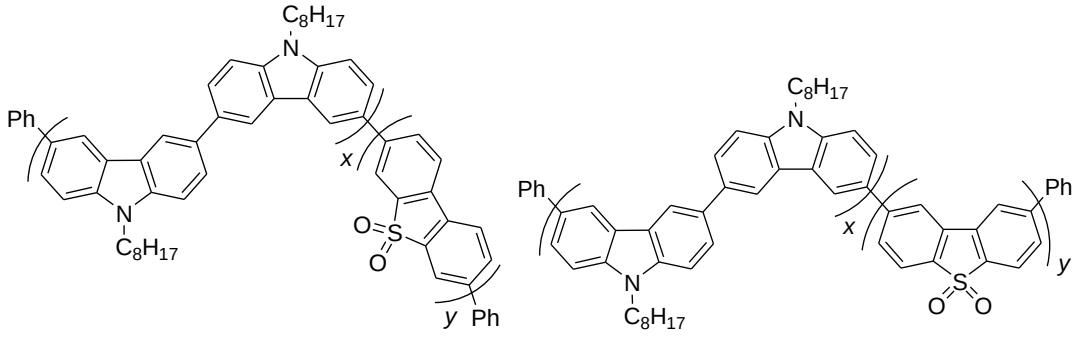

Figure 6.9 – Structures of carbazole/S co-polymers

Photophysical studies on all these materials are currently underway in order to compare the emission properties and triplet energy levels of the reduced conjugation **PF**s, the bent **F**/**S** co-polymers, and the carbazole-oxadiazole and carbazole-**S** co-oligomers in order to find materials capable of hosting green- or blue-emitting organometallic complexes.

6.3 Conclusions

"Bent" fluorene monomers (3,6-dibromo-9,9-dialkylfluorenes) have been synthesised where the alkyl chains are hexyl and octyl. The reactivity of these compounds to substitution in the 3,6-positions has been shown to be very low (particularly for the octyl substituted compounds) and numerous unsuccessful attempts have been made to functionalise fluorene in these positions. The dibrominated monomers have been successfully used to synthesise "fully bent" and "partly bent" PFs, as well as analogous trimers.

Initial photophysical results (together with related literature reports) suggest that these polymers may have the potential to act as host materials for OLEDs, to host green- and possibly even blue-emitting iridium complexes. Further investigation into the photophysics of these systems including determining the triplet energy levels will demonstrate whether these materials are good host candidates or not.

The concept of reducing the extent of conjugation to blue-shift emission has also been utilised to extend our previously discussed PF co-polymer systems where dibenzothiophene-*S*,*S*-dioxide (**S**) is used as a co-monomer. A "bent" system has been shown to exhibit blue shifted emission where the effect of the red-shifted ICT band has been significantly reduced. Reduced conjugation carbazole/**S** systems have also been synthesised and investigations into their photophysical properties are currently underway with the aim of synthesising oligomeric/polymeric, reduced conjugation materials capable of hosting green or blue light-emitting complexes for OLEDs.

Chapter 7: Experimental Procedures

7.1 General Experimental Procedures

All air-sensitive reactions were conducted under a blanket of argon which was dried by passage through a column of phosphorus pentoxide. All commercial chemicals were used without further purification unless otherwise stated. Solvents were dried and degassed following standard procedures. Column chromatography was carried out using 40-60 µm mesh silica. Analytical thin layer chromatography was performed on pre-coated plates of silica gel (Merck, silica gel $60F_{254}$), visualization was made using ultraviolet light (254 nm). NMR spectra were recorded on: Bruker Avance 400, Varian VNMRS 700, Varian Inova 500 or Mercury 200 spectrometers. Melting points were determined in open-ended capillaries using a Stuart Scientific SMP3 melting point apparatus at a ramping rate of 5 °C/min or Stuart Scientific SMP40 melting point apparatus at a ramping rate of 2 °C/min. Mass spectra were measured on a Waters Xevo OTofMS with an ASAP probe, a Thermoquest Trace or a Thermo-Finnigan DSQ. Elemental analyses were performed on a CE-400 Elemental Analyzer. HPLC analysis was carried out using a PerkinElmer Series 200 HPLC instrument equipped with a diode array detector, usually monitoring at 254 nm. The column was a Phenomenex HyperClone 5 µm ODS (C18) 120 Å, 250 x 4.6 mm; flow rate 1 mL min^{-1}. Gel permeation chromatography was carried out on a Viscotek TDA 302 with refractive index, viscosity, and light scattering detectors and 2 x 300 mL PLgel 5 µm mixed C columns; THF was used as the eluent at a flow rate of 1.0 mL min^{-1} and at a constant temperature of 35 ˚C. Samples were analyzed using a conventional calibration generated with a series of narrow polydispersity polystyrene standards (192-1111 200 g mol^{-1}) obtained from Polymer Laboratories.

7.2 Experimental Procedures for Chapter 2

2; Dibenzothiophene-*S*,*S*-dioxide

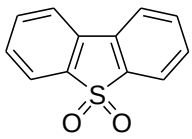

Dibenzothiophene (50.00 g, 0.27mol) was dissolved in glacial acetic acid (500 mL) at 55 °C with stirring. Hydrogen peroxide solution (30%, 76 mL) was added in small portions, not allowing the temperature to go above 60 °C. The mixture was stirred at 55 °C for 24 h, followed by further addition of hydrogen peroxide solution (30%, 10 mL) and heated at 100 °C for 4 h. Upon cooling to room temperature a white solid was isolated by filtration and washed (70% acetic acid, 30% acetic acid and water). The solid was dried in an oven overnight (70 °C) to give

2 as a white crystalline solid (53.50 g, 93%). ^{1}H NMR (400 MHz) DMSO-d_6 δ 8.20 (d, *J* = 8.0 Hz, 2H), 7.98 (d, *J* = 8.0 Hz, 2H), 7.81 (t, *J* = 8.0 Hz, 2H), 7.66 (t, *J* = 8.0 Hz, 2H). MS-ES^{+} *m/z* (%) 238.9 ([M+Na]$^{+}$, 100). Data consistent with the literature.[68]

87; 3,7-Dibromodibenzothiophene-*S*,*S*-dioxide

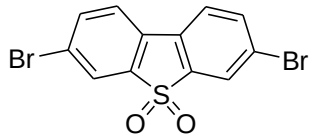

Dibenzothiophene-*S*,*S*-dioxide (**2**) (50.00 g, 0.23 mol) was dissolved in conc. sulphuric acid (1.5 L). N-bromosuccinimide (41.15 g, 0.23 mol) was added in portions. The mixture was stirred at room temperature for 1 h. Additional N-bromosuccinimide (41.15 g, 0.23 mol) was added and the mixture was stirred at room temperature for 24 h. The crude product was isolated by filtration as a white solid which was washed (conc. sulphuric acid, then water until neutral) and dried in an oven overnight (70 °C). Recrystallisation from chlorobenzene gave **87** as white needles (61.66 g, 72%). ^{1}H NMR (400 MHz) $CDCl_3$ δ 7.93 (d, *J* = 1.6 Hz, 2H), 7.77 (dd, *J* = 2.0 Hz, *J* = 8.0 Hz, 2H), 7.64 (d, *J* = 8.0 Hz, 2H). MS-EI *m/z* (%) 373.8 ([M], 100). Data consistent with the literature.[65]

88; 2,8-Dibromodibenzothiophene

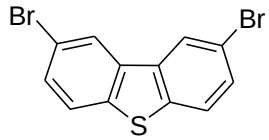

Dibenzothiophene (20.00 g, 0.109 mol) was dissolved in chloroform (120 mL) and the solution cooled to 0 °C. Bromine (12.2 mL, 0.239 mol) was added in portions under argon. The solution was allowed to warm to room temperature with stirring over 24 h. The resulting precipitate was isolated by filtration and washed with saturated sodium thiosulfate solution, then methanol, before drying in an oven (70 °C) overnight. Recrystallisation from chloroform gave **88** as a white solid (27.00 g, 66%).^{1}H NMR (400 MHz) $CDCl_3$ δ 8.21 (d, *J* = 1.8 Hz, 2H), 7.69 (d, *J* = 8.5 Hz, 2H), 7.56 (dd, *J* = 8.5, 1.9 Hz, 2H). Data consistent with the literature.[180]

89; 2,8-Dibromodibenzothiophene-*S*,*S*-dioxide

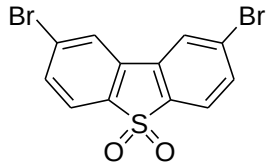

2,8-Dibromodibenzothiophene (**88**) (5.00 g, 14.6 mmol) was suspended in glacial acetic acid (200 mL). Hydrogen peroxide (30%, 35 mL) was added and the mixture heated at 140 °C for 2 h. Additional hydrogen peroxide (30%, 35 mL) was added and heating continued for 18 h. Upon cooling to room temperature distilled water (100 mL) was added and the crude product was isolated by filtration as a white solid. Recrystallisation from acetic acid gave **89** as white needles (4.15 g, 76%). ^{1}H NMR (400 MHz) DMSO-d_6 δ 8.64 (d, *J* = 1.6 Hz, 2H), 7.99 (d, *J* = 8.0 Hz, 2H), 7.90 (dd, *J* = 8.0 Hz, *J* = 4.0 Hz, 2H). ^{13}C NMR (100 MHz) DMSO-d_6 δ 136.2, 134.2, 131.9, 128.5, 126.7, 123.9. Anal. Calcd. for $C_{12}H_6Br_2O_2S$: C 38.53; H 1.62. Found: C 38.73; H 1.62. Mpt. > 350 °C.

112; 2-Nitrodibenzothiophene-*S*,*S*-dioxide

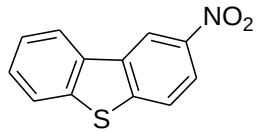

Conc. sulfuric acid (2.4 mL) was added to a mixture of dibenzothiophene (1.0 g, 5.4 mmol) in glacial acetic acid (40 mL) at 0 ˚C. Fuming nitric acid (2.6 mL) was then added slowly with stirring. The resultant yellow precipitate was isolated by filtration, washed with water and dried over magnesium sulfate. Recrystallisation from ethanol gave **112** as a pale yellow solid (0.426 g, 34%).^{1}H NMR (400 MHz) $CDCl_3$ δ 9.06 (d, *J* = 4.0 Hz, 1H), 8.36 (dd, *J* = 4.0 Hz, 8.0 Hz, 1H), 8.31-8.27 (m, 1H), 8.00 (d, *J* = 8.0 Hz, 1H), 7.95-7.92 (m, 1H), 7.62-7.57 (m, 2H). Data consistent with the literature.[181]

113; 2-Aminodibenzothiophene-*S*,*S*-dioxide

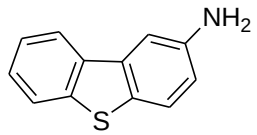

2-Nitrodibenzothiophene-*S*,*S*-dioxide (**112**) (0.263 g, 1.15 mmol) was dissolved in a mixture of ethanol:conc. hydrochloric acid (3:2 *v*/*v*). Granulated tin (0.50 g, 4.2 mmol) was added and the mixture refluxed for 1 h before being poured over ice. The organic products were extracted into diethyl ether and washed with sodium hydroxide solution. Removal of the solvent under vacuum gave the crude product which was purified by column chromatography (eluent: DCM) to give **113** as a yellow solid (0.073 g, 32%).^{1}H NMR (400 MHz) $CDCl_3$ δ 8.04 (t, *J* = 5.2 Hz, 1H), 7.81 (t, *J* = 4.4 Hz, 1H), 7.60 (d, *J* = 8.8 Hz, 1H), 7.46-7.40 (m, 3H), 6.90-6.87 (m, 1H), 4.21 (s, br, 2H, -NH_2). MS-EI *m/z* (%) 199.0 ([M]$^{+}$, 100). Data consistent with the literature.[182]

120; 2,8-Difluorodibenzothiophene-*S*,*S*-dioxide

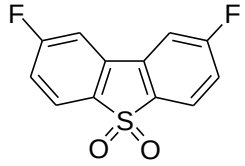

Bis(4-fluorophenyl) sulfone (5.00 g, 19.67 mmol) was dissolved in anhydrous THF (50 mL) at -78 °C, under argon. ^{n}BuLi (2.5 M in hexanes, 19 mL, 47.21 mmol) was added dropwise and the mixture stirred for 10 min. Dry copper (II) chloride (6.61 g, 49.18 mmol) was added in portions and the mixture stirred at - 78 °C for 30 min, before being allowed to warm to room temperature and stirred overnight. Saturated ammonium chloride solution (100 mL) was added to the mixture and the organic layer was extracted into DCM. The combined organic extracts were washed with brine and dried over magnesium sulfate. The solvent was removed under vacuum and the residual solid recrystallised from ethanol to give **120** as a white solid (1.12 g, 23%). ^{1}H NMR (400 MHz) DMSO-d_6 δ 8.16 (dd, *J* = 2.4 Hz, *J* = 9.0 Hz, 2H), 8.09 (q, *J* = 4.8 Hz, 2H), 7.54-7.49 (m, 2H). ^{13}C NMR (100 MHz) DMSO-d_6 δ 167.0 164.5, 133.9, 133.2, 124.9, 118.7, 111.1. ^{19}F NMR (376 MHz) DMSO-d_6 δ -103.0. MS-EI *m/z* (%) 251.9 ([M], 100). Anal. Calcd. for $C_{12}H_6F_2O_2S$: C 57.14; H 2.40; F 15.06; S 12.71. Found: C 56.76; H 2.53; F 15.43; S 12.17. Mpt. 290.3-291.0 °C.

124; 3,7-Dibromo-2,8-difluorodibenzothiophene-*S*,*S*-dioxide

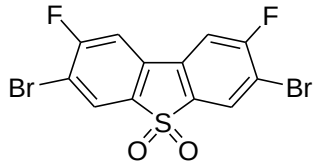

2,8-Difluorodibenzothiophene-*S*,*S*-dioxide (**120**) (1.14 g, 4.52 mmol) was suspended in conc. sulphuric acid (50 mL). N-bromosuccinimide (0.89 g, 4.97 mmol) was added in portions and the mixture stirred at room temperature for 1 h. Additional N-bromosuccinimide (0.804 g, 4.70 mmol) was added and the mixture stirred vigorously for 24 h. The solution was precipitated into an ice/water mix to obtain the crude product, which was recrystallised from chlorobenzene to give **124** as a white solid (0.80 g, 43%). ^{1}H NMR (700 MHz) DMSO-d_6 δ 8.60 (d, *J* = 7.0 Hz, 2H), 8.31 (d, *J* = 14.0 Hz, 2H). ^{13}C NMR (126 MHz) DMSO-d_6 δ 163.2, 161.8, 134.8, 132.0, 128.4, 112.6, 112.2. ^{19}F NMR (376 MHz) DMSO-d_6 δ -98.1. MS-EI *m/z* (%) 409.7 ([M], 100). Anal. Calcd. for $C_{12}H_4Br_2F_2O_2S$: C 35.15; H 0.98; Br 38.97; F 9.27; S 7.82. Found: C 35.41; H 1.02; Br 38.10; F 9.23; S 7.67. Mpt. 336.1-336.9 °C.

303; **2-Bromo-9,9-dihexyl-9*H*-fluorene**

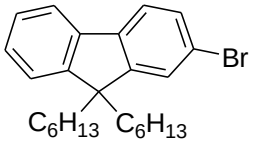

2-Bromofluorene (10.0 g, 40.8 mmol), tetra-*n*-butylammonium bromide (2.6 g, 8.16 mmol), aqueous sodium hydroxide (12.5 M; 40.0 g in 80 mL water) and bromohexane (34 mL, 245 mmol) were heated at 95 °C for 18 h. Water (200 mL) was added to the cloudy yellow solution and the organic layer extracted into DCM. The combined organic layers were washed with water until neutral pH, dried over magnesium sulfate and the solvent removed under vacuum to give the crude product as a yellow oil. Purification by column chromatography (eluent: petroleum ether) gave **303** as a colourless oil (15.56 g, 92%). ^{1}H NMR (400 MHz) $CDCl_3$ δ 7.65 (dd, *J* = 2.2, 7.0 Hz, 1H), 7.54 (d, *J* = 7.9 Hz, 1H), 7.46–7.41 (m, 2H), 7.32–7.29 (m, 3H), 1.97–1.88 (m, 4H), 1.15–0.98 (m, 12H), 0.76 (t, *J* = 7.1 Hz, 6H), 0.58 (d, *J* = 6.7 Hz, 4H). Data consistent with the literature.[65]

125; 9,9-Dihexyl-9*H*-fluoren-2-ylboronic acid

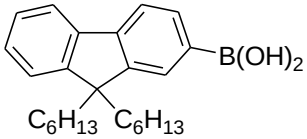

2-Bromo-9,9-dihexyl-9*H*-fluorene (**303**) (3.062 g, 7.406 mmol) was dissolved in anhydrous THF (150 mL) under argon at - 78 °C. ^{n}BuLi (2.5 M in hexanes, 3.85 mL, 9.628 mmol) was added dropwise and the mixture stirred at this temperature for 1 h. Triisopropyl borate (3.40 mL, 14.81 mmol) was added dropwise and the mixture was stirred at - 78 °C for 1 h. After warming to - 20 °C, the reaction mixture was quenched by the addition of a saturated solution of ammonium chloride and stirred overnight whilst warming to room temperature. The organic layer was extracted into DCM, washed with brine, dried over magnesium sulfate and the solvent removed under vacuum to give the crude product. Purification by column chromatography (eluent: petroleum ether:DCM 1:1 *v*/*v*) gave **125** as a white sticky solid (1.821 g, 65%). ^{1}H NMR (400 MHz) $CDCl_3$ δ 8.32 (d, *J* = 8.0 Hz, 1H), 8.21 (s, 1H), 7.89 (d, *J* = 8.0 Hz, 1H), 7.85-7.80 (m, 1H), 7.44-7.33 (m, 3H), 2.16-2.03 (m, 4H), 1.19-0.96 (m, 12H), 0.76 (t, *J* = 8.0 Hz, 6H), 0.71-0.65 (m, 4H). Data consistent with the literature.[65]

126; 3,7-Bis(9,9-dihexylfluoren-2-yl)-2,8-difluorodibenzothiophene-*S,S*-dioxide

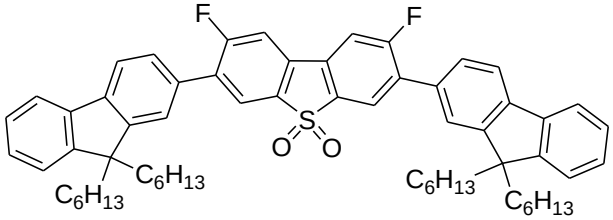

3,7-Dibromo-2,8-difluorodibenzothiophene-*S*,*S*-dioxide (**124**) (0.80 g, 0.195 mmol) and 9,9-dihexylfluoren-2-yl-2-boronic acid (**125**) (0.19 g, 0.488 mmol) were dissolved in 1,4-dioxane (10 mL) and the solution was degassed by bubbling through argon for 15 min. $Pd(PPh_3)_4$ (0.0113 g, 5 mol%) was added and the solution was degassed further. Degassed sodium carbonate solution (1 M, 5 mL) was added and the solution heated at 85 °C for 24 h. The mixture was poured into brine and the crude product extracted into DCM. Removal of the solvent under vacuum gave the crude product as an oily solid. Purification by column chromatography (eluent: petroleum ether: DCM 1:1 *v*/*v*), followed by recrystallisation from ethanol gave **126** as a white solid (0.85 g, 50%). ^{1}H NMR (400 MHz) $CDCl_3$ δ 8.03 (d, *J* = 8.0 Hz, 2H), 7.81 (d, *J* = 8.0 Hz, 2H), 7.77-7.75 (m, 2H), 7.59-7.54 (m, 6H), 7.39-7.35 (m, 6H), 2.04-2.00 (m, 8H), 1.12-1.06 (m, 32H), 0.77 (t, *J* = 8.0 Hz, 12H). ^{13}C NMR (100 MHz) $CDCl_3$ δ 164.5, 162.5, 151.7, 151.4, 142.4, 140.4, 134.8, 133.0, 132.9, 132.2, 128.0, 127.2, 125.2, 123.5, 123.2, 120.4, 120.2, 110.5, 110.3, 55.6, 40.6, 31.7, 29.9, 24.0, 22.8, 14.3. ^{19}F NMR (376 MHz) $CDCl_3$ δ -107.1. MS-MALDI *m/z* (%) 916.6 ([M], 100). Anal. Calcd. for $C_{62}H_{70}F_2O_2S$: C 81.18; H 7.69; F 4.14; S 3.50. Found: C 81.04; H 7.64; F 4.13; S 3.62. Mpt. 189.5-190.1 °C.

127; pFS_F (30:70)

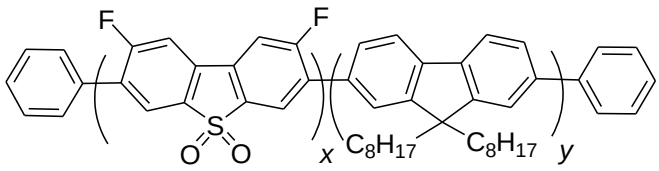

x:y 30:70

2,2'-(9,9-Dioctyl-9H-fluorene-2,7-diyl)bis(1,3,2-dioxaborinane) (**108**) (0.400 g, 0.619 mmol), 2,7-dibromo-9,9-dioctyl-9*H*-fluorene (**107**) (0.135 g, 0.248 mmol) and 3,7-dibromo-2,8-difluorodibenzothiophene-*S*,*S*-dioxide (**124**) (0.165 g, 0.374 mmol) were dissolved in a mixture of toluene (18 mL) and 1,4-dioxane (6 mL). The mixture was stirred and degassed by bubbling through argon for 15 min. $PdCl_2[P(o\text{-}tol_3)]_2$ (0.003 g, 1 mol%) and $P(o\text{-}tol)_3$ (0.006 g, 5 mol%) were added and degassing continued for 15 min. Degassed tetraethylammonium hydroxide solution (20%, 6 mL) was added and the mixture refluxed at 115 °C under argon for 20 h. Bromobenzene (0.1 mL, 0.950 mmol) was added and the mixture refluxed for 1 h.

Phenylboronic acid (0.100 g, 0.819 mmol) was added and the mixture refluxed for an additional 1 h. Upon cooling to room temperature, the mixture was poured into methanol (250 mL) and stirred for 30 min to precipitate the crude polymer as a green/yellow solid, which was isolated by filtration and washed (methanol, then water). The crude solid was dissolved in a toluene:1,4-dioxane mixture (30 mL 5:1 *v*/*v*), to which was added a solution of sodium diethyldithiocarbamic trihydrate (1 g in 10 mL water) and the mixture heated at 65 °C for 12 h. The organic layer was separated and washed (10% hydrochloric acid, sodium acetate solution and water), filtered through celite and concentrated under vacuum to give a viscous dark yellow oil. This oil was then precipitated dropwise into vigorously stirred methanol (~ 200 mL) to give **127** as a fluffy yellow solid (0.210 g, 49%). ^{1}H NMR (400 MHz) $CDCl_3$ δ 8.09-8.00 (m), 7.88-7.81 (m), 7.69-7.53 (m), 7.36-7.32 (m), 2.08-2.02 (m), 1.18-1.11 (m), 0.81-0.64 (m). M_n = 5,629 Da, M_w = 13,459 Da.

128; pFS_F (15:85)

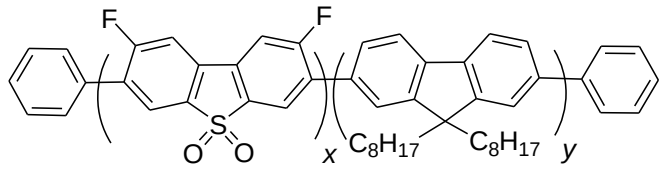

x:y 15:85

Synthesised using the same procedure as for pFS_F (30:70) (**127**) using the following quantities: 2,2'-(9,9-dioctyl-9*H*-fluorene-2,7-diyl)bis(1,3,2-dioxaborinane) (**108**) (0.400 g, 0.619 mmol), 2,7-dibromo-9,9-dioctyl-9*H*-fluorene (**107**) (0.237 g, 0.435 mmol), 3,7-dibromo-2,8-difluorodibenzothiophene-*S*,*S*-dioxide (**124**) (0.083 g, 0.187 mmol) in a mixture of toluene (9 mL) and 1,4-dioxane (3 mL) with $PdCl_2[P(o\text{-}tol_3)]_2$ (0.002 g, 1 mol%) and $P(o\text{-}tol)_3$ (0.003 g, 5 mol%) to give **128** as a fluffy yellow solid (0.395 g, 87%). ^{1}H NMR (400 MHz) $CDCl_3$ δ 8.06-8.05 (m), 7.83-7.82 (m), 7.70-7.50 (m), 2.20-2.05 (m), 1.20-1.12 (m), 0.81-0.65 (m). M_n = 45,583 Da, M_w = 191,448 Da.

132; Bis(4-trifluoromethylphenyl)sulfone

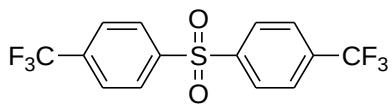

Magnesium turnings (0.24 g, 9.81 mmol) and iodine (~ 0.001 g) were added to a dry round bottomed flask under argon, which was sealed and briefly heated with a flame until a pink vapour was seen. Anhydrous THF (20 mL) was added and the mixture stirred under argon at room temperature. 4-Bromobenzotrifluoride (1.37 mL, 9.81 mmol) in anhydrous THF (20 mL)

was added dropwise. Once all the magnesium was dissolved, a solution of 4-trifluoromethylbenzene sulfonyl chloride (2.00 g, 8.18 mmol) in anhydrous THF (20 mL) was added dropwise and the mixture stirred under argon for 18 h. Saturated ammonium chloride solution (40 mL) was added and the organic layer extracted into DCM. The combined organic extracts were washed with water and dried over magnesium sulfate. Removal of the solvent under vacuum gave the crude product as an orange/yellow solid. Purification by column chromatography (eluent: DCM:hexane 1:1 *v*/*v*) followed by recrystallisation from hexane gave **132** as a white solid (0.46 g, 16%). ^{1}H NMR (400 MHz) $CDCl_3$ δ 8.08 (s, 4H), 7.80 (s, 4H). ^{13}C NMR (100 MHz) $CDCl_3$ δ 144.2, 135.6, 135.3, 128.5, 126.8, 126.7, 126.7, 124.3. ^{19}F NMR (376 MHz) $CDCl_3$ δ -63.7. MS-EI *m/z* 354.1 (%) ([M], 14), 144.7 ([ar-CF_3], 92). Anal. Calcd. for $C_{14}H_8F_6O_2S$: C 47.46; H 2.28. Found: C 47.56; H 2.42. Mpt. 153.4-153.9 °C.

133; 2,8-Di(trifluoromethyl)dibenzothiophene-*S*,*S*-dioxide

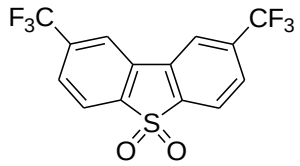

Bis(4-trifluoromethylphenyl)sulfone (**132**) (1.00 g, 2.82 mmol) was dissolved in anhydrous THF (20 mL) at - 78 °C under argon. ^{n}BuLi (2.5 M in hexanes, 4.52 mL, 11.28 mmol) was added dropwise and the mixture stirred at this temperature for 30 min. Dry copper(II)chloride (0.95 g, 7.05 mmol) was added in portions and the mixture stirred for a further 30 min before being allowed to warm to room temperature overnight. The reaction was quenched with saturated ammonium chloride solution and extracted into DCM. Upon removal of the solvent under vacuum, the crude product was obtained as a green/white solid. Purification by column chromatography (eluent: DCM) gave **133** as a white solid (0.21 g, 21%). ^{1}H NMR (400 MHz) $CDCl_3$ δ 8.12 (s, 2H), 8.00 (d, *J* = 8.0 Hz, 2H), 7.89 (d, *J* = 8.0 Hz, 2H). ^{13}C NMR (126 MHz) $CDCl_3$ δ 140.8, 136.5, 136.3, 131.2, 128.4, 123.6, 123.2, 122.0, 119.2. ^{19}F NMR (376 MHz) $CDCl_3$ δ - 63.6. MS-ES^{-} *m/z* (%) 350.9 ($[M-H]^{-}$, 100). HRMS-ES^{-} *m/z* calculated for $C_{14}H_6F_6O_2S$: $[M-H]^{-}$ 350.99199, Found: 350.99201. Anal. Calcd. for $C_{14}H_6F_6O_2S$: C 47.74; H 1.72. Found: C 47.13; H 1.70. Mpt. 287.5-288.7 °C.

135; 2,8-Di(*N*-morpholino)dibenzothiophene-*S*,*S*-dioxide

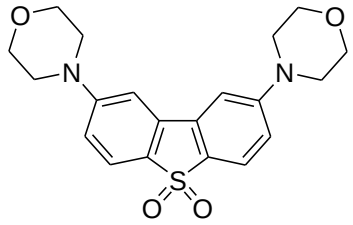

2,8-Dibromodibenzothiophene-*S*,*S*-dioxide (**89**) (1.00 g, 2.67 mmol) was dissolved in anhydrous toluene (50 mL) under argon. To this were added $Pd_2(dba)_3$ (0.049 g, 2 mol%), xphos (0.127 g, 10 mol%), sodium *tert*-butoxide (0.720 g, 7.48 mmol), morpholine (0.56 mL, 6.41 mmol) and *tert*-butanol (2 mL). The mixture was heated at 110 °C for 3.5 h. After cooling to room temperature, the mixture was filtered through celite, washing extensively with ethyl acetate. The filtrate was concentrated under vacuum to give the crude product. Recrystallisation from ethanol gave **135** as a yellow solid (0.68 g, 66%). ^{1}H NMR (500 MHz) $CDCl_3$ δ 7.67 (d, *J* = 10.0 Hz, 2H), 7.13 (s, 2H), 6.93 (d, *J* = 10.0 Hz, 2H), 3.91 (t, *J* = 5.0 Hz, 8H), 3.36 (t, *J* = 5.0 Hz, 8H). ^{13}C NMR (500 MHz) $CDCl_3$ δ 155.3, 133.9, 128.8, 123.4, 115.8, 106.3, 66.8, 48.3. MS-MALDI *m/z* (%) 386.1 ([M], 100). Mpt. 341.2-342.4 °C.

136; 3,7-Dibromo-2,8-di(*N*-morpholino)dibenzothiophene-*S*,*S*-dioxide

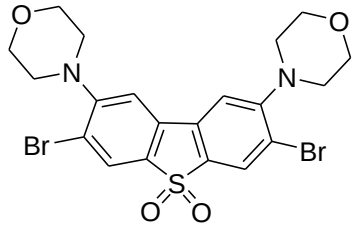

2,8-Di(*N*-morpholino)dibenzothiophene-*S*,*S*-dioxide (**135**) (0.095 g, 0.246 mmol) was suspended in a mixture of glacial acetic acid (15 mL) and chloroform (5 mL) at 0 °C. N-bromosuccinimide (0.048 g, 0.271 mmol) was added and the mixture was stirred for 1 h with protection from sunlight. Additional N-bromosuccinimide (0.048 g, 0.271 mmol) was then added, the mixture was allowed to warm to room temperature and stirred for 24 h. Distilled water (30 mL) was added and the organic layer extracted into chloroform. The organic layer was washed with water until pH neutral and the solvent removed under vacuum to give the crude product as a yellow solid. Recrystallisation from ethanol gave **136** as a pale yellow solid (0.100 g, 75%). ^{1}H NMR (400 MHz) $CDCl_3$ δ 7.95 (s, 2H), 7.27 (s, 2H), 3.91 (t, *J* = 4.0 Hz, 8H), 3.18 (t, *J* = 4.0 Hz, 8H). ^{13}C NMR (100 MHz) $CDCl_3$ δ 155.6, 132.9, 131.6, 128.0, 120.9, 112.6, 66.8, 51.8. MS-ES$^+$ *m/z* 566.9 (%) ($[M+Na]^+$, 100). HRMS-ES$^+$ *m/z* calculated for $C_{20}H_{21}O_4N_2Br_2S$: $[M+H]^+$ 544.95628, Found: 544.95647. Mpt. 342.3-343.3 °C.

137; 3,7-Bis(9,9-dihexylfluoren-2-yl)-2,8-di(*N*-morpholino)dibenzothiophene-*S,S*-dioxide

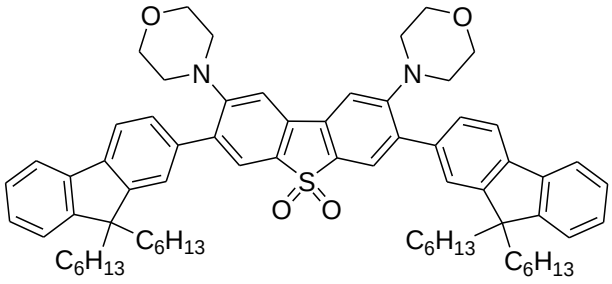

3,7-Dibromo-2,8-di(*N*-morpholino)dibenzothiophene-*S,S*-dioxide (**136**) (0.10 g, 0.184 mmol) and 9,9-dihexylfluoren-2-yl-2-boronic acid (**125**) (0.21 g, 0.570 mmol) were dissolved in 1,4-dioxane (25 mL) and the solution was degassed by bubbling through argon for 15 min. $Pd(PPh_3)_4$ (0.011 g, 5 mol%) was added and the solution degassed further. Degassed sodium carbonate solution (1 M, 5 mL) was added and the solution heated at 85 °C under argon for 24 h. The mixture was poured into brine and extracted into DCM. Removal of the solvent under vacuum gave the crude product as an oily yellow solid. Purification by column chromatography (eluent: DCM), followed by recrystallisation from ethanol gave **137** as a yellow solid (0.098 g, 51%). ^{1}H NMR (700 MHz) $CDCl_3$ δ 7.75 (d, *J* = 14.0 Hz, 2H), 7.72-7.71 (m, 4H), 7.59 (d, *J* = 14.0 Hz, 2H), 7.52 (s, 2H), 7.34-7.32 (m, 8H), 3.61 (s, 8H), 3.01 (s, 8H), 2.02-1.97 (m, 8H), 1.10-1.01 (m, 24H), 0.75 (t, *J* = 7.0 Hz, 12H), 0.62-0.61 (m, 8H). ^{13}C NMR (126 MHz) $CDCl_3$ δ 155.4, 151.4, 150.7, 141.0, 140.5, 138.3, 137.1, 131.8, 127.4, 127.1, 126.9, 125.4, 122.9, 122.6, 119.8, 110.0, 66.6, 55.3, 51.1, 40.5, 31.6, 29.7, 23.8, 22.5, 14.0. Anal. Calcd. for $C_{70}H_{86}N_2O_4S$: C 79.96; H 8.24; N 2.66. Found: C 79.72; H 8.19; N 2.57. MS-MALDI *m/z* (%) 1050.8 ([M], 100). Mpt. 229.0-230.1 °C.

7.3 Experimental Procedures for Chapter 3

General polymerisation procedure Chapter 3: All monomer units were dissolved in toluene and the mixture stirred and degassed by bubbling through argon for 15 min. $PdCl_2[P(o\text{-}tol_3)]_2$ catalyst (~ 11 mg) was added and degassing was continued for 15 min. Degassed tetraethylammonium hydroxide solution (20%, ~ 3.5 mL) was added and the mixture refluxed at 115 °C under argon for 20 h. Bromobenzene (0.1 mL, 0.950 mmol) was added and the mixture refluxed for 1 h. Phenylboronic acid (0.100 g, 0.819 mmol) was added and the mixture refluxed for an additional 1 h. Upon cooling to room temperature, the mixture was poured into methanol (250 mL) and stirred for 30 min to precipitate the crude polymer, which was filtered off and washed (methanol, then water). The crude solid was dissolved in a toluene (20 mL) and a solution of sodium diethyldithiocarbamic trihydrate (1 g in 10 mL water) was added and the mixture heated at 65 °C for 12 h. The organic layer was separated, washed (10% hydrochloric

acid, sodium acetate solution and water), filtered through celite (eluting with toluene), concentrated under vacuum and then precipitated dropwise into vigorously stirred methanol (300 mL). After stirring in methanol for 30 min, the pure polymer was isolated by filtration.

150; 3-Bromo-9-(2-ethylhexyl)-9*H*-carbazole

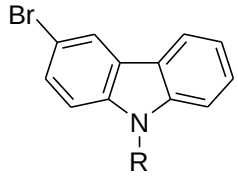

R = 2-ethylhexyl

Potassium-*tert*-butoxide (2.96 g, 26.4 mmol) was added to a solution of 3-bromocarbazole (5.00 g, 20.32 mmol) in anhydrous DMF (100 mL) under argon and the mixture stirred at room temperature for 1 h. 2-Ethylhexylbromide (6.13 mL, 34.34 mmol) was added and the reaction heated at 130 °C for 65 h. Water (100 mL) was added and the organic layer extracted into DCM. The solvent was removed under vacuum to give the crude product as a brown oil. Purification by column chromatography (eluent: DCM) gave **150** as a pale yellow oil (9.29 g, 63%). ^{1}H NMR (400 MHz) $CDCl_3$ δ 8.18 (s, 1H), 8.02 (d, J = 7.8 Hz, 1H), 7.53-7.43 (m, 2H), 7.37 (d, J = 8.3 Hz, 1H), 7.25-7.20 (m, 2H), 4.12 (dd, J = 7.5, 2.8 Hz, 2H), 2.06-1.99 (m, 1H), 1.41-1.19 (m, 8H), 0.93-0.80 (m, 6H). ^{13}C NMR (100 MHz) $CDCl_3$ δ 141.2, 139.6, 128.2, 126.3, 124.5, 123.0, 121.8, 120.5, 119.2, 111.5, 110.4, 109.2, 47.6, 39.4, 31.0, 28.8, 24.4, 23.0, 14.0, 10.9. MS-MALDI *m/z* 359.2 ([M+H], 100%). HRMS-MALDI *m/z* calculated for $C_{20}H_{25}NBr$ [M+H]: 358.1170, Found: 358.1170.

151; 9-(2-ethylhexyl)-9*H*-carbazol-3-yl boronic acid

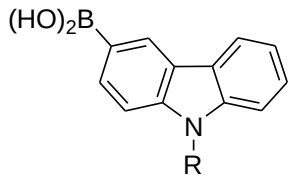

R = 2-ethylhexyl

3-bromo-9-(2-ethylhexyl)-9*H*-carbazole (**150**) (9.214 g, 2.71 mmol) was dissolved in anhydrous THF (200 mL) under argon at - 78 °C. ^{n}BuLi (2.5 M in hexanes, 13.4 mL, 3.52 mmol) was added dropwise and the mixture stirred at this temperature for 1 h. Triisopropyl borate (11.8 mL, 5.42 mmol) was added dropwise and the mixture was stirred at - 78 °C for 1 h. After warming to - 20 °C, the reaction mixture was quenched by the addition of a saturated solution of ammonium chloride and stirred overnight whilst warming to room temperature. The organic

layer was extracted into DCM, washed with brine and dried over magnesium sulfate. The solvent was removed under vacuum to give the crude product as a cream oily solid. Purification by column chromatography (eluent: DCM then DCM:ethyl acetate 1:1 *v*/*v*, then ethyl acetate) gave **151** as a white solid (5.084 g, 61%). ^{1}H NMR (400 MHz) $CDCl_3$ δ 9.08 (s, 1H), 8.40 (dd, J = 7.9, 45.8 Hz, 2H), 7.58-7.28 (m, 4H), 4.31-4.14 (m, 2H), 2.19-2.03 (m, 1H), 1.49-1.20 (m, 8H), 0.99-0.79 (m, 6H). ^{19}B NMR (400 MHz) $CDCl_3$ δ 29.6. MS-MALDI *m/z* 323.2 ([M], 100%). Mpt. 156.0–157.5 °C.

152; 3,7-Bis(9-(2-ethylhexyl)-9*H*-carbazol-3-yl)dibenzothiophene-*S*,*S*-dioxide

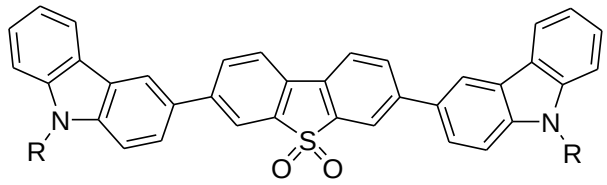

R = 2-ethylhexyl

9-(2-ethylhexyl)-9*H*-carbazol-3-ylboronic acid (**151**) (4.00 g, 12.37 mmol) and 3,7-dibromodibenzothiophene-*S*,*S*-dioxide (**87**) (2.013 g, 5.38 mmol) were dissolved in 1,4-dioxane (100 mL) and the solution was degassed by bubbling through argon for 15 min. $Pd(PPh_3)_4$ (0.124 g, 2 mol%) was added and the solution was degassed further. Degassed sodium carbonate solution (1 M, 40 mL) was added under argon and the solution was heated at 85 °C for 24 h. The mixture was poured into brine and the crude product was extracted into DCM. Removal of the solvent gave the crude product as an oily solid. Purification by column chromatography (eluent: petroleum ether: DCM 1:1 *v*/*v*) gave **152** as a bright yellow solid (3.412 g, 82%). ^{1}H NMR (400 MHz) $CDCl_3$ δ 8.34 (d, *J* = 1.8 Hz, 2H), 8.19-8.12 (m, 4H), 7.95-7.92 (m, 2H), 7.83 (dd, *J* = 5.5, 8.0 Hz, 2H), 7.71 (dd, *J* = 1.8, 8.5 Hz, 2H), 7.51-7.40 m (6H), 7.27 (t, *J* = 7.4 Hz, 2H), 4.21-4.10 (m, 4H), 2.09-2.06 (m, 2H), 1.48-1.21 (m, 18H), 0.90-0.84 (m, 12H). ^{13}C NMR (100 MHz) $CDCl_3$: δ 144.4, 141.0, 138.7, 132.4, 129.4, 123.5, 122.8, 121.8, 120.4, 119.3, 118.8, 109.5, 109.3, 47.6, 39.4, 31.0, 28.8, 24.4, 23.1, 14.0, 10.9. MS-MALDI *m/z* 770 ([M], 100%). Anal. Calcd. for $C_{52}H_{54}N_2O_2S$: C 81.00; H 7.06; N 3.63. Found: C 80.86; H 7.02, N 3.53. Mpt. 210.5-212.0 °C.

154; 2,8-Bis(9-(2-ethylhexyl)-9*H*-carbazol-3-yl)dibenzothiophene-*S*,*S*-dioxide

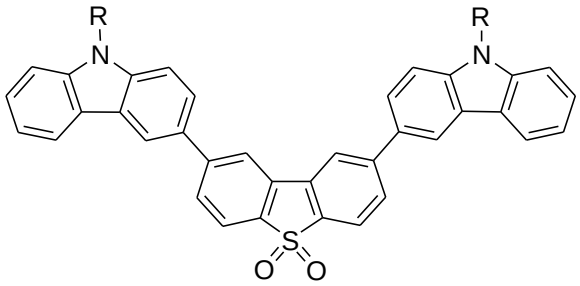

R = 2-ethylhexyl

2,8-Dibromodibenzothiophene-*S*,*S*-dioxide (**89**) (0.151 g, 0.404 mmol) and 9-(2-ethylhexyl)-9*H*-carbazol-3-ylboronic acid (**151**) (0.300 g, 0.928 mmol) were suspended in 1,4-dioxane (20 mL) and the solution degassed by bubbling through argon for 15 min. $Pd(PPh_3)_2Cl_2$ (0.014 g, 5 mol%) was added and the solution degassed for 15 min. Degassed sodium carbonate solution (1 M, 5 mL) was added and the solution heated at 85 °C under argon for 20 h. Upon cooling to room temperature brine (100 mL) was added and the organics extracted into DCM. Removal of the solvent under vacuum gave the crude product as a brown oil. Purification by column chromatography (eluent: DCM:petroleum ether 6:4 *v*/*v*, then DCM), followed by recrystallisation from ethanol gave **154** as a white solid (0.23 g, 74%). ^{1}H NMR (400 MHz) $CDCl_3$ δ 8.38 (s, 2H), 8.18 (d, J = 8.0 Hz, 4H), 7.90 (d, *J* = 8.0 Hz, 2H), 7.83 (d, *J* = 8.0 Hz, 2H), 7.75 (d, *J* = 8.0 Hz, 2H), 7.51-7.48 (m, 4H), 7.42 (d, *J* = 8.0 Hz, 2H), 7.27 (t , *J* = 7.4 Hz, 2H), 4.25-4.15 (m, 4H), 2.10-2.07 (m, 2H), 1.40-1.21 (m, 16H), 0.94-0.82 (m, 12H). ^{13}C NMR (100 MHz) $CDCl_3$ δ 148.5, 141.7, 141.4, 136.1, 132.8, 129.4, 126.4, 120.7, 120.3, 119.5, 119.5, 109.8, 109.6, 47.9, 39.7, 31.3, 29.1, 24.7, 23.3, 14.3, 11.2. MS-MALDI *m/z* 770 ([M], 100%). Anal. Calcd. for $C_{52}H_{54}N_2O_2S$: C 81.00; H 7.06; N 3.63. Found: C 80.80; H 7.06, N 3.71. Mpt. 176.5–178.0 ^{o}C.

159; 2,8-Bis(9,9-dihexyl-9*H*-fluoren-2-yl)dibenzothiophene

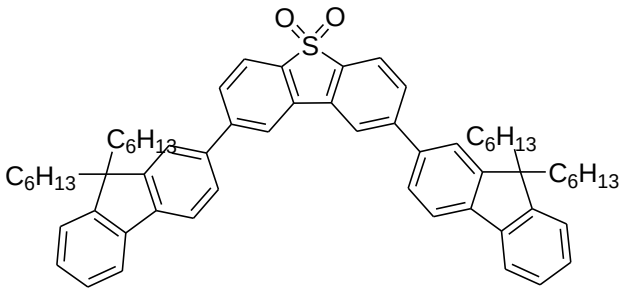

2,8-dibromodibenzothiophene-*S*,*S*-dioxide (**89**) (0.200 g, 0.535 mmol) and 9,9-dihexyl-9*H*-fluoren-2-ylboronic acid (**125**) (0.510 g, 0.34 mmol) were suspended in 1,4-dioxane (20 mL) and the solution degassed by bubbling through argon for 15 min. $Pd(PPh_3)_4$ (0.031 g, 5 mol%) was added and the solution degassed further. Degassed sodium carbonate solution (1M, 7 mL)

was added and the mixture heated at 85 °C for 18 h under argon. The organic product was extracted into DCM, washed with brine and dried over magnesium sulfate. The crude product was purified by column chromatography (eluent: petroleum ether:DCM 1:1 *v*/*v*), followed by repeated recrystallisations from ethanol to give **159** as a white solid (0.101 g, 21%). ^{1}H NMR (400 MHz) $CDCl_3$ δ 8.11 (s, 2H), 7.93 (d, *J* = 8.0 Hz, 2H), 7.83–7.78 (m, 4H), 7.77–7.72 (m, 2H), 7.64 (dd, *J* = 1.6, 7.9 Hz, 2H), 7.58 (s, 2H), 7.39–7.30 (m, 6H), 2.06–1.97 (m, 8H), 1.08 (m, 24H), 0.73 (t, *J* = 7.0 Hz, 12H), 0.65 (m, 8H). ^{13}C NMR (100 MHz) $CDCl_3$ δ 151.9, 151.1, 147.9, 142.0, 140.2, 138.0, 136.6, 132.4, 129.5, 127.6, 127.0, 126.4, 123.0, 122.6, 121.6, 120.3, 120.2, 120.1, 55.4, 40.4, 31.5, 29.7, 23.8, 22.6, 14.0. MS-EI *m/z* (%) ([M+H], 100) Anal. Calcd. for $C_{62}H_{72}O_2S$: C 84.50; H 8.23. Found: C 84.56; H 8.22. Mpt. 163.0-165.0 °C.

161; 3,7-Di(9*H*-carbazol-9-yl)dibenzothiophene-*S*,*S*-dioxide

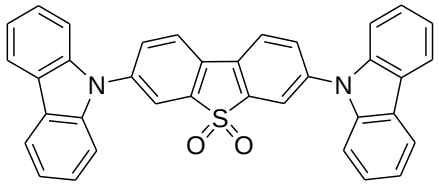

Carbazole (1.07 g, 6.43 mmol) was added to a mixture of 3,7-dibromodibenzothiophene-*S*,*S*-dioxide (**87**) (1.00 g, 2.68 mmol), $Pd_2(dba)_3$ (0.050 g, 2 mol%), xphos (0.127 g, 10 mol%), sodium *tert*-butoxide (0.72 g, 7.49 mmol) and *tert*-butanol (2.0 mL) in anhydrous toluene (80 mL) under argon. The mixture was heated at 110 °C for 18 h. After cooling to room temperature, the mixture was filtered through celite, eluting extensively with ethyl acetate. The filtrate was concentrated under vacuum to give the crude product as a brown solid. Recrystallisation from toluene gave **161** as a yellow solid (0.352 g, 24%). ^{1}H NMR (400 MHz) $CDCl_3$ δ 8.17–8.07 (m, 8H), 7.93 (dd, *J* = 1.9, 8.2 Hz, 2H), 7.51–7.43 (m, 8H), 7.35 (m, 4H). ^{13}C NMR (100 MHz) $CDCl_3$ δ 140.1, 140.0, 132.2, 129.3, 126.5, 123.1, 121.0, 120.6, 109.5. MS-MALDI *m/z* (%) 546.1 ([M], 100). HRMS-MALDI *m/z* calculated for $C_{36}H_{22}N_2O_2S$ [M+H]: 547.1480, Found: 547.1480. Mpt. >350 °C.

162; 2,8-Di(9*H*-carbazol-9-yl)dibenzothiophene-*S*,*S*-dioxide

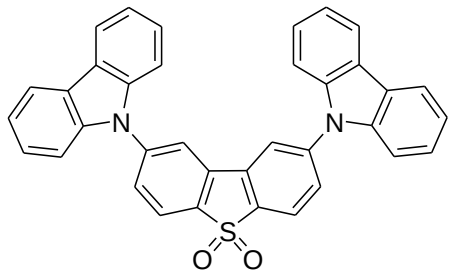

Carbazole (0.536 g, 3.22 mmol) was added to a mixture of 2,8-dibromodibenzothiophene-*S*,*S*-dioxide (**89**) (0.500 g, 1.34 mmol), $Pd_2(dba)_3$ (0.025 g, 2 mol%), tri-*tert*-butylphosphonium tetrafluoroborate (0.039 g, 10 mol%), sodium *tert*-butoxide (0.360 g, 3.8 mmol) and *tert*-butanol (2.0 mL) in anhydrous toluene (50 mL) under argon. The mixture was heated at 110 °C for 18 h. After cooling to room temperature, the mixture was filtered through celite, eluting extensively with ethyl acetate. The filtrate was concentrated under vacuum to give the crude product as a brown solid. Recrystallization from toluene gave **162** as a white solid (0.149 g, 20%). ^{1}H NMR (700 MHz) CDCl3 δ 8.13 (dd, *J* = 3.2, *J* = 7.9 Hz, 6H), 8.00 (s, 2H), 7.83 (dd, *J* = 1.7, *J* = 8.1 Hz, 2H), 7.46-7.40 (m, 8H), 7.32 (t, *J* = 8.0 Hz, 4H). ^{13}C NMR (126 MHz) CDCl3 δ 143.6, 140.0, 136.2, 133.2, 129.0, 126.5, 124.2, 124.0, 121.1, 120.6, 119.9, 109.4. MS-MALDI *m/z* (%) 546.1 ([M], 100). Anal. Calcd. for $C_{36}H_{22}N_2O_2S$: C 79.10; H 4.06; N 5.12. Found: C 79.33; H 4.11; N 5.13. Mpt. > 350 °C.

173; p[F-S-ArN-TBT$_{(0\%)}$-BT$_{(0\%)}$]

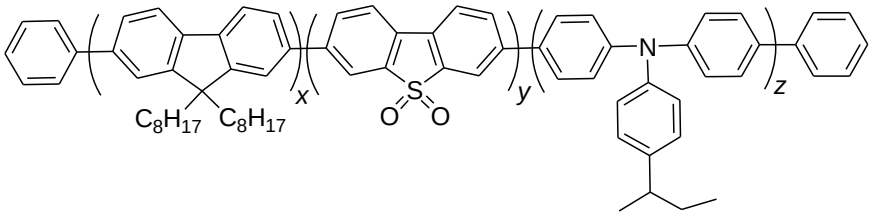

x = 90%, y = 5%, z = 5%

The general polymerisation procedure for Chapter 3 was followed using the following quantities of reagents: 3,7-Dibromodibenzothiophene-*S*,*S*-dioxide (**87**) (0.0233 g, 0.0619 mmol), 2,2'-(9,9-dioctyl-9*H*-fluorene-2,7-diyl)bis(4,4,5,5-tetramethyl-1,3,2-dioxaborolane) (**174**) (0.400 g, 0.619 mmol), 2,7-dibromo-9,9-dioctyl-9*H*-fluorene (**107**) (0.2725 g, 0.496 mmol) and 4-bromo-*N*-(4-bromophenyl)-*N*-(4-*sec*-butylphenyl)benzenamine (**176**) (0.0286 g, 0.0620 mmol) in toluene (12 mL). **173** was isolated by filtration as a fluffy yellow solid (415 mg, 89%). ^{1}H NMR (700 MHz) $CDCl_3$ δ 8.17 (s, br), 7.97-7.55 (m), 7.16-7.11 (m), 2.11 (s, br), 1.22-1.08 (m), 0.83-0.71 (m). M_n = 51,376 Da, M_w = 173, 823 Da.

175; 3,7-Bis-6-bromo-(9-(2-ethylhexyl)-9*H*-carbazol-3-yl)dibenzothiophene-*S*,*S*-dioxide

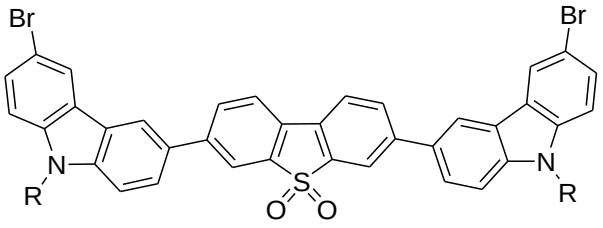

R = 2-ethylhexyl

Compound **152** (0.300 g, 0.389 mmol) was dissolved in anhydrous THF (100 mL) under argon at 0 °C and the solution degassed. N-bromosuccinimde (0.142 g, 0.797 mmol) was added in portions and the mixture stirred vigorously for 18 h with protection from the light. Water (100 mL) was added and the organic layer extracted into DCM. Removal of the solvent under vacuum gave the crude product as a yellow solid. Recrystallisation from a mixture of ethanol and toluene (~1:5 *v*/*v*) gave **175** as a fluffy yellow solid (0.279 g, 77%). ^{1}H NMR (400 MHz) $CDCl_3$ δ 8.24-8.18 (m, 4H), 8.16-8.12 (m, 2H), 7.92-7.86 (m, 2H), 7.86-7.79 (m, 2H), 7.77-7.70 (m, 2H), 7.59-7.52 (m, 2H), 7.46-7.39 (m, 2H), 7.28-7.23 (m, 2H), 4.16-4.02 (m, 4H), 2.10-1.95 (m, 2H), 1.45-1.21 (m, 16H), 0.99-0.82 (m, 12H). ^{13}C NMR (100 MHz) $CDCl_3$ δ 141.0, 141.2, 140.0, 138.7, 132.3, 130.1, 129.5, 128.7, 125.4, 124.4, 123.2, 122.4, 121.9, 120.3, 118.9, 112.1, 110.7, 109.8, 47.7, 39.4, 28.8, 24.4, 23.0, 14.0, 10.9. MS-ASAP$^+$ *m/z* (%) 929.21 ([M]$^+$, 100). HRMS-ASAP$^+$ *m/z* calculated for $C_{52}H_{52}Br_2N_2O_2S$: [M]$^+$ 926.2116, Found: 926.2086. Mpt. 252.9-253.8 °C.

304; 2,8-Bis-6-bromo-(9-(2-ethylhexyl)-9*H*-carbazol-3-yl)dibenzothiophene-*S*,*S*-dioxide

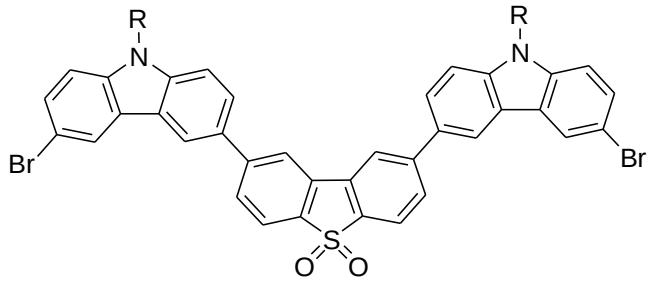

R = 2-ethylhexyl

Compound **154** (0.190 g, 0.246 mmol) was dissolved in anhydrous THF (15 mL) under argon at 0 °C and the solution degassed by bubbling through argon for 15 min. N-bromosuccinimide (0.090 g, 0.505 mmol) was added in portions and the mixture stirred vigorously for 18 h with protection from the light. Water (80 mL) was added and the organic layer extracted into DCM. Removal of the solvent under vacuum gave the crude product as a light yellow oily solid. Recrystallisation from a mixture of ethanol and toluene (~ 1:5 *v*/*v*) gave **304** as a fluffy white solid (0.189 g, 83%). ^{1}H NMR (400 MHz) $CDCl_3$ δ 8.31 (dd, *J* = 1.7, 11.1 Hz, 4H), 8.15 (s, 2H), 7.92 (d, *J* = 8.0 Hz, 2H), 7.86-7.77 (m, 4H), 7.56 (dd, *J* = 1.8, 8.7 Hz, 2H), 7.49 (d, *J* = 8.6 Hz, 2H), 7.29 (d, *J* = 8.7 Hz, 2H), 4.22-4.14 (m, 4H), 2.08-2.01 (m, 2H), 1.36-1.23 (m, 16H), 0.92-0.83 (m, 12H). ^{13}C NMR (100 MHz) $CDCl_3$ δ 147.9, 141.4, 140.1, 136.1, 132.5, 130.6, 129.2, 128.9, 125.8, 124.4, 123.3, 122.6, 122.5, 120.1, 119.4, 112.2, 110.8, 109.9, 47.7, 39.4, 31.0, 28.8, 24.4, 23.0, 14.0, 10.9. MS-ASAP$^+$ *m/z* (%) 929.2 ([M]$^+$, 100). HRMS-ASAP$^+$ *m/z* calculated for $C_{52}H_{52}O_2Br_2N_2S$: [M]$^+$ 926.2116, Found: 926.2149. Mpt. 252.9-253.8 °C.

305; 4,7-Di(thiophen-2-yl)benzo[*c*][1,2,5]thiadiazole

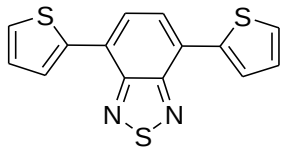

4,7-Dibromobenzo[*c*][1,2,5]thiadiazole (**178**) (0.250 g, 0.850 mmol) was dissolved in anhydrous 1,4-dioxane (8mL) and the solution degassed by bubbling through argon for 30 min. Thiophen-2-ylboronic acid (0.229 g, 1.786 mmol) was added and the solution degassed further. $PdCl_2$(dppf) (0.031 g, 5mol%), tribasic potassium phosphate (0.542 g, 2.55 mmol) and degassed water (2 mL) were added and the mixture heated at 80 °C for 24 h. Upon cooling to room temperature water was added and the organic products extracted into ethyl acetate. The organic layer was washed with brine and dried over magnesium sulfate. Removal of the solvent under vacuum gave the crude product, which was purified using column chromatography (eluent: petroleum ether:DCM 6:4 *v*/*v*) followed by recrystallisation from hexane to give **305** as red needles (0.110 g, 43%).[1]H NMR (400 MHz) $CDCl_3$ δ 8.10 (dd, *J* = 3.7, 1.1 Hz, 2H), 7.86 (s, 2H), 7.44 (dd, *J* = 5.1, 1.1 Hz, 2H), 7.20 (dd, *J* = 5.1, 3.7 Hz, 2H). Data consistent with the literature.[183]

177; 4,7-Bis(5-bromothiophen-2-yl)benzo[*c*][1,2,5]thiadiazole

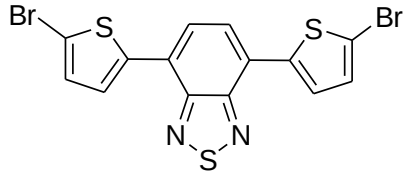

4,7-Di(thiophen-2-yl)benzo[*c*][1,2,5]thiadiazole (**305**) (0.216 g, 0.719 mmol) was dissolved in chloroform (50 mL) and the solution degassed by bubbling through argon for 30 min. N-bromosuccinimide (0.522 g, 1.582 mmol) was added, together with acetic acid (50 mL). The mixture was then stirred under argon at room temperature for 6 h. The resulting precipitate was isolated by filtration and recrystallised from chloroform to give **177** as dark red needles (0.114 g, 35%). [1]H NMR (400 MHz) $CDCl_3$ δ 7.85–7.77 (m, 4H), 7.16 (d, *J* = 4.0 Hz, 2H). Data consistent with the literature.[183]

178; 4,7-Dibromobenzo[*c*][1,2,5]thiadiazole

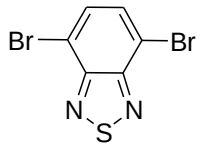

2,13-Benzothiadiazole (2. 5 g, 18.4 mmol) was dissolved in hydrobromic acid (48% aq., 40 mL). A solution of bromine (2.8 mL, 55.1 mmol) in hydrobromic acid (48% aq., 25 mL) was added dropwise. The mixture was heated at 100 °C for 6 h. After cooling to room temperature, sodium thiosulfate solution was added to neutralize the excess bromine. The precipitated product was isolated by filtration and recrystallised from acetonitrile to give **178** as colourless needles (4.903 g, 90%). ^{1}H NMR (400 MHz) DMSO-d_6 δ 7.97 (s, 1H). Data consistent with the literature.[184]

179; p[F-Cz/S/Cz/TBT$_{(0.05\%)}$]

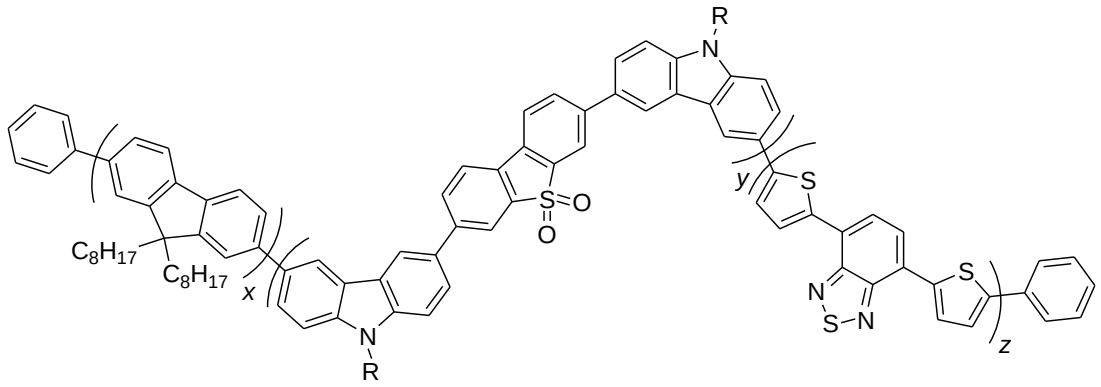

R = 2-ethylhexyl

x = 69.95%, y = 30%, z = 0.05%

The general polymerisation procedure for Chapter 3 was followed using the following quantities of reagents: 3,7-bis-6-bromo-(9-(2-ethylhexyl)-9*H*-carbazol-3-yl)dibenzothiophene-*S*,*S*-dioxide (**175**) (0.3452 g, 0.372 mmol), 2,2'-(9,9-dioctyl-9*H*-fluorene-2,7-diyl)bis(4,4,5,5-tetramethyl-1,3,2-dioxaborolane) (**174**) (0.400 g, 0.619 mmol), 2,7-dibromo-9,9-dioctyl-9*H*-fluorene (**107**) (0.1359 g, 0.247 mmol), 4,7-bis(5-bromothiophen-2-yl)benzo[*c*][1,2,5]thiadiazole (**177**) (0.000285 g, 0.000619 mmol) in toluene (30 mL). **179** was isolated by filtration as a fluffy orange/yellow solid (0.331 g, 53%). ^{1}H NMR (700 MHz) $CDCl_3$ δ 8.49-8.19 (m), 8.03-7.65 (m), 7.51-7.29 (m), 4.29-4.09 (m), 2.13 (s, br), 1.42-1.30 (m), 1.18-1.06 (m), 0.95-0.74 (m). M_n = 10,234 Da, M_w = 24,748 Da.

180; p[F-Cz/S/Cz-TBT$_{(0.075\%)}$]

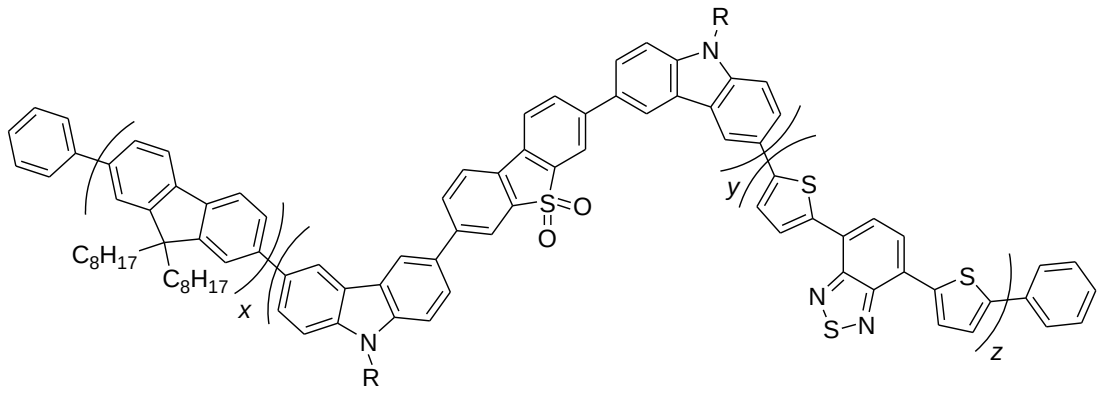

R = 2-ethylhexyl

x = 69.925%, y = 30%, z = 0.075%

The general polymerisation procedure for Chapter 3 was followed using the following quantities of reagents: 3,7-bis-6-bromo-(9-(2-ethylhexyl)-9*H*-carbazol-3-yl)dibenzothiophene-*S*,*S*-dioxide (**175**) (0.250 g, 0.269 mmol), 2,2'-(9,9-dioctyl-9*H*-fluorene-2,7-diyl)bis(4,4,5,5-tetramethyl-1,3,2-dioxaborolane) (**174**) (0.2477 g, 0.441 mmol), 2,7-dibromo-9,9-dioctyl-9*H*-fluorene **(107)** (0.0965 g, 0.176 mmol) and 4,7-bis(5-bromothiophen-2-yl)benzo[c][1,2,5]thiadiazole (**177**) (0.00304 g, 0.00066 mmol) in toluene (30 mL). **180** was isolated by filtration as an orange/red solid (0.356 g, 80%). ^{1}H NMR (500 MHz) $CDCl_3$ δ 8.51-8.39 (m), 8.22-8.15 (m), 8.04-7.98 (m), 7.90-7.61 (m), 7.52-7.35 (m), 4.27-4.11 (m), 2.15 (s, br), 1.44-1.30 (m), 1.19-1.11 (m), 0.95-0.74 (m). M_n = 14,041 Da, M_w = 42,823 Da.

181; p[F-S-ArN-TBT$_{(0.075\%)}$-BT$_{(0\%)}$]

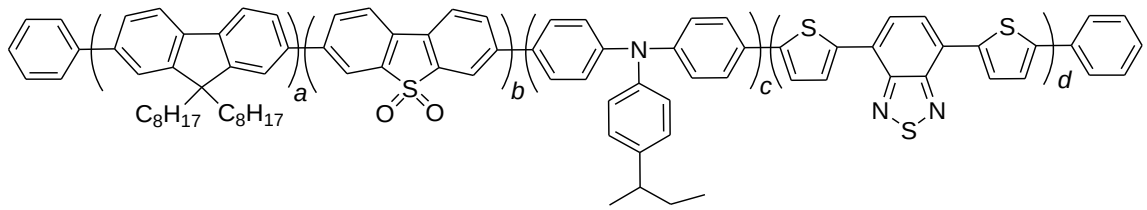

a = 84.925%, b = 5%, c = 10%, d = 0.075%

The general polymerisation procedure for Chapter 3 was followed using the following quantities of reagents: 3,7-dibromodibenzothiophene-*S*,*S*-dioxide (**87**) (0.0233 g, 0.0619 mmol), 2,2'-(9,9-dioctyl-9*H*-fluorene-2,7-diyl)bis(4,4,5,5-tetramethyl-1,3,2-dioxaborolane) (**174**) (0.400 g, 0.619 mmol), 2,7-dibromo-9,9-dioctyl-9*H*-fluorene (**107**) (0.2379 g, 0.433 mmol), 4,7-bis(5-bromothiophen-2-yl)benzo[c][1,2,5]thiadiazole (**177**) (0.0043 g, 0.000936 mmol) and 4-bromo-*N*-(4-bromophenyl)-*N*-(4-*sec*-butylphenyl)benzenamine (**176**) (0.0572 g, 0.124 mmol) in toluene (12 mL). **181** was isolated by filtration as a fluffy orange/pink solid

(0.386 g, 84%). ^{1}H NMR (700 MHz) $CDCl_3$ δ 8.18 (s, br), 7.97-7.55 (m), 7.15-7.10 (m), 2.10 (s, br), 1.20-1.08 (m), 0.84-0.71 (m). M_n = 48,000 Da, M_w = 138,204 Da.

182; p[F-*S*-ArN-TBT$_{(0.075\%)}$-BT$_{(0.1\%)}$]

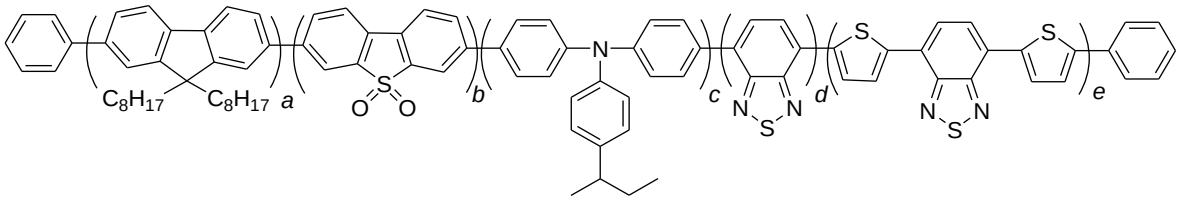

a = 84.825%, b = 10%, c = 5%, d = 0.1%, e = 0.075%

The general polymerisation procedure for Chapter 3 was followed using the following quantities of reagents: 2,2'-(9,9-dioctyl-9*H*-fluorene-2,7-diyl)bis(4,4,5,5-tetramethyl-1,3,2-dioxaborolane) (**174**) (0.400 g, 0.619 mmol), 2,7-dibromo-9,9-dioctyl-9*H*-fluorene (**107**) (0.2372 g, 0.431 mmol), 3,7-dibromodibenzothiophene-*S*,*S*-dioxide (**87**) (0.0233 g, 0.0619 mmol), 4,7-bis(5-bromothiophen-2-yl)benzo[*c*][1,2,5]thiadiazole (**177**) (0.000427 g, 0.000929 mmol), 4-bromo-*N*-(4-bromophenyl)-*N*-(4-*sec*-butylphenyl)benzenamine (**176**) (0.0572 g, 0.124 mmol), and 4,7-dibromobenzo[*c*][1,2,5]thiadiazole (**178**) (0.000364 g, 0.00124mmol) in toluene (12 mL). **182** was isolated by filtration as a pink fluffy solid (0.397 g, 87%). ^{1}H NMR (500 MHz) $CDCl_3$ δ 8.18 (s, br), 7.97-7.55 (m), 7.17-7.10 (m), 2.10 (s, br), 1.22-1.04 (m), 0.88-0.74 (m). M_n = 46,952 Da, M_w = 139,110 Da.

183; p[F-ArN-TBT$_{(0.075\%)}$-BT$_{(0.1\%)}$]

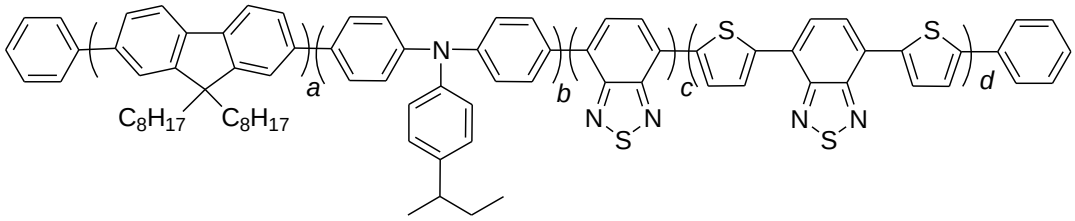

a = 89.825%, b = 10%, c = 0.1%, d = 0.075%

The general polymerisation procedure for Chapter 3 was followed using the following quantities of reagents: 2,2'-(9,9-dioctyl-9*H*-fluorene-2,7-diyl)bis(4,4,5,5-tetramethyl-1,3,2-dioxaborolane) (**174**) (0.400 g, 0.619 mmol), 2,7-dibromo-9,9-dioctyl-9*H*-fluorene (**107**) (0.2713 g, 0.495 mmol), 4,7-bis(5-bromothiophen-2-yl)benzo[*c*][1,2,5]thiadiazole (**177**) (0.000427 g, 0.000929 mmol), 4-bromo-*N*-(4-bromophenyl)-*N*-(4-*sec*-butylphenyl)benzenamine (**176**) (0.0572 g, 0.124 mmol), and 4,7-dibromobenzo[*c*][1,2,5]thiadiazole (**178**) (0.000364 g, 0.00124mmol) in toluene (12 mL). **183** was isolated by filtration as a pink fluffy solid (0.385 g, 82%). ^{1}H NMR (500 MHz) $CDCl_3$ δ 7.85-7.80 (m), 7.70-7.60 (m), 7.17 (s, br), 2.13 (s, br), 1.22-1.11 (m), 0.85-0.80 (m). M_n = 49,174 Da, M_w = 151,250 Da.

188; 3,6-Di-*tert*-butyl-9*H*-carbazole

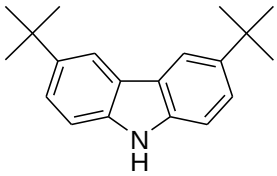

Carbazole (8.00 g, 0.048 mol) and zinc(II)chloride (19.56 g, 0.144 mol) were dissolved in nitromethane (150 mL) under argon. 2-chloro-2-methylpropane (15.70 mL, 0.144 mol) was added dropwise and the mixture stirred for 3 h. The reaction mixture was hydrolysed with water (100 mL) and the organic products extracted into DCM. The solvent was removed under vacuum and the crude product purified by column chromatography (eluent: petroleum ether:DCM 1:1 *v*/*v*). The product fraction was recrystallised from methanol to give **188** as a white crystalline solid (4.954 g, 37%). ^{1}H NMR (400 MHz) $CDCl_3$ δ 8.06 (d, *J* = 1.5 Hz, 2H), 7.84 (s, 1H), 7.45 (dd, *J* = 8.5, 1.9 Hz, 2H), 7.32 (dd, *J* = 8.5, 0.7 Hz, 2H), 1.43 (s, 18H). Data consistent with the literature.[185]

189; 3,7-Bis(3,6-di-*tert*-butyl-9*H*-carbazol-9-yl)dibenzothiophene-*S*,*S*-dioxide

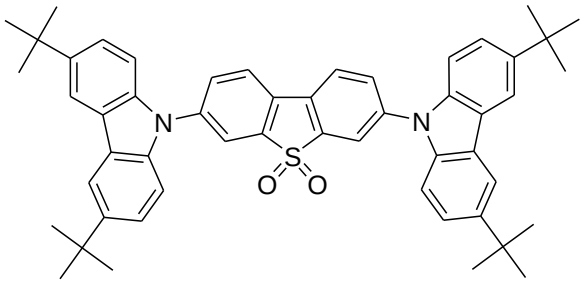

3,7-Dibromodibenzothiophene-*S*,*S*-dioxide (**87**) (0.112 g, 0.298 mmol) and 3,6-di-*tert*-butyl-9*H*-carbazole (**188**) (0.200 g, 0.716 mmol) were dissolved in anhydrous toluene (60 mL) and the solution degassed by bubbling through argon for 15 min. $Pd_2(dba)_3$ (0.006 g, 2 mol%) and xphos (0.014 g, 10 mol%) were added and the solution degassed further. Sodium *tert*-butoxide (0.080 g, 0.834 mmol) and *tert*-butanol (1.5 mL) were added and the mixture heated at 110 °C under argon for 18 h. Upon cooling, water (~ 150 mL) was added and the organic products extracted into DCM, washed with water and brine. The organic layer was dried over magnesium sulfate and the solvent removed under vacuum to give the crude product. Purification by column chromatography (eluent: petroleum ether:DCM 1:1 *v*/*v*) gave **189** as an amorphous yellow powder (0.147 g, 64%). ^{1}H NMR (500 MHz) $CDCl_3$ δ 8.15 (s, 4H), 8.11 (s, 2H), 8.06 (d, *J* = 8.2 Hz, 2H), 7.91 (d, *J* = 8.2 Hz, 2H), 7.52 (d, *J* = 8.7 Hz, 4H), 7.44 (d, *J* = 8.6 Hz, 4H), 1.49 (s, 36H). ^{13}C NMR (126 MHz) $CDCl_3$ δ 144.3, 140.8, 140.0, 138.7, 131.8, 129.3, 129.1, 128.5, 125.5, 124.4, 124.3, 123.2, 120.2, 116.8, 109.3, 35.1, 32.2. MS-ASAP^{+} *m/z* (%) 771.4

([M+H]$^+$, 100). HRMS-ASAP$^+$ *m/z* calculated for $C_{52}H_{55}N_2O_2S$ [M]$^+$ 771.3984 Found: 771.4017. Anal. Calcd. for $C_{52}H_{54}N_2O_2S$: C 81.00; H 7.06; N 3.63. Found: C 81.13; H 7.02, N 3.29. Mpt. > 350 °C.

190; 2,8-Bis(3,6-di-*tert*-butyl-9*H*-carbazol-9-yl)dibenzothiophene-*S*,*S*-dioxide

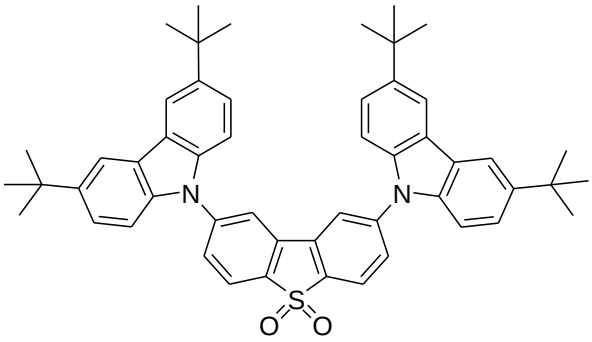

2,8-Dibromodibenzothiophene-*S*,*S*-dioxide (**89**) (0.112 g, 0.298 mmol) and 3,6-di-*tert*-butyl-9*H*-carbazole (**188**) (0.200 g, 0.716 mmol) were dissolved in anhydrous toluene (60 mL) and degassed by bubbling through argon for 15 min. $Pd_2(dba)_3$ (0.006 g, 2 mol%) and xphos (0.014 g, 10 mol%) were added and the solution degassed further. Sodium *tert*-butoxide (0.080 g, 0.834 mmol, 2.8 equiv.) and *tert*-butanol (1.5 mL) were added and the mixture heated at 110 °C under argon for 18 h. Upon cooling, water (~ 150 mL) was added and the organic products extracted into DCM and washed with water and brine. The organic layer was dried over magnesium sulfate and the solvent removed under vacuum to give the crude product. Purification by column chromatography (eluent: petroleum ether:DCM 1:1 *v*/*v*) and recrystallisation from ethanol gave **190** as a white solid (0.135 g, 59%).^{1}H NMR (500 MHz) $CDCl_3$ δ 8.13 (d, *J* = 1.6 Hz, 4H), 8.11 (d, *J* = 8.2 Hz, 2H), 7.99 (d, *J* = 1.7 Hz, 2H), 7.82 (dd, *J* = 8.2, 1.8 Hz, 2H), 7.48 (dd, *J* = 8.7, 1.9 Hz, 4H), 7.40 (d, *J* = 8.6 Hz, 4H), 1.45 (s, 36H). ^{13}C NMR (126 MHz) $CDCl_3$ δ 144.4, 144.3, 138.5, 135.8, 133.5, 128.5, 124.4, 124.3, 119.5, 116.8, 109.2, 35.0, 32.2 MS-ASAP$^+$ *m/z* (%) 771.4 ([M+H]$^+$, 60%). HRMS-ASAP$^+$ *m/z* calculated for $C_{52}H_{54}N_2O_2S$ [M]$^+$ 770.3906 Found: 770.3928. Anal. Calcd. for $C_{52}H_{54}N_2O_2S$: C 81.00; H 7.06; N 3.63. Found: C 80.69; H 7.00, N 3.56. Mpt. > 350 °C.

192; 2,8-Bis(3,6-di-*tert*-butyl-9*H*-carbazol-9-yl)dibenzothiophene

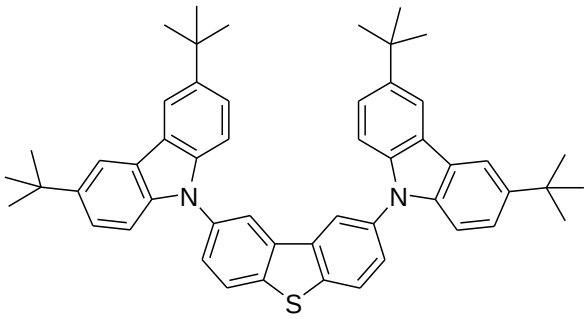

2,8-Dibromodibenzothiophene (**88**) (0.128 g, 0.373 mmol) and 3,6-di-*tert*-butyl-9*H*-carbazole (**188**) (0.250 g, 0.895 mmol) were dissolved in anhydrous toluene (20 mL) and the solution degassed by bubbling through argon for 15 min. To the solution was added *tert*-butanol (1.5 mL), $Pd_2(dba)_3$ (0.010 g, 3 mol%) and xphos (0.018 g, 10 mol%) and degassing continued for an additional 15 min. Sodium *tert*-butoxide (0.108 g, 1.12 mmol) was added and the mixture heated at 110 °C under argon for 18 h. Upon cooling to room temperature, water (~ 150 mL) was added and the organic products extracted into DCM. The organic layer was washed with brine and water and the solvent removed under vacuum to give the crude product as an oily brown solid. Purification by column chromatography (eluent: petroleum ether:DCM 1:1 *v*/*v*) gave **192** as an amorphous white solid (0.238 g, 86%). ^{1}H NMR (700 MHz) $CDCl_3$ δ 8.28 (s, 2H), 8.15 (s, 4H), 8.10 (d, *J* = 8.4 Hz, 2H), 7.71 (d, *J* = 8.4 Hz, 2H), 7.45 (d, *J* = 8.6 Hz, 4H), 7.36 (d, *J* = 8.6 Hz, 4H), 1.46 (s, 36H). ^{13}C NMR (176 MHz) $CDCl_3$ δ 143.0, 139.5, 138.7, 136.6, 135.4, 126.2, 124.2, 123.7, 123.4, 120.1, 116.3, 109.0, 34.7, 32.0. MS-ASAP$^+$ *m/z* (%) 738.4 ($[M]^+$, 100%). HRMS-ASAP$^+$ *m/z* calculated for $C_{52}H_{54}N_2S$: $[M]^+$ 738.4008, found: 738.4001. Anal. Calcd. for $C_{52}H_{54}N_2S$: C 84.51; H 7.36; N 3.79. Found: C 84.34; H 7.33; N 4.09. Mpt. 231.2-233.0 °C.

193; 9,9'-(9,9-Dihexyl-9*H*-fluorene-3,6-diyl)bis(3,6-di-*tert*-butyl-9*H*-carbazole)

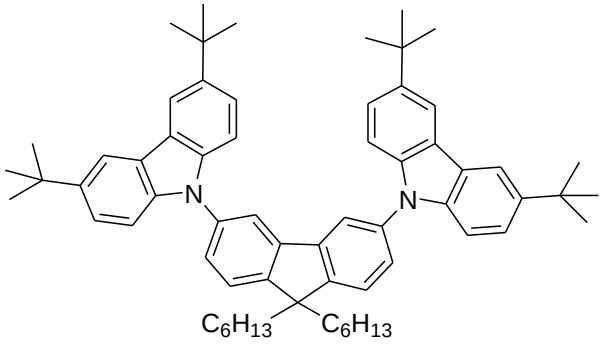

3,6-Dibromo-9,9-dihexyl-9*H*-fluorene (**194**) (0.184 g, 0.373 mmol) and 3,6-di-*tert*-butyl-9*H*-carbazole (**188**) (0.250 g, 0.895 mmol) were dissolved in anhydrous toluene (40 mL) and the solution degassed by bubbling through argon for 15 min. To the solution was added *tert*-butanol (1.5 mL), $Pd_2(dba)_3$ (0.010 g, 3 mol%) and xphos (0.018 g, 10 mol%) and degassing

continued for an additional 15 min. Sodium *tert*-butoxide (0.108 g, 1.12 mmol) was then added and the mixture heated at 110 °C under argon for 18 h. Upon cooling to room temperature, water (~ 150 mL) was added and the organic products extracted into DCM. The organic layer was washed with brine and water and the solvent removed under vacuum to give the crude product as a brown oil. Purification by column chromatography (eluent: petroleum ether:DCM 1:1 v/*v*) gave the product as a yellow oil, which upon triturating in ethanol for 30 min precipitated **193** as an amorphous white solid which was isolated by filtration (0.286 g, 86%). ^{1}H NMR (700 MHz) $CDCl_3$ δ 8.14 (s, 4H), 7.82 (s, 2H), 7.57 (d, *J* = 8.2 Hz, 2H), 7.52 (d, *J* = 7.8 Hz, 2H), 7.46 (d, *J* = 8.6 Hz, 4H), 7.41 (d, *J* = 8.5 Hz, 4H), 2.16-2.10 (m, 4H), 1.46 (s, 36H), 1.23-1.19 (m, 12H), 0.90-0.84 (m, 10H). ^{13}C NMR (176 MHz) $CDCl_3$ δ 149.8, 142.7, 141.9, 139.4, 137.2, 125.9, 124.0, 123.5, 123.3, 118.2, 116.1, 109.2, 55.2, 40.3, 34.7, 32.0, 31.5, 29.7, 24.0, 22.6, 14.0. MS-ASAP$^+$ *m/z* (%) 888.5 ([M]$^+$, 100%). HRMS-ASAP$^+$ *m/z* calculated for $C_{65}H_{80}N_2$: [M]$^+$ 888.6322, found: 888.6322. Anal. Calcd. for $C_{65}H_{80}N_2$: C 87.78; H 9.07; N 3.15. Found: C 87.81; H 9.06; N 3.18. Mpt. decomposed at > 200 °C.

194; 3,6-Dibromo-9,9-dihexyl-9*H*-fluorene

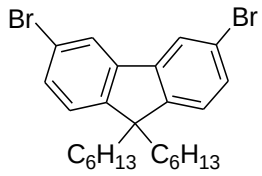

3,6-Dibromo-9*H*-fluorene (**270**) (4.50 g, 13.89 mmol), tetra-*n*-butylammonium bromide (0.896 g, 2.78 mmol), aqueous sodium hydroxide (12.5 M; 14 g in 28 mL water) and bromohexane (11.7 mL, 83.34 mmol) were heated at 95 °C for 18 h. Water (100 mL) was added to the cloudy yellow solution and the organic layer extracted into DCM. The combined organic layers were washed with water until neutral pH, dried over magnesium sulfate and the solvent removed under vacuum to give the crude product. Purification by column chromatography (eluent: petroleum ether) followed by recrystallisation from ethanol gave **194** as a white crystalline solid (3.946 g, 58%). ^{1}H NMR (400 MHz) $CDCl_3$ δ 7.76 (d, *J* = 1.8 Hz, 2H), 7.42 (dd, *J* = 1.8, 8.0 Hz, 2H), 7.17 (d, *J* = 8.0 Hz, 2H), 1.95-1.85 (m, 4H), 1.14-0.95 (m, 12H), 0.75 (t, *J* = 7.1 Hz, 6H), 0.59-0.50 (m, 4H). ^{13}C NMR (100 MHz) $CDCl_3$ δ 149.7, 141.9, 130.5, 124.4, 123.2, 120.8, 55.0, 40.0, 31.4, 29.6, 23.7, 22.5, 14.0. MS-EI *m/z* (%) 406.8 ([M-C_6H_{13}], 100), 491.9 ([M], 12%). Data consistent with literature.[173]

195; 9-(3-Bromophenyl)-3,6-di-*tert*-butyl-9*H*-carbazole

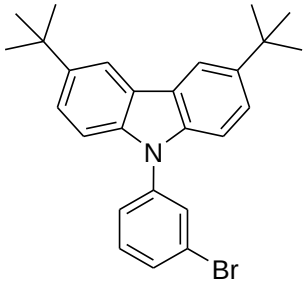

3,6-Di-*tert*-butyl-9*H*-carbazole (**188**) (0.500 g, 1.789 mmol) was dissolved in anhydrous DMF (15 mL) under argon and degassed by bubbling through argon for 15 min. 1-bromo-3-iodobenzene (0.25 mL, 1.968 mmol) was added. Copper(I)iodide (0.034 g, 0.179 mmol, 10 mol%), 1,10-phenanthroline (0.064 g, 0.356 mmol, 20 mol%) and potassium carbonate (0.742 g, 5.367 mmol) were added and the mixture heated at 120 °C under argon for 18 h. Upon cooling, the reaction solvent was removed under vacuum, the residue purified by column chromatography (eluent: petroleum ether:DCM 8:2 *v*/*v*) and the solid product recrystallised from ethanol to give **195** as white crystals (0.397 g, 51%). ^{1}H NMR (400 MHz) $CDCl_3$ δ 8.13 (dd, *J* = 1.9, 0.6 Hz, 2H), 7.74 (t, *J* = 1.8 Hz, 1H), 7.57-7.51 (m, 2H), 7.49-7.43 (m, 3H), 7.35 (dd, *J* = 8.6, 0.6 Hz, 2H), 1.47 (s, 18H). ^{13}C (126 MHz) δ 143.5, 139.8, 139.1, 131.2, 130.2, 129.9, 125.5, 124.0, 123.8, 123.3, 116.6, 109.3, 35.0, 32.2. MS-ASAP$^+$ *m/z* (%) 433.3 ([M]$^+$, 90%). HRMS-ASAP$^+$ *m/z* calculated for $C_{26}H_{28}NBr$: [M]$^+$ 433.1405, found: 433.1385. Mpt. 154.6-155.7 °C.

196; 3,6-Di-*tert*-butyl-9-(3-(4,4,5,5-tetramethyl-1,3,2-dioxaborolan-2-yl)phenyl)-9*H*-carbazole

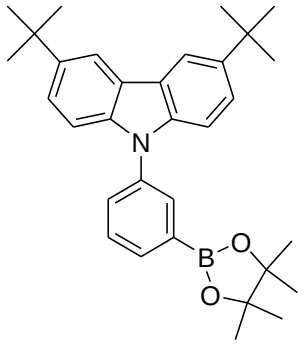

9-(3-Bromophenyl)-3,6-di-*tert*-butyl-9*H*-carbazole (**195**) (0.166 g, 0.382 mmol) was dissolved in anhydrous 1,4-dioxane (5 mL) under argon and the solution was degassed by bubbling through argon for 15 min. Bis(pinacolato) diboron (0.146 g, 0.573 mmol), tris(dibenzylideneacetone) dipalladium(0) (0.0035 g, 0.00382 mmol, 1 mol%), 1,1'-bis(diphenylphosphino)ferrocene (0.005 g, 0.00955 mmol, 2.5 mol%) and potassium acetate (0.112 g, 1.146 mmol) were added and the mixture was heated at 80 °C under argon for 24 h. The organics were extracted into DCM and washed with brine. The solvent was removed under vacuum and the residue purified

by column chromatography (eluent: 5% ethyl acetate in petroleum ether) to give **196** as a white solid (0.081 g, 44%).^{1}H NMR (400 MHz) $CDCl_3$ δ 8.12 (d, *J* = 1.4 Hz, 2H), 7.98-7.95 (m, 1H), 7.84 (d, *J* = 7.0 Hz, 1H), 7.63-7.53 (m, 2H), 7.43 (dd, *J* = 8.6, 2.0 Hz, 2H), 7.29 (d, *J* = 8.6 Hz, 2H), 1.45 (s, 18H), 1.33 (s, 12H). ^{19}B NMR (128 MHz) $CDCl_3$ δ 13.78. ^{13}C NMR (100 Mz) $CDCl_3$ δ 142.6, 139.5, 137.7, 133.4, 133.2, 129.7, 129.1, 123.5, 123.3, 116.1, 109.2, 84.0, 34.7, 32.0, 24.9. MS-ASAP$^+$ *m/z* (%) 481.4 ([M]$^+$, 100%). HRMS-ASAP$^+$ *m/z* calculated for $C_{32}H_{40}BNO_2$: [M]$^+$ 480.3188, found: 480.3168. Mpt. 234.8-235.9 °C.

197; 2,8-Bis(3-(3,6-di-*tert*-butyl-9*H*-carbazol-9-yl)phenyl)dibenzothiophene-*S*,*S*-dioxide

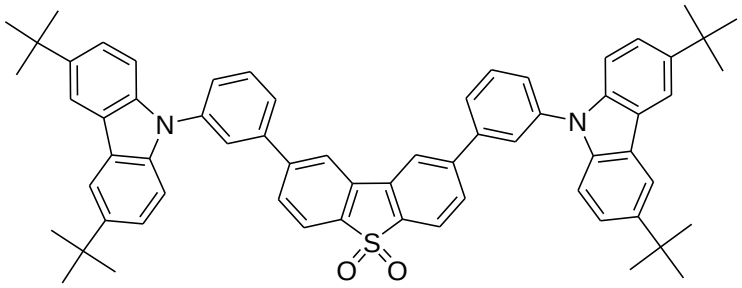

3,6-Di-*tert*-butyl-9-(3-(4,4,5,5-tetramethyl-1,3,2-dioxaborolan-2-yl)phenyl)-9*H*-carbazole (**196**) (0.075 g, 0.156 mmol) and 2,8-dibromodibenzothiophen-*S*,*S*-dioxide (**89**) (0.028 g, 0.074 mmol) were dissolved in anhydrous 1,4-dioxane (10 mL) under argon and the mixture was degassed by bubbling through argon for 15 min. Tetrakis(triphenylphosphine)palladium(0) (0.005 g, 0.0037 mmol, 5 mol%) was added and degassing continued for 15 min. A degassed solution of potassium carbonate (41 mg in 1 mL water, 4 equiv.) was added and the mixture heated at 85 °C for 24 h. The organics were then extracted into DCM and washed with brine and water. The solvent was removed under vacuum and the residue purified by column chromatography (eluent: petroleum ether:DCM 1:1 *v/v* then DCM) to give **197** as an amorphous white powder (0.035 g, 51%).^{1}H NMR (700 MHz) $CDCl_3$ δ 8.15 (s, 4H), 8.06 (s, 2H), 7.94 (d, *J* = 8.3 Hz, 2H), 7.85 (s, 2H), 7.81 (d, *J* = 7.7 Hz, 2H), 7.71 (d, *J* = 5.8 Hz, 4H), 7.65 (s, 2H), 7.47 (dd, *J* = 8.6, 1.6 Hz, 4H), 7.37 (d, *J* = 8.6 Hz, 4H), 1.46 (s, 36H). ^{13}C NMR (176 Mz) $CDCl_3$ δ 146.3, 143.2, 140.9, 139.1, 137.2, 134.0, 132.2, 130.6, 129.5, 128.8, 127.0, 125.8, 125.5, 125.1, 123.7, 123.6, 123.5, 122.8, 120.3, 116.3, 109.0, 34.7, 32.0. MS-ASAP$^+$ *m/z* (%) 922.4 ([M]$^+$, 75%). HRMS-ASAP$^+$ *m/z* calculated for $C_{64}H_{62}N_2O_2S$: [M]$^+$ 922.4532, found: 922.4520. Mpt. 234.8-235.9 °C.

198; 9-(2-Ethylhexyl)-3-iodo-9*H*-carbazole

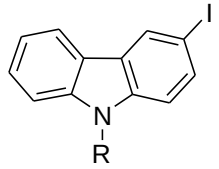

R = 2-ethylhexyl

3-Iodocarbazole (0.400 g, 1.365 mmol) was dissolved in anhydrous DMF (5 mL) under argon and the solution was degassed by bubbling through argon for 15 min. Sodium hydride (0.086 mg, 3.549 mmol) and 2-ethylhexyl bromide (0.43 mL, 2.457 mmol) were added and the solution was stirred under argon at room temperature for 18 h. Water (50 mL) was added and the organics extracted into ethyl acetate. The solvent was removed under vacuum and the resulting oil was purified by column chromatography (eluent: hexane:DCM 7:3 *v*/*v*) to give **198** as a pale yellow oil (0.492 mg, 89%). ^{1}H NMR (400 MHz) $CDCl_3$ δ 8.37 (d, *J* = 1.4 Hz, 1H), 8.01 (dd, *J* = 8.0, 2.0 Hz, 1H), 7.67 (dd, *J* = 8.6, 1.7 Hz, 1H), 7.48-7.43 (m, 1H), 7.36 (d, *J* = 8.3 Hz, 1H), 7.23-7.19 (m, 1H), 7.15 (d, *J* = 8.6 Hz, 1H), 4.16-4.06 (m, 2H), 2.07-1.95 (m, 1H), 1.36-1.22 (m, 8H), 0.92-0.84 (m, 6H). Data consistent with the literature.[186]

199; 9-(2-Ethylhexyl)-3-((trimethylsilyl)ethynyl)-9*H*-carbazole

200; 9-(2-Ethylhexyl)-3-ethynyl-9*H*-carbazole

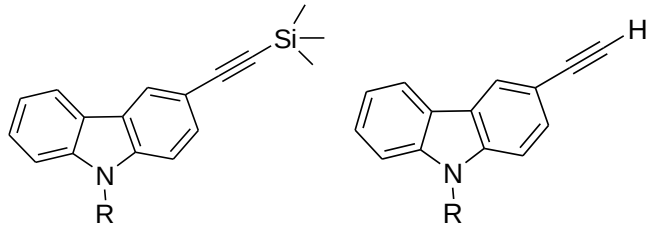

199 **200**

R = 2-ethylhexyl

9-(2-Ethylhexyl)-3-iodo-9*H*-carbazole (**198**) (0.246 g, 0.607 mmol) was dissolved in a mixture of anhydrous THF (5 mL) and triethylamine (5 mL) under argon. The solution was then degassed by bubbling through argon for 15 min. Tetrakis(triphenylphosphine)palladium(0) (0.050 g, 7 mol%) and copper(I)iodide (0.017 g, 15 mol%) were added and degassing continued for 15 min. Ethynyltrimethylsilane (0.34 mL, 2.428 mmol) was added and the mixture stirred under argon at room temperature for 18 h. Upon cooling the solvent was removed under vacuum and the residue was purified by column chromatography (eluent: 10% DCM in petroleum ether) to give (9-(2-ethylhexyl)-3-((trimethylsilyl)ethynyl)-9*H*-carbazole) (**199**) as a colourless oil (0.150 g, 66%).^{1}H NMR (400 MHz) $CDCl_3$ δ 8.24 (d, *J* = 1.2 Hz, 1H), 8.06 (d, *J* = 7.6 Hz, 1H), 7.56 (dd, *J* = 8.4, 1.6 Hz, 1H), 7.47 (t, *J* = 7.2 Hz, 1H), 7.38 (d, *J* = 8.0 Hz, 1H), 7.30 (d, *J* = 8.4 Hz, 1H), 7.23 (d, *J*

= 6.8 Hz, 1H), 4.16-4.14 (m, 2H), 2.07-2.01 (m, 1H), 1.37-1.23 (m, 8H), 0.92-0.83 (m, 6H), 0.29 (s, 9H). Compound **199** was then reacted on by dissolving in a mixture of THF (2 mL) and methanol (10 mL). To the solution was added potassium carbonate (0.276 g, 1.995 mmol) and the mixture stirred at room temperature for 18 h. The organic product was extracted into diethyl ether and washed with brine and water. Removal of the solvent under vacuum gave **200** as a yellow oil (0.099 g, 82% for deprotection step; 54% overall yield). ^{1}H NMR (400 MHz) $CDCl_3$ δ 8.26 (d, *J* = 1.1 Hz, 1H), 8.07 (d, *J* = 7.4 Hz, 1H), 7.58 (dd, *J* = 8.5, 1.6 Hz, 1H), 7.51 – 7.44 (m, 1H), 7.39 (d, *J* = 8.2 Hz, 1H), 7.32 (d, *J* = 8.5 Hz, 1H), 7.28–7.22 (m, 1H), 4.17-4.15 (m, 2H), 3.07 (s, 1H), 2.07-2.03 (m, 1H), 1.37-1.28 (m, 8H), 0.93-0.84 (m, 6H). ^{13}C NMR (176 MHz) $CDCl_3$ δ 140.8, 129.6, 126.1, 124.6, 122.7, 122.4, 120.4, 119.3, 111.9, 109.2, 108.9, 85.1, 75.0, 47.6, 39.4, 31.0, 28.8, 24.4, 23.0, 14.0, 10.9. MS-ASAP$^+$ *m/z* (%) 303.4 ([M]$^+$, 100%). HRMS-ASAP$^+$ *m/z* calculated for $C_{22}H_{25}N$: [M]$^+$ 303.1987, found: 303.1987.

201; 2,8-Bis((9-(2-ethylhexyl)-9*H*-carbazol-3-yl)ethynyl)dibenzothiophene-*S*,*S*-dioxide

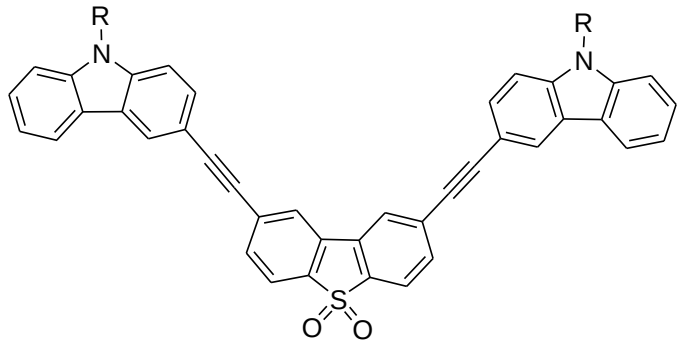

R = 2-ethylhexyl

9-(2-Ethylhexyl)-3-ethynyl-9*H*-carbazole (**200**) (0.090 g, 0.297 mmol) and 2,8-dibromodibenzothiophene-*S*,*S*-dioxide (**89**) (0.053 g, 0.141 mmol) were dissolved in anhydrous THF (25 mL) under argon. Triethylamine (10 mL) was added and the solution was degassed by bubbling through argon for 15 min. Tetrakis(triphenylphosphine)palladium(0) (0.010 g) and copper(I)iodide (0.010 g) were added and the mixture was heated at 60 °C under argon for 18 h. Upon cooling the solvent was removed under vacuum and the residue was purified by column chromatography (eluent: petroleum ether:DCM 1:1 *v*/*v* then DCM) to give the product as a glassy yellow film. Triturating this material in hexane (25 mL) for 1 h precipitated **201** which was isolated by filtration as a fine, yellow amorphous powder (0.070 g, 61%).^{1}H NMR (700 MHz) $CDCl_3$ δ 8.35 (s, 2H), 8.13 (d, *J* = 7.7 Hz, 2H), 8.00 (s, 2H), 7.82 d, *J* = 7.8 Hz, 2H), 7.69 (dd, *J* = 22.5, 8.1 Hz, 4H), 7.51 (t, *J* = 7.5 Hz, 2H), 7.41 (dd, *J* = 13.8, 8.3 Hz, 4H), 7.29 (t, *J* = 7.3 Hz, 2H), 4.20-4.16 (m, 4H), 2.09-2.06 (m, 2H), 1.45-1.24 (m, 16H), 0.90 (dt, *J* = 46.1, 7.2 Hz, 12H). ^{13}C NMR (176 MHz) $CDCl_3$ δ 141.3, 141.1, 136.3, 133.1, 131.4, 130.2, 129.3, 126.3, 124.5,

124.2, 122.9, 122.3, 122.2, 120.5, 119.6, 111.9, 109.3, 109.2, 95.6, 86.3, 47.6, 39.4, 31.0, 28.8, 24.4, 23.0, 14.0, 10.9. MS-ASAP$^+$ *m/z* (%) 818.3 ([M]$^+$, 20%). HRMS-ASAP$^+$ *m/z* calculated for $C_{56}H_{54}N_2O_2S$: [M]$^+$ 818.3906, found: 818.3921. Mpt. 282.9-284.2 °C.

202; 3'-(9,9-Dihexyl-9*H*-fluoren-2-yl)-9,9,9',9'-tetrahexyl-2,6'-bi(9*H*-fluorene)

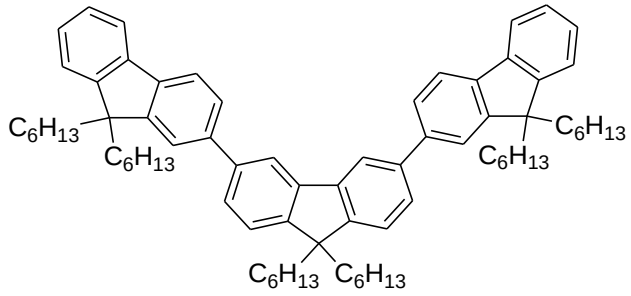

3,6-Dibromo-9,9-dihexyl-9*H*-fluorene (**194**) (0.200 g, 0.406 mmol) and 9,9-dihexylfluoren-2-yl-2-boronic acid (**125**) (0.385 g, 1.02 mmol) were suspended in 1,4-dioxane (20 mL) and the solution degassed. $Pd(PPh_3)_4$ (0.024 g, 5 mol%) was added and the solution degassed further. Degassed sodium carbonate solution (1M, 7 mL) was added and the mixture heated at 85 °C for 18 h under argon. The organic product was extracted into DCM, washed with brine and dried over magnesium sulfate. The crude product was purified by column chromatography (eluent: DCM), followed by recrystallisation from ethanol (at low temperature) to give **202** as a sticky white solid (0.190 g, 47%). ^{1}H NMR (400 MHz) $CDCl_3$ δ 8.06 (d, *J* = 1.3 Hz, 2H), 7.69-7.59 (m, 10H), 7.43 (d, *J* = 7.8 Hz, 2H), 7.36-7.25 (m, 6H), 2.08-1.94 (m, 12H), 1.18-0.95 (m, 36H), 0.78-0.65 (m, 30H). Data consistent with the literature.[174]

7.4 Experimental Procedures for Chapter 4

General Procedure (A) for Ferrocene Suzuki Coupling Reactions:

The required aryl boronic ester (1.2-2 equiv.) was dissolved in a mixture of ethanol:water 9:1 *v*/*v* and the solution degassed by bubbling through argon for 2 h. Bromoferrocene (1 equiv.) was added and degassing continued for 15 min. Potassium carbonate (1.1-1.4 equiv.) and palladium(II)acetate (0.2 equiv.) were added and the mixture stirred vigorously under argon at room temperature for 24 h. The reaction was stopped by removal of the solvent under vacuum. The residue was then dissolved in diethyl ether (~ 50 mL) and washed with brine, before drying over magnesium sulfate. Removal of the solvent under vacuum followed by purification using column chromatography (eluent: petroleum ether:DCM 1:1 *v*/*v*) gave the required compounds.

General Procedure (B) for C_{60} Reactions:

Fullerene-C_{60} (4 equiv.) was dissolved in chlorobenzene (100 mL per 200 mg of C_{60}) and the mixture sonicated for 10 min. The resulting purple solution was heated at 130 °C under argon for 10 min before the addition of sarcosine (5 equiv.) and the ferrocene/fluorene-based aldehdye (1 equiv.) Reflux was continued for 4-7 h, monitoring reaction progress by TLC. The reaction was stopped by the removal of the solvent under vacuum and the final products were purified by column chromatography.

213; 2,7-Dibromo-9,9-dihexyl-9*H*-fluorene

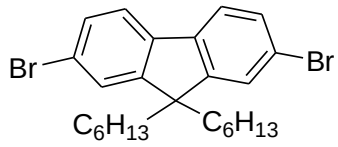

2,7-Dibromofluorene (20 g, 61.73 mmol) was suspended in DMSO (20 mL) with stirring. 1-bromohexane (21.7 mL, 154.32 mmol), tetra-*n*-butylammonium bromide (3.980 g, 12.35 mmol), sodium hydroxide (6.173 g, 154.32 mmol) and water (8 mL) were added. The mixture was stirred at room temperature for 18 h. The organic products were extracted into ethyl acetate and washed with dilute HCl and water, before being dried over magnesium sulfate. Removal of the solvent under vacuum gave the crude product which was purified by column chromatography (eluent: petroleum ether) followed by recrystallisation from ethanol to give **213** as a white crystalline solid (21.88 g, 72%). ^{1}H NMR (400 MHz) $CDCl_3$ δ 7.52 (dd, *J* = 7.6, 0.9 Hz, 2H), 7.48–7.42 (m, 4H), 1.96–1.83 (m, 4H), 1.18–0.98 (m, 12H), 0.78 (t, *J* = 7.1 Hz, 6H), 0.58 (s, 4H). Data consistent with the literature.[133]

214; 7-Bromo-9,9-dihexyl-9*H*-fluorene-2-carbaldehyde

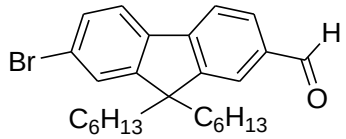

2,7-Dibromo-9,9-dihexyl-9*H*-fluorene (**213**) (3.00 g, 6.094 mmol) was dissolved in anhydrous diethyl ether (35 mL) at - 78 °C under argon. ^{n}BuLi (2.5 M in hexanes, 2.7 mL, 6.703 mmol) was added dropwise and the solution stirred at - 78 °C for 30 min. The solution was then warmed to room temperature and stirred for 30 min, before being cooled to - 78 °C and DMF (0.63 mL, 1.3 equiv.) added dropwise. The reaction was then stirred under argon for 18 h slowly warming to room temperature. Hydrochloric acid (2M, ~ 30 mL) was added to quench the reaction and the mixture stirred for 2 h. The organic products were extracted into diethyl ether, washed with brine and dried over magnesium sulfate. After removal of the solvent under vacuum,

purification by column chromatography (eluent: petroleum ether:DCM 7:3 *v*/*v*) gave **214** as a colourless oil, which upon standing overnight became a white solid (1.968 g, 73%).[1]H NMR (400 MHz) $CDCl_3$ δ 10.06 (s, 1H), 7.93–7.73 (m, 3H), 7.73–7.56 (m, 1H), 7.57–7.43 (m, 2H), 2.20–1.85 (m, 4H), 1.17–0.90 (m, 12H), 0.76 (t, *J* = 7.1 Hz, 6H), 0.61-0.52 (m, 4H). Data consistent with the literature.[133]

215; 9,9-Dihexyl-7-(4,4,5,5-tetramethyl-1,3,2-dioxaborolan-2-yl)-9*H*-fluorene-2-carbaldehyde

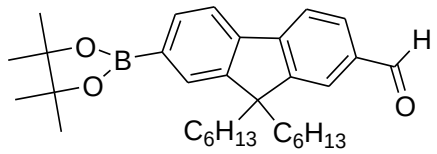

7-Bromo-9,9-dihexyl-9*H*-fluorene-2-carbaldehyde (**214**) (0.50 g, 1.2 mmol) was dissolved in anhydrous DMF (10 mL) and the solution degassed by bubbling through argon for 30 min. Bis(pinacolato)diboron (0.73 g, 2.9 mmol), potassium acetate (0.90 g, 9.2 mmol) and palladium(II) acetate (~ 15 mg) were added and the mixture heated at 90 °C under argon for 18 h. The organic products were extracted into DCM, washed with brine and dried over magnesium sulfate. Purification by column chromatography (eluent: petroleum ether:DCM 1:1 *v*/*v*) gave **215** as a sticky white solid (0.400 g, 68%). [1]H NMR (400 MHz) $CDCl_3$ δ 10.07 (s, 1H), 7.87-7.83 (m, 4H), 7.81–7.74 (m, 2H), 2.09–1.99 (m, 4H), 1.40 (s, 12H), 1.10-1.00 (m, 12H), 0.74 (t, *J* = 7.1 Hz, 6H), 0.57-0.51 (m, 4H). Data consistent with the literature.[133]

216; 7-Bromo-9,9,9',9'-tetrahexyl-2,2'-bi(9*H*-fluorene)-7'-carbaldehyde

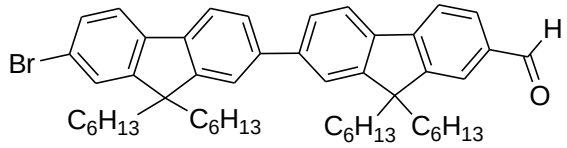

9,9-Dihexyl-7-(4,4,5,5-tetramethyl-1,3,2-dioxaborolan-2-yl)-9*H*-fluorene-2-carbaldehyde (**215**) (0.800 g, 1.637 mmol) and 2,7-dibromo-9,9-dihexyl-9*H*-fluorene (**213**) (2.42 g, 4.911 mmol) were dissolved in a mixture of toluene (10 mL) and water (5 mL) and the solution degassed by bubbling through argon for 30 min. Potassium carbonate (1.81 g, 13.096 mmol) and $Pd(PPh_3)_2Cl_2$ (~ 20 mg) were added and the mixture heated at 110 °C for 18 h. The organic products were extracted into DCM, washed with brine and dried over magnesium sulfate. Purification by column chromatography (eluent: petroleum ether:DCM 8:2 *v*/*v*) removed unreacted starting material (**213**), then further purification by column chromatography (eluent: petroleum ether:DCM 4:6 *v*/*v*) gave **216** as a fluffy pale yellow solid (0.570 g, 45%).[1]H NMR (400 MHz) $CDCl_3$ δ 10.08 (s, 1H), 7.95–7.82 (m, 4H), 7.76 (d, *J* = 7.7 Hz, 1H), 7.71–7.56 (m,

5H), 7.53–7.46 (m, 2H), 2.17–1.94 (m, 8H), 1.20-0.99 (m, 24H), 0.79-0.62 (m, 20H). Data consistent with the literature.[133]

217;9,9,9',9'-Tetrahexyl-7-(4,4,5,5-tetramethyl-1,3,2-dioxaborolan-2-yl)-2,2'-bi(9*H*-fluorene)-7'-carbaldehyde

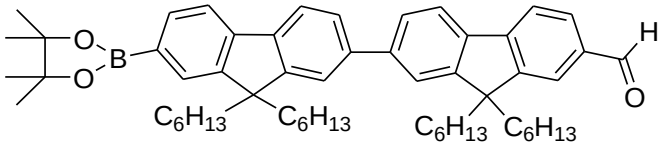

7-Bromo-9,9,9',9'-tetrahexyl-2,2'-bi(9*H*-fluorene)-7'-carbaldehyde (**216**) (0.593 g, 0.766 mmol) was dissolved in anhydrous DMF (10 mL) and the solution degassed by bubbling through argon for 30 min. Bis(pinacolato)diboron (0.467 g, 1.84 mmol), potassium acetate (0.579 g, 5.90 mmol) and palladium(II) acetate (~ 15 mg) were added and the mixture heated at 90 °C under argon for 18 h. The organic products were extracted into DCM, washed with brine and dried over magnesium sulfate. Purification by column chromatography (eluent: petroleum ether:DCM 3:7 *v*/*v*) gave **217** as a pale yellow fluffy solid (0.394 g, 63%). ^{1}H NMR (400 MHz) $CDCl_3$ δ 10.08 (s, 1H), 8.04–7.51 (m, 12H), 2.10-2.03 (m, 8H), 1.40 (s, 12H), 1.22–0.95 (m, 24H), 0.75 (t, *J* = 6.9 Hz, 12H), 0.70-0.64 (m, 8H). Data consistent with the literature.[133]

218; Trimethyl(4-(4,4,5,5-tetramethyl-1,3,2-dioxaborolan-2-yl)phenyl)silane

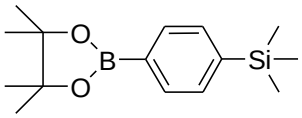

(4-Bromophenyl)trimethylsilane (**222**) (1.00 g, 4.363 mmol) was dissolved in anhydrous DMF (10 mL) and the solution degassed by bubbling through argon for 30 min. Bis(pinacolato) diboron (1.77 g, 6.981 mmol), potassium acetate (1.285 g, 13.09 mmol) and $Pd(dppf)Cl_2$ (0.160 g, 0.218 mmol, 5 mol%) were added and the mixture heated at 80 °C under argon for 18 h. The organic products were extracted into DCM, washed with brine and dried over magnesium sulfate. Purification by column chromatography (eluent: DCM) gave **218** as a white solid (0.900 g, 75%).^{1}H NMR (400 MHz) $CDCl_3$ δ 7.82-7.76 (m, 2H), 7.56-7.51 (m, 2H), 1.34 (s, 12H), 0.27 (s, 9H). ^{19}B NMR (128 MHz) δ 31.01. ^{13}C NMR (100 MHz) $CDCl_3$ δ 145.5, 135.1, 133.9, 85.0, 26.1, 0.0. MS-MALDI *m/z* 261.1 (%) ($[M-CH_3]^+$, 100). Mpt. 119.9-120.3 °C.

219; 9,9-Dihexyl-7-(4-(trimethylsilyl)phenyl)-9*H*-fluorene-2-carbaldehyde

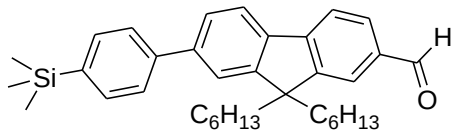

7-Bromo-9,9-dihexyl-9*H*-fluorene-2-carbaldehyde (**214**) (0.600 g, 1.359 mmol) and trimethyl(4-(4,4,5,5-tetramethyl-1,3,2-dioxaborolan-2-yl)phenyl)silane (**218**) (0.413 g, 1.495 mmol) were dissolved in 1,4-dioxane (20 mL) and the solution degassed by bubbling through argon for 15 min. $Pd(PPh_3)_4$ (0.047 g, 0.0408 mmol, 3 mol%) was added together with a degassed solution of potassium carbonate (0.564 g, 4.078 mmol) in water (5 mL). The reaction mixture was heated at 85 °C for 18 h. The organic products were then extracted into DCM, washed with brine and dried over magnesium sulfate. Purification by column chromatography (eluent: petroleum ether:DCM 1:1 *v*/*v*) gave **219** as a viscous yellow oil (0.580 g, 84%). ^{1}H NMR (400 MHz) $CDCl_3$ δ 10.07 (s, 1H), 7.89-7.83 (m, 4H), 7.66-7.59 (m, 6H), 2.09-2.00 (m, 4H), 1.15-0.97 (m, 12H), 0.75 (t, *J* = 7.1 Hz, 6H), 0.65-0.62 (m, 4H), 0.32 (s, 9H). ^{13}C NMR (100 MHz) $CDCl_3$ δ 190.9, 151.4, 150.3, 140.3, 133.8, 132.4, 129.2, 125.1, 124.9, 121.6, 120.3, 119.8, 118.5, 53.9, 38.8, 30.0, 28.1, 22.3, 21.1, 12.5, -2.6. MS-ASAP$^+$ *m/z* 510.2 (%) ([M]$^+$, 100). HRMS-ASAP$^+$ *m/z* calculated for $C_{35}H_{46}OSi$: [M]$^+$ 510.3318, Found: 510.3335.

220; 9,9-Dihexyl-7-(4-iodophenyl)-9*H*-fluorene-2-carbaldehyde

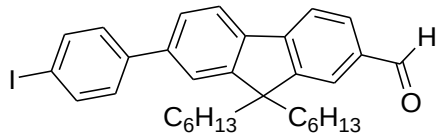

9,9-Dihexyl-7-(4-(trimethylsilyl)phenyl)-9*H*-fluorene-2-carbaldehyde (**219**) (0.570 g, 1.116 mmol) was dissolved in anhydrous DCM (20 mL) and the solution degassed by bubbling through argon for 15 min, whilst cooling to 0 °C. Iodine monochloride (1M solution in DCM, 2.80 mL, 2.5 equiv.) was added dropwise. The mixture was stirred under argon at 0 °C for 1.5 h before warming to room temperature with stirring overnight. The reaction was quenched with an aqueous solution of sodium thiosulfate and extracted into DCM. Purification by column chromatography (eluent: petroleum ether:DCM 1:1 *v*/*v*) gave **220** as a light yellow oil (quantitative yield). ^{1}H NMR (400 MHz) $CDCl_3$ δ 10.08 (s, 1H), 7.95–7.76 (m, 6H), 7.64–7.50 (m, 2H), 7.46–7.36 (m, 2H), 2.12–1.97 (m, 4H), 1.16–0.97 (m, 12H), 0.74 (t, *J* = 8.0 Hz, 6H), 0.66-0.60 (m, 4H). ^{13}C NMR (100 MHz) $CDCl_3$ δ 192.2, 153.1, 151.8, 147.0, 140.8, 139.2, 137.9, 135.5, 130.5, 129.1, 126.2, 123.1, 121.4, 120.1, 93.2, 55.4, 40.2, 31.4, 29.6, 23.8, 22.5, 13.9. MS-ASAP$^+$ *m/z* 564.3 (%) ([M]$^+$, 100). HRMS-ASAP$^+$ *m/z* calculated for $C_{32}H_{47}IO$: [M]$^+$ 565.1967, Found: 565.1970.

221;9,9-Dihexyl-7-(4-(4,4,5,5-tetramethyl-1,3,2-dioxaborolan-2-yl)phenyl)-9*H*-fluorene-2-carbaldehyde

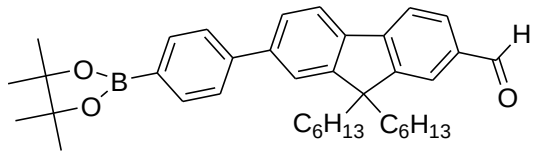

9,9-Dihexyl-7-(4-iodophenyl)-9*H*-fluorene-2-carbaldehyde (**220**) (0.452 g, 0.801 mmol) was dissolved in anhydrous DMF (10 mL) and the solution degassed by bubbling through argon for 30 min. Bis(pinacolato)diboron (0.488 g, 1.92 mmol), potassium acetate (0.605 g, 6.16 mmol) and palladium(II)acetate (15 mg) were added and the mixture heated at 90 °C under argon for 18 h. The organic products were extracted into DCM, washed with brine and dried over magnesium sulfate. Purification by column chromatography (eluent: hexane:DCM 1:3 *v*/*v*) gave **221** as a fluffy white solid (0.273 g, 60%). ^{1}H NMR (400 MHz) $CDCl_3$ δ 10.08 (s, 1H), 7.95–7.82 (m, 6H), 7.71–7.59 (m, 4H), 2.10-2.02 (m, 4H), 1.39 (s, 12H), 1.13-1.01 (m, 12H), 0.75 (t, *J* = 7.0 Hz, 6H), 0.71–0.57 (m, 4H). ^{11}B NMR (128 MHz) $CDCl_3$ δ 34.3. ^{13}C NMR (100 MHz) $CDCl_3$ δ 192.3, 152.9, 151.8, 147.1, 143.9, 141.6, 139.0, 135.3, 130.5, 126.5, 123.1, 121.7, 121.2, 120.0, 83.9, 55.4, 40.2, 31.4, 29.5, 24.9, 23.7, 22.5, 13.9. MS-ASAP$^+$ *m/z* 564.4 (%) ([M]$^+$, 100). HRMS-ASAP$^+$ *m/z* calculated for $C_{38}H_{50}BO_3$: [M+H]$^+$ 565.3853, Found: 565.3866. Mpt. 103.7-105.3 °C.

222; (4-Bromophenyl)trimethylsilane

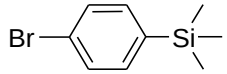

1,4-Dibromobenzene (5.00 g, 21.20 mmol) was dissolved in anhydrous diethyl ether (70 mL) under argon and cooled to - 78 °C. ^{n}BuLi (2.5 M in hexanes, 9.33 mL, 23.32 mmol) was added dropwise and the mixture stirred at - 78 °C for 1.5 h. Chlorotrimethylsilane (3.23 mL, 25.44 mmol) was added and the mixture warmed to room temperature and stirred for 2 h. The organic products were extracted into diethyl ether, washed with water and dried over magnesium sulfate. Removal of the solvent under vacuum gave **222** as a colourless liquid (quantitative yield). ^{1}H NMR (400 MHz) $CDCl_3$ δ 7.51 (d, *J* = 8.2 Hz, 2H), 7.40 (d, *J* = 8.2 Hz, 2H), 0.29 (s, 9H). Data consistent with the literature.[187]

223; 9,9,9',9'-Tetrahexyl-7-(4-(trimethylsilyl)phenyl)-2,2'-bi(9*H*-fluorene)-7'-carbaldehyde

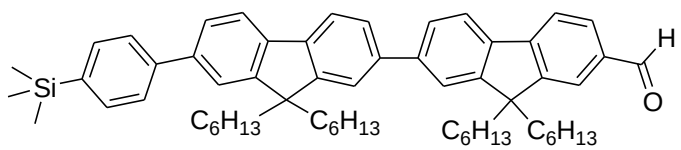

9,9,9',9'-tetrahexyl-7-(4,4,5,5-tetramethyl-1,3,2-dioxaborolan-2-yl)-2,2'-bi(9*H*-fluorene)-7'-carbaldehyde (**217**) (0.411 g, 0.501 mmol) was dissolved in a mixture of toluene (10 mL) and water (5 mL) and the solution degassed by bubbling through argon for 15 min. (4-bromophenyl)trimethylsilane (**222**) (0.104 g, 0.451 mmol), potassium carbonate (0.498 g, 3.608 mmol) and $Pd(PPh_3)_2Cl_2$ (15 mg) were then added and the reaction heated at 110 °C for 18 h. The organic products were extracted into DCM. Purification by column chromatography (eluent: petroleum ether:DCM 1:4 *v*/*v*) gave **223** as a light yellow sticky solid (0.332 g, 87%). ^{1}H NMR (400 MHz) $CDCl_3$ δ 10.08 (s, 1H), 7.88 (t, *J* = 9.7 Hz, 4H), 7.82-7.79 (m, 2H), 7.72–7.58 (m, 10H), 2.11-2.05 (m, 8H), 1.17–1.02 (m, 24H), 0.81–0.62 (m, 20H), 0.33 (s, 9H). ^{13}C NMR (100 MHz) $CDCl_3$ δ 191.9, 151.3, 141.9, 139.7, 139.5, 138.2, 134.8, 133.4, 126.1, 125.8, 121.2, 120.8, 119.5, 54.9, 54.8, 39.7, 31.0, 29.2, 23.3, 22.1, 13.5, -1.5. MS-ASAP$^+$ *m/z* 842.5 (%) ([M]$^+$, 100). HRMS-ASAP$^+$ *m/z* calculated for $C_{60}H_{78}OSi$: [M]$^+$ 842.5822, Found: 842.5860.

224; 9,9,9',9'-Tetrahexyl-7-(4-iodophenyl)-2,2'-bi(9*H*-fluorene)-7'-carbaldehyde

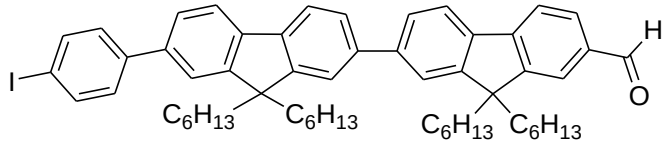

9,9,9',9'-Tetrahexyl-7-(4-(trimethylsilyl)phenyl)-2,2'-bi(9*H*-fluorene)-7'-carbaldehyde (**223**) (0.320 g, 0.379 mmol) was dissolved in anhydrous DCM (15 mL) and the solution degassed by bubbling through argon for 15 min, whilst cooling to 0 °C. Iodine monochloride (1M solution in DCM, 0.95 mL, 2.5 equiv.) was added dropwise. The mixture was stirred under argon at 0 °C for 0.5 h before warming to room temperature over ~4 h. The reaction was quenched with an aqueous solution of sodium thiosulfate and extracted into DCM. Purification by column chromatography (eluent: petroleum ether:DCM 1:1 *v*/*v*) gave **224** as an oily solid (quantitative yield).^{1}H NMR (400 MHz) $CDCl_3$ δ 10.08 (s, 1H), 7.92–7.77 (m, 8H), 7.71-7.53 (m, 6H), 7.44-7.40 (m, 2H), 2.11-2.03 (m, 8H), 1.16-1.04 (m, 24H), 0.79-0.66 (m, 20H). ^{13}C NMR (176 MHz) $CDCl_3$ δ 192.3, 152.9, 151.9, 147.2, 141.1, 140.4, 140.2, 138.7, 137.8, 130.6, 129.0, 126.5, 126.3, 125.9, 123.1, 121.5, 121.2, 120.1, 120.0, 92.7, 55.4, 40.3, 31.4, 29.6 23.8, 22.5, 13.94. MS-ASAP$^+$ *m/z* 896.4 (%) ([M]$^+$, 100). HRMS-ASAP$^+$ *m/z* calculated for $C_{57}H_{69}IO$: [M]$^+$ 896.4393, Found: 896.4431. Mpt. 85.2-86.9 °C.

225;9,9,9',9'-Tetrahexyl-7-(4-(4,4,5,5-tetramethyl-1,3,2-dioxaborolan-2-yl)phenyl)-2,2'-bi(9*H*-fluorene)-7'-carbaldehyde

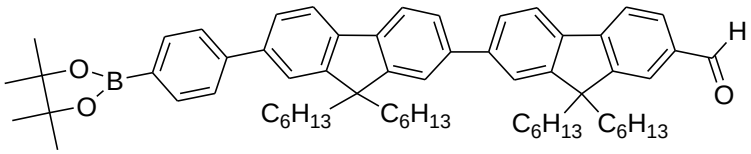

9,9,9',9'-Tetrahexyl-7-(4-iodophenyl)-2,2'-bi(9*H*-fluorene)-7'-carbaldehyde (**224**) (0.332 g, 0.370 mmol) was dissolved in anhydrous DMF (10 mL) and the solution degassed by bubbling through argon for 30 min. Bis(pinacolato)diboron (0.226 g, 0.89 mmol), potassium acetate (0.280 g, 2.85 mmol) and palladium(II)acetate (15 mg) were added and the mixture heated at 90 °C under argon for 18 h. The organic products were extracted into ethyl acetate, washed with brine and dried over magnesium sulfate. Purification by column chromatography (eluent: petroleum ether:DCM 3:7 *v*/*v*) gave **225** as a yellow oil (0.220 g, 66%).^{1}H NMR (400 MHz) $CDCl_3$ δ 10.08 (s, 1H), 7.93-7.86 (m, 6H), 7.82-7.79 (m, 2H), 7.71-7.60 (m, 8H), 2.10-2.07 (m, 8H), 1.38 (s, 12H), 1.14-1.04 (m, 24H), 0.78-0.63 (m, 20H). ^{13}C NMR (176 MHz) $CDCl_3$ δ 192.3, 152.9, 151.9, 147.3, 144.3, 142.3, 140.3, 138.6, 135.3, 126.4, 126.2, 123.1, 121.6, 121.2, 120.1, 120.0, 83.8, 55.4, 40.3, 31.4, 29.6, 24.9, 23.8, 14.0, 13.9. MS-MALDI *m/z* 896.5 (%) ([M], 100).

226; Fc – F – CHO

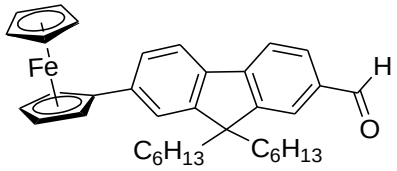

General procedure **A** was followed using boronic ester (**215**) (0.234 g, 0.479 mmol) in 20 mL of solvent, together with bromoferrocene (0.063 g, 0.24 mmol), potassium carbonate (0.048 g, 0.347 mmol) and palladium(II)acetate (0.011 g, 0.049 mmol). Purification by column chromatography gave **226** as a viscous red oil (64 mg, 49%). ^{1}H NMR (400 MHz) $CDCl_3$ δ 10.05 (s, 1H), 7.91–7.74 (m, 3H), 7.67 (d, *J* = 8.6 Hz, 1H), 7.48 (dd, *J* = 7.1, 1.5 Hz, 2H), 4.78–4.71 (m, 2H), 4.40–4.34 (m, 2H), 4.02 (s, 5H), 2.11–1.98 (m, 4H), 1.15–0.96 (m, 12H), 0.74 (t, *J* = 7.0 Hz, 6H), 0.65-0.61 (m, 4H). ^{13}C NMR (101 MHz) $CDCl_3$ δ 192.3, 152.4, 151.4, 147.6, 140.5, 137.5, 135.0, 130.7, 124.9, 123.0, 120.9, 120.4, 119.5, 85.0, 69.8, 69.3, 66.6, 55.1, 40.4, 31.5, 29.6, 23.8, 22.5, 13.9. MS-ASAP^{+} *m/z* 546.3 (%) ([M]$^{+}$, 100). HRMS-ASAP^{+} *m/z* calculated for $C_{36}H_{42}{}^{56}FeO$: [M+H]$^{+}$ 547.2663, Found: 547.2664.

227; Fc – F_2 – CHO

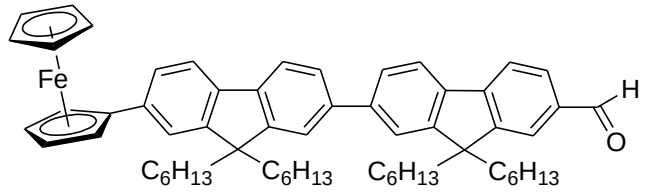

General procedure **A** was followed using boronic ester (**217**) (0.214 g, 0.261 mmol) in a solvent mixture of ethanol (9 mL), water (2 mL) and THF (5 mL), together with bromoferrocene (0.053 g, 0.201 mmol), potassium carbonate (0.033 g, 0.239 mmol) and palladium(II)acetate (0.009 g, 0.040 mmol). Purification by column chromatography gave **227** as a viscous red oil (52 mg, 29%). ^{1}H NMR (400 MHz, $CDCl_3$) δ 10.08 (s, 1H), 7.88 (dd, *J* = 12.1, 9.5 Hz, 4H), 7.77 (d, *J* = 7.9 Hz, 1H), 7.71 (dd, *J* = 7.9, 1.4 Hz, 1H), 7.68–7.60 (m, 4H), 7.51–7.45 (m, 2H), 4.75 (t, *J* = 1.8 Hz, 2H), 4.40–4.33 (m, 2H), 4.05 (s, 5H), 2.12-2.04 (m, 8H), 1.19–0.98 (m, 24H), 0.78–0.62 (m, 20H). ^{13}C NMR (101 MHz) $CDCl_3$ δ 192.4, 153.0, 151.8, 151.5, 151.2, 147.3, 142.4, 140.8, 139.6, 138.7, 138.6, 138.4, 135.2, 130.6, 130.4, 126.5, 126.3, 124.7, 123.1, 121.5, 121.3, 121.2, 120.5, 120.0, 119.7, 85.7, 69.7, 69.0, 66.5, 55.4, 55.1, 40.5, 40.2, 31.5, 29.7, 29.6, 23.8, 22.5, 14.0. MS-ASAP$^+$ *m/z* 878.5 (%) ([M]$^+$, 100). HRMS-ASAP$^+$ *m/z* calculated for $C_{61}H_{74}{}^{54}FeO$: [M]$^+$ 876.5136, Found: 876.5135.

228; Fc – Ph – F – CHO

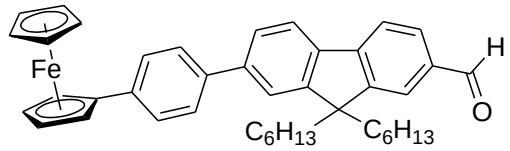

General procedure **A** was followed using boronic ester (**221**) (0.276 g, 0.489 mmol) in 40 mL of solvent, together with bromoferrocene (0.086 g, 0.326 mmol), potassium carbonate (0.063 g, 0.456 mmol) and palladium(II)acetate (0.015 g, 0.067 mmol). Purification by column chromatography gave **228** as a viscous red oil (76 mg, 37%). ^{1}H NMR (500 MHz) $CDCl_3$ δ 10.07 (s, 1H), 7.91–7.81 (m, 4H), 7.69-7.58 (m, 6H), 4.74–4.68 (m, 2H), 4.38–4.34 (m, 2H), 4.09 (s, 5H), 2.12–1.99 (m, 4H), 1.16–0.98 (m, 12H), 0.76 (t, *J* = 7.1 Hz, 6H), 0.70–0.59 (m, 4H). ^{13}C NMR (126 MHz) $CDCl_3$ δ 192.3, 153.1, 152.0, 147.6, 141.8, 139.1, 138.8, 138.7, 135.4, 130.9, 129.1, 127.5, 127.3, 126.8, 126.2, 123.3, 121.5, 121.4, 120.2, 85.1, 69.9, 69.3, 66.8, 55.6, 40.5, 31.7, 29.9, 24.0, 22.8, 14.2. MS-ASAP$^+$ *m/z* 622.3 (%) ([M]$^+$, 100). HRMS-ASAP$^+$ *m/z* calculated for $C_{42}H_{47}{}^{54}FeO$: [M+H]$^+$ 621.3023, Found: 621.3040.

229; Fc – Ph – F_2 – CHO

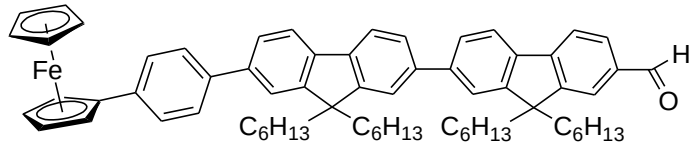

General procedure **A** was followed using boronic ester (**225**) (0.215 g, 0.240 mmol) in 20 mL of solvent (with 4 mL THF added for solubility), together with bromoferrocene (0.049 g, 0.184 mmol), potassium carbonate (0.028 g, 0.202 mmol) and palladium(II)acetate (0.008 g, 0.037 mmol). Purification by column chromatography gave **229** as a viscous red oil (0.050 g, 28%). ^{1}H NMR (400 MHz) $CDCl_3$ δ 10.09 (s, 1H), 7.89 (t, *J* = 9.7 Hz, 4H), 7.81 (dd, *J* = 7.8, 4.4 Hz, 2H), 7.74– 7.57 (m, 10H), 4.71 (t, *J* = 1.8 Hz, 2H), 4.40–4.33 (m, 2H), 4.09 (s, 5H), 2.15–2.03 (m, 8H), 1.17–1.04 (m, 24H), 0.81–0.62 (m, 20H). ^{13}C NMR (101 MHz) $CDCl_3$ δ 192.4, 153.0, 151.8, 147.3, 142.3, 140.5, 139.9, 139.8, 139.0, 138.7, 138.4, 135.2, 130.6, 127.0, 126.5, 126.3, 125.7, 123.1, 121.6, 121.5, 121.2, 121.1, 120.1, 120.0, 85.1, 69.7, 69.1, 66.6, 55.4, 55.3, 40.4, 31.5, 29.7, 23.8, 22.6, 14.0. MS-ASAP$^+$ *m/z* 954.5 (%) ([M]$^+$, 100). HRMS-ASAP$^+$ *m/z* calculated for $C_{67}H_{79}{}^{54}FeO$: [M+H]$^+$ 953.5527, Found: 953.5554.

230; Fc – F – C_{60}

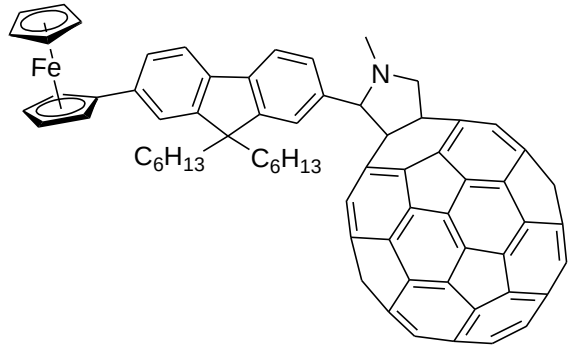

General procedure **B** was followed using fullerene-C_{60} (0.280 g), sarcosine (0.043 g) and compound (**226**) (0.053 g, 0.0970 mmol), refluxing for 4.5 h. Purification using column chromatography (eluent: CS_2; then hexane:toluene 1:1 *v*/*v*) gave **230** as an amorphous black solid (0.065 g, 52%). ^{1}H NMR (500 MHz) $CDCl_3$ δ 7.97 (s, 1H, br), 7.69 (s, 1H, br), 7.58 (d, *J* = 8.3 Hz, 2H), 7.41 (d, *J* = 6.8 Hz, 2H), 5.03 (t, *J* = 4.6 Hz, 2H), 4.75–4.66 (m, 2H), 4.34-4.31 (m, 3H), 3.99 (s, 5H), 2.88 (s, 3H), 2.18 (s, 1H, br), 1.99 (s, 3H, br), 1.14-0.66 (m, 20H), 0.41 (s, 1H, br), 0.24 (s, 1H, br). ^{13}C NMR (126 MHz) $CDCl_3$ δ 156.5, 153.9, 153.8, 147.5, 147.1, 146.8, 146.6, 146.5, 146.4, 146.2, 146.0, 145.8, 145.7, 145.6, 145.5, 145.4, 144.9, 144.6, 143.4, 143.2, 142.9, 142.8, 142.5, 142.4, 142.3, 142.1, 142.0, 141.9, 140.4, 139.7, 139.0, 136.8, 136.1, 124.8, 120.4, 119.9, 85.8, 84.2, 70.3, 69.9, 69.3, 66.6, 55.3, 40.9, 40.3, 31.9, 30.0, 24.1, 22.8, 14.3. MS-MALDI$^+$ *m/z* 1294.2 (%) ([M+1]$^+$, 90), 573.2 (%) ([M-C_{60}]$^+$, 100).

231; Fc – F_2 – C_{60}

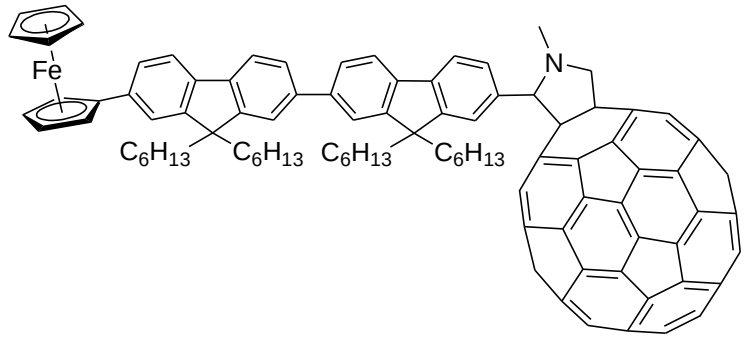

General procedure **B** was followed using fullerene-C_{60} (0.213 g), sarcosine (0.033 g) and compound (**227**) (0.065 mg, 0.0739 mmol). After refluxing for 7 h, the reaction was stopped. Purification using column chromatography (eluent: CS_2:hexane 8:2 *v*/*v*; then hexane:toluene 1:1 *v*/*v*) gave **231** as an amorphous black solid (80 mg, 67%). ^{1}H NMR (700 MHz) $CDCl_3$ δ 8.02 (s, 1H, br), 7.75 (dd, *J* = 14.5, 7.9 Hz, 3H), 7.61 (dd, *J* = 19.6, 13.0 Hz, 6H), 7.51–7.41 (m, 2H), 5.05 (d, *J* = 9.7 Hz, 2H), 4.74 (s, 2H), 4.42–4.28 (m, 3H), 4.04 (s, 5H), 2.89 (s, 3H), 2.31–1.94 (m, 8H, br), 1.24–0.56 (m, 40H), 0.41 (s, 2H, br), 0.26 (s, 2H, br). ^{13}C NMR (176 MHz) $CDCl_3$ δ 156.1, 154.1, 151.4, 151.1, 147.6, 147.3, 146.8, 146.5, 146.3, 146.2, 146.1, 145.9, 145.7, 145.6, 145.5, 145.2, 145.1, 144.9, 144.7, 144.4, 143.1, 143.0, 142.7, 142.6, 142.3, 142.2, 142.1, 142.0, 141.7, 140.3, 140.1, 140.0, 139.4, 138.9, 138.1, 137.1, 136.6, 135.8, 126.0, 124.6, 121.3, 120.4, 120.0, 119.5, 83.9, 69.7, 69.1, 69.0, 66.5, 55.0, 54.1, 40.5, 40.0, 31.5, 29.7, 23.8, 22.5, 14.0. MS-MALDI$^+$ *m/z* 1626.4 (%) ([M+1]$^+$, 25), 905.4 (%) ([M-C_{60}]$^+$, 100).

232; Fc – Ph – F – C_{60}

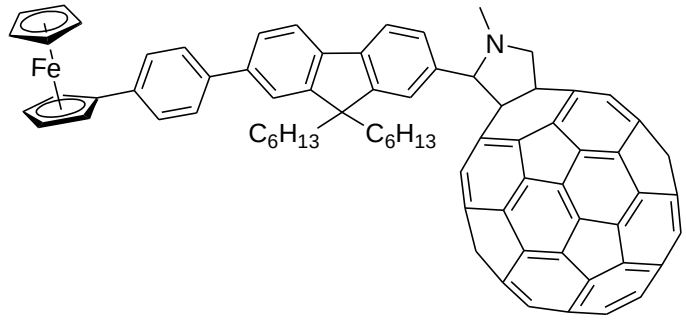

General procedure **B** was followed using fullerene-C_{60} (0.278 g), sarcosine (0.043 g) and compound (**228**) (0.060 g, 0.0964 mmol). After refluxing for 4.5 h, the reaction was stopped. Purification using column chromatography (eluent: CS_2; then hexane:toluene 1:1 *v*/*v*) gave **232** as an amorphous black solid (90 mg, 68%). ^{1}H NMR (700 MHz) $CDCl_3$ δ 8.00 (s, 1H, br), 7.73 (d, *J* = 7.9 Hz, 2H), 7.60-7.55 (m, 7H), 5.04 (d, *J* = 7.5 Hz, 2H), 4.70 (s, 2H), 4.40–4.26 (m, 3H), 4.08 (s, 5H), 2.88 (s, 3H), 2.21 (s, 1H, br), 2.04 (d, *J* = 52.1 Hz, 3H, br), 1.22–0.57 (m, 20H), 0.40 (s, 1H, br), 0.23 (s, 1H, br). ^{13}C NMR (176 MHz) $CDCl_3$ δ 156.2, 154.0, 153.6, 153.5, 151.5, 147.3, 146.8,

146.5, 146.3, 146.2, 146.1, 145.9, 145.7, 145.5, 145.3, 145.2, 145.1, 144.7, 144.4, 143.1, 143.0, 142.7, 142.5, 142.2, 142.1, 142.0, 141.9, 141.7, 140.2, 140.1, 139.8, 139.4, 138.9, 138.3, 136.6, 135.8, 126.9, 126.5, 125.6, 120.9, 120.0, 83.9, 70.1, 69.7, 67.9, 66.5, 55.3, 40.6, 40.0, 31.6, 29.7, 23.9, 22.6, 14.1, 14.0. MS-MALDI$^+$ *m/z* 1370.3 (%) ([M+1]$^+$, 10), 649.3 (%) ([M-C_{60}]$^+$, 100).

233; Fc – Ph – F_2 – C_{60}

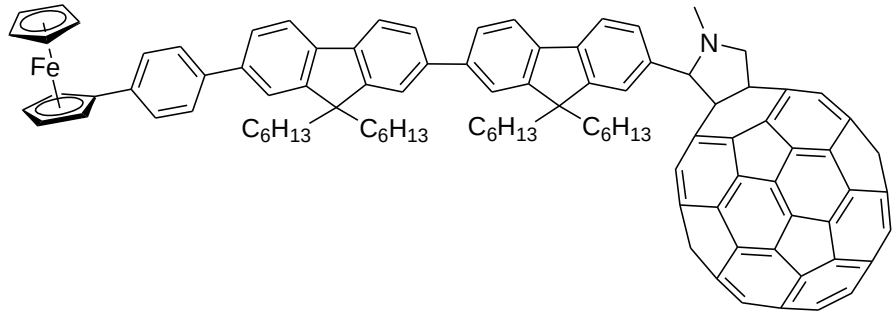

General procedure **B** was followed using fullerene-C_{60} (0.136 g), sarcosine (0.021 g) and compound (**229**) (0.045 g, 0.0471 mmol). After refluxing for 6 h, the reaction was stopped. Purification using column chromatography (eluent: CS_2; then hexane:toluene 1:1 *v*/*v*) gave **233** as an amorphous black solid (0.045 g, 56%). ^{1}H NMR (700 MHz) $CDCl_3$ δ 8.02 (s, 1H, br), 7.79-7.75 (m, 4H),7.68 (s, 1H, br), 7.67–7.59 (m, 9H), 7.52-7.45 (m, 1H, br), 5.05 (d, *J* = 10.2 Hz, 2H), 4.71 (s, 2H), 4.45 – 4.22 (m, 3H), 4.09 (s, 5H), 2.89 (s, 3H), 2.33–1.91 (m, 8H), 1.23–0.63 (m, 40H), 0.45 (s, 2H, br), 0.25 (s, 2H, br). ^{13}C NMR (176 MHz) $CDCl_3$ δ 156.2, 153.9, 153.6, 153.5, 151.7, 147.3, 146.5, 146.3, 146.2, 146.1, 145.9, 145.7, 145.5, 145.3, 145.2, 145.1, 144.4, 143.1, 142.5, 142.3, 142.1, 142.0, 141.9, 141.7, 140.4, 140.2, 139.9, 139.4, 139.0, 138.3, 136.6, 135.8, 127.0, 126.5, 126.1, 126.0, 125.6, 121.4, 121.3, 121.1, 120.0, 119.9, 83.9, 70.1, 69.6, 69.1, 69.0, 66.5, 55.2, 40.4, 40.0, 31.6, 31.4, 29.7, 23.8, 22.5, 14.1, 14.0. MS-MALDI$^+$ *m/z* 1702.5 (%) ([M+1]$^+$, 10), 981.5 (%) ([M-C_{60}]$^+$, 100).

235; Vinyl Ferrocene

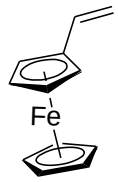

Methyl triphenylphosphonium bromide (1.836 g, 5.14 mmol) was dissolved in anhydrous THF (50 mL) under argon and cooled to 0 °C. ^{n}BuLi (2.5 M in hexanes, 2.1 mL, 5.14 mmol) was added dropwise and the mixture stirred for 30 min. A solution of ferrocenecarboxaldehyde (1.00 g, 4.72 mmol) in anhydrous THF (5 mL) was added and the mixture stirred for 18 h, gradually warming to room temperature. Water (150 mL) was added and the organic products

extracted into ethyl acetate. The organic layer was washed with brine and dried over magnesium sulfate. Removal of the solvent under vacuum gave the crude product. Purification by column chromatography (eluent: petroleum ether:ethyl acetate 4:1 *v*/*v*) gave **235** as a red/orange solid (0.710 g, 72%). ^{1}H NMR (400 MHz) $CDCl_3$ δ 6.45 (dd, *J* = 17.5, 10.7 Hz, 1H), 5.33 (d, *J* = 17.5, 1H), 5.02 (d, *J* = 10.7, 1H), 4.36 (s, 2H), 4.21 (s, 2H), 4.11 (s, 5H). Data consistent with the literature.[188]

236; Fc - C = C - F - CHO

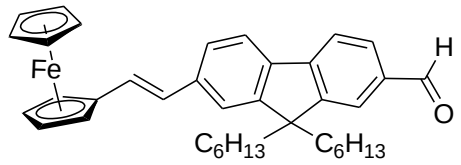

7-Bromo-9,9-dihexyl-9*H*-fluorene-2-carbaldehyde (**214**) (0.250 g, 0.566 mmol) was dissolved in anhydrous DMF (20 mL) under argon. Vinyl ferrocene (**235**) (0.144 g, 0.680 mmol), potassium carbonate (0.939 g, 6.792 mmol), tetra-*n*-butyl ammonium bromide (0.912 g, 2.83 mmol) and palladium(II)acetate (0.015 g, 0.068 mmol) were added and the mixture was heated at 95 °C for 36 h. Upon cooling the organic products were extracted into DCM, washed with brine, dried over magnesium sulfate and the solvent removed under vacuum. Purification by column chromatography (eluent: 10% ethyl acetate in petroleum ether) gave **236** as a viscous red oil (0.202 g, 62%). ^{1}H NMR (600 MHz) $CDCl_3$ δ 10.05 (s, 1H), 7.88 – 7.82 (m, 2H), 7.80 (d, *J* = 7.7 Hz, 1H), 7.72 (d, *J* = 7.9 Hz, 1H), 7.47 (dd, *J* = 7.9, 1.3 Hz, 1H), 7.39 (s, 1H), 6.97 (d, *J* = 16.1 Hz, 1H), 6.80 (d, *J* = 16.1 Hz, 1H), 4.50 (t, *J* = 1.8 Hz, 2H), 4.34 – 4.30 (m, 2H), 4.18 (s, 5H), 2.07 – 1.98 (m, 4H), 1.14 – 0.99 (m, 12H), 0.76 (t, *J* = 7.2 Hz, 6H), 0.69 – 0.54 (m, 4H). ^{13}C NMR (151 MHz) $CDCl_3$ δ 192.3, 152.8, 151.6, 147.4, 138.7, 138.3, 135.0, 130.6, 127.6, 126.3, 124.9, 123.0, 121.2, 120.3, 119.7, 83.3, 69.2, 66.9, 55.2, 40.2, 31.4, 29.6, 23.7, 22.5, 14.0. MS-ASAP^{+} *m/z* 572.3 (%) ([M]$^{+}$, 100). HRMS-ASAP^{+} *m/z* calculated for $C_{38}H_{45}{}^{54}FeO$: [M+H]$^{+}$ 571.2867, Found: 571.2840.

237; Fc - C = C - F_2 - CHO

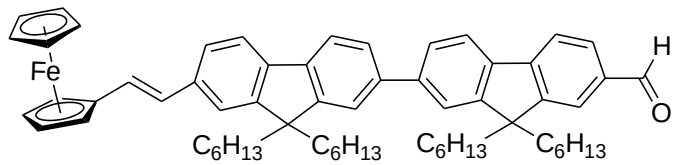

7-Bromo-9,9,9',9'-tetrahexyl-2,2'-bi(9*H*-fluorene)-7'-carbaldehyde (**216**) (0.250 g, 0.323 mmol) was dissolved in anhydrous DMF (20 mL) under argon. Vinyl ferrocene (**235**) (0.082 g, 0.388 mmol), potassium carbonate (0.536 g, 3.876 mmol), tetra-*n*-butyl ammonium bromide (0.521 g, 1.615 mmol) and palladium(II)acetate (0.009 g, 0.040 mmol) were added and the mixture

was heated at 95 °C for 24 h. Upon cooling, the organic products were extracted into DCM, washed with brine, dried over magnesium sulfate and the solvent removed under vacuum. Purification by column chromatography (eluent: petroleum ether:DCM 1:1 v/v) gave **237** as a viscous red oil (0.197 g, 67%). ^{1}H NMR (600 MHz) $CDCl_3$ δ 10.08 (s, 1H), 7.92 – 7.83 (m, 4H), 7.77 (d, *J* = 7.8 Hz, 1H), 7.72 – 7.67 (m, 2H), 7.66 – 7.62 (m, 2H), 7.61 (s, 1H), 7.46 (dd, *J* = 8.0, 1.1 Hz, 1H), 7.40 (s, 1H), 6.94 (d, *J* = 16.1 Hz, 1H), 6.82 (d, *J* = 16.1 Hz, 1H), 4.51 (t, *J* = 1.8 Hz, 2H), 4.34 – 4.28 (m, 2H), 4.18 (s, 5H), 2.14 – 2.01 (m, 8H), 1.18 – 0.99 (m, 24H), 0.81 – 0.60 (m, 20H). ^{13}C NMR (151 MHz) $CDCl_3$ δ 192.3, 152.9, 151.8, 151.7, 151.6, 147.3, 142.4, 140.6, 139.7, 139.6, 138.6, 137.0, 135.2, 130.6, 126.8, 126.4, 126.3, 126.2, 124.7, 123.1, 121.5, 121.5, 121.2, 120.2, 120.0, 119.9, 119.8, 83.7, 69.2, 69.0, 66.8, 55.4, 55.1, 40.3, 40.2, 31.4, 29.6, 29.5, 23.8, 22.5, 14.0, 13.9. MS-ASAP^{+} *m/z* 904.6 (%) ([M]$^{+}$, 100). HRMS-ASAP^{+} *m/z* calculated for $C_{63}H_{77}{}^{54}FeO$: [M+H]$^{+}$ 903.5371, Found: 903.5336.

238; Fc – C=C – F – C_{60}

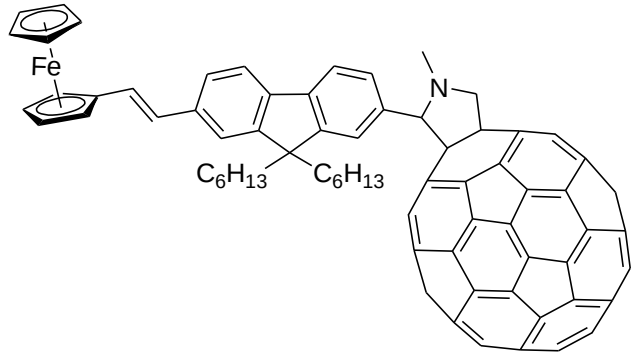

General procedure **B** was followed using fullerene-C_{60} (0.403 g), sarcosine (0.062 g) and compound (**236**) (0.080 mg, 0.140 mmol). After refluxing for 5.5 h, the reaction was stopped. Purification using column chromatography (eluent: CS_2; then hexane:toluene 1:1 *v*/*v*) gave **238** as an amorphous black solid (0.102 g, 55%). ^{1}H NMR (700 MHz) $CDCl_3$ δ 7.97 (s, 1H, br), 7.68 (s, 1H, br), 7.62 (d, *J* = 7.9 Hz, 1H), 7.56 (s, 1H, br), 7.40 (d, *J* = 7.9 Hz, 1H), 7.33 (s, 1H), 6.90 (d, *J* = 16.1 Hz, 1H), 6.77 (d, *J* = 16.1 Hz, 1H), 5.03 (d, *J* = 7.6 Hz, 2H), 4.47 (s, 2H), 4.34 – 4.27 (m, 3H), 4.16 (s, 5H), 2.87 (s, 3H), 2.04 – 1.97 (m, 4H, br), 1.17 – 0.67 (m, 20H, br), 0.37 (s, 1H, br), 0.21 (s, 1H, br). ^{13}C NMR (176 MHz) $CDCl_3$ δ 156.2, 154.0, 153.6, 151.5, 147.3, 146.8, 146.5, 146.3, 146.2, 146.1, 145.9, 145.7, 145.5, 145.3, 145.2, 145.1, 144.7, 144.4, 143.1, 143.0, 142.7, 142.5, 142.2, 142.1, 142.0, 141.9, 141.7, 141.5, 140.2, 140.1, 139.7, 139.4, 137.1, 136.6, 135.8, 126.8, 126.3, 124.7, 120.1, 119.9, 83.9, 83.7, 70.1, 69.2, 69.0, 66.8, 55.1, 40.0, 31.6, 29.7, 23.8, 22.6, 14.1, 14.0. MS-MALDI^{+} *m/z* 1320.4 (%) ([M+1]$^{+}$, 20), 599.2 (%) ([M-C_{60}]$^{+}$, 100).

239; Fc – C=C – F_2 – C_{60}

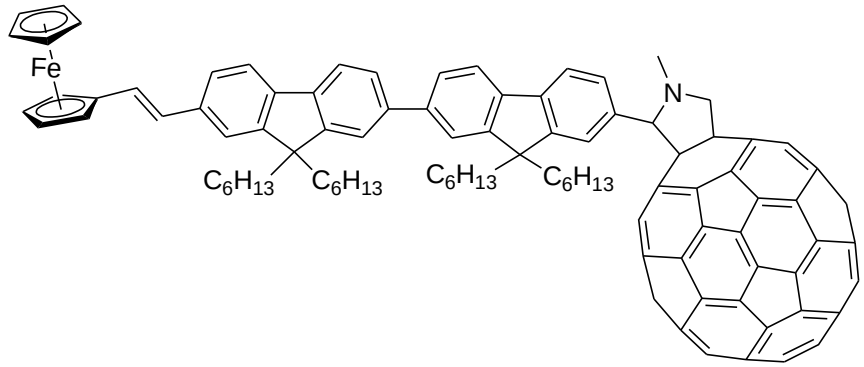

General procedure **B** was followed using fullerene-C_{60} (0.255 g), sarcosine (0.039 g) and compound (**237**) (0.080 mg, 0.088 mmol). After refluxing for 5.5 h, the reaction was stopped. Purification using column chromatography (eluent: CS_2; then hexane:toluene 1:1 *v*/*v*) gave **239** as an amorphous black solid (0.070 g, 48%). ^{1}H NMR (700 MHz) $CDCl_3$ δ 8.02 (s, 1H, br), 7.75 (dd, *J* = 12.2, 7.9 Hz, 3H), 7.67 (d, *J* = 7.9 Hz, 1H), 7.64 – 7.56 (m, 5H), 7.44 (d, *J* = 7.8 Hz, 1H), 7.38 (s, 1H), 6.92 (d, *J* = 16.1 Hz, 1H), 6.81 (d, *J* = 16.1 Hz, 1H), 5.05 (d, *J* = 10.6 Hz, 2H), 4.50 (s, 2H), 4.35 – 4.28 (m, 3H), 4.18 (s, 5H), 2.89 (s, 3H), 2.16 – 1.96 (m, 8H), 1.20 – 0.66 (m, 40H), 0.43 (s, 2H, br), 0.26 (s, 2H, br). ^{13}C NMR (176 MHz) $CDCl_3$ δ 155.2, 152.7, 152.5, 150.6, 146.3, 145.8, 145.5, 145.3, 145.2, 145.1, 144.9, 144.7, 144.6, 144.5, 144.4, 144.3, 144.2, 144.1, 143.7, 143.4, 142.1, 142.0, 141.7, 141.6, 141.3, 141.2, 141.1, 141.0, 140.9, 140.8, 140.7, 139.8, 139.2, 139.1, 138.9, 138.7, 138.4, 135.8, 135.6, 134.9, 134.8, 128.0, 127.2, 125.9, 125.2, 125.1, 125.0, 123.7, 120.4, 120.3, 119.2, 119.0, 118.9, 118.7, 82.9, 68.2, 68.0, 65.8, 54.1, 39.3, 39.0, 30.6, 30.4, 28.7, 22.8, 21.5, 13.1, 13.0. MS-MALDI$^+$ *m/z* 1652.5 (%) ([M+1]$^+$, 100), 931.6 (%) ([M-C_{60}]$^+$, 100).

7.5 Experimental Procedures for Chapter 5

General polymerisation procedure (Chapter 5): All monomer units were dissolved in toluene and the mixture stirred and degassed by bubbling through argon for 15 min. $PdCl_2[P(o\text{-}tol_3)]_2$ catalyst (~ 11 mg) was added and degassing was continued for 15 min. Degassed tetraethylammonium hydroxide solution (20%, ~ 3.5 mL) was added and the mixture was refluxed at 115 °C under argon for 20 h. Bromobenzene (0.1 mL, 0.950 mmol) was added and the mixture was refluxed for 1 h. Phenylboronic acid (0.100 g, 0.819 mmol) was added and the mixture was refluxed for an additional 1 h. Upon cooling to room temperature, the mixture was poured into methanol (250 mL) and stirred for 30 min to precipitate the crude polymer, which was filtered off and washed (methanol, then water). The crude solid was dissolved in a toluene (20 mL) and a solution of sodium diethyldithiocarbamic trihydrate (1 g in 10 mL water)

was added and the mixture was heated at 65 °C for 12 h. The organic layer was separated, washed (10% hydrochloric acid, sodium acetate solution and water), filtered through celite (eluting with toluene), concentrated under vacuum and then precipitated dropwise into vigorously stirred methanol (300 mL). After stirring in methanol for 30 min, the pure polymer was isolated by filtration.

PF8-S-y% co-polymers

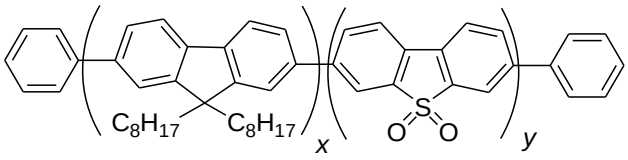

245; PF8-S-2%

The general polymerisation procedure from Chapter 5 was followed using the following quantities of reagents: 2,2'-(9,9-dioctyl-9*H*-fluorene-2,7-diyl)bis(4,4,5,5-tetramethyl-1,3,2-dioxaborolane) (**174**) (0.2000 g, 0.310 mmol), 2,7-dibromo-9,9-dioctyl-9*H*-fluorene (**107**) (0.1635 g, 0.298 mmol) and 3,7-dibromodibenzothiophene-*S*,*S*-dioxide (**87**) (0.0047 g, 0.012 mmol) in toluene (10 mL) with $PdCl_2[P(o\text{-}tol_3)]_2$ catalyst (0.0060 g) and tetraethylammonium hydroxide solution (20%, 3.0 mL). **245** was isolated by filtration as a pale yellow fluffy solid (0.173 g, 72%). ^{1}H NMR (700 MHz) $CDCl_3$ δ 7.85-7.83 (m), 7.71-7.68 (m), 2.13 (br, s), 1.22-1.15 (m), 0.83-0.81 (m). M_n = 57,214 Da, M_w = 219,715 Da.

247; PF8-S-8%

The general polymerisation procedure from Chapter 5 was followed using the following quantities of reagents: 2,2'-(9,9-dioctyl-9*H*-fluorene-2,7-diyl)bis(4,4,5,5-tetramethyl-1,3,2-dioxaborolane) (**174**) (0.2000 g, 0.310 mmol), 2,7-dibromo-9,9-dioctyl-9*H*-fluorene (**107**) (0.1431 g, 0.261 mmol) and 3,7-dibromodibenzothiophene-*S*,*S*-dioxide (**87**) (0.0187 g, 0.0499 mmol) in toluene (10 mL) with $PdCl_2[P(o\text{-}tol_3)]_2$ catalyst (0.0060 g) and tetraethylammonium hydroxide solution (20%, 3.0 mL). **247** isolated as a fluffy pale yellow solid (0.168 g, 72%). ^{1}H NMR (700 MHz) $CDCl_3$ δ 8.18 (s, br), 7.98-7.92 (m), 7.83-7.82 (m), 7.69-7.66 (m), 2.11 (s, br), 1.22-1.08 (m), 0.84-0.78 (m). M_n = 53,985 Da, M_w = 210,283 Da.

248; PF8-S-12%

The general polymerisation procedure from Chapter 5 was followed using the following quantities of reagents: 2,2'-(9,9-dioctyl-9*H*-fluorene-2,7-diyl)bis(4,4,5,5-tetramethyl-1,3,2-dioxaborolane) (**174**) (0.2000 g, 0.310 mmol), 2,7-dibromo-9,9-dioctyl-9*H*-fluorene (**107**)

(0.1294 g, 0.236 mmol) and 3,7-dibromodibenzothiophene-*S*,*S*-dioxide (**87**) (0.028 g, 0.075 mmol) in toluene (10 mL) with $PdCl_2[P(o\text{-}tol_3)]_2$ catalyst (0.0060 g) and tetraethylammonium hydroxide solution (20%, 3.0 mL). **248** isolated as a fluffy pale yellow solid (0.204 g, 89%). ^{1}H NMR (500 MHz) $CDCl_3$ δ 8.19 (s, br), 7.99-7.85 (m), 7.71-7.68 (m), 2.13 (s, br), 1.22-1.14 (m), 0.85-0.81 (m). M_n = 35,053 Da, M_w = 130,874 Da.

250; 3,7-Dibromodibenzothiophene

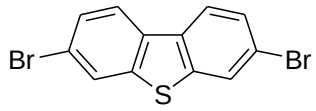

Compound (**87**) (1.00 g, 2.67 mmol) was suspended in anhydrous diethyl ether (40 mL) under argon. Lithium aluminium hydride (0.50 g, 13.35 mmol) was added in portions in order to maintain a moderate reflux. The mixture was then heated at reflux for 6 h, before water was added dropwise to destroy excess lithium aluminium hydride. More water (~ 80 mL) was then added and the mixture heated with stirring. The reaction was then acidified with conc. hydrochloric acid (5 mL). Upon cooling, the organic products were extracted into diethyl ether and washed with water. The solvent was removed under vacuum and the crude product recrystallised from chloroform to give **250** as white needles (0.305 g, 33%). ^{1}H NMR (400 MHz) $CDCl_3$ δ 7.96 (d, *J* = 1.8 Hz, 2H), 7.94 (d, *J* = 8.5 Hz, 2H), 7.55 (dd, *J* = 8.4, 1.8 Hz, 2H). Data consistent with the literature.[69]

PF8-DBT-y% co-polymers

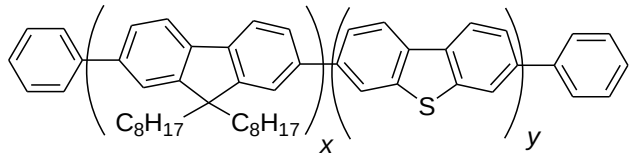

251; PF8-DBT-8%

The general polymerisation procedure from Chapter 5 was followed using the following quantities of reagents: 2,2'-(9,9-dioctyl-9*H*-fluorene-2,7-diyl)bis(4,4,5,5-tetramethyl-1,3,2-dioxaborolane) (**174**) (0.2000 g, 0.310 mmol), 2,7-dibromo-9,9-dioctyl-9*H*-fluorene (**107**) (0.1431 g, 0.2609 mmol) and 3,7-dibromodibenzothiophene (**250**) (0.0170 g, 0.0497 mmol) in toluene (10 mL) with $PdCl_2[P(o\text{-}tol_3)]_2$ catalyst (0.0060 g) and tetraethylammonium hydroxide solution (20%, 3.0 mL). **251** isolated as a fluffy pale yellow solid (0.195 g, 84%). ^{1}H NMR (500 MHz) $CDCl_3$ δ 8.30 (s, br), 8.20 (s, br), 7.86-7.84 (m), 7.72-7.68 (m), 2.13 (s, br), 1.22-1.15 (m), 0.87-0.81 (m). M_n = 47,252 Da, M_w = 157,429 Da.

252; PF8-DBT-12%

The general polymerisation procedure from Chapter 5 was followed using the following quantities of reagents: 2,2'-(9,9-dioctyl-9*H*-fluorene-2,7-diyl)bis(4,4,5,5-tetramethyl-1,3,2-dioxaborolane) (**174**) (0.2000 g, 0.310 mmol), 2,7-dibromo-9,9-dioctyl-9*H*-fluorene (**107**) (0.1294 g, 0.236 mmol) and 3,7-dibromodibenzothiophene (**250**) (0.0255 g, 0.075 mmol) in toluene (10 mL) with $PdCl_2[P(o\text{-}tol_3)]_2$ catalyst (0.0060 g) and tetraethylammonium hydroxide solution (20%, 3.0 mL). **252** isolated as a fluffy yellow solid (0.193 g, 85%). ^{1}H NMR (500 MHz) $CDCl_3$ δ 8.33-8.28 (m), 8.21 (br), 7.87-7.85 (m), 7.73-7.69 (m), 2.15 (s, br), 1.24-1.16 (m), 0.89-0.82 (m). M_n = 39,670 Da, M_w = 140,466 Da.

253; PF8-DBT-15%

The general polymerisation procedure from Chapter 5 was followed using the following quantities of reagents: 2,2'-(9,9-dioctyl-9*H*-fluorene-2,7-diyl)bis(4,4,5,5-tetramethyl-1,3,2-dioxaborolane) (**174**) (0.2000 g, 0.310 mmol), 2,7-dibromo-9,9-dioctyl-9*H*-fluorene (**107**) (0.1192 g, 0.2174 mmol) and 3,7-dibromodibenzothiophene (**250**) (0.0319 g, 0.0932 mmol) in toluene (10 mL) with $PdCl_2[P(o\text{-}tol_3)]_2$ catalyst (0.0060 g) and tetraethylammonium hydroxide solution (20%, 3.0 mL). **253** isolated as a fluffy yellow solid (0.185 g, 83%). ^{1}H NMR (500 MHz) $CDCl_3$ δ 8.29 (s, br), 8.19 (s, br), 7.85-7.82 (m), 7.71-7.66 (m), 2.13 (s, br), 1.22-1.15 (m), 0.85-0.80 (m). M_n = 54,633 Da, M_w = 180,795 Da.

254; PF8-DBT-20%

The general polymerisation procedure from Chapter 5 was followed using the following quantities of reagents: 2,2'-(9,9-dioctyl-9*H*-fluorene-2,7-diyl)bis(4,4,5,5-tetramethyl-1,3,2-dioxaborolane) (**174**) (0.1500 g, 0.2325 mmol), 2,7-dibromo-9,9-dioctyl-9*H*-fluorene (**107**) (0.0766 g, 0.1397 mmol) and 3,7-dibromodibenzothiophene (**250**) (0.0319 g, 0.0932 mmol) in toluene (8 mL) with $PdCl_2[P(o\text{-}tol_3)]_2$ catalyst (0.0050 g) and tetraethylammonium hydroxide solution (20%, 3.0 mL). **254** isolated as a fluffy yellow solid (0.138 g, 85%). ^{1}H NMR (500 MHz) $CDCl_3$ δ 8.29 (s, br), 8.20 (s, br), 7.87-7.68 (m), 2.13 (s, br), 1.22-1.10 (m), 0.86-0.80 (m). M_n = 52,953 Da, M_w = 158,464 Da.

PF8-keto-y% co-polymers

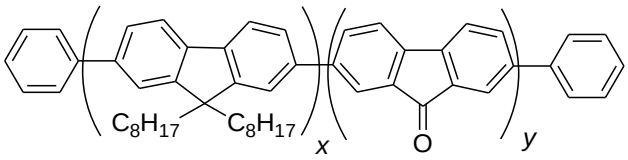

255; PF8-keto-0.05%

The general polymerisation procedure from Chapter 5 was followed using the following quantities of reagents: 2,2'-(9,9-dioctyl-9*H*-fluorene-2,7-diyl)bis(4,4,5,5-tetramethyl-1,3,2-dioxaborolane) (**174**) (0.400 g, 0.619 mmol), 2,7-dibromo-9,9-dioctyl-9*H*-fluorene (**107**) (0.3403 g, 0.6204 mmol), 2,7-dibromo-9*H*-fluoren-9-one (**29**) (0.000211 g, 0.000623 mmol) in toluene (12 mL). **255** was isolated by filtration as a pale yellow fluffy solid (0.423 g, 88%). ^{1}H NMR (700 MHz) $CDCl_3$ δ 7.83-7.82 (m), 7.70-7.65 (m), 2.11 (s, br), 1.22-10 (m), 0.82-0.78 (m). M_n = 41,904 Da, M_w = 162,504 Da.

257; PF8-keto-0.2%

The general polymerisation procedure from Chapter 5 was followed using the following quantities of reagents: 2,2'-(9,9-dioctyl-9*H*-fluorene-2,7-diyl)bis(4,4,5,5-tetramethyl-1,3,2-dioxaborolane) (**174**) (0.400 g, 0.619 mmol), 2,7-dibromo-9,9-dioctyl-9*H*-fluorene (**107**) (0.3393 g, 0.6186 mmol), 2,7-dibromo-9*H*-fluoren-9-one (**29**) (0.000843 g, 0.00249 mmol) in toluene (12 mL). **257** was isolated by filtration as a pale yellow fluffy solid (0.401 g, 83%). ^{1}H NMR (500 MHz) $CDCl_3$ δ 7.85-7.81 (m), 7.70-7.65 (m), 2.12 (s, br), 1.21-1.12 (m), 0.81-0.78 (m). M_n = 28,302 Da, M_w = 152,157 Da.

258; PF8-keto-0.5%

The general polymerisation procedure from Chapter 5 was followed using the following quantities of reagents: 2,2'-(9,9-dioctyl-9*H*-fluorene-2,7-diyl)bis(4,4,5,5-tetramethyl-1,3,2-dioxaborolane) (**174**) (0.400 g, 0.619 mmol), 2,7-dibromo-9,9-dioctyl-9*H*-fluorene (**107**) (0.3372 g, 0.615 mmol) 2,7-dibromo-9*H*-fluoren-9-one (**29**) (0.00211 g, 0.00623 mmol) in toluene (12 mL). **258** was isolated by filtration as a bright yellow fluffy solid (0.388 g, 81%). ^{1}H NMR (700 MHz) $CDCl_3$ δ 7.84-7.82 (m), 7.70-7.65 (m), 2.11 (s, br), 1.21-1.11 (m), 0.85-0.78 (m). M_n = 38,085 Da, M_w = 166,445 Da.

259; PF8-keto-1.0%

The general polymerisation procedure from Chapter 5 was followed using the following quantities of reagents: 2,2'-(9,9-dioctyl-9*H*-fluorene-2,7-diyl)bis(4,4,5,5-tetramethyl-1,3,2-dioxaborolane) (**174**) (0.400 g, 0.619 mmol), 2,7-dibromo-9,9-dioctyl-9*H*-fluorene (**107**) (0.3338 g, 0.609 mmol) 2,7-dibromo-9*H*-fluoren-9-one (**29**) (0.00421 g, 0.0125 mmol) in toluene (12 mL). **259** was isolated by filtration as a bright yellow fluffy solid (0.385 g, 80%). ^{1}H NMR (700 MHz) $CDCl_3$ δ 7.84-7.82 (m), 7.71-7.66 (m), 2.12 (s, br), 1.23-1.10 (m), 0.86-0.80 (m). M_n = 47,896 Da, M_w = 164,664 Da.

260; PF8-keto-1.5%

The general polymerisation procedure from Chapter 5 was followed using the following quantities of reagents: 2,2'-(9,9-dioctyl-9*H*-fluorene-2,7-diyl)bis(4,4,5,5-tetramethyl-1,3,2-dioxaborolane) (**174**) (0.400 g, 0.619 mmol), 2,7-dibromo-9,9-dioctyl-9*H*-fluorene (**107**) (0.3304 g, 0.602 mmol) 2,7-dibromo-9*H*-fluoren-9-one (**29**) (0.00632 g, 0.0187 mmol) in toluene (12 mL). **260** was isolated by filtration as a dark yellow fluffy solid (0.386 g, 81%).^{1}H NMR (700 MHz) $CDCl_3$ δ 7.86-7.84 (m), 7.72-7.66 (m), 2.14 (s, br), 1.22-1.15 (m), 0.85-0.80 (m). M_n = 42,463 Da, M_w = 143,047 Da.

261; PF8-keto-2.0%

The general polymerisation procedure from Chapter 5 was followed using the following quantities of reagents: 2,2'-(9,9-dioctyl-9*H*-fluorene-2,7-diyl)bis(4,4,5,5-tetramethyl-1,3,2-dioxaborolane) (**174**) (0.400 g, 0.619 mmol), 2,7-dibromo-9,9-dioctyl-9*H*-fluorene (**107**) (0.3270 g, 0.596 mmol) 2,7-dibromo-9*H*-fluoren-9-one (**29**) (0.00843 g, 0.0249 mmol) in toluene (12 mL). **261** was isolated by filtration as a light orange fluffy solid (0.401 g, 84%). ^{1}H NMR (700 MHz) $CDCl_3$ δ 7.86-7.84 (m), 7.71-7.68 (m), 2.13 (s, br), 1.22-1.15 (m), 0.85-0.81 (m). M_n = 51,991 Da, M_w = 220,695 Da.

7.6 Experimental Procedures for Chapter 6

268; 3,6-Dibromophenanthrene-9,10-dione

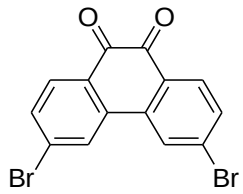

Phenanthrenequinone (12.89 g, 61.88 mmol), *tert*-butyl peroxide (0.50 mL) and bromine (9.5 mL, 185.64 mmol) were dissolved in nitrobenzene (100 mL). The mixture was heated at 110 °C and irradiated with a tungsten lamp for 1 h. After cooling to room temperature, the precipitate was isolated by filtration and washed extensively with hexane to give **268** as an orange solid (18.20 g, 80%).^{1}H NMR (400 MHz) $CDCl_3$ δ 8.14 (d, *J* = 1.6 Hz, 2H), 8.10 (d, *J* = 12 Hz, 2H), 7.69 (dd, *J* = 1.6 Hz, *J* = 8.0 Hz, 2H). ^{13}C NMR (126 MHz) $CDCl_3$ δ 178.9, 135.9, 133.4, 132.1, 129.9, 127.4. MS-ES^{+} *m/z* (%) 389.2 ([M+Na]$^{+}$, 100). Data consistent with the literature.[173]

269; 3,6-Dibromo-9*H*-fluoren-9-one

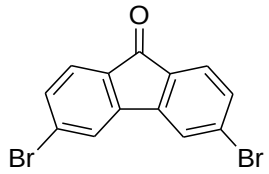

3,6-Dibromophenanthrene-9,10-dione (**268**) (5.00 g, 13.67 mmol) was gradually added to a solution of potassium hydroxide (21.50 g, 380 mmol) in water (200 mL) at 85 °C. The mixture was stirred at this temperature for 12 h. Powdered potassium permanganate (11.15 g, 71.15 mmol) was then added over 30 min. After complete addition, the reaction was heated at reflux for 2 h. On cooling to room temperature the mixture was diluted with water (200 mL) and the dark green solid filtered off. The crude product was then suspended in water (250 mL) and boiled with enough sodium bisulfite to remove the dark colour of the solution. On cooling to room temperature the crude product was isolated by filtration as an amorphous yellow powder. Soxlet extraction in toluene gave **269** as yellow flakes (3.71 g, 80%).[1]H NMR (400 MHz) $CDCl_3$ δ 7.70 (d, *J* = 4.0 Hz, 2H), 7.57 (dd, *J* = 1.6 Hz, *J* = 8.0 Hz, 2H), 7.52 (dd, *J* = 1.6 Hz, *J* = 8.0 Hz, 2H). Data consistent with the literature.[173]

270; 3,6-Dibromo-9*H*-fluorene

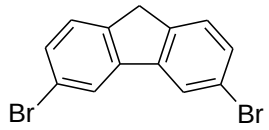

3,6-Dibromo-9*H*-fluoren-9-one (**269**) (2.00 g, 5.92 mmol) was suspended in a glycerol/ethylene glycol mix (50 mL 1:1 *v*/*v*) Hydrazine monohydrate (1.72 mL, 35.6 mmol) was added and the mixture heated at 80 °C for 12 h. The mixture was then refluxed at 160 °C for 2 h. After cooling to 60 °C, an aqueous solution of potassium hydroxide (2.00 g, 35.6 mmol) in water (20 mL) was added and the mixture heated at 110 °C for 2 h. The product was precipitated by addition of water (150 mL), filtered and washed (water and methanol) to give **270** as a yellow/orange solid (1.25 g, 65%), no further purification was necessary. [1]H NMR (400 MHz) $CDCl_3$ δ 7.88 (s, 2H), 7.45-7.41 (m, 4H), 3.81 (s, 2H).[13]C NMR (100 MHz) $CDCl_3$ δ 142.6, 142.2, 130.2, 126.5, 123.4, 121.0, 36.3. Data consistent with the literature.[173]

278; 3,6-Dibromo-9,9-dioctyl-9*H*-fluorene

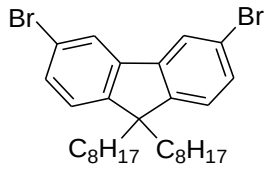

3,6-Dibromo-9*H*-fluorene (**270**) (5.53 g, 17.08 mmol), tetra-*n*-butylammonium bromide (1.01 g, 3.42 mmol), aqueous sodium hydroxide (12.5 M; 20 g in 40 mL water) and bromooctane (18 mL, 102.48 mmol) were heated at 95 °C for 18 h. Water (100 mL) was added to the cloudy yellow solution and the organic layer extracted into DCM. The combined organic layers were washed with water until neutral pH, dried over magnesium sulfate and the solvent removed under vacuum to give the crude product. Purification by column chromatography (eluent: petroleum ether) followed by recrystallisation from ethanol gave **278** as a white crystalline solid (5.90 g, 63%). ^{1}H NMR (400 MHz) $CDCl_3$ δ 7.75 (s, 2H), 7.41 (d, *J* = 8.0 Hz, 2H), 7.17 (d, *J* = 8.0 Hz, 2H), 1.91-1.87 (m, 4H), 1.18-1.00 (m, 20H), 0.80 (t, *J* = 8.0 Hz, 6H), 0.56-0.52 (m, 4H). ^{13}C NMR (100 MHz) $CDCl_3$ δ 149.7, 141.9, 130.5, 124.4, 123.2, 120.8, 55.0, 40.0, 31.7, 29.9, 29.2, 28.7, 33.7, 22.6, 14.0. MS-ASAP^{+} *m/z* (%) 548.2 ([M]$^{+}$, 100). HRMS-ASAP^{+} *m/z* calculated for $C_{29}H_{40}O_4Br_2$: [M]$^{+}$ 546.1497, Found: 546.1523. Mpt. 40.8-41.1 °C.

281; 2,2'-(9,9-Dihexyl-9*H*-fluorene-2,7-diyl)bis(4,4,5,5-tetramethyl-1,3,2-dioxaborolane)

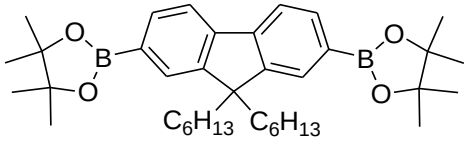

2,7-Dibromo-9,9-dihexyl-9*H*-fluorene (**213**) (2.80 g, 5.69 mmol) was dissolved in anhydrous THF (100 mL) under argon and cooled to - 78 °C. ^{n}BuLi (2.5 M in hexanes, 5.23 mL, 2.3 equiv.) was added dropwise and the solution stirred at - 78 °C for 2 h. Triisopropylborate (3.11 mL, 13.54 mmol) was added in portions and the mixture warmed to room temperature over 3 h. Water (80 mL) was added and the mixture stirred overnight. The THF was removed under vacuum, then water (10 mL) and conc. hydrochloric acid (20 mL) were added to precipitate the boronic acid. The solid was extracted into diethylether and washed until neutral. The diethylether was removed under reduced pressure to give a light pink slurry which was then dissolved in acetone and added dropwise to a mixture of water (40 mL) and conc. hydrochloric acid (20 mL) to precipitate a pink/white solid which was isolated by filtration and washed with water. The solid was combined with pinacol (1.546 g, 13.08 mmol) and toluene (150 mL) and refluxed with a Dean-Stark apparatus at 115 °C for 18 h. The toluene was removed under reduced pressure to give the crude product which was recrystallised multiple times from acetonitrile to give **281** as white crystals (1.071 g, 10%). ^{1}H NMR (400 MHz) $CDCl_3$ δ 7.78 (dd, *J* = 1.0, 7.5 Hz, 2H), 7.74-7.67 (m, 4H), 2.00-1.96 (m, 4H), 1.25 (s, 24H), 1.09-0.91 (m, 12H), 0.72 (t, *J* = 7.1 Hz, 6H), 0.56-0.48 (m, 4H). Data consistent with the literature.[189]

283; 2,2'-(9,9-Dihexyl-9*H*-fluorene-3,6-diyl)bis(4,4,5,5-tetramethyl-1,3,2-dioxaborolane)

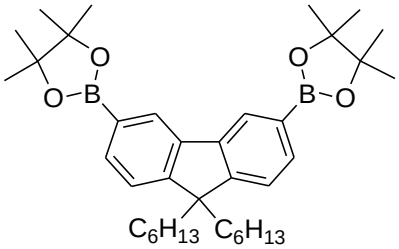

3,6-Dibromo-9,9-dihexyl-9*H*-fluorene (**194**) (1.00 g, 2.031 mmol) was dissolved in anhydrous THF (240 mL) under argon and the solution cooled to - 78 °C. ^{n}BuLi (2.5 M in hexanes, 3.74 mL, 4.6 equiv.) was added dropwise and the mixture stirred at - 78 °C for 2 h. 2-Isopropoxy-4,4,5,5-tetramethyl-1,3,2-dioxaborolane (2.07 mL, 10.16 mmol) was added in portions and the mixture stirred for 2 h at - 78 °C before warming to room temperature overnight. The reaction was quenched by the addition of brine (100 mL) and the organics extracted into DCM. The DCM was removed under vacuum to give the crude product as a colourless oil. Recrystallisation from acetonitrile gave **283** as white crystals (0.596 g, 50%).[1]H NMR (400 MHz) $CDCl_3$ δ 8.21 (s, 2H), 7.73 (d, J = 8.0 Hz, 2H), 7.32 (d, J = 8.0 Hz, 2H), 1.95-1.91 (m, 4H), 1.28 (s, 24H), 1.09-0.91 (m, 12H), 0.72 (t, *J* = 7.1 Hz, 6H), 0.57-0.50 (m, 4H). Data consistent with the literature.[174]

284; "Fully bent" PF6

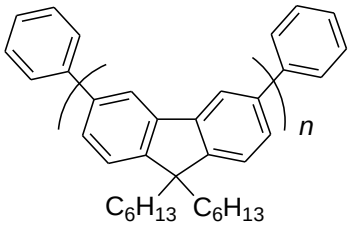

Compound **283** (0.190 g, 0.324 mmol) and compound **194** (0.1624 g, 0.321 mmol) were dissolved in toluene (5 mL). The mixture was stirred and degassed by bubbling through argon for 15 min. $PdCl_2[P(o\text{-}tol_3)]_2$ (0.003 g, 1 mol%) and $P(o\text{-}tol)_3$ (0.006 g, 5 mol%) were added and degassing was continued for 15 min. Degassed tetraethylammonium hydroxide solution (20%, 3 mL) was added and the mixture was refluxed at 115 °C under argon for 20 h. Bromobenzene (0.1 mL, 0.950 mmol) was added and the mixture was refluxed for 1 h. Phenylboronic acid (0.100 g, 0.819 mmol) was added and the mixture was refluxed for an additional 1 h. Upon cooling to room temperature, the mixture was poured into methanol (250 mL) and stirred for 30 min to precipitate the crude polymer as a white/grey solid, which was filtered off and washed (methanol, then water). The crude solid was dissolved in a toluene (20 mL) and a solution of sodium diethyldithiocarbamic trihydrate (1 g in 10 mL water) was added and the mixture was heated at 65 °C for 12 h. The organic layer was separated, washed (10%

hydrochloric acid, sodium acetate solution and water), filtered through celite (eluting with toluene), concentrated under vacuum and precipitated dropwise into vigorously stirred methanol (300 mL). After stirring in methanol for 30 min, **284** was isolated by filtration as a white solid (0.118 g, 55%).[1]H NMR (500 MHz) $CDCl_3$ δ 8.32 (s, br), 8.14 (s, br), 7.73-7.67 (m), 7.48-7.45 (m), 2.09-2.04 (m), 1.16-1.07 (m), 0.80-0.75 (m). [13]C NMR (126 MHz) $CDCl_3$ δ 150.3, 140.6, 126.7, 123.3, 119.0, 118.8, 55.0, 40.9, 30.0, 22.8, 14.3. M_n = 4,963 Da, M_w = 14,852 Da. Data consistent with the literature.[174]

285; "Partly bent" PF6

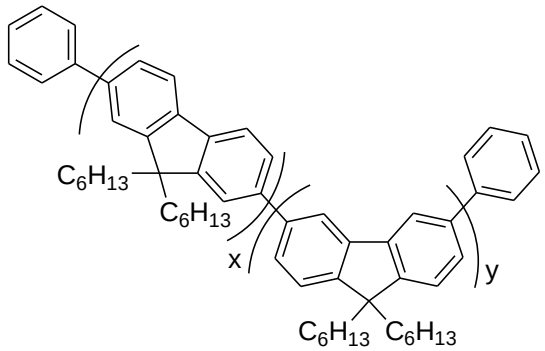

x:y 1:1

Synthesised according to the procedure for polymer **284** using the following quantities: Compound **281** (0.400 g, 0.638 mmol) and compound **194** (0.323 g, 0.656 mmol) in toluene (20 mL) with $PdCl_2[P(o\text{-}tol_3)]_2$ (0.005 g, 1 mol%), $P(o\text{-}tol)_3$ (0.010 g, 5 mol%) and tetraethylammonium hydroxide solution (20%, 5 mL). **285** was isolated by filtration as a white solid (330 mg, 77%). [1]H NMR (400 MHz) $CDCl_3$ δ 8.10 (s, br), 7.83-7.63 (m), 7.47-7.44 (m). [13]C NMR (126 MHz) $CDCl_3$ δ 151.9, 150.4, 141.8, 140.8, 140.6, 140.3, 126.8, 126.4, 123.4, 121.7, 120.2, 118.9, 55.6, 55.0, 40.9, 31.8, 30.0, 24.2, 22.9, 14.3. M_n = 12,515 Da, M_w = 27,084 Da. Data consistent with the literature.[174]

286; "Partly bent" PF8

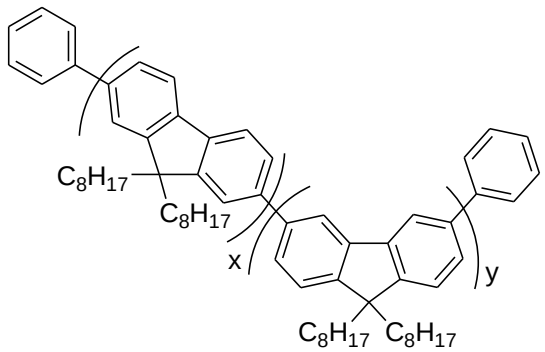

x:y 1:1

Synthesised according to the procedure for polymer **284** using the following quantities: Compound **278** (0.3397 g, 0.619 mmol), compound **174** (0.400 g, 0.619 mmol) in toluene (12 mL) with $PdCl_2[P(o\text{-}tol_3)]_2$ (0.011 g, 2 mol%), $P(o\text{-}tol)_3$ (0.009 g, 5 mol%) and tetraethylammonium hydroxide solution (20%, 3.5 mL). **286** was isolated by filtration as a white solid (0.386 g, 80%). ^{1}H NMR (500 MHz) $CDCl_3$ δ 8.10 (s, br), 7.83-7.64 (m), 7.46-7.43 (m), 2.11-2.03 (m), 1.20-1.07 (m), 0.82-0.73 (m). ^{13}C NMR (126 MHz) $CDCl_3$ δ 151.9, 150.4, 141.8, 140.7, 140.6, 140.3, 126.7, 126.4, 123.3, 120.3, 120.2, 118.7, 55.6, 55.0, 40.9, 40.7, 32.0, 29.5, 24.3, 24.2, 24.1, 22.9, 22.8, 14.3. M_n = 13,422 Da, M_w = 39,407 Da.

306; 2-Bromo-9,9-dioctyl-9*H*-fluorene

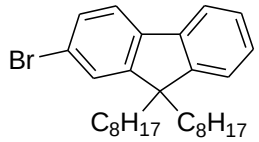

2-Bromofluorene (3.00 g, 12.24 mmol), tetra-*n*-butylammonium bromide (0.789 g, 2.45 mmol), aqueous sodium hydroxide (12.5 M; 12.00 g in 24 mL water) and bromooctane (12.7 mL, 73.44 mmol) were heated at 95 °C for 18 h. Water (100 mL) was added and the organic layer extracted into DCM. The combined organic layers were washed with water until neutral pH, dried over magnesium sulfate and the solvent removed under vacuum to give the crude product as a yellow oil. Purification by column chromatography (eluent: petroleum ether) gave **306** as a colourless oil (5.17 g, 90%).^{1}H NMR (400 MHz) $CDCl_3$ δ 7.67-7.60 (m, 1H), 7.53 (dd, *J* = 1.5, 7.3 Hz, 1H), 7.42 (dd, *J* = 1.6, 7.4 Hz, 2H), 7.33-7.27 (m, 3H), 1.98-1.80 (m, 4H), 1.22-0.99 (m, 20H), 0.80 (t, *J* = 7.1 Hz, 6H), 0.66-0.48 (m, 4H). Data consistent with the literature.[190]

287; 9,9-Dioctyl-9*H*-fluoren-2-ylboronic acid

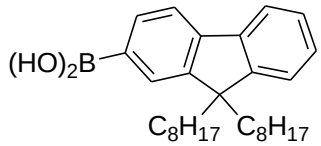

2-Bromo-9,9-dioctyl-9*H*-fluorene (**306**) (2.58 g, 5.510 mmol) was dissolved in anhydrous THF (140 mL) under argon at - 78 °C. ^{n}BuLi (2.5 M in hexanes, 2.87 mL, 1.3 equiv.) was added dropwise and the mixture stirred at this temperature for 1 h. Triisopropyl borate (2.53 mL, 11.02 mmol) was added dropwise and the mixture was stirred at - 78 °C for 1 h. After warming to - 20 °C, the reaction mixture was quenched by the addition of a saturated solution of ammonium chloride and stirred overnight whilst warming to room temperature. The organic layer was extracted into DCM, washed with brine, dried over magnesium sulfate and the

solvent removed under vacuum to give the crude product. Purification by column chromatography (eluent: petroleum ether:DCM 1:1 *v*/*v*) gave **287** as a white sticky solid (1.39 g, 58%).[1]H NMR (400 MHz) $CDCl_3$ δ 8.30 (d, *J* = 8.0 Hz, 1H), 8.21 (s, 1H), 7.88 (d, *J* = 8.0 Hz, 1H), 7.82-7.80 (m, 1H), 7.41-7.37 (m, 3H), 2.13-2.03 (m, 4H), 1.13-0.97 (m, 20H), 0.76 (t, *J* = 8.0 Hz, 6H), 0.69-0.66 (m, 4H). Data consistent with the literature.[191]

288; 6'-(9,9-Dioctyl-9*H*-fluoren-2-yl)-9,9,9',9'-tetraoctyl-2,3'-bi(9*H*-fluorene)

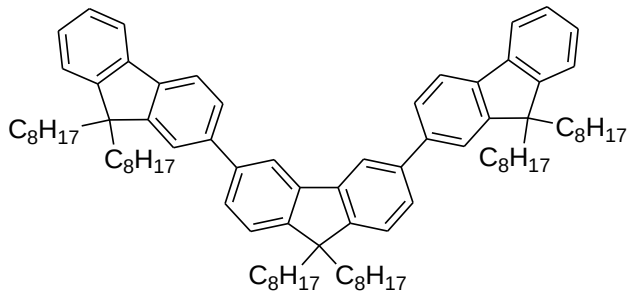

3,6-Dibromo-9,9-dioctyl-9*H*-fluorene (**278**) (0.200 g, 0.365 mmol), and 9,9-dioctyl-9*H*-fluoren-2-ylboronic acid (**287**) (0.396 g, 0.9117 mmol) were suspended in 1,4-dioxane (20 mL) and the solution degassed. $Pd(PPh_3)_2Cl_2$ (0.013 g, 5 mol%,) was added and the solution degassed further. Degassed sodium carbonate solution (1M, 5 mL) was added and the mixture heated at 85 °C for 18 h under argon. The organic product was extracted into DCM, washed with brine and dried over magnesium sulfate. The crude product was purified by column chromatography (eluent: DCM) to give **288** as a viscous colourless oil (0.221 g, 52%). ^{1}H NMR (400 MHz) $CDCl_3$ δ 8.07 (d, *J* = 1.4 Hz, 2H), 7.80-7.57 (m, 10H), 7.43 (d, *J* = 7.8 Hz, 2H), 7.36-7.27 (m, 6H), 2.08-1.94 (m, 12H), 1.24-0.99 (m, 60H), 0.84-0.59 (m, 30H). ^{13}C NMR (126 MHz) $CDCl_3$ δ 151.4, 150.9, 150.1, 141.5, 140.9, 140.5, 140.4, 140.2, 126.9, 126.7, 126.4, 126.0, 123.1, 122.8, 121.4, 119.6, 118.3, 55.2, 54.7, 40.4, 31.8, 30.0, 29.2, 24.0, 23.8, 22.6, 14.0. MS-ASAP$^+$ *m/z* (%) 1168.0 ($[M+H]^+$). HRMS-ASAP$^+$ *m/z* calculated for $C_{87}H_{122}$ $[M]^+$ 1166.9547 Found: 1166.9524.

289; "Fully bent" PF8

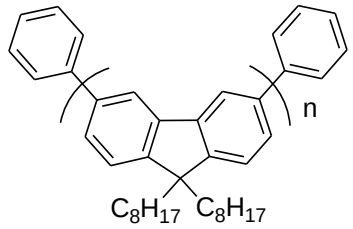

$Ni(COD)_2$ (0.166 g, 0.60 mmol) and 2,2'-bipyridyl (0.094 g, 0.60 mmol) were dissolved in anhydrous, degassed DMF (2.5 mL) with stirring under nitrogen. Degassed COD (0.074 mL, 0.60 mmol) was added to this and the resultant purple solution stirred at 75 °C for 1 h. Compound

(**278**) (0.300 g, 0.55 mmol) was dissolved in anhydrous, degassed toluene (4 mL) under nitrogen in a separate flask, added to the catalyst solution and heated at 75 °C for 24 h. Bromobenzene (0.1 mL) was added and the mixture stirred at this temperature for an additional 12 h. Upon cooling to room temperature the reaction mixture was poured into a stirred solvent mix of methanol:acetone:*conc*.hydrochloric acid 1:1:1 *v*/*v*. A small amount of light brown solid was isolated by filtration and determined to be **289** (0.055 g, 26%). ^{1}H NMR (400 MHz) $CDCl_3$ δ 8.10-8.08 (m), 7.98-7.89 (m), 7.68-7.61 (m), 7.45-7.38 (m), 2.05-1.93 (m), 1.19-1.04 (m), 0.81-0.77 (m), 0.72-0.62 (m). ^{13}C NMR (700 MHz) $CDCl_3$ δ 150.2, 149.9, 143.3, 140.5, 140.4, 129.8, 126.3, 123.0, 118.7, 118.5, 54.9, 40.2, 31.8, 31.7, 29.3, 29.2, 23.8, 22.6, 14.0. M_n = 45,391 Da, M_w = 87,367 Da.

290; p[F-(2,8)S]

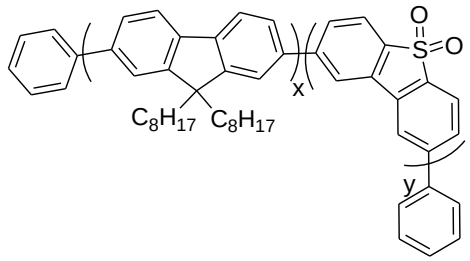

x = 85%, y = 15%

2,8-Dibromodibenzothiophene-*S*,*S*-dioxde (**89**) (0.0965 g, 0.186 mmol), 2,2'-(9,9-dioctyl-9*H*-fluorene-2,7-diyl)bis(4,4,5,5-tetramethyl-1,3,2-dioxaborolane) (**174**) (0.400 g, 0.619 mmol), and 2,7-dibromo-9,9-dioctyl-9*H*-fluorene (**107**) (0.2384 g, 0.434 mmol) were dissolved in toluene (15 mL) and the mixture stirred and degassed by bubbling through argon for 15 min. $PdCl_2[P(o\text{-}tol_3)]_2$ catalyst (~ 11 mg) was added and degassing was continued for 15 min. Degassed tetraethylammonium hydroxide solution (20%, ~3.5 mL) was added and the mixture was refluxed at 115 °C under argon for 20 h. Bromobenzene (0.1 mL, 0.950 mmol) was added and the mixture was refluxed for 1 h. Phenylboronic acid (0.100 g, 0.819 mmol) was added and the mixture was refluxed for an additional 1 h. Upon cooling to room temperature, the mixture was poured into methanol (250 mL) and stirred for 30 min to precipitate the crude polymer, which was filtered off and washed (methanol, then water). The crude solid was dissolved in a toluene (20 mL) and a solution of sodium diethyldithiocarbamic trihydrate (1 g in 10 mL water) was added and the mixture was heated at 65 °C for 12 h. The organic layer was separated, washed (10% hydrochloric acid, sodium acetate solution and water), filtered through celite (eluting with toluene), concentrated under vacuum and then precipitated dropwise into vigorously stirred methanol (300 mL). After stirring in methanol for 30 min, polymer **290** was isolated by filtration as a fluffy pale yellow solid (0.265 g, 59%). ^{1}H NMR (700

MHz) $CDCl_3$ δ 8.16 (s, br), 7.97-7.81 (m), 7.69-7.63 (m), 2.11 (s, br), 1.20-1.08 (m), 0.83-0.76 (m). M_n = 22,421 Da, M_w = 67,690 Da.

297; 9-Octyl-9*H*-carbazole

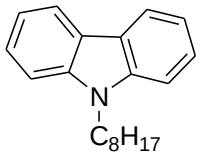

Carbazole (5.00 g, 29.90 mmol) and tetra-*n*-butyl ammonium bromide (1.93 g, 5.98 mmol) were suspended in toluene (50 mL) under argon and aqueous sodium hydroxide (18.0 g in 20 mL water) was added. Bromooctane (6.2 mL, 35.88 mmol) was added dropwise and the mixture heated at reflux for 18 h. Upon cooling, the organic products were extracted into toluene, washed with water and dried over magnesium sulfate. After removal of the solvent under vacuum, purification by column chromatography (eluent: petroleum ether:DCM 7:3 *v*/*v*) gave **297** as a colourless oil (7.69 g, 92%).^{1}H NMR (400 MHz) $CDCl_3$ δ 8.14 (d, *J* = 7.8 Hz, 2H), 7.55 – 7.40 (m, 4H), 7.26 (dd, *J* = 11.5, 4.4 Hz, 2H), 4.33 (t, *J* = 7.2 Hz, 2H), 1.97 – 1.80 (m, 2H), 1.50 – 1.18 (m, 10H), 0.90 (dd, *J* = 7.0, 5.7 Hz, 3H). Data consistent with the literature.[106]

298; 9-Octyl-3-(9-octyl-9*H*-carbazol-6-yl)-9*H*-carbazole

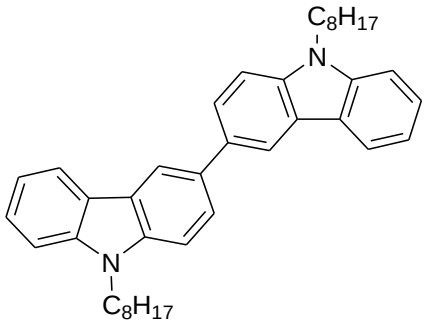

9-Octyl-9*H*-carbazole (**297**) (3.84 g, 13.7 mmol) was dissolved in chloroform (50 mL) under argon. Iron(III)chloride (4.46 g, 27.5 mmol) was then added in one portion and the mixture stirred at room temperature for 18 h. Water (50 mL) was added and the organic product extracted into chloroform, washed with water and dried over magnesium sulfate. The solvent was removed under vacuum and purification by column chromatography (eluent: petroleum ether:DCM 8:2 *v*/*v*) followed by recrystallisation from hexane gave **298** as a white crystalline solid (2.204 g, 58%).^{1}H NMR (400 MHz) $CDCl_3$ δ 8.41 (s, 2H), 8.20 (d, *J* = 7.6 Hz, 2H), 7.84 (d, *J* = 8.6 Hz, 2H), 7.55 – 7.39 (m, 6H), 7.30 – 7.19 (m, 2H), 4.35 (t, *J* = 7.4 Hz, 4H), 2.01 – 1.82 (m, 4H), 1.49 – 1.16 (m, 20H), 0.88 (t, *J* = 6.8 Hz, 6H). Data consistent with the literature.[106]

299; 3-Bromo-6-(3-bromo-9-octyl-9*H*-carbazol-6-yl)-9-octyl-9*H*-carbazole

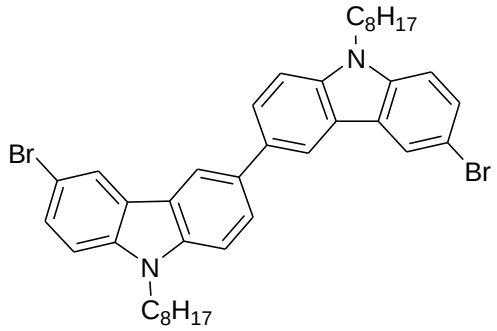

9-Octyl-3-(9-octyl-9*H*-carbazol-6-yl)-9*H*-carbazole (**298**) (2.00 g, 3.592 mmol) was dissolved in anhydrous THF (100 mL) under argon and the solution cooled to 0 °C. N-bromosuccinimide (1.279 g, 7.184 mmol) was added in portions and the mixture stirred for 18 h, whilst being allowed to warm to room temperature. The THF was removed under vacuum and the organic product extracted into DCM, washed with water and dried over magnesium sulfate. Removal of the solvent under vacuum followed by purification by column chromatography (eluent: petroleum ether:DCM 8:2 *v*/*v*) and recrystallisation from hexane gave **299** as a white solid (2.282 g, 89%).[1]H NMR (400 MHz) $CDCl_3$ δ 8.33 (d, *J* = 1.7 Hz, 2H), 8.29 (d, *J* = 1.9 Hz, 2H), 7.83 (dd, *J* = 8.5, 1.8 Hz, 2H), 7.55 (dd, *J* = 8.7, 1.9 Hz, 2H), 7.49 (d, *J* = 8.5 Hz, 2H), 7.30 (d, *J* = 8.7 Hz, 2H), 4.31 (t, *J* = 7.2 Hz, 4H), 1.97 – 1.80 (m, 4H), 1.45 – 1.19 (m, 20H), 0.87 (t, *J* = 6.6 Hz, 6H). Data consistent with the literature.[106]

300;3-(4,4,5,5-Tetramethyl-1,3,2-dioxaborolan-2-yl)-6-(3-(4,4,5,5-tetramethyl-1,3,2-dioxaborolan-2-yl)-9-octyl-9*H*-carbazol-6-yl)-9-octyl-9*H*-carbazole

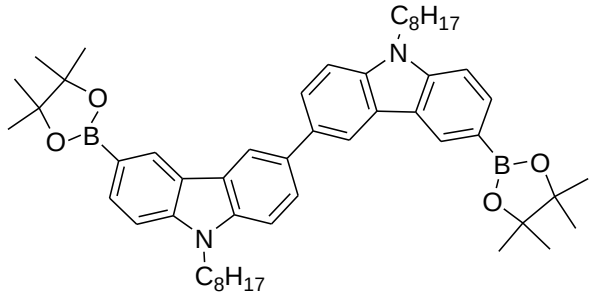

3-Bromo-6-(3-bromo-9-octyl-9*H*-carbazol-6-yl)-9-octyl-9*H*-carbazole (**299**) (1.00 g, 1.40 mmol) was dissolved in anhydrous DMF (20 mL) and the solution degassed for 30 min. Bis(pinacolato)diboron (0.859 g, 3.38 mmol), potassium acetate (0.962 g, 9.8 mmol) and palladium acetate (~ 15 mg) were added and the mixture heated at 90 °C for 18 h. Upon cooling, the organics were extracted into DCM and washed with brine. Removal of the solvent under vacuum, followed by column chromatography (eluent: petroleum ether:DCM 6:4 *v*/*v*) and recrystallisation from ethanol:toluene gave **300** as a white solid (0.300 g, 26%). [1]H NMR

(400 MHz) $CDCl_3$ δ 8.70 (s, 2H), 8.49 (d, *J* = 1.5 Hz, 2H), 7.94 (dd, *J* = 8.2, 1.1 Hz, 2H), 7.84 (dd, *J* = 8.5, 1.7 Hz, 2H), 7.50 (d, *J* = 8.5 Hz, 2H), 7.42 (d, *J* = 8.2 Hz, 2H), 4.35 (t, *J* = 7.2 Hz, 4H), 2.00 – 1.82 (m, 4H), 1.42 (s, 24H), 1.38 – 1.13 (m, 20H), 0.87 (t, *J* = 6.8 Hz, 6H). Data consistent with the literature.[179]

301; p-Cbz/Cbz-*meta*-S

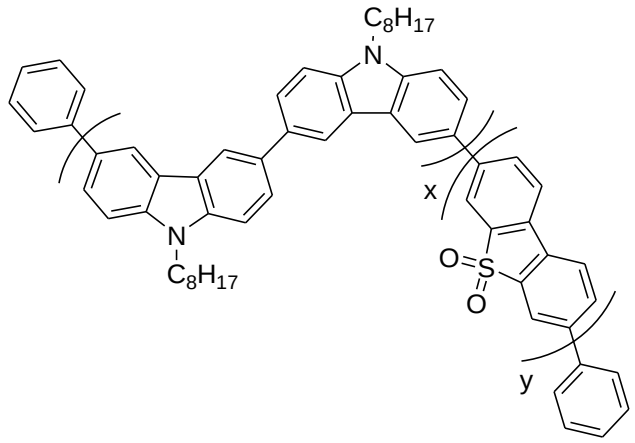

x:y 1:1

3-(4,4,5,5-Tetramethyl-1,3,2-dioxaborolan-2-yl)-6-(3-(4,4,5,5-tetramethyl-1,3,2-dioxaborolan-2-yl)-9-octyl-9*H*-carbazol-6-yl)-9-octyl-9*H*-carbazole (**300**) (0.200 g, 0.232 mmol) and 3,7-dibromodibenzothiophene-*S*,*S*-dioxide (**87**) (0.0875 g, 0.234 mmol) were dissolved in toluene (5 mL) and the mixture stirred and degassed by bubbling through argon for 15 min. $PdCl_2[P(o\text{-}tol_3)]_2$ catalyst (6 mg) was added and degassing was continued for 15 min. Degassed tetraethylammonium hydroxide solution (20%, 2.5 mL) was added and the mixture was refluxed at 115 °C under argon for 48 h. Bromobenzene (0.1 mL, 0.950 mmol) was added and the mixture was refluxed for 1 h. Phenylboronic acid (0.080 g, 0.819 mmol) was added and the mixture was refluxed for an additional 1 h. Upon cooling to room temperature, the mixture was poured into methanol (250 mL) and stirred for 30 min to precipitate the crude polymer, which was filtered off and washed (methanol, then water). The crude solid was dissolved in DCM (10 mL) and a solution of sodium diethyldithiocarbamic trihydrate (1 g in 10 mL water) was added and the mixture was heated at 50 °C for 12 h. The organic layer was separated, washed (10% hydrochloric acid, sodium acetate solution and water), filtered through celite (eluting with DCM), concentrated under vacuum and then precipitated dropwise into vigorously stirred methanol (250 mL). After stirring in methanol for 30 min, polymer **301** was isolated by filtration as a yellow solid (0.119 g, 67%). ^{1}H NMR (700 MHz) $CDCl_3$ δ 8.57-7.12 (m), 4.32 (s, br), 1.94-1.38 (m), 1.26 (s, br), 1.11-0.70 (m). M_n = 4,914 Da, M_w = 8,522 Da.

302; p-Cbz/Cbz-*para*-S

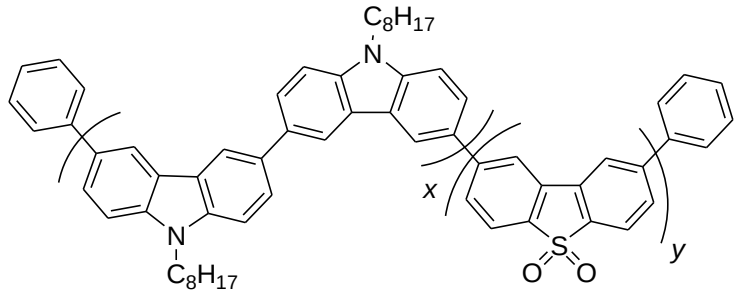

x:y 1:1

Synthesised according to the procedure for polymer **301** with 3-(4,4,5,5-tetramethyl-1,3,2-dioxaborolan-2-yl)-6-(3-(4,4,5,5-tetramethyl-1,3,2-dioxaborolan-2-yl)-9-octyl-9*H*-carbazol-6-yl)-9-octyl-9*H*-carbazole (**300**) (0.200 g, 0.232 mmol) and 2,8-dibromodibenzothiophene-*S*,*S*-dioxide (**89**) (0.0919 g, 0.246 mmol). Polymer **302** was obtained as a yellow solid (0.103 g, 57%).^{1}H NMR (700 MHz) $CDCl_3$ δ 8.45-7.15 (m), 4.29 (s, br), 2.00-1.53 (m), 1.27 (s, br), 1.07-0.51 (m). M_n = 3,677 Da, M_w = 5,656 Da.

Appendix I: Additional CV scans of ambipolar trimers from Chapter 3.2

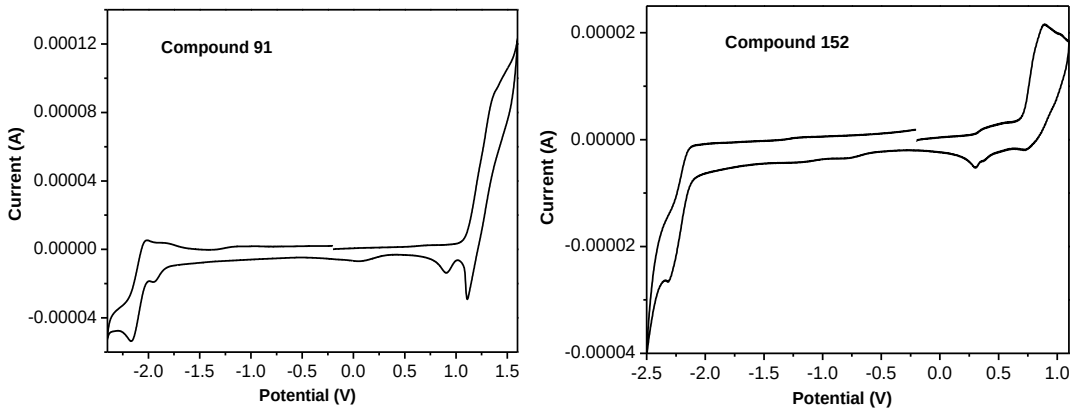

Figure I.I – CV scans of compounds 91 and 152

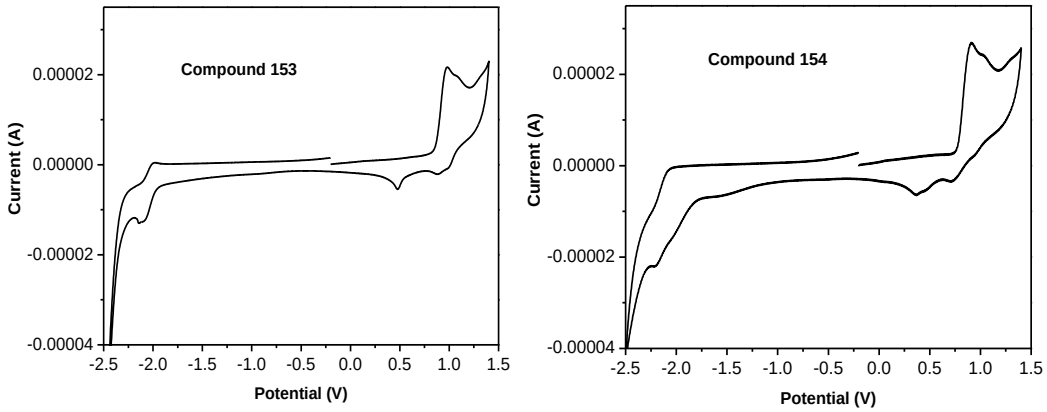

Figure I.II – CV scans of compounds 153 and 154

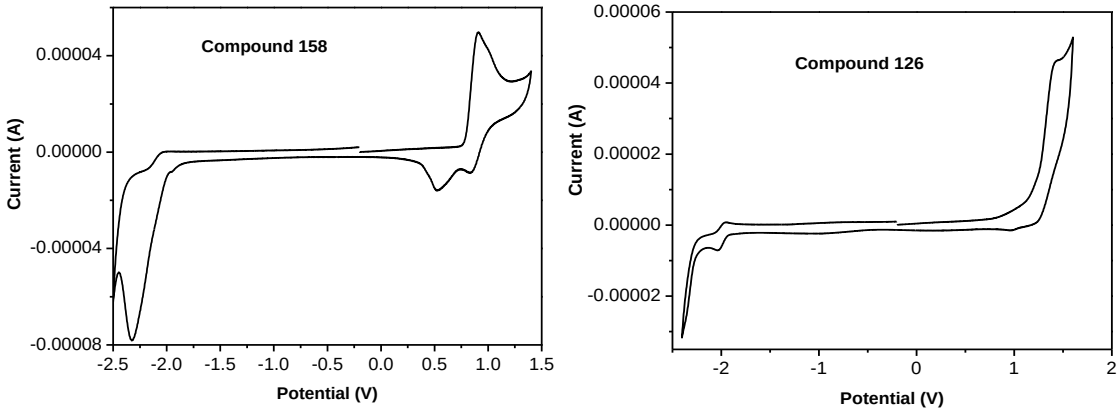

Figure I.III – CV scans of compounds 158 and 126

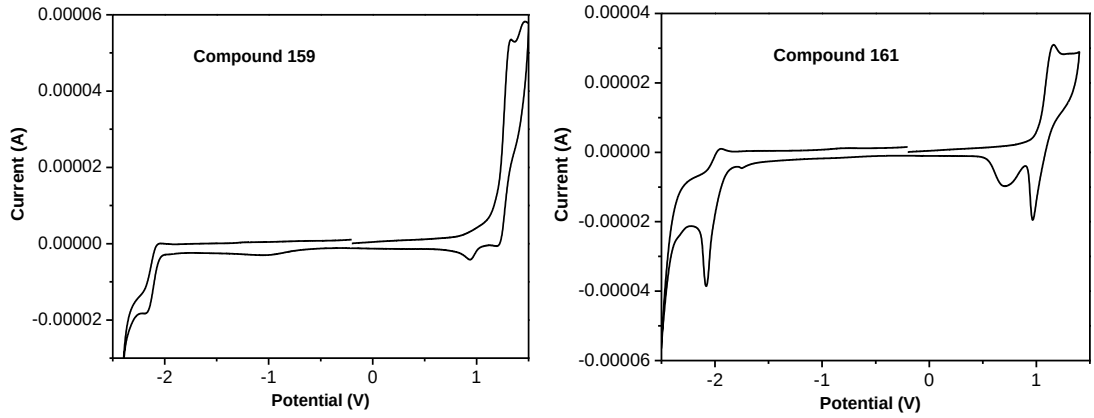

Figure I.IV – CV scans of compounds 159 and 161

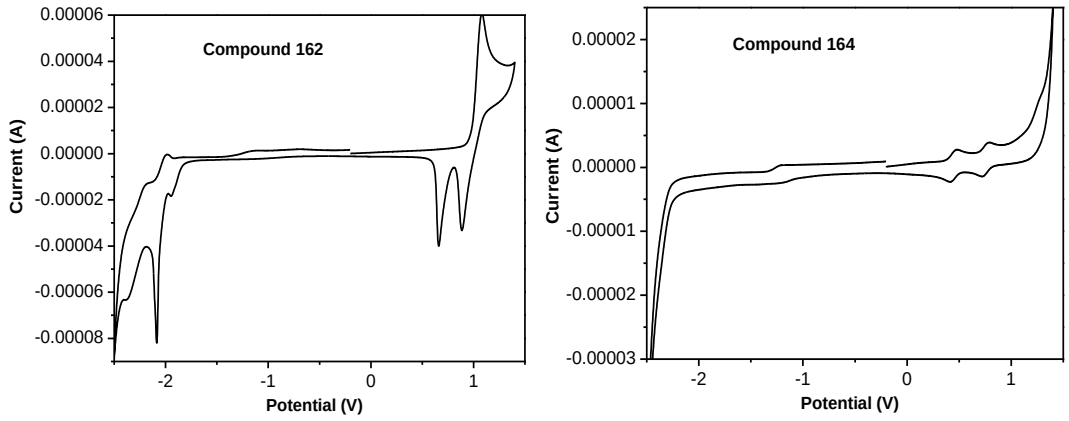

Figure I.V – CV scans of compounds 162 and 164

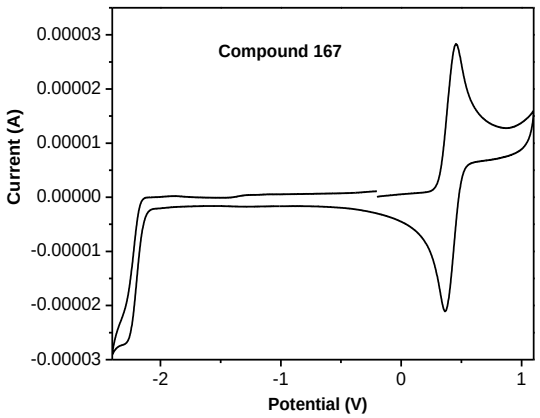

Figure I.VI – CV scan of compound 167

Potentials in V; scan rate 100 mVs^{-1}; Pd/C working electrode; Pt wire pseudo-reference electrode; Pt wire counter electrode; 0.2 M NBu_4PF_4 in DCM as electrolyte. Redox potentials reported with the ferrocene/ferrocenium (Fc/Fc^+) redox couple used as an internal reference system: 0.00 V.

Appendix II: Additional CV scans of Fc-C_{60} oligomers from Chapter 4

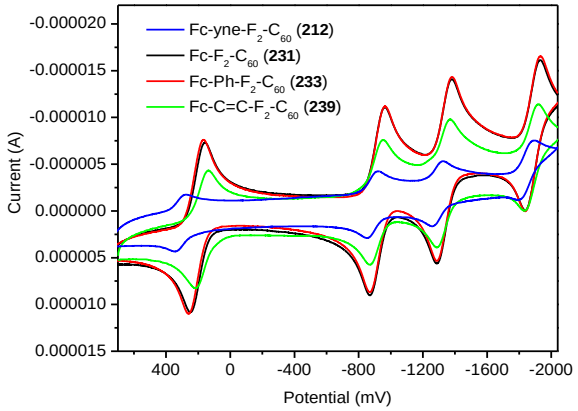

Figure II.I – Scans of (*n* = 2) final compounds (between + 700 and - 2000 mV)

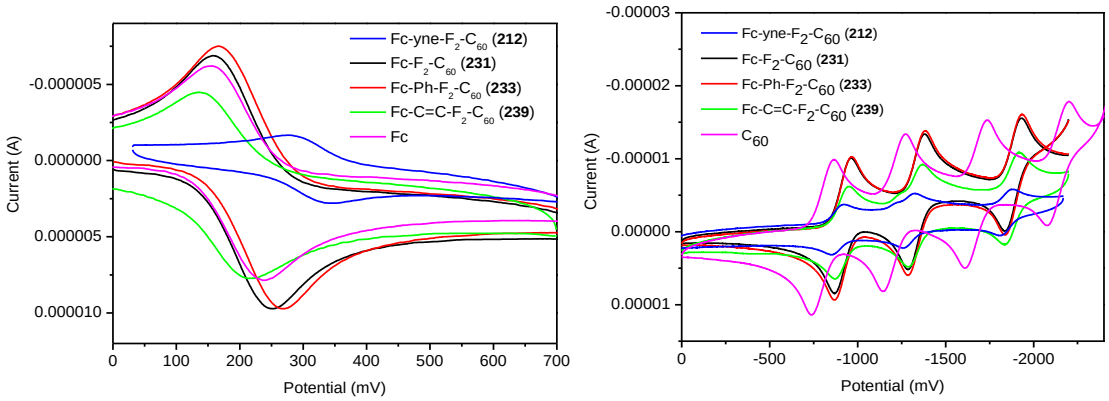

Figure II.II – Oxidation (a) and reduction (b) scans of (*n* = 2) compounds

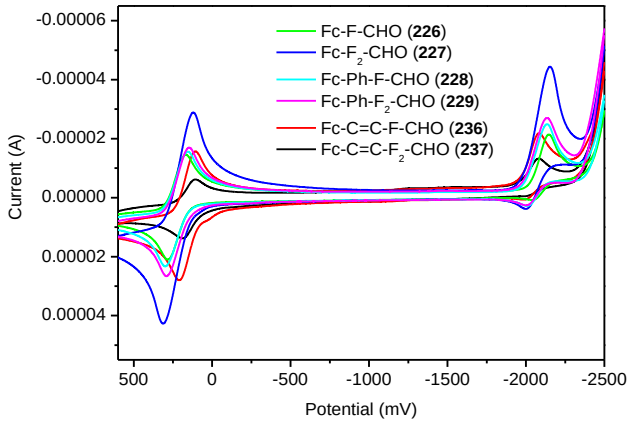

Figure II.III – Full scans of intermediate (*n* = 1) and (*n* = 2) compounds

Potentials in mV; scan rate 100 mVs^{-1}; glassy carbon working electrode; $Ag/AgNO_3$ reference electrode; Pt wire counter electrode; 0.1 M Bu_4NClO_4 in *o*DCB/CH_3CN (4:1 *v*/*v*) as electrolyte.

Appendix III: List of Seminars Attended

- 15/10/08: Rob Field, “From Biofuels to Homeland Security”
- 22/10/08: Mike Ward, “Self Assembly and Host Guest Chemistry of Polyhedral Coordination Chemistry”
- 29/10/08: Naokazu Kano, “Development of Organic Fluorescent Materials by Taking Advantage of the N-B interaction”
- 5/11/08: Paul Beer, “Anion Templated Assembly of Interlocked Host Structures”
- 12/11/08: A. M. Bond, “Electrochemistry and Photoelectrochemistry in Ionic Liquids”
- 14/01/09: Darren Dixon, “Enantioselective Bifunctional Organocatalysis”
- 24/03/09: Tim Glass, “Fluorescent Chemical Sensors for Bioactive Compounds”
- 08/06/09: H. Yersin, “Triplet States and Photophysical Properties of Organo-Transition Metal Compounds Towards Optimization of OLED Emitter Materials”
- 23/06/09: Michael Hon-Wah Lam, Hong Kong, “Versatile Luminescent Organometallic Pt(II) Systems for Bio-Labelling Applications”
- 07/07/09: Tim Swager, MIT, “Polymer Electronics in the Design of Chemical Sensors”
- 17/07/09: Uwe Bunz, Georgia Tech, “Cruciform Fluorophores”
- 13/01/10: Hugh Burrows, Coimbra, Portugal, RSC Photochemistry Meeting
- 11/03/10: Frieder Jakle, Rutgers, “Organoborane functionalised conjugated polymers”
- 15/04/10: Dr. Anne Routledge, York, RSC Organic Division NE Region Symposium
- 15/04/10: Dr. Valery Kozhenikov, Northumbria, RSC NE Region Symposium
- 10/05/10-12/05/10: Dan Nocera, MIT, USA, “The Global Energy Challenge”; “The Chemistry of Solar Fuels”; “Personalised Energy”
- 28/09/10: L-O. Pålsson, Durham, “Time-Resolved Optical Microscopy”
- 28/09/10: Claude Lapinte, Rennes, “Molecular Organometallic Wires”
- 10/11/10: Martyn Twigg, Johnson Matthey, “Controlling Emissions from Cars”
- 12/11/10: Michael Bendikov, “Novel Organic Electronic Materials”
- 23/02/11: Laura Herz, “Ultrafast Photoexcitation Dynamics in Hybrid Materials”
- 11/05/11: M. C. Nicasio, Seville, “C-Heteroatom Bond Formation Using Ni and Cu”
- 11/05/11: Pete Skabara, Strathclyde, “Complex Conjugated Architectures”
- 13/05/11: Henri Doucet, Rennes, “Pd-Catalysed Arylations via C-H Bond Activation”
- 18/05/11: Randy Thummel, Houston, “Heterocyclic Ligands to Capture Sun’s Energy”
- 12/09/11: Chihaya Adachi, Kyushu, Japan
- 01/11/11: Igor Larrosa, Queen Mary, “C-H Activation to C-C Activation”

Chapter 8: Bibliography

(1) Kamtekar, K. T.; Monkman, A. P.; Bryce, M. R. *Adv. Mater.* **2010**, *22*, 572.
(2) Duan, L.; Qiao, J.; Sun, Y.; Qiu, Y. *Adv. Mater.* **2011**, *23*, 1137.
(3) Chaskar, A.; Chen, H.-F.; Wong, K.-T. *Adv. Mater.* **2011**, *23*, 3876.
(4) Jiang, H. *Macromol. Rapid Commun.* **2010**, *31*, 2007.
(5) Beaujuge, P. M.; Amb, C. M.; Reynolds, J. R. *Accts. Chem. Res.* **2010**, *43*, 1396.
(6) Facchetti, A. *Chem. Mater.* **2011**, *23*, 733.
(7) Zhu, X.-H.; Peng, J.; Cao, Y.; Roncali, J. *Chem. Soc. Rev.* **2011**, *40*, 3509.
(8) Grimsdale, A. C.; Leok, C. K.; Martin, R. E.; Jokisz, P. G.; Holmes, A. B. *Chem. Rev.* **2009**, *109*, 897.
(9) Shirota, Y.; Kageyama, H. *Chem. Rev.* **2007**, *107*, 953.
(10) Zhu, Y.; Kulkarni, A. P.; Wu, P.-T.; Jenekhe, S. A. *Chem. Mater.* **2008**, *20*, 4200.
(11) Kulkarni, A. P.; Zhu, Y.; Babel, A.; Wu, P.-T.; Jenekhe, S. A. *Chem. Mater.* **2008**, *20*, 4212.
(12) Jenekhe, S. A.; Lu, L.; Alam, M. M. *Macromolecules* **2001**, *34*, 7315.
(13) Kwon, T. W.; Kulkarni, A. P.; Jenekhe, S. A. *Synthetic Met.* **2008**, *158*, 292.
(14) Zhang, W.-W.; Mao, W.-L.; Hu, Y.-X.; Tian, Z.-Q.; Wang, Z.-L.; Meng, Q.-J. *J. Phys. Chem. A* **2009**, *113*, 9997.
(15) Lin, S.-L.; Chan, L.-H.; Lee, R.-H.; Yen, M.-Y.; Kuo, W.-J.; Chen, C.-T.; Jeng, R.-J. *Adv. Mater.* **2008**, *20*, 3947.
(16) Chen, L.; Wang, L.; Jing, X.; Wang, F. *J. Mater. Chem.* **2011**, *21*, 10265.
(17) Tao, Y.; Wang, Q.; Yang, C.; Zhong, C.; Zhang, K.; Qin, J.; Ma, D. *Adv. Funct. Mater.* **2010**, *20*, 304.
(18) Zheng, Y.; Batsanov, A. S.; Jankus, V.; Dias, F. B.; Bryce, M. R.; Monkman, A. P. *J. Org. Chem.* **2011**, *76*, 8300.
(19) Thompson, A. L.; Ahn, T.-S.; Thomas, K. R. J.; Thayumanavan, S.; Martinez, T. J.; Bardeen, C. J. *J. Am. Chem. Soc.* **2005**, *127*, 16348.
(20) Tang, Z.-M.; Lei, T.; Wang, J.-L.; Ma, Y.; Pei, J. *J. Org. Chem.* **2010**, *75*, 3644.
(21) Wu, J.-S.; Cheng, Y.-J.; Dubosc, M.; Hsieh, C.-H.; Chang, C.-Y.; Hsu, C.-S. *Chem. Commun.* **2010**, *46*, 3259.
(22) Xin, H.; Guo, X.; Kim, F. S.; Ren, G.; Watson, M. D.; Jenekhe, S. A. *J. Mater. Chem.* **2009**, *19*, 5303.
(23) Guo, X.; Xin, H.; Kim, F. S.; Liyanage, A. D. T.; Jenekhe, S. A.; Watson, M. D. *Macromolecules* **2011**, *44*, 269.
(24) Zhang, X.; Shim, J. W.; Tiwari, S. P.; Zhang, Q.; Norton, J. E.; Wu, P.-T.; Barlow, S.; Jenekhe, S. A.; Kippelen, B.; Bredas, J.-L.; Marder, S. R. *J. Mater. Chem.* **2011**, *21*, 4971.
(25) Kim, F. S.; Guo, X.; Watson, M. D.; Jenekhe, S. A. *Adv. Mater.* **2010**, *22*, 478.
(26) Wu, P.-T.; Kim, F. S.; Champion, R. D.; Jenekhe, S. A. *Macromolecules* **2008**, *41*, 7021.
(27) Chua, L.-L.; Zaumseil, J.; Chang, J.-F.; Ou, E. C. W.; Ho, P. K. H.; Sirringhaus, H.; Friend, R. H. *Nature* **2005**, *434*, 194.
(28) Yamamoto, T.; Morita, A.; Miyazaki, Y.; Maruyama, T.; Wakayama, H.; Zhou, Z. H.; Nakamura, Y.; Kanbara, T.; Sasaki, S.; Kubota, K. *Macromolecules* **1992**, *25*, 1214.
(29) Miyaura, N.; Suzuki, A. *Chem. Rev.* **1995**, *95*, 2457.
(30) Bliznyuk, V. N.; Carter, S. A.; Scott, J. C.; Klarner, G.; Miller, R. D.; Miller, D. C. *Macromolecules* **1999**, *32*, 361.

(31) List, E. J. W.; Guentner, R.; Scanducci de Freitas, P.; Scherf, U. *Adv. Mater.* **2002**, *14*, 374.
(32) Liu, L.; Yang, B.; Zhang, H.; Tang, S.; Xie, Z.; Wang, H.; Wang, Z.; Lu, P.; Ma, Y. *J. Phys. Chem. C.* **2008**, *112*, 10273.
(33) Pei, J.; Ni, J.; Zhou, X.-H.; Cao, X.-Y.; Lai, Y.-H. *J. Org. Chem.* **2002**, *67*, 4924.
(34) Cho, S. Y.; Grimsdale, A. C.; Jones, D. J.; Watkins, S. E.; Holmes, A. B. *J. Am. Chem. Soc.* **2007**, *129*, 11910.
(35) Kappaun, S.; Scheiber, H.; Trattnig, R.; Zojer, E.; List, E. J. W.; Slugovc, C. *Chem. Commun.* **2008**, 5170.
(36) Saragi, T. P. I.; Spehr, T.; Siebert, A.; Fuhrmann-Lieker, T.; Salbeck, J. *Chem. Rev.* **2007**, *107*, 1011.
(37) Miteva, T.; Meisel, A.; Knoll, W.; Nothofer, H. G.; Scherf, U.; Müller, D.; Meerholz, K.; Yasuda, A.; Neher, D. *Adv. Mater.* **2001**, *13*, 565.
(38) Ego, C.; Grimsdale, A. C.; Uckert, F.; Yu, G.; Srdanov, G.; Müllen, K. *Adv. Mater.* **2002**, *14*, 809.
(39) Giovanella, U.; Pasini, M.; Destri, S.; Porzio, W.; Botta, C. *Synthetic Met.* **2008**, *158*, 113.
(40) Jiang, Z.; Zhang, W.; Yao, H.; Yang, C.; Cao, Y.; Qin, J.; Yu, G.; Liu, Y. *J. Polym. Sci. Part A: Polym. Chem.* **2009**, *47*, 3651.
(41) Zhang, X.; Quan, Y.; Cui, Z.; Chen, Q.; Ding, J.; Lu, J. *Eur. J. Org. Chem.* **2010**, 2295.
(42) Li, Y. N.; Ding, J. F.; Day, M.; Tao, Y.; Lu, J. P.; D'Iorio, M. *Chem. Mater.* **2004**, *16*, 2165.
(43) Zhu, Y.; Gibbons, K. M.; Kulkarni, A. P.; Jenekhe, S. A. *Macromolecules* **2007**, *40*, 804.
(44) Wang, M.; Tong, H.; Cheng, Y.; Xie, Z.; Wang, L.; Jing, X.; Wang, F. *J. Polym. Sci. Part A: Polym. Chem.* **2010**, *48*, 1990.
(45) Zou, L.; Liu, Z.; Yan, X.; Liu, Y.; Fu, Y.; Liu, J.; Huang, Z.; Chen, X.; Qin, J. *Eur. J. Org. Chem.* **2009**, *2009*, 5587.
(46) Chen, Z.; Fang, J.; Gao, F.; Brenner, T. J. K.; Banger, K. K.; Wang, X.; Huck, W. T. S.; Sirringhaus, H. *Org. Electron.* **2011**, *12*, 461.
(47) Kajii, H.; Koiwai, K.; Hirose, Y.; Ohmori, Y. *Org. Electron.* **2010**, *11*, 509.
(48) Lee, W.-Y.; Cheng, K.-F.; Wang, T.-F.; Chen, W.-C.; Tsai, F.-Y. *Thin Solid Films* **2010**, *518*, 2119.
(49) Wu, P. L.; Feng, X. J.; Tam, H. L.; Wong, M. S.; Cheah, K. W. *J. Am. Chem. Soc.* **2009**, *131*, 886.
(50) Feng, X. J.; Wu, P. L.; Tam, H. L.; Li, K. F.; Wong, M. S.; Cheah, K. W. *Chem. Eur. J.* **2009**, *15*, 11681.
(51) Lin, Y.; El-Khouly, M. E.; Chen, Y.; Supur, M.; Gu, L.; Li, Y.; Fukuzumi, S. *Chem. Eur. J.* **2009**, *15*, 10818.
(52) Wu, F.-I.; Shih, P.-I.; Tseng, Y.-H.; Shu, C.-F.; Tung, Y.-L.; Chi, Y. *J. Mater. Chem.* **2007**, *17*, 167.
(53) Wang, K.-L.; Leung, M.-K.; Hsieh, L.-G.; Chang, C.-C.; Lee, K.-R.; Wu, C.-L.; Jiang, J.-C.; Tseng, C.-Y.; Wang, H.-T. *Org. Electron.* **2011**, *12*, 1048.
(54) Kamtekar, K. T.; Wang, C.; Bettington, S.; Batsanov, A. S.; Perepichka, I. F.; Bryce, M. R.; Ahn, J. H.; Rabinal, M.; Petty, M. C. *J. Mater. Chem.* **2006**, *16*, 3823.
(55) Fisher, A. L.; Linton, K. E.; Kamtekar, K. T.; Pearson, C.; Bryce, M. R.; Petty, M. C. *Chem. Mater.* **2011**, *23*, 1640.
(56) Chan, K. L.; McKiernan, M. J.; Towns, C. R.; Holmes, A. B. *J. Am. Chem. Soc.* **2005**, *127*, 7662.

(57) Wong, W. W. H.; Holmes, A. B. *Polyfluorenes*; Springer-Verlag Berlin, 2008; Vol. 212, p 85-98.
(58) Chan, K. L.; Watkins, S. E.; Mak, C. S. K.; McKiernan, M. J.; Towns, C. R.; Pascu, S. I.; Holmes, A. B. *Chem. Commun.* **2005**, 5766.
(59) Keyworth, C. W.; Chan, K. L.; Labram, J. G.; Anthopoulos, T. D.; Watkins, S. E.; McKiernan, M.; White, A. J. P.; Holmes, A. B.; Williams, C. K. *J. Mater. Chem.* **2011**, *21*, 11800.
(60) Wang, E.; Wang, L.; Lan, L.; Luo, C.; Zhuang, W.; Peng, J.; Cao, Y. *Appl. Phys. Lett.* **2008**, *92*, 033307.
(61) Duan, C.; Cai, W.; Huang, F.; Zhang, J.; Wang, M.; Yang, T.; Zhong, C.; Gong, X.; Cao, Y. *Macromolecules* **2010**, *43*, 5262.
(62) Geramita, K.; McBee, J.; Tao, Y.; Segalman, R. A.; Tilley, T. D. *Chem. Commun.* **2008**, 5107.
(63) Geramita, K.; McBee, J.; Tilley, T. D. *J. Org. Chem.* **2009**, *74*, 820.
(64) Geramita, K.; Tao, Y.; Segalman, R. A.; Tilley, T. D. *J. Org. Chem.* **2010**, *75*, 1871.
(65) Perepichka, I. I.; Perepichka, I. F.; Bryce, M. R.; Palsson, L. O. *Chem. Commun.* **2005**, 3397.
(66) Barbarella, G.; Favaretto, L.; Sotgiu, G.; Zambianchi, M.; Bongini, A.; Arbizzani, C.; Mastragostino, M.; Anni, M.; Gigli, G.; Cingolani, R. *J. Am. Chem. Soc.* **2000**, *122*, 11971.
(67) Charas, A.; Morgado, J.; Martinho, J. M. G.; Alcacer, L.; Cacialli, F. *Chem. Commun.* **2001**, 1216.
(68) Dias, F. B.; Pollock, S.; Hedley, G.; Palsson, L.-O.; Monkman, A. P.; Perepichka, I. I.; Perepichka, I. F.; Tavasli, M.; Bryce, M. R. *J. Phys. Chem. B* **2006**, *110*, 19329.
(69) Dias, F. B.; King, S.; Monkman, A. P.; Perepichka, I. I.; Kryuchkov, M. A.; Perepichka, I. F.; Bryce, M. R. *J. Phys. Chem. B* **2008**, *112*, 6557.
(70) King, S. M.; Perepichka, I. I.; Perepichka, I. F.; Dias, F. B.; Bryce, M. R.; Monkman, A. P. *Adv. Funct. Mater.* **2009**, *19*, 586.
(71) Li, Y. Y.; Wu, H. B.; Zou, J. H.; Ying, L.; Yang, W.; Cao, Y. *Org. Electron.* **2009**, *10*, 901.
(72) Kamtekar, K. T.; Dahms, K.; Batsanov, A. S.; Jankus, V.; Vaughan, H. L.; Monkman, A. P.; Bryce, M. R. *J. Polym. Sci. Part A: Polym. Chem.* **2011**, *49*, 1129.
(73) Yang, F.; Sun, K.; Cao, Z. J.; Li, Z. H.; Wong, M. S. *Synthetic Met.* **2008**, *158*, 391.
(74) Huang, T. H.; Lin, J. T.; Chen, L. Y.; Lin, Y. T.; Wu, C. C. *Adv. Mater.* **2006**, *18*, 602.
(75) Grisorio, R.; Melcarne, G.; Suranna, G. P.; Mastrorilli, P.; Nobile, C. F.; Cosma, P.; Fini, P.; Colella, S.; Fabiano, E.; Piacenza, M.; Sala, F. D.; Ciccarella, G.; Mazzeo, M.; Gigli, G. *J. Mater. Chem.* **2010**, *20*, 1012.
(76) Liu, H.; Zou, J. H.; Yang, W.; Wu, H. B.; Li, C.; Zhang, B.; Peng, J. B.; Cao, Y. *Chem. Mater.* **2008**, *20*, 4499.
(77) Grisorio, R.; Piliego, C.; Cosma, P.; Fini, P.; Mastrorilli, P.; Gigli, G.; Suranna, G. P.; Nobile, C. F. *J. Polym. Sci. Part A: Polym. Chem.* **2009**, *47*, 2093.
(78) Grabowski, Z. R.; Rotkiewicz, K.; Rettig, W. *Chem. Rev.* **2003**, *103*, 3899.
(79) Demeter, A.; Bérces, T.; Zachariasse, K. A. *J. Phys. Chem. A* **2001**, *105*, 4611.
(80) Yoshihara, T.; Druzhinin, S. I.; Zachariasse, K. A. *J. Am. Chem. Soc.* **2004**, *126*, 8535.
(81) Druzhinin, S. I.; Kovalenko, S. A.; Senyushkina, T. A.; Demeter, A.; Januskevicius, R.; Mayer, P.; Stalke, D.; Machinek, R.; Zachariasse, K. A. *J. Phys. Chem. A* **2009**, *113*, 9304.
(82) Druzhinin, S. I.; Kovalenko, S. A.; Senyushkina, T. A.; Demeter, A.; Zachariasse, K. A. *J. Phys. Chem. A* **2010**, *114*, 1621.

(83) Zachariasse, K. A.; Druzhinin, S. I.; Galievsky, V. A.; Demeter, A.; Allonas, X.; Kovalenko, S. A.; Senyushkina, T. A. *J. Phys. Chem. A* **2010**, *114*, 13031.
(84) Cogan, S.; Zilberg, S.; Haas, Y. *J. Am. Chem. Soc.* **2006**, *128*, 3335.
(85) Neubauer, A.; Bendig, J.; Rettig, W. *Chem. Phys.* **2009**, *358*, 235.
(86) Ooyama, Y.; Ito, G.; Kushimoto, K.; Komaguchi, K.; Imae, I.; Harima, Y. *Org. Biomol. Chem.* **2010**, *8*, 2756.
(87) Kotaka, H.; Konishi, G.-i.; Mizuno, K. *Tetrahedron Lett.* **2010**, *51*, 181.
(88) Kamtekar, K. T.; Vaughan, H. L.; Lyons, B. P.; Monkman, A. P.; Pandya, S. U.; Bryce, M. R. *Macromolecules* **2010**, *43*, 4481.
(89) Fyaz, M. D. I. *J. Fluorine Chem.* **2002**, *118*, 27.
(90) Brinon, M. C.; Debertorello, M. M.; Bertorello, H. E. *An. Asoc. Quim. Argent.* **1983**, *71*, 571.
(91) Soki, F.; Neudorfl, M.; Goldfuss, B. *Tetrahedron* **2005**, *61*, 10449.
(92) Yamazaki, D.; Nishinaga, T.; Komatsu, K. *Org. Lett.* **2004**, *6*, 4179.
(93) Li, H.; Batsanov, A. S.; Moss, K. C.; Vaughan, H. L.; Dias, F. B.; Kamtekar, K. T.; Bryce, M. R.; Monkman, A. P. *Chem. Commun.* **2010**, *46*, 4812.
(94) Babudri, F.; Farinola, G. M.; Naso, F.; Ragni, R. *Chem. Commun.* **2007**, 1003.
(95) Wallace, J. U.; Chen, S. H. *Fluorene-based conjugated oligomers for organic photonics and electronics*; Springer-Verlag Berlin: Berlin, 2008; Vol. 212.
(96) Liu, J.; Zou, J.; Yang, W.; Wu, H.; Li, C.; Zhang, B.; Peng, J.; Cao, Y. *Chem. Mater.* **2008**, *20*, 4499.
(97) Morin, J. F.; Leclerc, M.; Ades, D.; Siove, A. *Macromol. Rapid Commun.* **2005**, *26*, 761.
(98) Boudreault, P.-L. T.; Beaupre, S.; Leclerc, M. *Polym. Chem.* **2010**, *1*, 127.
(99) Shirota, Y. *J. Mater. Chem.* **2000**, *10*, 1.
(100) Kulkarni, A. P.; Kong, X. X.; Jenekhe, S. A. *Adv. Funct. Mater.* **2006**, *16*, 1057.
(101) Brunner, K.; van Dijken, A.; Borner, H.; Bastiaansen, J. J. A. M.; Kiggen, N. M. M.; Langeveld, B. M. W. *J. Am. Chem. Soc.* **2004**, *126*, 6035.
(102) van Dijken, A.; Bastiaansen, J.; Kiggen, N. M. M.; Langeveld, B. M. W.; Rothe, C.; Monkman, A. P.; Bach, I.; Stossel, P.; Brunner, K. *J. Am. Chem. Soc.* **2004**, *126*, 7718.
(103) Chen, Y. C.; Huang, G. S.; Hsiao, C. C.; Chen, S. A. *J. Am. Chem. Soc.* **2006**, *128*, 8549.
(104) Estrada, L. A.; Neckers, D. C. *J. Org. Chem.* **2009**, *74*, 8484.
(105) Estrada, L. A.; Cai, X.; Neckers, D. C. *J. Phys. Chem. A* **2011**, *115*, 2184.
(106) Farinola, G. M.; Ragni, R. *Chem. Soc. Rev.* **2011**, *40*, 3467.
(107) Wu, H. B.; Ying, L.; Yang, W.; Cao, Y. *Chem. Soc. Rev.* **2009**, *38*, 3391.
(108) Raja, I. U.; Lee, J. Y.; Kim, I. T.; Lee, S. H. *Monatsh Chem.* **2008**, *139*, 725.
(109) Liu, J.; Shao, S. Y.; Chen, L.; Xie, Z. Y.; Cheng, Y. X.; Geng, Y. H.; Wang, L. X.; Jing, X. B.; Wang, F. S. *Adv. Mater.* **2007**, *19*, 1859.
(110) Hu, B.; Zhang, J. P. *Polymer* **2009**, *50*, 6172.
(111) Liu, J.; Cheng, Y. X.; Xie, Z. Y.; Geng, Y. H.; Wang, L. X.; Jing, X. B.; Wang, F. S. *Adv. Mater.* **2008**, *20*, 1357.
(112) Liu, J.; Chen, L.; Shao, S. Y.; Xie, Z. Y.; Cheng, Y. X.; Geng, Y. H.; Wang, L. X.; Jing, X. B.; Wang, F. S. *Adv. Mater.* **2007**, *19*, 4224.
(113) Luo, J.; Li, X. Z.; Hou, Q.; Peng, J. B.; Yang, W.; Cao, Y. *Adv. Mater.* **2007**, *19*, 1113.
(114) Zhu, D. X.; Zhen, H. Y.; Ye, H.; Liu, X. *Appl. Phys. Lett.* **2008**, *93*, 1633091.
(115) Zhang, L.; Hu, S.; Chen, J.; Chen, Z.; Wu, H.; Peng, J.; Cao, Y. *Adv. Funct. Mater.* **2011**, *21*, 3760.
(116) Strohriegl, P.; Grazulevicius, J. V. *Adv. Mater.* **2002**, *14*, 1439.

(117) Turro, N. J.; Ramamurthy, V.; Scaiano, J. C. *Principles of Molecular Photochemistry An Introduction*; University Science Books, 2009.
(118) Beljonne, D.; Shuai, Z.; Pourtois, G.; Bredas, J. L. *J. Phys. Chem. A* **2001**, *105*, 3899.
(119) Fonseca, S. M.; Pina, J.; Arnaut, L. G.; de Melo, J. S.; Burrows, H. D.; Chattopadhyay, N.; Alcacer, L.; Charas, A.; Morgado, J.; Monkman, A. P.; Asawapirom, U.; Scherf, U.; Edge, R.; Navaratnam, S. *J. Phys. Chem. B* **2006**, *110*, 8278.
(120) Rybicki, J.; Wohlgenannt, M. *Phys. Rev. B* **2009**, *79*, 153202.
(121) Parker, C. A.; Joyce, T. A. *Chem. Commun.* **1968**, 749.
(122) Hoshino, S.; Suzuki, H. *Appl. Phys. Lett.* **1996**, *69*, 224.
(123) Bolton, O.; Lee, K.; Kim, H. J.; Lin, K. Y.; Kim, J. *Nat. Chem.* **2011**, *3*, 205.
(124) Castex, M. C.; Olivero, C.; Pichler, G.; Ades, D.; Siove, A. *Synthetic Met.* **2006**, *156*, 699.
(125) Guldi, D. M.; Illescas, B. M.; Atienza, C. M.; Wielopolski, M.; Martin, N. *Chem. Soc. Rev.* **2009**, *38*, 1587.
(126) Lopez, M. A.; Mateo-Alonso, A.; Prato, M. *J. Mater. Chem.* **2011**, *21*, 1305.
(127) Prato, M.; Maggini, M. *Acc. Chem. Res.* **1998**, *31*, 519.
(128) Kharisov, B. I.; Kharissova, O. V.; Gomez, M. J.; Mendez, U. O. *Ind. Eng. Chem. Res.* **2009**, *48*, 545.
(129) Hummelen, J. C.; Knight, B. W.; LePeq, F.; Wudl, F.; Yao, J.; Wilkins, C. L. *J. Org. Chem.* **1995**, *60*, 532.
(130) Gendron, D.; Leclerc, M. *Energy Environ. Sci.* **2011**, *4*, 1225.
(131) Cheng, Y.-J.; Yang, S.-H.; Hsu, C.-S. *Chem. Rev.* **2009**, *109*, 5868.
(132) Boudreault, P.-L. T.; Najari, A.; Leclerc, M. *Chem. Mater.* **2010**, *23*, 456.
(133) van der Pol, C.; Bryce, M. R.; Wielopolski, M.; Atienza-Castellanos, C.; Guldi, D. M.; Filippone, S.; Martín, N. *J. Org. Chem.* **2007**, *72*, 6662.
(134) Figueira-Duarte, T. M.; Rio, Y.; Listorti, A.; Delavaux-Nicot, B.; Holler, M.; Marchioni, F.; Ceroni, P.; Armaroli, N.; Nierengarten, J.-F. *New J. Chem.* **2008**, *32*, 54.
(135) Atienza, C.; Martin, N.; Wielopolski, M.; Haworth, N.; Clark, T.; Guldi, D. M. *Chem. Commun.* **2006**, 3202.
(136) Vail, S. A.; Schuster, D. I.; Guldi, D. M.; Isosomppi, M.; Tkachenko, N.; Lemmetyinen, H.; Palkar, A.; Echegoyen, L.; Chen, X.; Zhang, J. Z. H. *J. Phys. Chem. B* **2006**, *110*, 14155.
(137) Kanato, H.; Takimiya, K.; Otsubo, T.; Aso, Y.; Nakamura, T.; Araki, Y.; Ito, O. *J. Org. Chem.* **2004**, *69*, 7183.
(138) Oswald, F.; Islam, D. M. S.; Araki, Y.; Troiani, V.; de la Cruz, P.; Moreno, A.; Ito, O.; Langa, F. *Chem.-Eur. J.* **2007**, *13*, 3924.
(139) Goldsmith, R. H.; Sinks, L. E.; Kelley, R. F.; Betzen, L. J.; Liu, W.; Weiss, E. A.; Ratner, M. A.; Wasielewski, M. R. *Proc. Nat. Acad. Sci.* **2005**, *102*, 3540.
(140) Leary, E.; González, M. T.; van der Pol, C.; Bryce, M. R.; Filippone, S.; Martín, N.; Rubio-Bollinger, G.; Agraït, N. *Nano Lett.* **2011**, *11*, 2236.
(141) Atienza-Castellanos, C.; Wielopolski, M.; Guldi, D. M.; van der Pol, C.; Bryce, M. R.; Filippone, S.; Martin, N. *Chem. Commun.* **2007**, 5164.
(142) Wielopolski, M.; de Miguel Rojas, G.; van der Pol, C.; Brinkhaus, L.; Katsukis, G.; Bryce, M. R.; Clark, T.; Guldi, D. M. *ACS Nano* **2010**, *4*, 6449.
(143) Wielopolski, M.; Santos, J.; Illescas, B. M.; Ortiz, A.; Insuasty, B.; Bauer, T.; Clark, T.; Guldi, D. M.; Martin, N. *Energy Environ. Sci.* **2011**, *4*, 765.
(144) Nakamura, T.; Kanato, H.; Araki, Y.; Ito, O.; Takimiya, K.; Otsubo, T.; Aso, Y. *J. Phys. Chem. A* **2006**, *110*, 3471.

(145) Araki, Y.; Chitta, R.; Sandanayaka, A. S. D.; Langenwalter, K.; Gadde, S.; Zandler, M. E.; Ito, O.; D'Souza, F. *J. Phys. Chem. C* **2008**, *112*, 2222.
(146) Guldi, D. M.; Aminur Rahman, G. M.; Marczak, R.; Matsuo, Y.; Yamanaka, M.; Nakamura, E. *J. Am. Chem. Soc.* **2006**, *128*, 9420.
(147) Cioffi, C. T.; Palkar, A.; Melin, F.; Kumbhar, A.; Echegoyen, L.; Melle-Franco, M.; Zerbetto, F.; Rahman, G. M. A.; Ehli, C.; Sgobba, V.; Guldi, D. M.; Prato, M. *Chem.-Eur. J.* **2009**, *15*, 4419.
(148) Imrie, C.; Loubser, C.; Engelbrecht, P.; McCleland, C. W. *J. Chem. Soc.-Perkin Trans. 1* **1999**, 2513.
(149) Sailer, M.; Rominger, F.; Muller, T. J. J. *J. Organomet. Chem.* **2006**, *691*, 299.
(150) Chen, S. A.; Lu, H. H.; Huang, C. W. *Polyfluorenes*; Springer-Verlag Berlin, 2008; Vol. 212, p 49.
(151) Knaapila, M.; Winokur, M. J. *Polyfluorenes*; Springer-Verlag Berlin, 2008; Vol. 212, p 227.
(152) Grell, M.; Bradley, D. D. C.; Long, X.; Chamberlain, T.; Inbasekaran, M.; Woo, E. P.; Soliman, M. *Acta Polym.* **1998**, *49*, 439.
(153) Grell, M.; Bradley, D. D. C.; Ungar, G.; Hill, J.; Whitehead, K. S. *Macromolecules* **1999**, *32*, 5810.
(154) Abbel, R.; Schenning, A. P. H. J.; Meijer, E. *J. Polym. Sci. Part A: Polym. Chem.* **2009**, *47*, 4215.
(155) Bright, D. W.; Dias, F. B.; Galbrecht, F.; Scherf, U.; Monkman, A. P. *Adv. Funct. Mater.* **2009**, *19*, 67.
(156) Da Como, E.; Becker, K.; Lupton, J. M. *Polyfluorenes*; Springer-Verlag Berlin; Vol. 212, p 293.
(157) Lu, H. H.; Liu, C. Y.; Chang, C. H.; Chen, S. A. *Adv. Mater.* **2007**, *19*, 2574.
(158) Prins, P.; Grozema, F. C.; Nehls, B. S.; Farrell, T.; Scherf, U.; Siebbeles, L. D. A. *Phys. Rev. B* **2006**, *74*, 113203.
(159) O'Carroll, D.; Lacopino, D.; O'Riordan, A.; Lovera, P.; O'Connor, É.; O'Brien, G. A.; Redmond, G. *Adv. Mater.* **2008**, *20*, 42.
(160) Monkman, A. P.; Rothe, C.; King, S.; Dias, F. B. *Polyfluorenes*; Springer-Verlag Berlin, 2008; Vol. 212, p 187.
(161) Rothe, C.; Galbrecht, F.; Scherf, U.; Monkman, A. P. *Adv. Mater.* **2006**, *18*, 2137.
(162) Tsoi, W. C.; Charas, A.; Cadby, A. J.; Khalil, G.; Adawi, A. M.; Iraqi, A.; Hunt, B.; Morgado, J.; Lidzey, D. G. *Adv. Funct. Mater.* **2008**, *18*, 600.
(163) Knaapila, M.; Garamus, V. M.; Dias, F. B.; Almásy, L.; Galbrecht, F.; Charas, A.; Morgado, J.; Burrows, H. D.; Scherf, U.; Monkman, A. P. *Macromolecules* **2006**, *39*, 6505.
(164) Knaapila, M.; Dias, F. B.; Garamus, V. M.; Almásy, L.; Torkkeli, M.; Leppänen, K.; Galbrecht, F.; Preis, E.; Burrows, H. D.; Scherf, U.; Monkman, A. P. *Macromolecules* **2007**, *40*, 9398.
(165) Bright, D. W.; Galbrecht, F.; Scherf, U.; Monkman, A. P. *Macromolecules* **2010**, *43*, 7860.
(166) Lee, S. K.; Ahn, T.; Park, J.-H.; Jung, Y. K.; Chung, D.-S.; Park, C. E.; Shim, H. K. *J. Mater. Chem.* **2009**, *19*, 7062.
(167) Niu, X.; Liu, J.; Xie, Z. *Organic Electronics* **2010**, *11*, 1273.
(168) Knaapila, M.; Stepanyan, R.; Torkkeli, M.; Garamus, V. M.; Galbrecht, F.; Nehls, B. S.; Preis, E.; Scherf, U.; Monkman, A. P. *Phys. Rev. E* **2008**, *77*, 051803.
(169) Moss, K. C.; Bourdakos, K. N.; Bhalla, V.; Kamtekar, K. T.; Bryce, M. R.; Fox, M. A.; Vaughan, H. L.; Dias, F. B.; Monkman, A. P. *J. Org. Chem.* **2010**, *75*, 6771.
(170) Wu, Z.; Xiong, Y.; Zou, J.; Wang, L.; Liu, J.; Chen, Q.; Yang, W.; Peng, J.; Cao, Y. *Adv. Mater.* **2008**, *20*, 2359.

(171) Mo, Y.; Tian, R.; Shi, W.; Cao, Y. *Chem. Commun.* **2005**, 4925.
(172) Mo, Y.; Jiang, X.; Cao, D. *Org. Lett.* **2007**, *9*, 4371.
(173) Fomina, N.; Hogen-Esch, T. E. *Macromolecules* **2008**, *41*, 3765.
(174) Fomina, N.; Bradforth, S. E.; Hogen-Esch, T. E. *Macromolecules* **2009**, *42*, 6440.
(175) Beaupre, S.; Leclerc, M. *Macromolecules* **2003**, *36*, 8986.
(176) Beaupre, S.; Dumas, J.; Leclerc, M. *Chem. Mat.* **2006**, *18*, 4011.
(177) Li, Y.; Wu, H.; Zou, J.; Ying, L.; Yang, W.; Cao, Y. *Org. Electron.* **2009**, *10*, 901.
(178) Huang, W. S.; Wu, Y. H.; Hsu, Y. C.; Lin, H. C.; Lin, J. T. *Polymer* **2009**, *50*, 5945.
(179) Pandya, S. U.; Al Attar, H. A.; Jankus, V.; Zheng, Y.; Bryce, M. R.; Monkman, A. P. *J. Mater. Chem.* **2011**, *21*, 18439.
(180) Yang, W.; Hou, Q.; Liu, C.; Niu, Y.; Huang, J.; Yang, R.; Cao, Y. *J. Mater. Chem.* **2003**, *13*, 1351.
(181) Klemm, L. H.; Porter, Q. N. *J. Org. Chem.* **1981**, *46*, 2184.
(182) Gilman, H.; Nobis, J. F. *J. Am. Chem. Soc.* **1949**, *71*, 274.
(183) Huang, F.; Hou, L.; Shen, H.; Jiang, J.; Wang, F.; Zhen, H.; Cao, Y. *J. Mater. Chem.* **2005**, *15*, 2499.
(184) Mancilha, F. S.; DaSilveira Neto, B. A.; Lopes, A. S.; Moreira, P. F.; Quina, F. H.; Gonçalves, R. S.; Dupont, J. *Eur. J. Org. Chem.* **2006**, *2006*, 4924.
(185) Ishow, E.; Camacho-Aguilera, R.; Guérin, J.; Brosseau, A.; Nakatani, K. *Adv. Funct. Mater.* **2009**, *19*, 796.
(186) Vaitkeviciene, V.; Grigalevicius, S.; Grazulevicius, J. V.; Jankauskas, V.; Syromyatnikov, V. G. *Eur. Polym. J.* **2006**, *42*, 2254.
(187) Wang, D.; Niu, Y.; Wang, Y.; Han, J.; Feng, S. *J. Organomet. Chem.* **2010**, *695*, 2329.
(188) Valderrama, M. I. R.; García, R. A. V.; Klimova, T.; Klimova, E.; Ortiz-Frade, L.; García, M. M. *Inorg. Chim. Acta* **2008**, *361*, 1597.
(189) Dudek, S. P.; Pouderoijen, M.; Abbel, R.; Schenning, A. P. H. J.; Meijer, E. W. *J. Am. Chem. Soc.* **2005**, *127*, 11763.
(190) Belletête, M.; Beaupré, S.; Bouchard, J.; Blondin, P.; Leclerc, M.; Durocher, G. *J. Phys. Chem. B* **2000**, *104*, 9118.
(191) Ding, J.; Day, M.; Robertson, G.; Roovers, J. *Macromolecules* **2002**, *35*, 3474.